SynDLP: A new bacterial dynamin-like protein and its potential involvement in thylakoid membrane biogenesis

The identification and characterization of new DLPs from *Synechocystis* sp. PCC 6803

Dissertation zur Erlangung des akademischen Grades eines „Doctor rerum naturalium (Dr. rer. nat.)“ der Fachbereiche

08 – Physik, Mathematik und Informatik

09 – Chemie, Pharmazie und Geowissenschaften

10 – Biologie

Universitätsmedizin

der Johannes Gutenberg-Universität

von Ruven Jilly geboren am 04.12.1986 in Langen (Hessen)

1. Gutachter:

2. Gutachter:

Tag der mündlichen Prüfung: 26.04.2018

Nichts endet wirklich, es ist nur der Anfang von etwas Neuem

Frei nach Miguel de Unamuno y Yugo

I. Table of contents

II. Abstract

Billion years ago, the photosynthetic light reaction was a very successful invention of the nature. Primordial cyanobacteria were the first organism, which were able to cover their energy needs with almost endless resources (water, CO_2 and sun light). During the earth history, the photosynthetic system has become a very successful way to provide energy not only for cyanobacteria. Some early eukaryotes engulfed cyanobacteria in an endosymbiotic event that led to the development of algae and plants. However, the photosynthesis light reaction is localized within a special membrane system, the thylakoid membrane. In this thesis, a protein was studied, which is potentially involved in the biogenesis of thylakoid membranes. Dynamin-like proteins (DLPs) from eukaryotes or bacterial DLPs (BDLPs) are mechanochemical large GTPase, which share membrane remodeling or membrane protection properties. They are involved in several processes affecting membranes, like fission, fusion and division of cell organelles as well as viral protection and membrane stress response. With the help of bioinformatic analysis, five potential BDLPs were identified in the genome of the model organism *Synechocystis* sp. PCC 6803. These five candidates were investigated in order to figure out if they are BDLPs. Moreover, the influence of the phenotype was studied by creating *Synechocystis* deletion or depletion strains, lacking the corresponding genes. Out of the five candidates only one was confirmed being a BDLP and subsequently be named SynDLP. During this project, expression and purification of this new BDLP was established and it has been shown that SynDLP is an asymmetric disulfide-linked dimer, *in vitro*. With the purified protein, a continuous, regenerative coupled GTPase assay confirmed the GTPase activity. In addition, membrane interaction studies with Laurdan fluorescence showed, that SynDLP interacts with negatively charged membranes. Moreover, SFG spectroscopy, TEM micrographs and a sedimentation assay revealed a nucleotide depending change in the conformation and in the oligomeric state. In addition, a SynDLP mutant was created, which does not form dimers and was compared to the WT. Besides the *in vitro* experiments, a *Synechocystis* deletion mutant was generated, lacking in the SynDLP gene. *In vivo* analysis suggested that the phenotype is slightly different, especially under high light growth conditions, compared to the WT strain.

III. Zusammenfassung

Vor Milliarden Jahren änderte eine evolutionäre Entwicklung das damalige Leben auf der Erde grundlegend. Urahnen von Cyanobakterien waren in der Lage, mit Hilfe von Licht, CO_2 und Wasser, ihren Energiebedarf zu decken. Als Abfallprodukt gelangte dabei erstmalig freier Sauerstoff in die Umwelt. Das dem zu grundliegende System der oxygenen Photosynthese hat sich bis heute erhalten und findet sich außer in Cyanobakterien auch in Algen und Pflanzen. Dies geht wahrscheinlich auf eine Endosymbiose zurück. Frühe eukaryotische Lebensformen nahmen Cyanobakterien auf, aus denen sich nach und nach Chloroplasten entwickelt haben. Die photosynthetische Lichtreaktion ist in einem speziellen Membransystem lokalisiert, der Thylakoidmembran. Die Biogenese der Thylakoidmembran ist nur rudimentär verstanden. Ziel dieser Arbeit war es, neue Proteine zu charakterisieren, die an der Thylakoidmembran-Biogenese beteiligt sein könnten. DLPs (*eng. dynamin-like proteins*) oder BDLPs (bakterielle DLPs) sind GTPase, die an verschiedenen Membranen zu finden sind und deren Struktur beeinflussen können. So sind sie an der Fusion und Teilung von Zellorganellen, sowie an viralen Schutzmechanismen und der Instandhaltung von bakteriellen Membransystemen beteiligt. Im Genom des Cyanobakteriums *Synechocystis* sp. PCC 6803 konnten fünf potentielle BDLPs identifiziert werden. *In vitro* Analysen konnten bestätigen, dass es sich bei einem der Kandidaten höchstwahrscheinlich um ein BDLP handelt. Dieses Protein wurde daraufhin in SynDLP umbenannt. *In vitro* liegt SynDLP als asymmetrisch Disulfid-verknüpftes Dimer vor. Die GTPase-Aktivität des Proteins konnte mittels eines regenerativen, gekoppelten Assays bestätigt werden. Eine spezifische Interaktion mit negativ geladenen biologischen Modelmembranen wurde mittels Laurdan-Fluoreszenzspektroskopie gezeigt. Weiter konnte mit SFG-Spektroskopie, TEM Aufnahmen und einem Sedimentation-Assay gezeigt werden, dass sich die Konformation und der oligomere Zustand von SynDLP, abhängig vom zugesetzten Nukleotid ändert. Zudem wurde eine SynDLP Mutante kreiert, die keine Dimere mehr bildet. Zur Untersuchung der Auswirkung auf die Thylakoidmembran wurde eine *Synechocystis* Mutante etabliert, in der das SynDLP Gen deletiert werden konnte. Dabei zeigt die Mutante einen leicht veränderten Phänotyp im Gegensatz zum wildtypischen Stamm, der besonders unter Starklichtbedingungen ausgeprägt ist.

IV. Publications

Some parts of this thesis are published:

- Jilly, R., Khan, N.Z., Aronsson, H., Schneider, D., 2018. Dynamin-Like Proteins Are Potentially Involved in Membrane Dynamics within Chloroplasts and Cyanobacteria. Front. Plant Sci. 9, 1–13. doi:10.3389/fpls.2018.00206

V. Collaborations

With the following groups and persons collaborations due to data used in this thesis:

- [redacted] (Prof. Markl group), Institut für Molekularbiologie Johannes Gutenberg-Universität Mainz
- [redacted] (Prof. Markl group), Institut für Molekularbiologie, Johannes Gutenberg-Universität Mainz
- [redacted]. Molecular spectroskopy group, Max Planck-Institut für Polymerforschung
- [redacted], Laboratoire de Bioélectrochimie et Spectroscopie, University Strassburg
- [redacted], Institute for Molecular Sciences Van't Hoff, University of Amsterdam

The following diploma thesis were supervised during this thesis.

"Expression, Reinigung und Charakterisierung des hypothetischen BDLP Homologes Sll0804 aus dem Cyanobakterium *Synechocystis* sp. PCC 6803", [redacted]

Data obtained from the previous mentioned collaborations are marked.

1. Introduction

1.1 Oxygen evolution, the revolution of cyanobacteria

Around 4.5 billion years ago, the earth was formed out of dust and stones within our solar system. Only a few billion years later, the first living cells emerged, as supported by ^{13}C isotope analysis of old rocks (McCollom and Seewald, 2006). Evidences of anoxygenic photosynthesis can be predated 4.2 billion years ago, but are still controversially discussed (Blankenship, 2010). A following event changed the complete environmental conditions dramatically. 3.5 to 2.7 billion years ago, first organisms appeared and were able to convert CO_2 and H_2O to carbohydrates and O_2, only with the help of light energy. The released oxygen in the atmosphere oxidized the previous reduced earth and thereby founded our oxygen based life. This process was not continuous, but includes several steps and stages (see also Figure 1). The first hints of cyanobacteria can be dated back 3.5 billion years, as fossils might show cyanobacteria-like shapes (Schopf, 1993). Moreover, a biological marker for cyanobacteria, methyl-substituted hopanoids, were discovered in a 2.5 billion years old shale (Summons et al., 1999). In this period also free oxygen occurred the first time on earth (Hohmann-Marriott and Blankenship, 2011). The oceans started to become slightly oxidized and oxygen accumulated in the atmosphere to approx. 0.04 atm from 2.5 to 1.9 billion years (Holland, 2006). This event is called the great oxygen event (GOE), which is roughly the point where the “reduced” earth changed to an “oxidized” world. Before the GOE, the produced oxygen might have reacted directly with its environment. Afterwards, the oxygen level in the atmosphere remained stable for approx. 1 billion years. With the upcoming of oxygenic photosynthetic eukaryotes (likely resulting out of one or even more endosymbiotic events), like algae and first plants, the atmospheric oxygen level increased to a maximum of more than 0.3 atm in the Carboniferous, and with emergence of the first mammals the O_2 level reached the 0.2 atm of today (Holland, 2006). In all of these stages, cyanobacteria were present and had conquered nearly every habitat on earth, which makes them also extremely successful from an evolutionary point of view. Nowadays, they can be found in freshwater, seawater, on rocks (including Antarctic and dessert rocks), in soil and even endolithic as well as endosymbionts in some other organism (Büdel, 2011; de los Ríos et al., 2007).

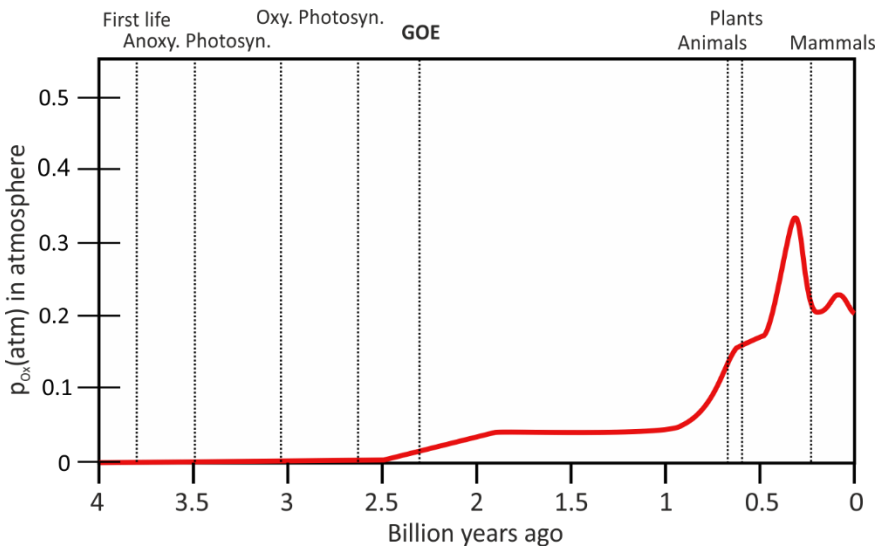

Figure 1: Oxygenic evolution during the last 4 billion years. The partial pressure of oxygen in the atmosphere is indicted by the red line. GOE: Great oxygen event

1.2 Cyanobacteria between model organism and industrial applications

Cyanobacteria are very modest and the few resources they need are nearly endlessly available. Thus, the usage in a wide range of biotechnical applications is discussed and tested. The first description of cyanobacteria used as a food source can be dated back to the year 1520. Spanish conquistadores observed the harvesting of green mud from a lake in Mexico, which was dried and eaten (Siva Kiran et al., 2015). Later, similar observations were made in Africa (Sánchez et al., 2003). Indeed, such crude extracts contain a numerous amount of different cyanobacteria and micro algae, but the main component is the cyanobacterium *Arthrospira*, which is better known as *Spirulina* (Sánchez et al., 2003). Beginning in the 1970s this strain was planted systematically in tropical and subtropical areas. The corresponding extract is distributed worldwide as food supplementary, animal feed and fertilizer (Siva Kiran et al., 2015).

Besides food and feed production, other cyanobacterial strains were and are still genetically engineered to produce several organic compounds, like ethanol and alkanes for biofuel production (recently reviewed (Al-Haj et al., 2016)). But there are also efforts to use them in direct photosynthetic biofuel cells (Morishima et al., 2007), as the producer of anti-inflammatory

substances (Choi et al., 2012) and as potential food and oxygen source on a future mars outpost (Verseux et al., 2016).

But in the end, all these undoubtedly interesting applications go back on efficiency in photosynthesis and the efficiency in turnover light to carbohydrates. To tune this system, a deep understanding of the photosynthetic machinery is necessary, not only in cyanobacteria, but also in chloroplasts. It seems to be very likely that in one or even more endosymbiotic events, primordial cyanobacteria were engulfed by eukaryotic organisms, which lead to a deep connection and a high genomic similarity between both (reviewed in reference (Hohmann-Marriott and Blankenship, 2011)). The endosymbiotic theory suggests that cell organelles, such as mitochondria or chloroplasts, originate from early prokaryotic cells, which were engulfed from another cell. Over the time, the DNA of the prokaryotic cell was incorporated in the DNA of the host cell and e.g. thus 18 % of the *Arabidopsis thaliana* (hereafter just *Arabidopsis*) genome is of cyanobacterial origin (Martin et al., 2002). However, to study the photosynthesis light reaction, the cyanobacterial strain *Synechocystis* sp. PCC 6803 (hereafter just *Synechocystis*) is used frequently. It was the first cyanobacterium, whose full length amino acid sequence was provided in 1996 (Kaneko et al., 1996). Furthermore, *Synechocystis* is naturally competent, (Barten and Lill, 1995) benefits from a relatively short doubling time of approx. 12 h (Vermass et al., 1988) and is able to grow under light-activated heterotrophic growth conditions, where it growth on glucose (Anderson and McIntosh, 1991). Thus, besides several biotechnical aspects, *Synechocystis* is a widely-used model organism to study photosynthesis.

Figure 2 illustrates the structure of a *Synechocystis* cell. The photosynthetic light reaction is localized in the thylakoid membrane (green), which is distributed in the cytoplasm (light blue).

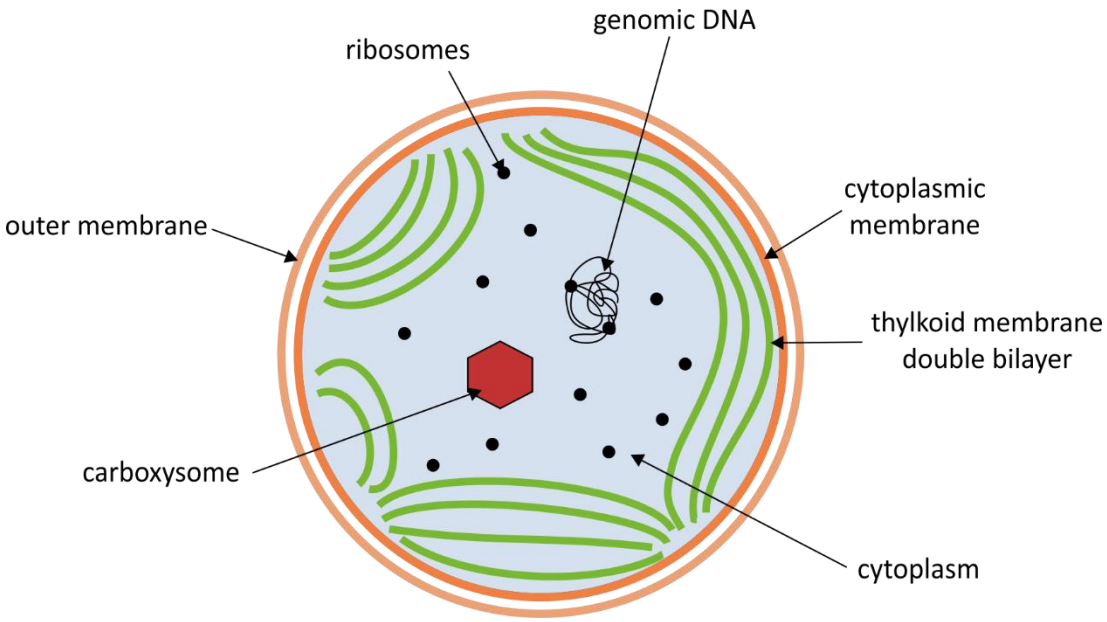

Figure 2: Schematic view on a *Synechocystis* cell. The thylakoid membranes (green) are distributed in the cytoplasm (light blue) along the cytoplasmic membrane.

1.3 The thylakoid membrane or the home of nature solar cells

In chloroplast and in cyanobacteria, the photosynthesis light reaction is localized within a special membrane system, the thylakoid membrane (TM). The TM harbors the proteins, cofactors, pigments and lipids of the light reaction. Together they are involved in the fixation of carbon dioxide and splitting of water to generate carbohydrates. This process can be expressed by the overall photosynthesis equation:

$$6CO_2 + 6H_2O \rightarrow C_6H_{12}O_6 + 6O_2$$

Here water and CO_2 are utilized to create carbohydrates and oxygen as a reaction side product. Behind this simple equation the proteins, cofactors and pigments have to be highly synchronized in time and place to reach a maximum of photosynthetic efficiency. However, a more detailed description can be found elsewhere (e.g. here (Shevela et al., 2013)) and will be discussed only briefly in this thesis (Figure 3). Light energy is collected by phycobilisome complexes, which channel the light energy to the photosystem II (PSII). There, the energy excites electrons in the

reaction center (P680→P680*), containing a pair of chlorophyll molecules. Thereby, the excited reaction center (P680*) feeds the electron transport chain with electrons and the resulting electron gap is filled by electrons provided by water oxidation. Via the cofactor plastoquinone (PQ) and the cytochrome b_6f complex (Cyt b_6f) the electrons are transferred to the photosystem I (PSI), where the reaction center is excited again (P700→P700*) and $NADP^+$ is finally reduced to NADPH. Formally, for all steps the charge need to be balanced, which is provided by a proton flux from the cyanobacterial cytoplasm into the thylakoid lumen. The resulting proton gradient is used for the synthesis of ATP out of ADP and inorganic phosphate. ATP, together with NADPH, is utilized to fix CO_2 in the Calvin-Benson cycle.

Noteworthy, parts of the respiratory electron transport complexes are also localized within the TM in cyanobacteria (Mullineaux, 2014). Consequently, the photosynthetic and respiratory electron transport are closely interlinked and can be regulated, depending on the environmental conditions (reviewed e.g. here (Lea-Smith et al., 2016; Liu, 2016)).

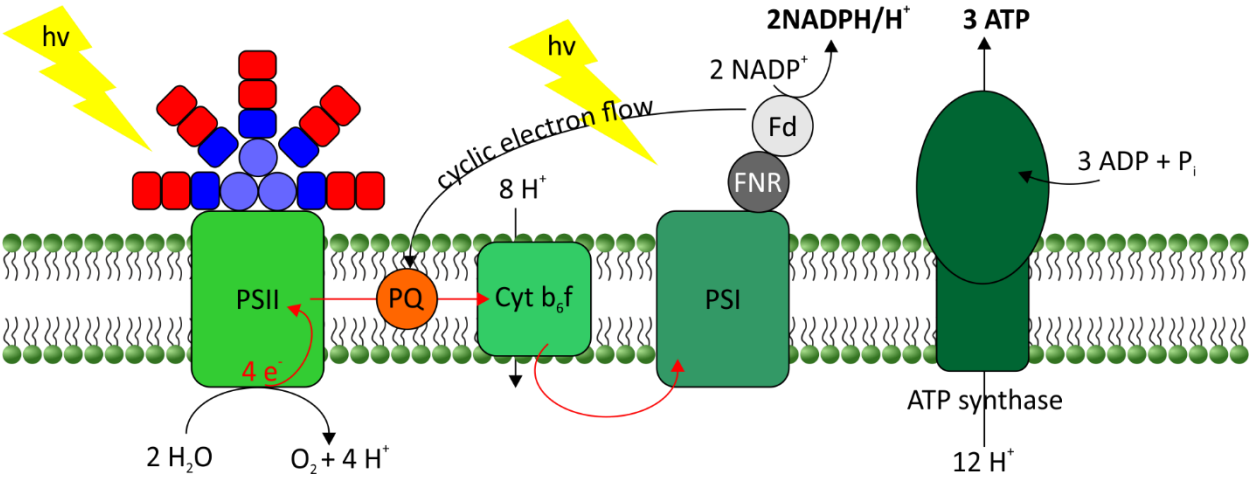

Figure 3: The photosynthetic light reaction is localized in the TM. The light energy (hv) is collected by phycobilisomes (red and blue) and utilized to oxidize water. From photosystem II (PSII) the electrons are transported to the cytochrome *b_6f*-Komplex (Cyt b_6f) via plastoquinone (PQ). Finally, the electrons reach photosystem I and reduce NADP to $NADPH/H^+$. The overall generated proton gradient drives the ATP synthesis at the ATP synthase. Fd: Ferredoxin; FNR: Ferredoxin-$NADP^+$ reductase

1.3.1 Composition and arrangement of the thylakoid membrane

Chloroplasts are cell organelles in algae and plants in which the TMs are localized. In the chloroplast stroma the TMs arrange in multiple cylindrical stacks (grana), which are connected by unstacked TMs (stroma lamellae). The TMs enclose the so called thylakoid lumen (Adam et al., 2011). In cyanobacteria the TMs order in a sheet like structure in the cytoplasm and can differ significantly between the different strains (Herrero and Flores, 2008). Although the fine structure of TMs in cyanobacteria and chloroplasts differs, the lipid composition of the TM is very similar (Boudière et al., 2014; Jouhet et al., 2007). The main lipid compounds of TMs are monogalactosyldiacylglycerol (MGDG) and digalactosyldiacylglycerol (DGDG), the negatively charged galactolipid sulfoquinovosyldiacylglycerol (SQDG), as well as the phosphoglycerolipid phosphatidylglycerol (PG), which is also negatively charged. The amount of the different lipids can vary from species to species and may include other lipids in case of chloroplasts (Table 1) (Block et al., 2007; Boudière et al., 2014; Jouhet et al., 2007).

Table 1: TM composition in different species from cyanobacteria to higher plants in percentage of the whole TM lipids. PI: Phosphatidylinositol; Phosphatidylethanolamine; PC: Phosphatidylcholine.

Structure/Name	***Synechocystis*** (Boudière et al., 2014)	***C. reinhardtii*** (Mendiola-Morgenthaler et al., 1985)	***Arabidopsis*** (Dörmann et al., 1995)	***S. oleracea*** (Dorne et al., 1990)
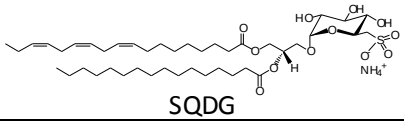 SQDG	22	13	2.4	6.5
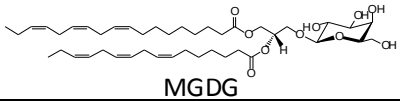 MGDG	52	55	51.3	52
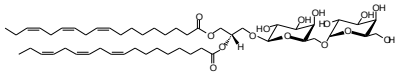 DGDG	11.7	20	16.0	26
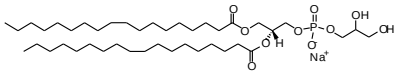 PG	11.4	6	8.1	9.5
PI	-	2.7	-	1.5
PE	-	-	9.3	-
PC	-	-	12.8	4.5

In all species, the amount of MGDG is always above 50 %, and thus MGDG appears to have a key role in TMs. However, in contrast to the other thylakoid lipids, MGDG alone forms an inverse hexagonal lipid phase, due to its small headgroup (Lee, 2000). Consequently, a lamellar, functional TM bilayer is only formed in presence of the other lipids and membrane proteins (Simidjiev et al., 2000). While the high MGDG content in fact severely destabilizes TMs, in curved TM regions the MGDG/DGDG ratio is significantly higher compared to the stroma lamella region (Gounaris et al., 1983), and MGDG destabilized membrane regions are discussed to be crucial for the formation of inter-membrane contact sides (Heidrich et al., 2017). Moreover, due to the lipids SQDG and PG the TM is partly negative charged, which seems to be very important for the TM, because the loss of negative charges is always compensated. Thus, in the cyanobacterium *Synechococus* sp. PCC7942 and in the plant *Arabidopsis*, PG synthesis stops under phosphate deficient growth conditions coupled with an increase of the SQDG content to compensate for the loss of negative charges (Essigmann et al., 1998; Güler et al., 1996). In addition, the negative charge of the TM is important to coordinate the lipid protein interaction within the membrane. For example, in plant chloroplasts, the negative surface charge affects aggregation/dis-aggregation of antenna complexes (Schaller-Laudel et al., 2017; Schaller et al., 2014, 2011), and recent studies have indicated that assembly and activity of serval membrane associated compounds of the photosynthetic electron transfer chain depend on the lipid environment (Boudière et al., 2014). Especially PSII is strongly influenced by its lipid environment and e.g. SQDG and PG are needed to stabilize its structure (Mizusawa and Wada, 2012).

Beside the lipids, the TM also contains cofactors, pigments and ca. 60 % proteins (Chapman et al., 1983). Thus, TM biogenesis must be highly synchronized in time and place to work efficiently and successfully. There are several unanswered questions regarding the biogenesis of the TM. The knowns and unknowns are summarized in Figure 4.

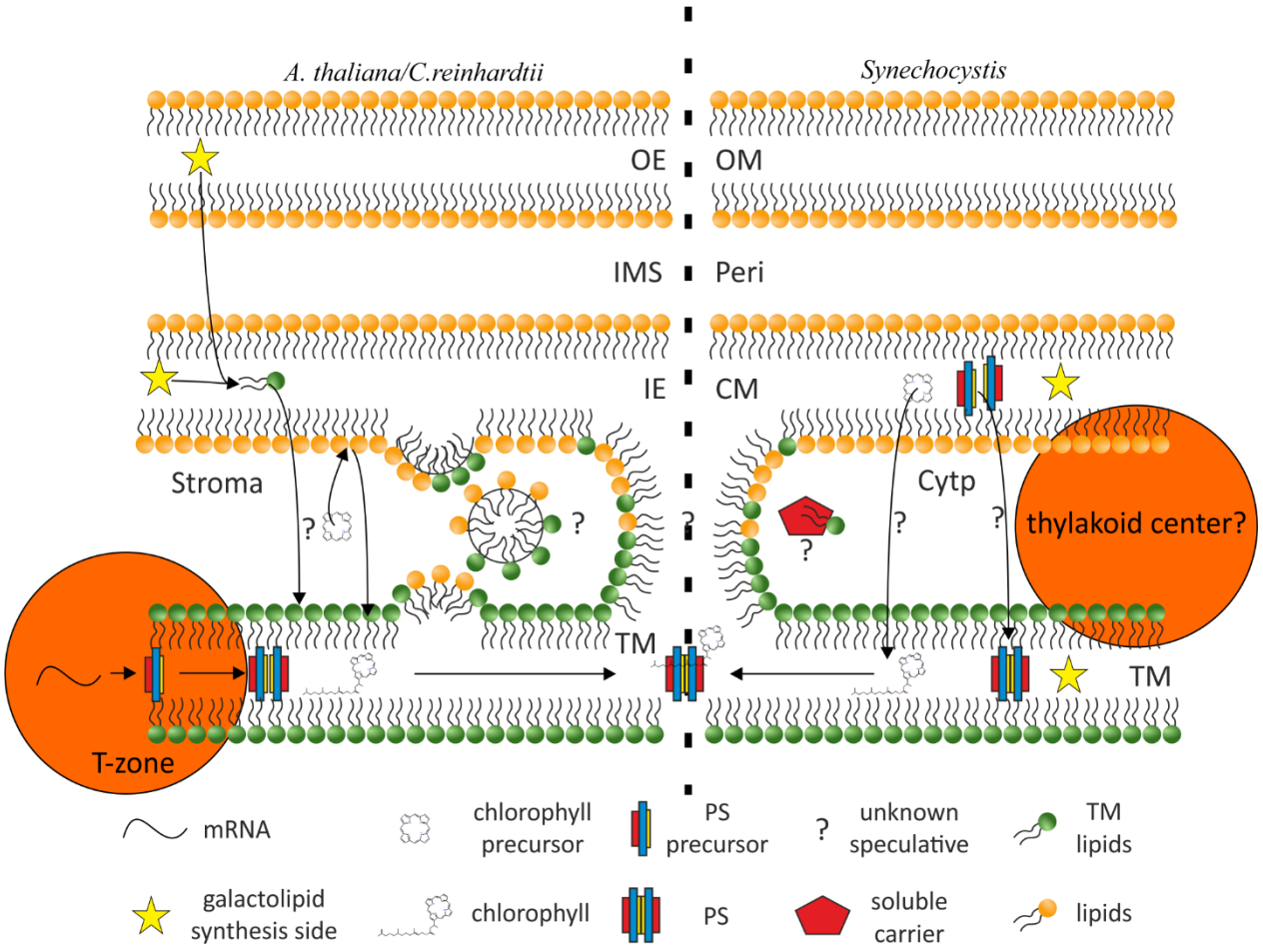

Figure 4: The knowns and unknows of TM biogenesis. For details see the text below. OE: Outer envelope; OM: Outer membrane; IMS: Inner membrane space; Peri: Periplasm; IE: Inner envelope; CM: Cytoplasmic membrane; Cytp: Cytoplasmic membrane; TM: Thylakoid membrane.

Possibly, defined TM regions exist, where protein, pigments and lipids are synthesized and holo-protein assembly takes place. In *Chlamydomonas reinhardtii* so called T-zones have been identified (Uniacke and Zerges, 2007). These T(translation)-zones are areas localized close to the pyrenoid. Pyrenoids are sub organelle compartments in chloroplast and ensure a carbon dioxide rich environment close to the photosynthetic light reaction (Giordano et al., 2005). mRNA, which encodes PSII subunits, was found exclusively in this defined membrane regions (Uniacke and Zerges, 2007). Such defined structures were also discussed for cyanobacteria. So called thylakoid centers, where different TM layers merge and are in close contact to the CM, could represent specialized biogenesis zones (Rast et al., 2015). However, this is highly speculative and experimental evidence is missing so far.

A key step in the development, dynamics and maintenances of TMs is the transport of lipids to their destination. In chloroplasts, lipid biosynthesis starts in the chloroplast stroma, where acetyl-CoA is converted into the lipid precursor phosphatidic acid (PA) (Benning, 2009; Rolland et al., 2012). Subsequently, the enzyme MGD1, which is localized within the chloroplast inner envelope (IE) membrane, as well as the outer envelope (OE) membrane enzyme DGD1 catalyze synthesis of MGDG and DGDG, respectively (Benning, 2009; Joyard et al., 2010; Rolland et al., 2012). Since in chloroplasts membrane lipids are synthesized within the envelope membranes, lipids need to be translocated to the TM system after synthesis, for membrane biogenesis and/or maintenance. However, while in chloroplasts lipid transfer between the IE and TMs clearly needs to be organized, the need for lipid transfer is not obvious in cyanobacteria. In cyanobacteria, galactolipids appear to be synthesized at both membranes, the PM and the TM (Koichiro Awai et al., 2006; Selão et al., 2014), and thus the CM and TMs might not need to exchange membrane lipids. Nevertheless, in cyanobacteria, synthesis of chlorophyll might be delocalized, as chlorophyll precursors were exclusively found in the CM, whereas enzymes catalyzing subsequent synthesis steps are mainly localized within the TMs (Peschek et al., 1989; Schottkowski et al., 2009). Consequently, potentially chlorophyll precursors have to exchange in between cyanobacterial membranes. In contrast, the initial step of chlorophyll biosynthesis takes place in the *A. thaliana* chloroplast stroma, while the final steps are localized at the TM or the IE (Eckhardt et al., 2004; Nickelsen et al., 2011). Thus, mechanisms ensuring the transport of lipids in between inner membranes are needed both, in chloroplasts and cyanobacteria. Transfer proteins can transport lipids from the ER to chloroplasts in plants (K. Awai et al., 2006; Lu et al., 2007; Roston et al., 2011; Wang et al., 2012; Xu et al., 2008, 2003), but within chloroplasts and cyanobacteria a lipid carrier protein has not been identified yet. The second possibility is an exchange of compound in between inner membranes via a vesicle transport system. In fact, in chloroplast the formation of vesicular structures has been observed, supporting the assumption that a vesicular transfer system operates in chloroplasts (Khan et al., 2013; Lindquist et al., 2016; Westphal et al., 2001). In addition, similar systems are suggested to work in cyanobacteria (Keller and Schneider, 2013; Nevo et al., 2007; Schneider et al., 2007). Alternatively, a material exchange in between the IE/CM and the TM via lateral fusion is conceivable. Indeed, in chloroplast (Charuvi et al., 2012;

Engel et al., 2015; Hoober et al., 1991) and in *Synechocystis* (Van De Meene et al., 2006) regions were identified, which seems to show such connections. Nevertheless, the existence of these fusion events is discussed controversial, as they were observed only rarely in cyanobacteria. However, that TMs arose from the CM might be highlighted by the observation that the primitive cyanobacterium *Gloeobacter violaceus* is lacking internal TMs (Rippka et al., 1974). Here, the components of the photosynthetic light reaction are localized within defined regions within the CM (Mimuro et al., 2008; Rexroth et al., 2011). These areas might represent primordial TM-precursors and the TM system might has arisen from similar structures during evolution. In addition, TMs do not form *de novo* in cyanobacteria, indicated by the presence of rudimentary TMs in dark-adapted *Synechocystis* cells (Barthel et al., 2013).

In *Arabidopsis* chloroplasts, the structure and interconnection of the TM system is highly dynamic, depending on the environmental conditions (Chuartzman et al., 2008; Herbstova et al., 2012; Iwai et al., 2015; Kirchhoff et al., 2011), which underlines the requirement of controlled fission and fusion processes. In cyanobacteria, similar dynamic events are not described, but observation in *Cyanothece* sp. ATCC 51142 reveal interconnected TM layers, which are essential for transport of e.g. proteins (Liberton et al., 2011a, 2011b), suggesting a chloroplast-like TM dynamic.

In recent years many proteins were discussed to be involved in the TM biogenesis in *Synechocystis*. E.g., a SPHF homologue (Slr1768), the chaperone DnaK3 (Sll1932) and the IM30 protein (Sll0617) (Bryan et al., 2011; E. Fuhrmann et al., 2009; Rupprecht et al., 2007). Especially, IM30 is part of actual studies and it has been shown, that it fuses membrane vesicles in presence of Mg^{2+}, at least *in vitro* (Hennig et al., 2015) IM30-depelted chloroplasts and cyanobacteria have significantly reduced TM contains (Eva Fuhrmann et al., 2009; Kroll et al., 2001).

1.4 The dynamin superfamily

Since TM biogenesis involves membrane reorganization, a protein family became into our focus, which are associated with different membrane remodeling processes. Dynamin-like proteins or dynamin-related proteins are found in eukaryotic and in prokaryotic organisms. Beside the "small GTPases", which are e.g. involved in signal transduction, such as Ras-like GTPases, dynamin-like proteins (DLPs) or dynamin-related proteins (DRPs) are "large" GTPases and members of the dynamin superfamily (hereafter just DLPs) (Lu et al., 2016; Praefcke and McMahon, 2004). They can bind GTP and hydrolyze it (GTP → GDP + P_i). The released energy is utilized to remodel membranes (Daumke and Praefcke, 2016; Praefcke and McMahon, 2004). The DLPs can be further separated into the better characterized eukaryotic and the recently discovered prokaryotic or bacterial DLPs, BDLPs. Especially the eukaryotic branch harbors various of well characterized DLP subfamilies.

Approx. 30 years ago the first member of the DLP subfamily Mx (interferon-induced GTP-binding proteins) was suggested to be involved in interferon mediated influenza resistance (Mx1) (Staeheli et al., 1986). In further studies of the human Mx (MxA) protein, the structure and function were clarified (Gao et al., 2011, 2010; Kochs and Haller, 1999). Shortly afterwards, dynamin, which lent its name to the superfamily, was first isolated from a calf brain and a tubulin-activated GTPase activity was discovered (Shpetner and Vallee, 1992; Shpetner et al., 1989). Later, the essential role of dynamin in clathrin-mediated endocytosis was revealed (Hinshaw and Schmid, 1995; Mettlen et al., 2009). While the prototypic dynamin (Dyn) is mainly expressed in the synapse, two other isoforms exist in mammals. Dynamin II is expressed in all cell types and dynamin III is restricted to lung, brain and testis tissue (Cook et al., 1996, 1994).

In addition, several dynamin related proteins exist, which are acting at different cell organelles and membrane systems. For example, Atlastin from the organism *Drosophila melanogaster* was suggested to be required for the homotypic fusion of ER membranes (Orso et al., 2010). The division of mitochondria is supported by Drp1 via promoting membrane intermediates (Smirnova et al., 2001; Ugarte-Uribe et al., 2014). The counterparts of Drp1 are mitofusin and OPA1. They are involved in the fusion of mitochondrial inner and outer membrane, respectively (Frezza et al.,

2006; Santel and Fuller, 2001). Guanylate-binding proteins (GBPs) create another subfamily. Like the Mx subfamily, proteins of the GBP subfamily are interferon induced protectors against pathogens (reviewed by (Vestal and Jeyaratnam, 2011)). Especially GBP1 was extensively studied and it has been shown that GTPase hydrolysis of GBP1 is essential for suppression of hepatitis C virus replication (Itsui et al., 2009). Although they are no GTPases but ATPases, the Eps15 homology domain-containing proteins (EHDs) are claimed to be DLPs (Daumke et al., 2007). Recent studies suggest that EHD2, a member of this subfamily, is involved in the regulation of caveolar dynamics (Moren et al., 2012).

Besides in insects and mammalian cells, DLPs are also encoded in plants. This class of DLPs is mainly investigated in *Arabidopsis*. The first identified representative was the *Arabidopsis* dynamin-like protein 1 (ADL1) that was initially suggested to be involved in TM biogenesis in chloroplasts (Park et al., 1998), although this function was not confirmed in later studies. Instead, ADL1 (later renamed to ADL1A and sometimes named DRP1A) and its homolog ADL1E were proposed to be essential for polarized cell growth and plant cytokinesis (Kang et al., 2003). Additionally, the DLPs ADL2a (also DRP3A) and ADL2b (also DRP3B) were suggested to be involved in mitochondria division in *Arabidopsis* (Arimura and Tsutsumi, 2002; Arimura et al., 2004), whereas ADL6 is involved in vesicle transport from the trans-Golgi network to vacuoles (Jin et al., 2001). Later studies claimed that DRP3A and DRP3B participate in the division of mitochondria and peroxisomes, while DRP5B is involved in the division of chloroplast (Aung and Hu, 2012, 2009; Fujimoto et al., 2009; Mano et al., 2004; Zhang and Hu, 2010). The DLP DRP1E, initially discovered in rice, controls the release of cytochrome c from mitochondria and is involved in apoptosis (Li et al., 2017). The *Arabidopsis* proteins ADL1 and ADL3 (also DRP2B) were suggested to cooperate, during the formation of clathrin-coated endocytic vesicles (Fujimoto et al., 2010). At the chloroplast OM facing the cytosol, the (thus far only identified and characterized) plant-specific DLP ARC5 (or DRP5B) is involved in organelle division (Gao et al., 2003). Moreover, in *Arabidopsis* the FZL protein was found, which is related to fuzzy onion (FZO) proteins and belongs to the mitofusin subfamily. FZL is the only protein, which might be involved in the TM biogenesis. Pioneer work by H. Gao et al. showed that FZL is located at the chloroplasts TM/IE. Furthermore,

in absence of FZL, vesicles in the chloroplast appear to not fuse and abnormal TM morphology was observed, indicating an important role of FZL in the TM biogenesis (Gao et al., 2006).

Noteworthy, DLPs in algae are not studied, although a search in the Kegg genome database identified 8 potential DLPs (DRPs) in the model alga *C. reinhardtii* (Kanehisa et al., 2017; Merchant et al., 2007).

Besides DLPs in eukaryotic organisms, including the prototypical dynamin, recent studies suggested an important role of DLPs in prokaryotic cells. Although it is known widely that in many bacteria DLP homologues are encoded, the first thorough investigation of a bacterial DLP (BDLP) was published in 2006 by Low et al. (Low and Löwe, 2006; Van Der Bliek, 1999). To distinguish BDLP from other bacterial dynamin-like proteins (hereafter BDLPs), it is named to NosDLP. NosDLP is hosted in the cyanobacterium *Nostoc punctiforme*, and NosDLP behaves like a "classical" DLPs *in vitro* (Low and Löwe, 2006; Low et al., 2009). Although the protein is expressed *in vivo*, its function remains still mysterious (Low and Löwe, 2006). In recent years, three more BDLPs were discovered: DynA was found in *Bacillus subtilis* where it is involved in membrane fusion events, at least *in vitro* (Bürmann et al., 2011). Moreover, a recent study strongly suggested a membrane repair function of DynA (Sawant et al., 2016). The third member of the BDLP subfamily is LeoA. LeoA likely is involved in the secretion of heat labile enterotoxin (Brown and Hardwidge, 2007; Fleckenstein et al., 2000). Recently, LeoA together with its gene neighbors (LeoB and LeoC), are identified as BDLPs (Michie et al., 2014). The youngest members of the BDLP family are DynA and DynB of *Streptomyces venezuelae*, which play a key role in bacterial cytokinesis (Schlimpert et al., 2017).

Figure 5 shows potential functions of selected (B)DLPs in opisthokonts (right), in plants (left) and in a prokaryotic cell (blue, middle). Interestingly, while the exact function is different, the (B)DLPs can be roughly categorized into two groups: One group is crucial for different membrane remodeling processes, whereas the other group is known to protect animal cells against pathogens and/or membrane disruption.

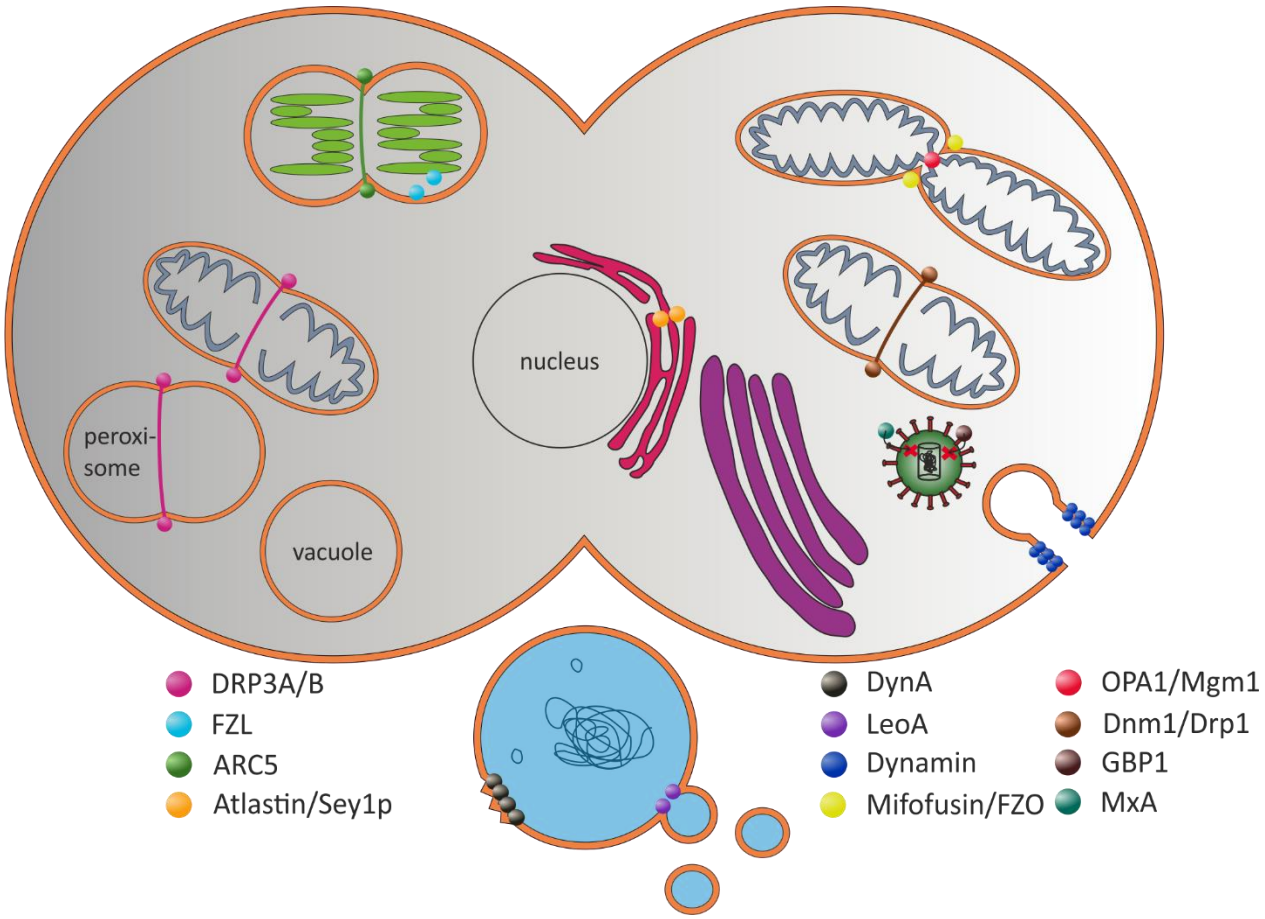

Figure 5: Selected (B)DLPs and their localization as well as proposed functions. On the left side, a plant cell and on the right side, an animal cell is shown with selected DLPs and their suggested function**.** The light blue background illustrates a schematic bacteria cell. For more details see the text. This figure is adapted and modified from Jilly et al (Jilly et al., 2018).

1.4.1 Common structure elements of (B)DLPs

The diversity within the howl DLP superfamily is great, regarding the membranes they interact with, the organisms they are encoded in and the function they are made for. Nevertheless, especially on the level of the protein domain structure elements can be identified, which are similar for all DLPs. Many DLPs harbor a G-domain (GD), a middle domain (MD), a membrane interacting domain (MID) and a GTPase effector domain (GED). It should be noted that the nomenclature is not totally strict. In this thesis, the domains are defined as followed: The GD typically starts at the N-terminus of (B)DLPs, harbors the GTPase activity and ends right before the MD. The MD typically starts directly after the GD and ends before the MID. The MID is followed by the GED at the C-terminal end of the protein. Note that the here chosen parameters are not necessarily in agreement with the literature, but should unify the structure elements.

Figure 6 shows the domain structure of 13 (B)DLP representatives. Besides the common domains, some (B)DLPs own additional domains and/or lack some. The only plant DLP (FZL) has an additional chloroplast transit peptide (CTP), which is necessary for chloroplast input (Gao et al., 2006). Similarly, OPA1 exhibits a mitochondrial interaction side (MIS) within the GD before the GTPase region (Belenguer and Pellegrini, 2013). Interestingly, OPA1 is the only DLP, whose MID is not between the MD and the GED, but between the MIS and the GD (Belenguer and Pellegrini, 2013). Atlastin and GBP1 do not contain the GED. The MID in Drp1 is replaced by a variable region. The variable region can be post-translational modified to promote protein activity (Cho et al., 2013). While in EHD2 the MID is missing, the GED is replaced by an EH domain, which can interact with special peptide motifs (de Beer et al., 1998). Noteworthy, in dynamin the GED contains an additional proline rich domain (Zheng et al., 1996). The BDLPs show all a very strict domain organization, except DynA. DynA is composed of two subunits (D1 and D2), which are both BDLPs (Bürmann et al., 2011).

While the overall domain structure of all (B)DLPs are highly conserved, the amino acid sequence is not. The GD harbors the only conserved region in the GTPase subdomain. The GTPase domain is large with approx. 280 aa and owns a central global β-sheet structure, surrounded by α-helices (Faelber et al., 2011). The phosphate groups of GTP are guided to the active side by the P-loop or G1 motif (GxxxxGKS/T). The G2/Switch I (T/S) or G3/Switch II (DxxG) are necessary for Mg^{2+} binding. The G4 (N/TxxD or RD) might bind directly to guanin bases (Leipe et al., 2002). The MD is dominated by α-helical structures and mediates interactions of (B)DLPs (e.g. for Dyn, MxA and NosDLP) (Gao et al., 2010; Low et al., 2009; Reubold et al., 2015).

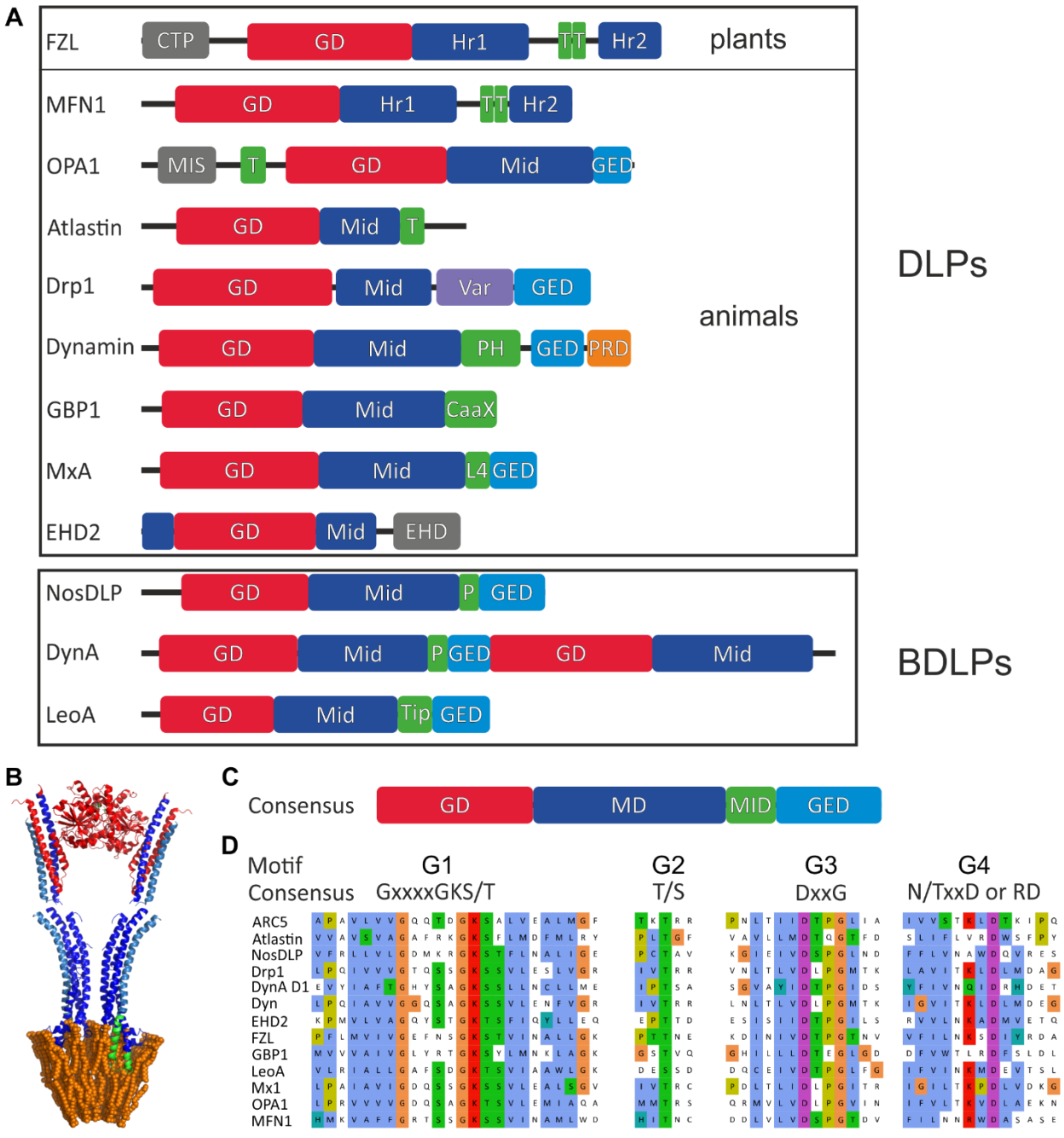

Figure 6: Structure elements of selected (B)DLPs. The domain structure of different (B)DLPs of plants, opisthokonts and prokaryotic cells (A). (B) shows the crystal structure of an open NosDLP dimer in its GDP bound form anchored in a tubulated lipid bilayer (orange) (PDB 2W6D) (Low et al., 2009). The typical domain structure consensus of (B)DLPs is illustrated in (C). The GTPase domain (GD, red) includes the nucleotide binding side, the middle domain (MD, blue) is part of alpha-helical bundles as well as the GTPase effector domain (GED, light blue). The membrane interacting domain (MID, green) is necessary for membrane interaction. In (D) amino acid motifs in the GD regions of (B)DLPs are aligned and shows the conserved amino acids. CTP: chloroplast transition peptide; Hr: heptad repeats; T: transmembrane helix; MIS: mitochondrial interaction side; Var: variable region; PH: pleckstrin homology domain; PRD: proline rich domain; L: loop; EHD: EPS15 homology domain; P: paddle

Since a lot of (B)DLPs can remodel membranes, a part of all the proteins must interact with membranes. As mentioned above, in this thesis this region is named MID. In case of FZL, MFN1,

OPA1 and Atlastin the MIDs are real transmembrane (T) helices, anchoring the proteins in mitochondria, endoplasmic reticulum (ER) and IE/TM membranes, respectively (Belenguer and Pellegrini, 2013; Cao et al., 2017; Gao et al., 2006; Liu et al., 2015). In BDLPs, the paddle (P) and the tip are hydrophobic loop regions, driving a strong lipid binding interface (Low and Löwe, 2006; Michie et al., 2014). A similar function is provided by a disordered loop region (L4) in MxA (Gao et al., 2010). Remarkably, Drp1 lacks a direct membrane interaction side, but the variable region mediates membrane binding after post-translational modification (Cho et al., 2013). In a similar way, the CaaX motif of GBP1 can be enzymatically isoprenylated to support membrane binding (Vestal and Jeyaratnam, 2011). Like the MD, the GED is dominated by α-helical structures and might play a role in formation of higher-ordered structures, as well as in the stimulation of the GTPase activity (Chappie et al., 2009). In addition, dynamin owns a proline-rich domain (PRD) to recruit clathrin-coated pits (Daumke et al., 2014) and the EHD2s' is reported to bind Asn-Pro-Phe (NPF) motifs for regulating assembly and membrane recruitment (Daumke et al., 2007).

1.4.2 Lipids can influence the GTPase activity of DLPs

All (B)DLPs appear to oligomerize and form higher ordered structures (Daumke and Praefcke, 2016). Furthermore, in case of Drp1, EHD2, NosDLP, Dyn, DynA and Dnm1 electron micrographs show that these (B)DLPs oligomerize and form helical structures around a liposome in the presence of a non-hydrolysable GTP analogue, resulting in formation of tube-like structures (Bürmann et al., 2011; Hinshaw, 2000; Low and Löwe, 2006; Mears et al., 2011; Shah et al., 2014; Ugarte-Uribe et al., 2014).

Dyn oligomerizes in a criss-cross way via the MID domains (Ford et al., 2011). Two dynamin dimers interact and form a tetramer. The dimers interact head to tail, i.e. the GTPase domains of one dimer interact with the PH domains of the adjacent dimer, resulting in autoinhibition. In the presence of lipids, the PH domain favors to interact with the lipids and thus the GTPase domain is released from the PH domain. This unlocks the autoinhibitory structure (Reubold et al., 2015). A similar regulation of the GTPase activity was observed in case of the DLPs MxA and EHD2. (Daumke et al., 2007; Gao et al., 2010). Thus, oligomerization appears to be key feature of DLPs.

The GTP hydrolysis rate of purified (B)DLPs ranges from 0.53 min^{-1} up to 6 min^{-1}. (Bürmann et al., 2011; Bustillo-Zabalbeitia et al., 2014; Gao et al., 2010; Low and Löwe, 2006; Song et al., 2004) Interestingly, in the presence of lipids, the GTP hydrolysis rates of Dyn and Drp1 increase from 2.6 min^{-1} to 105 min^{-1} and 3.2 min^{-1} to 20 min^{-1}, respectively (Bustillo-Zabalbeitia et al., 2014; Song et al., 2004), which is likely caused by disassembly of the autoinhibited tetrameric DLP structure (Reubold et al., 2015). While in case of MxA, lipids appear not to influence GTP hydrolysis, mutants that do not form tetramers also have a severely increased hydrolysis rate (Gao et al., 2010). In a mutant that still forms dimers, whereas formation of higher ordered oligomers is abolished, the GTP hydrolysis rate is not at all affected by lipids (Faelber et al., 2012; Ford et al., 2011; Fröhlich et al., 2013; Gao et al., 2010) Thus, oligomerization and lipid interaction together affect the GTPase activity of many DLPs. In contrast, the thus far analyzed BDLPs (NosDLP, DynA and LeoA) appear to operate completely different, at least on the first view. BDLPs hydrolyses GTP with lower rates when e.g. compared to Dyn, and GTP hydrolysis appears not to be affected at all by lipids (Low and Löwe, 2006). NosDLP homodimerizes in its GDP bound state via the GTPase domain and in the presence of GTP and lipids, self-assembles around liposomes and forms lipid tubes, a feature characteristic for DLPs (Low and Löwe, 2006). DynA from *Bacillus subtilis* is a special case, as it contains two GDs and two MIDs (Figure 6), and thus it is *de facto* a tandem of two fused BDLPs. This tandem also forms dimers, which can structurally be compared to the tetramers formed by other DLPs (as discussed above) (Bürmann et al., 2011). Formation of higher ordered oligomers was not observed for LeoA of *Escherichia coli* yet, and thus this BDLP might be active as a monomer or activated by other, yet to be identified proteins (Michie et al., 2014). Potentially, heterodimerization of different BDLPs is crucial for the proteins' activity, whereas in case of DLPs of eukaryotic origin homooligomerization controls the GTPase activity (Bramkamp, 2012; Michie et al., 2014).

1.4.3 The mechanisms of (B)DLPs membrane remodeling

(B)DLPs are GTPases that remodel membranes. However, (B)DLP family members act differently on/at membranes (reviewed e.g. here (Antonny et al., 2016; Bramkamp, 2012; Daumke and

Praefcke, 2016)), and we here briefly introduce proteins, where the molecular mechanisms are best studied (see also Figure 7).

The prototypical dynamin Dyn (Figure 7 A), the most studied DLP, constricts membranes during formation of clathrin-coated vesicles, and two mechanism are discussed finally leading to membrane fission. (Antonny et al., 2016). Either, dynamins first assemble at the membrane in a transition state corresponding to a dynamin dimer connected by GDP+P_i (Chappie et al., 2011), and this dimer forces the membrane in a second step into a hemi-fission intermediate. The fission process is then completed by the release of P_i (Mattila et al., 2015). Alternatively, Dyn assembles into helical filaments around the membrane mediated by the stalk domain (Reubold et al., 2015). Upon GTP binding, individual Dyns dimerize via their GTPase domains (head-to-head) (Chappie et al., 2010), followed by GTP hydrolysis. The free energy generated by GTP hydrolysis induces a conformational change within the protein structure and induces a mechanical movement of the protein. The proteins slide apart relative to the proteins in opposite direction of the helix turn, and these steps are repeated until a hemi-fission intermediate is reached (Morlot and Roux, 2015). This movement is reminiscent of a myosin movement on actin, with dynamin being both, myosin and actin simultaneous (Antonny et al., 2016). Due to membrane destabilization by the PH domain the membranes fuse triggered by dissociation of dynamins (Shnyrova et al., 2013).

Atlastin (Figure 7 B) is known to fuse adjacent ER membranes mediated by nucleotide-dependent formation of a stretched Atlastin dimer mediated by the G-domains (Orso et al., 2010). The dimer is anchored in two adjacent membranes via the TM regions of each Atlastin monomer (Bian et al., 2011; Byrnes and Sondermann, 2011). Upon GTP-hydrolysis, the previous open conformation of the Alastin dimer closes, bringing the two membranes in spatial proximity, finally resulting in membrane fusion at the anchor points (Liu et al., 2015).

Also, NosDLP (Figure 7 C) is thought to mediate membrane fusion by inducing formation of highly curved membrane regions. After GTP-binding, NosDLP self-oligomerizes around the membrane and forces the membrane into a tube-like structure with high curvature, similar to the prototypical Dyn protein. After GTP hydrolysis, BDLP is released from the lipid and adjacent lipids of the highly curved membrane region spontaneously fuse (Low et al., 2009).

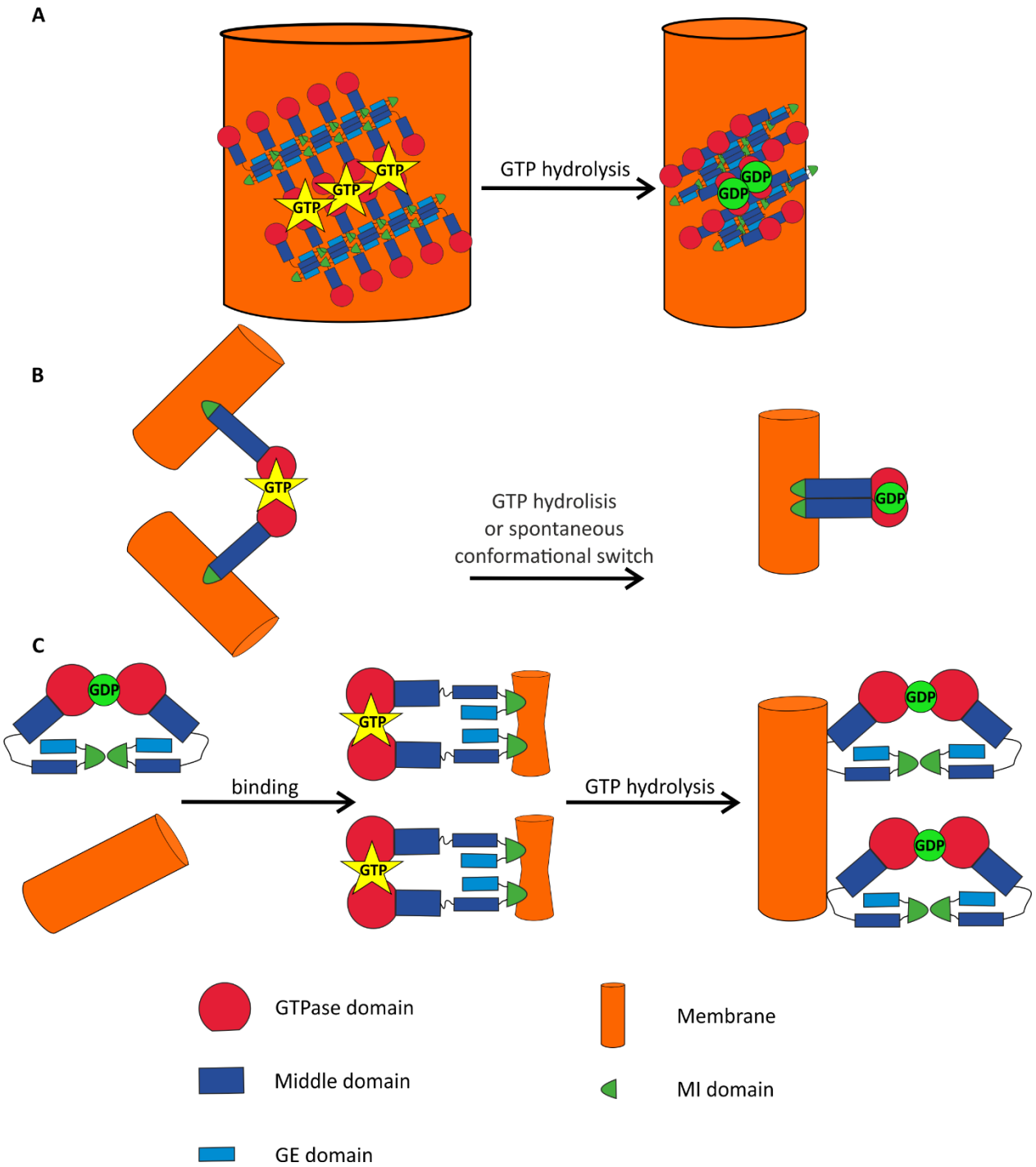

Figure 7: Three selected (B)DLPs and the proposed membrane remodeling mechanism. (A) shows dynamin oligomerization around a membrane, when GTP is bound. GTP hydrolysis results in a conformation collapse and the membrane is constricted. (B) Atlastin fuses membranes by dimerization. GTP hydrolysis is inducing in a MD-MD interaction, which brings to adjacent membranes in close contact. (C) GTP binding mediate a membrane interaction of NosDLP. GTP hydrolysis generates curved membrane regions and the resulting tension fuses membranes. MI: membrane interacting

Likewise, the bacterial DynA was suggested to protect membranes by moving along the membrane surface. When encountering a ruptured membrane region or a membrane pore (e.g.

induced by an antibiotic or phages), DynA accumulates at curved pore regions and interacts with a GTPase domain of another DynA, finally resulting in membrane sealing. This process was suggested to be independent of GTP hydrolysis and the need of GTP hydrolysis remains unclear (Bürmann et al., 2011; Sawant et al., 2016).

Although it seems like BDLPs work different, when compared to eukaryotic DLPs, all (B)DLPs share unique features: (i) large GTPase with a low nucleotide binding affinity, (ii) interaction with and remodeling of biological membranes, (iii) self-assembly into higher arranged oligomers and (iv) a similar domain structure with at least the GD, MD and MID.

2. Objectives of this thesis

The knowledge of (B)DLP in TM biogenesis is very limited. Indeed thus far, only FZL is connected to the TM biogenesis in chloroplasts (Gao et al., 2006). Other DLPs in plants, which are better studied, are involved in division of plant organelles (Aung and Hu, 2012, 2009; Zhang and Hu, 2010). In cyanobacteria, only BDLP (NosDLP) was studied in some extent, whose *in vivo* function is still enigmatic, as of today (Low and Löwe, 2006). Thus, very little is known about BDLPs. Only one could be characterized, and studies of cyanobacterial BDLPs (cBDLPs) involved in TM biogenesis are absent.

Accordingly, this work had the aim to close the lack of knowledge in this area. Therefore, new cBDLPs should be identified and analyzed in order to uncover whether they play a role in the TM biogenesis. Because nothing is known about this topic, several steps were necessary. At the beginning it was aimed to identify potential cBDLPs in the genome of *Synechocystis* and ranking them in the context of potential cBDLPs of other cyanobacterial strains. In the next step, the cBDLPs of *Synechocystis* should be cloned, expressed and purified to study them *in vitro*. Simultaneous, *Synechocystis* mutant strains were intended to generate. Here the influence of the phenotype should be analyzed, while the potential cBDLP are missing. The *in vitro* studies aimed to find out whether the potential cBDLPs share similar properties like the well-known (B)DLPs and consequently to answer the question if the candidates were cBDLPs or not. Therefore, the properties of known (B)DLPs were tested against the cBDLPs. Thus, the GTPase activity should be tested by establishing a proper GTPase assay and the membrane interacting properties should be investigated by using Laurdan fluorescence spectroscopy. Moreover, the nucleotide depending oligomerization and membrane interaction were planned to clarify. In addition, it was aimed to illuminate the conformation change during GTP hydrolysis at lipid monolayers in SFG experiments. In summary, the objectives of this thesis were to identify potential cBDLPs in *Synechocystis*, to purify them, to study their (B)DLPs properties and to connect them to TM biogenesis.

3. Experimental details and methods

3.1 Instruments

Table 2: In this study used instruments in an alphabetical order.

Instrument	Name	Manufacturer
Blotting system	Trans-Blot® Turbo™ Transfer System	BioRad (Hercules, CA, US)
CD spectrometer	J-815 Spectropolarimeter	Jasco (Pfungstadt, GER)
Centrifuge	Allegra X-15R Avanti J-26XP Optima Max XP UC Optima L-100K	Beckman Coulter (Krefeld, GER)
	Centrifuge 5415 R Centrifuge 5424	Eppendorf (Hamburg, GER)
Centrifuge rotors	70 Ti 90 Ti JA-25.50 JLA-8.1000 MLA-130 TLA-100	Beckman Coulter (Krefeld, GER
	F-45-24-11 FA-45-24-11	Eppendorf (Hamburg, GER)
Electron microscope	FEI Tecnai 12	FEI, Thermo Scientific (Darmstadt, GER)
Electrophoresis adapter	peqPOWER300	PeqLab (Erlangen, GER)
	PowerPac Basic	BioRad (Hercules, CA, US)
Electrophoresis chamber	Mini-Protean 3 Cell Min-Protean Tetra Cell	BioRad (Hercules, CA, US)
	PerfectBlue Gelsystem S, M, L	PeqLab (Erlangen, GER)
EMCCD camera	Newton	Andor Technology (Belfast, GB-NIR)
Extruder	Mini-Extruder	Avanti Polar Lipids (Alabaster, AL, US)
Fluorescence spectrometer	FluoroMax-4	Horiba Scientific (Bensheim, GER)
	Series 2	Aminco Bowman
Gel scanner	Quantum-ST4 1100/26M	PeqLab (Erlangen, GER)
	ViewPix 700	Biostep (Burkhardtsdorf, GER)
Heating bath	Thermomix 1420	Braun (Melsungen, GER)

Heating block	HBT-1 Heiz-Block-Thermostat	HLC BioTech (Pforzheim, GER)
Heating plate/magnetic stirrer	MR Hei-Standard	Heidolph (Schwabach, GER)
High shear fluid processor	Microfluidizer LM20	Microfluidics (Newton, MA, US)
Horizontal shaker	Duomax 1030	Heidolph (Schwabach, GER)
Immunoblot documentation system	STELLA	Raytest (Straubenhardt, GER)
Incubator (*E. coli*)	Binder Inkubator Serie BF	Binder (Tuttlingen, GER)
Incubator (*Synechocystis*)	Economic Delux, ECD01E	Snijders Scientific (Tilburg, NL)
Incubation shaker (*E. coli* and *Synechocystis*)	Multitron HT	Infors (Bottmingen, CHE)
Inverse laboratory microscope	Leica DM IL LED	Leica, Wetzlar
Lateral flow cabinet	Biological Safety Cabinet	Microflow (Kaufbeuren, GER)
Microplate reader	FlUOstar Omega	BMG Labtech (Ortenburg, GER)
Overhead shaker	Rollenmischer CMV-ROM	Fröbel (Lindau, GER)
Oxygen sensor	fiber-optic oxygen meter	PreSens (Regensburg, GER)
PAM system	Dual-PAM-100	Walz GmbH (Effeltrich, GER)
pH meter	pH 211 Microprocessor	Hanna Instruments (Vöhringen, GER)
Size exclusion system	ÄKTApurifier 10	GE Healthcare (München, GER)
Sum frequency generation setup	Self-made by the molecular spectroscopy group MPI-P Mainz with the following components	
Regenerative amplifier	Spitfire	Spectra-Physics (Santa Clara, CA, USA)
Paramagnetic amplifier	TOPAS-C	
Pump Laser	Empower	
Oscillator	MaiTai	
Tensiometer	DeltaPi	Kibron (Helsinki, FI)
Thermocycler	Thermocycler Primus 25	PeqLab (Erlangen, GER)

Thermomixer	Thermomixer comfort	Eppendorf (Hamburg, GER)
Ultrasonic cell homogenizer	Branson Sonifier 250	Branson, (Danbury, USA)
UV/Vis spectrometer	Lambda 35 Lambda 465	PerkinElmer (Rodgau, GER)
	NanoDrop	Thermo Scientific (Darmstadt, GER)
Visible spectrometer	Novaspec Plus	Amersham Biosciences (Little Chalfont, UK)
Vacuum coater	Vacuum Coater Auto 306	Edwards (Crawley, UK)
Vacuum pump	High Vacuum Pump	Edwards (Crawley, UK)
Vortex mixer	Vortex Mixer	VWR (Radnor, PA, US)

3.2 Consumables

Table 3: In this study used consumables in an alphabetical order.

Consumables	**Name**	**Manufacturer**
Agarose gel extraction	Gel/PCR DNA Fragments Kit	Geneaid Biotech (Taipei, TW)
Blotting paper	Thick Blot Paper	BioRad (Hercules, CA, US)
Copper grids	CF400-Cu, carbon film on 400 mesh copper grids	Electron Microscopy Sciences (Hatfield, UK)
Centrifugal concentrators	Vivaspin® 6 10,000 MWCO Vivaspin® 6 30,000 MWCO Vivaspin® 20 10,000 MWCO Vivaspin® 20 30,000 MWCO	Sartorius (Göttingen, GER)
DNA Ladder	GeneRuler™ 1kb FastRuler Middle Range	Thermo Scientific (Darmstadt, GER)
Extruder membrane	Polycarbonate membranes	Avanti Polar Lipids (Alabaster, AL, US)
Immunoblot membrane	Roti-PVDF	Roth (Karlsruhe, GER)
Immunostaining chemicals	Amersham ECL Prime Western Blotting Detection Reagent	GE Healthcare (München, GER)
Plasmid preparation Kit	Presto™ Mini Plasmid Kit	Geneaid Biotech (Taipei, TW)
Protein Ladder	PageRuler™ Prestained PageRuler™ Unstained Pierce Unstained MW	Thermo Scientific (Darmstadt, GER)
SEC column	Superdex-200-16/600	GE Healthcare (München, GER)

Further consumables were obtained from Bio-Rad (München), Braun (Melsungen), Roth (Karlsruhe), Sarstedt (Nümbrecht) and VWR (Darmstadt).

3.3 Bacteria strains

E. coli strains used in this thesis are listed in Table 4. Standard cloning procedures were done in XL1-Blue, whereas the other *E. coli* strains were utilized for heterologous protein expression.

Table 4: In this study used bacteria strains.

Escherichia coli	**Genotype**	**Ref.**
XL1-Blue	*recA1 endA1 gyrA96 thi*1 *hsdR17 supE44 relA1 lac* [F′ proAB lacI^{q} ZΔM15Tn10(Tet^{r})]	Stratagene, La Jolla
BL21 (DE3)	F^{-} *ompT hsdS*$_B$($r_B^-m_B^-$) *gal dcm* (DE3)	Novagen, Darmstadt
BL21 (DE3) plysS	F^{-} *ompT hsdS*$_B$($r_B^-m_B^-$) *gal dcm* (DE3) pLysS (Cam^R)	Novagen, Darmstadt
BL21(DE3 plysE)	F^{-} *ompT hsdS*$_B$($r_B^-m_B^-$) *gal dcm* (DE3) pLysE (Cam^R)	Novagen, Darmstadt
HMS174 (DE3) pLysS	F^{-} *rec*A1 *hsd*R(rK12^{-} mK12^{+}) (DE3) pLysS (Cam^R, Rif+R)	(Studier and Moffatt, 1986)
Origami (DE3) pLysS	Δ(*ara–leu)7697 ΔlacX74 ΔphoA PvuII phoR araD139 ahpC galE galK rpsL* F'[*lac^{+} lacI^{q} pro*] (DE3) *gor522*::Tn*10 trxB* pLysS (Cam^R, Kan^R, Str^R, Tet^R)	Novagen, Darmstadt
Rosetta2 (DE3)	F^{-} *ompT hsdS*$_B$(r_B^- m_B^-) *gal dcm* (DE3) pRARE2 *(*Cam^R)	Novagen, Darmstadt
Rosetta2 (DE3) pLysS	F^{-} *ompT hsdS*$_B$(r_B^- m_B^-) *gal dcm* (DE3) pLysSpRARE2 *(*Cam^R)	Novagen, Darmstadt

Rosetta-gami2 (DE3)	Δ(*ara–leu)7697 ΔlacX74 ΔphoA PvuII phoR araD139 ahpC galE galK rpsL* F'[*lac*$^+$ *lacI*^{q} *pro*] (DE3) *gor522*::Tn*10 trxB* pRARE2 (Cam^R, Str^R, Tet^R)	Novagen, Darmstadt
Rosetta-gami2 (DE3) pLysS	Δ(*ara–leu)7697 ΔlacX74 ΔphoA PvuII phoR araD139 ahpC galE galK rpsL* F'[*lac*$^+$ *lacI*^{q} *pro*] (DE3) *gor522*::Tn*10 trxB* pLysSRARE2 (Cam^R, Str^R, Tet^R)	Novagen, Darmstadt
Tuner (DE3)	F$^-$ *ompT hsdS*$_B$(r_B^- m_B^-) *gal dcm lacY1* (DE3)	Novagen, Darmstadt
Tuner (DE3) pLysS	F$^-$ *ompT hsdS*$_B$(r_B^- m_B^-) *gal dcm lacY1* (DE3) pLysS (Cam^R)	Novagen, Darmstadt

***Synechocystis* sp. PCC 6803**	**Genotype**	**Ref.**
Synechocystis sp. PCC 6803	WT	Pasteur Culture Collection of Cyanobacteria
Δ*slr0179*	*Δslr0179*::Kan^R	This thesis
Δ*slr0869*	*Δslr0869*::Kan^R	
Δ*slr1462*	*Δslr1462*::Kan^R	
Δ*sll0503*	*Δsll0503*::Kan^R	
Δ*sll0804*	*Δsll0804*::Kan^R	

3.4 Plasmids

Table 5: In this study used plasmids.

pET303/CT-His plasmids	**Resistance**	**Properties**	**Ref.**
pET303/CT-His	Amp^R	6xHis Taq at the C terminus, containing several mcs	Thermo Fisher Scientific, Darmstadt
pET303-*slr0179*/CT-His	Amp^R	*slr0179* insertion via XbaI and XhoI	This thesis
pET303-*slr0869*/CT-His	Amp^R	*slr0869* insertion via NsiI and XhoI	
pET303-*slr1462*/CT-His	Amp^R	*slr1462* insertion via XbaI and XhoI	This thesis
pET303-*sll0503*/CT-His	Amp^R	*sll0503* insertion via XbaI and XhoI	

pET303-*sll0804*/CT-His	Amp^R	*sll0804* insertion via XbaI and XhoI	

pBluescript II KS+ plasmids

pBluescript II KS+	Amp^R	Containing several mcs	Stratagene, La Jolla
pBluescriptΔ*slr0179*	Amp^R, Kan^R	*slr0179* replaced by a Kan^R cassette between the up and downstream region	Created in this thesis
pBluescriptΔ*slr0869*	Amp^R, Kan^R	*slr0869* replaced by a Kan^R cassette between the up and downstream region	
pBluescriptΔ*slr1462*	Amp^R, Kan^R	*slr1462* replaced by a Kan^R cassette between the up and downstream region	
pBluescriptΔ*sll0503*	Amp^R, Kan^R	*sll0503* replaced by a Kan^R cassette between the up and downstream region	
pBluescriptΔ*sll0804*	Amp^R, Kan^R	*sll0804* replaced by a Kan^R cassette between the up and downstream region	

3.5 Oligonucleotides

Oligonucleotides were purchased from Sigma Aldrich, München.

Table 6: In this study used oligonucleotides.

Name	Sequence (5`-3`)	Remarks
Gen Amplification		
fXbaIslr0179	GGCC TCTAGA ATGAATATTGAAGCTAAGCT	Restriction sites inserted: XbaI/XhoI
rXhoIslr0179	GGCC CTCGAG ACACTTCTGCTTCTGAGCAA	
fNsiIslr0869	GGCC ATGCAT ATGTCCAAGATTGCGCCCCA	Restriction sites inserted: NsiI/XhoI
rXhoIslr0869	GGCC CTCGAG TTCTACTATTTCCACAAAAT	
fXbaIslr1462	GGCC TCTAGA ATGCCCCTGCCCCGTTTACT	Restriction sites inserted: XbaI/XhoI
rXhoIslr1462	GGCC CTCGAG CCAATCATCCTGGCGCTGGG	

fXbaIsll0503	GGCC TCTAGA ATGAATAATAATTCCTTGAC	Restriction sites inserted: XbaI/XhoI
rXhoIsll0503	GGCC CTCGAG AGGAGAGGGGGACACAATTC	
fXbaIsll0804	GGCC TCTAGA ATGAATTCCCCTGCCCCTGA	Restriction sites inserted: XbaI/XhoI
rXhoIsll0804	GGCC CTCGAG CCCTTCGCCGCCTACATCAT	
Amplification of up- and downstream regions		
fPstIslr0179up	CGGG CTGCAG TAAAAGCTTTGTCCTACTCC	Primers matching the up- and downstream of the genes of interest
rBamHIslr0179up	TAGT GGATCC CGTGTACCTGTTCTAACGCC	
fBamHIslr0179down	TAGT GGATCC CATGAGAAATTTAAATCTGA	
rXbaIslr0179down	CCGC TCTAGA CCCTTTATTCTATCATTTTA	
fHindIIIslr0869up	TATC AAGCTT GGGAGTGGCACAAGAAACAA	
rPstIslr0869up	CGGG CTGCAG GCGGAGTGTGGGTTCCTGGC	
fPstIslr0869down	CGGG CTGCAG ATGTTTAAAAGCCATGCAAA	
rBamHIslr0869down	TAGT GGATCC TGCTTGTATGTCAGAAAGGT	
fPstIslr1462up	CGGG CTGCAG TATTTTTAAGAGTACCCAAG	
rBamHIslr1462up	TAGT GGATCC GGACAAACAGGGAATAATGC	
fBamHIslr1462down	TAGT GGATCC TTAGCCATGACGTGAGTCCG	
rXbaIslr1462down	CCGC TCTAGA ACAGGCCAAAGGGGAGGCCT	
fHindIIIsll0503up	TATC AAGCTT GGCAGGGGGATTTTTAATAC	
rBamHIsll0503up	TAGT GGATCC CTCCAGAAAGAATTGTGTCC	
fBamHIsll0503down	TAGT GGATCC CTCCTTGGTTTAAATTTTCT	
rXbaIsll0503down	CCGC TCTAGA CATGAATAATAATTCCTTGA	
fPstIsll0804up	CGGG CTGCAG CTCTCTTTTTCCCCGCGCTG	
rBamHIsll0804up	TAGT GGATCC AGTGGCCGCCTACAGCACCT	
fBamHIsll0804down	TAGT GGATCC ATACCCGTTGCTCCAGTTTG	
rXbaIsll0804down	CCGC TCTAGA TCTGTTGCCTAGCTGAATGA	
Sequencing primers		
slr0869seq1	TATGCGAGGCGGGGA	
slr0869seq2	GAAAATTATGTCAGA	
slr0869seq3	CAAGTTTATCGTTTG	
slr1462seq1	ACAGCGGCTCGGCAA	
slr1462seq2	ATTTCCCTGGGTAAA	
sll0503seq1	AATTGAGGGAAAATA	
sll0804seq1	CCCTAAGGGTTCTCG	
Site-directed mutagenesis		
TG22GC_F	CAAGATTGCGCCCCAAGCTCAGAATCTCCGTGAG	Matching the regions around the codon TGT for displacing TGT o GCT
TG22GC_R	CTCACGGAGATTCTGAGCTTGGGGCGCAATCTTG	
TG22GC_Fb	GATTGCGCCCCAAGCTCAGAATCTCCGTG	
TG22GC_Rb	CACGGAGATTCTGAGCTTGGGGCGCAATC	
TG22GC_Fc	GCCCCAAGCTCAGAATCTCCGTGAGCAAG	

TG22GC_Rc	GATTCTGAGCTTGGGGCGCAATCTTGGAC
TG256GC_F	CACGCCACGGGGACAGAAGCTCATATTGAATATGCTAAC
TG256GC_R	GTTAGCATATTCAATATGAGCTTCTGTCCCCGTGGCGTG
TG421GC_F	GAAGGTGGTTAGTCAATATGCTCAGAAAATAATTGCAGAAG
TG421GC_R	CTTCTGCAATTATTTTCTGAGCATATTGACTAACCACCTTC
TG652GC_F	CTTAAACGATTGGATTATTTTGCTAATCACTCATTATTAAAAG
TG652GC_R	CTTTTAATAATGAGTGATTAGCAAAATAATCCAATCGTTTAAG
TG778GC_F	GATACCTCAGCAGTGATCGCTGTGCTTAAACCAGCGG
TG778GC_R	CCGCTGGTTTAAGCACAGCGATCACTGCTGAGGTATC
TG1132GC_F	GCGAGTTTAATAACTACGCTGCTAATTCTGGTAAG
TG1132GC_R	CTTACCAGAATTAGCAGCGTAGTTATTAAACTCGC
TG1363GC_F	GATTTGCAACCGTTAGCTATTGCTCTACGGC
TG1363GC_R	GCCGTAGAGCAATAGCTAACGGTTGCAAATC
TG1807GC_F	CGCCTACGAAAAGTGGATGCTTACCATCAAGTTTATC
TG1807GC_R	GATAAACTTGATGGTAAGCATCCACTTTTCGTAGGCG

3.6 Antibodies

Table 7: Antibodies used in this study.

Name	Properties	Epitope	Source	Dilution
Primary antibody				
α-BDLP2	Polyclonal (rabbit)	BDLP2ΔG-Domain	Davids Biotechnologie, Regensburg	1:2000
Secondary antibody				
α-rabbit HRP	Polyclonal (goat)	Rabbit	Sigma-Aldrich, München	1:10000
Antibody conjugate				
His•Tag® Antibody HRP Conjugate	Monoclonal	His-Tag	Novagen, Darmstadt	1:2000

3.7 Chemicals, solutions, enzymes

Chemicals were purchased from Merck (Darmstadt), Roth (Karlsruhe), Sigma Aldrich (München), AppliChem (Darmstadt), Acros Organics (Geel, BEL), Alfa Aesar (Haverhill, MA, US), Fisher Scientific (Hampton, NH, US) and Avanti Polar Lipids (Alabaster, ALA, US) and have P.A. quality, at least. All buffer and solutions were prepared with deionized water. Buffers, which were

used for cyanobacteria studies were prepared using ultrapure water. Enzymes were purchased from New England Bio Labs (Frankfurt).

Buffers used for several applications are listed in Table 8 and Table 9.

Table 8: Buffers used for activity measurements and protein storage.

Component	GTPase Reaction buffer (RB)	Storage buffer (SB)
HEPES	20 mM	20 mM
NaCl	150 mM	-
$MgCl_2$	5 mM	-
KCl	7.5 mM	-
pH	7.4	7.4

Table 9: Buffers used for protein purification.

Component	Lysis buffer	Wash buffer	Elution buffer
NaH_2PO_4	50 mM	50 mM	50 mM
NaCl	150 mM	150 mM	150 mM
Imidazole	10 mM	20-95 mM	500 mM
Glycerol	10 % (v/v)	10 % (v/v	10 % (v/v
pH	8	8	8

3.8 Media

E. coli strains were grown in LB media (Miller J H, 1972) and *Synechocystis* strains were grown in BG-11 media (Rippka et al., 1979). The exact compositions are listed below.

Table 10: Media used for bacteria growth.

LB medium	
Trypton	10 g/l
Yeast extract	5 g/l
NaCl	10 g/l
pH	7.0 ± 0.2

BG-11 medium

Trace minerals		**BG-FBC**	
H_3BO_3	2.5 g/l	$NaNO_3$	149.58 g/l
$MnCl_2x4H_2O$	1.8 g/l	Citric acid	0.66 g/l
$Na_2MoO_4x2H_2O$	0.22 g/l	$CaCl_2x2H_2O$	3.6 g/l
$Co(NO_3)_2x6H_2O$	0.40 g/l	$MgSO_4x7H_2O$	7.49 g/l
$CuSO_4x5H_2O$	0.08 g/l	NaEDTA	0.3 mM g/l

5 ml	1M HEPES-KOH pH 8.2
10 ml	BG-FPC
1 ml	Trace minerals
1 ml	6 mg/ml Ammonium ferric citrate in ultrapure water
1 ml	190 mM Na_2CO3 in ultrapure water
1 ml	175 mM K_2HPO_4 in ultrapure water

Ad. 1 liter with ultrapure water

LB media was prepared with diluting of a ten-fold concentrated and autoclaved media stock. BG-11 media was sterilized directly after preparation. Sterile glucose was added to final concentration of 5 mM, when needed. The BG-11 agar plates contained 1.5 % Difco Bacto Agar and 3 g/l Sodium thiosulfate, in addition. When needed, kanamycin was added. For phosphate free BG-11 media K_3PO_4 was replaced by 175 mM KCl to keep the amount of K^+.

3.8.1 Media additives

LB media was supplemented with ampicillin (sterile filtrated), IPTG (sterile filtrated and to induce protein expression) and agar for LB agar plates. BG-11 media was supplemented with Kanamycin (sterile filtrated), glucose (sterilized, to reach mixotrophic growth conditions) and bacto agar as well as sodium thiosulfate for BG-11 agar plates. The media additives are listed in Table 11.

Table 11: Media additives used during this study.

Name	**Stock solution**	**Final concentration**	**Solvent**
Ampicillin	100 mg/ml	100 µg/ml	50% EtoH / 50% H_2O ultrapure
Kanamycin	50 mg/ml	10-100 µg/ml	H_2O ultrapure
Glucose	1 M	5 mM	H_2O ultrapure
IPTG	1 M	1 mM	H_2O ultrapure
Agar	Powder	1.5 g/l	LB media
Difco Bacto Agar	Powder	1.5 g/l	BG11 media
Sodium thiosulfate	Powder	3 g/l	BG11 media

3.9 Methods

3.9.1 Molecular biology

3.9.1.1 Bacteria cell culture

E. coli cells were cultivated either at 37 °C in liquid LB in a shaking incubator (Multitron Infors) at 220 rpm or on LB agar plates at 37°C in an incubator. *Synechocystis* strains were grown photo-mixotrophic in liquid BG-11 media (supplemented with 180 µg/ml kanamycin, when needed) in a shaking incubator at 130 rpm (Multitron Infors) or on BG-11 agar plates. The temperature was set to 30°C and the cells were illuminated with 30 µE of cold-white light. In case of phenotypic characterization, WT and mutant strains were grown phototrophic only with CO_2 (2 %) enriched air in glass bottles with a gas inlet in a water basin (30°C). Note that no kanamycin was used to ensure the absence of any side effects. The light intensity was varied from 20 µE (normal light: NL) to approx. 1000 µE (high light: HL). After reaching the exponential growth phase (OD_{750} = 0.6-1.5), the cells were harvested and adjusted to a chlorophyll concentration of approximately 3.5 µg/ml. The optical density (OD) of the cells was measured routinely with a diode array visible spectrophotometer (GE Healthcare) at 600 nm (*E. coli*) and 750 nm (*Synechocystis*). The cell concentration (cells/ml) was estimated by a thoma cell counting chamber. The chamber was filled with 10 µl cell suspension and the counted number of five big squares were averaged. The cell concentration is given by equation (1). $\overline{N}$ is the average of the counted cells, d the dilution factor, A the area and h the chamber height.

$$\frac{cells}{ml} = \frac{\overline{N} \cdot d}{A[mm^2] \cdot h[mm]} \quad (1)$$

3.9.1.2 DNA isolation

Plasmid DNA of *E. coli* was isolated using the High-Speed Plasmid Mini-Kit (Genaid, Taiwan) by following the manual. The genomic DNA (gDNA) of the *Synechocystis* strains was extracted manually. The cells were harvested (5200 g, 15 min, 4°C) at an OD > 2 and washed four times with TES buffer (5 mM Tris, 50 mM NaCl, 5 mM EDTA, pH 8.5). The cell pellet was resuspended in 450 µl TES buffer and incubated 30 min at 37°C in presence of 50 µl lysozyme (20 mg/ml; end

concentration of 2 mg/ml). Afterwards the cells were treated with 50 µl sodium lauryl sarcosinate (10 %) and 600 µl Roti®-Phenol. The suspension was incubated at RT for 15 min on an orbital shaker. The phases were separated by centrifugation (16,100 g, 5 min at 4 °C) and the upper aqueous phase was treated with 5 µl of 10 µg/ml RNAse (15 min at 37 °C). After addition of 100 µl 5 M NaCl, 80 µl CTAP (10 % solution in 0.7 M aqueous NaCl) and 600 µl of a 24:1 mixture of chloroform and isoamyl alcohol, the solution was incubated for 15 min on an orbital shaker. The phases were again separated by centrifugation (16,100 g, 5 min at 4 °C) and the DNA in the upper phase was precipitated with 600 µl isopropanol. The gDNA was obtained by centrifugation (16,100 g, 5 min at 4 °C), washed with 70 % EtOH, dried over night at RT and resuspended in 50 µl TE buffer (10 mM Tris, 0.1 mM EDTA, pH 7.5). The DNA concentration and purity were determined by measuring the OD_{260}, OD_{230} and OD_{280}.

3.9.1.3 Polymerase chain reaction (PCR)

To amplify DNA for analytical or preparative reasons, the polymerase chain reaction (PCR) was used. Analytical PCR was done with the Taq polymerase in a 25 µl sample volume, whereas preparative PCR and site-directed mutagenesis (SDM) was done with Phusion polymerase (NEB) in 50 µl sample volumes. The PCR cycle programs are summarized in Table 12.

Table 12: PCR cycling to amplify DNA, with number of cycles, melting temperature and time.

	Phusion PCR			**SDM PCR**			**Taq PCR**		
	T (°C)	t (sec)	cyc.	T (°C)	t (sec)	cyc.	T (°C)	t (sec)	cyc.
1.	98	120		98	60		95	30	
2.	98	20		98	30		95	20	
3.	72	30	30x	72	60	20x	51	30	25x
4.	72	150		72	240		68	90	
5.	72	600		72	300		68	300	

3.9.1.4 Agarose gel electrophoreses

Analytical and preparative separation of DNA were done using agarose gel electrophoreses. 1 % (w/v) agarose was dissolved in TAE buffer (400 mM Tris, 10 mM EDTA, 200 mM acetic acid) with microwave irradiation. Usually, six wells were generated for preparative and 12 wells for analytical electrophoresis. The wells were filled with 6 to 50 µl sample containing a loading dye

(x6). The DNA, including a DNA marker, was separated at constant voltage (135 V). The DNA was marked with 1 µg/ml ethidium bromide in water for 30 min and visualized with UV light. Finally, the gel was photographed (Transilluminator, peQLab Biotechnologie GmBH). In case of preparative gel electrophoreses, the gel parts containing the DNA fragments were sliced out of the gel on a UV table and recovered utilizing the Gel/PCR DNA Fragments Kit (Geneaid, Taiwan).

3.9.1.5 DNA digestion

To digest DNA fragments and DNA plasmids, different restriction enzymes (NEB) were utilized. The buffers were chosen following the manufactures instructions. The incubation time was 2 h at 37°C.

3.9.1.6 DNA ligation

The ligation of DNA fragments was catalyzed by T4 ligase (NEB). Success of the ligation was controlled by DNA digestion and sequencing (Eurofins Genomics).

3.9.1.7 Transformation of plasmids into Synechocystis and E. coli

All *E. coli* strains were made chemical competent using the method of Chung et al. (Chung et al., 1989). The transformation of plasmid into *E. coli* could be realized by a short heat shock treatment. 50 µl of cells were thawed on ice. 3 µl of plasmid (approx. 200 ng) was added and the cells were incubated on ice for 30 min. Afterwards, cells were incubated at 41 °C for 90 s. The cells were stored on ice for 2 min and LB was added to a total volume of 800 µl. The cell suspension was incubated at 37 °C for 1 h. The cells were collected and resuspended in approx. 50 µl of LB. Cells containing the plasmids, were selected on LB agar plates containing the appropriate antibiotics. The bacteria grew overnight at 37 °C.

Since the cyanobacterium *Synechocystis* sp. PCC 6803 is naturally competent, it can take up DNA efficiently without any special treatment. For transformation, a fresh photomixotrophically grown culture (OD_{750} = 1) was harvested (4,400 g, 15 min, RT) and resuspended in fresh BG-11 to an OD_{750} of 2.5. 400 µl of the cell suspension was transferred into a new sterile glass culture tube including 5 µl plasmid and 5 mM glucose. Cells were incubated over night at 30 °C and 30 µE. On the next day, the cell suspension was plated on BG-11 agarose plates including 5 mM glucose and

10 µg/ml kanamycin (Kan). After approx. 2 weeks a few colonies appeared. Each single colony was picked with a sterile toothpick and spread onto a new BG-11 agarose plate with a Kan concentration of 20 µg/ml. The concentration of Kan was increased in several steps up to 200 µg/ml by spreading the colonies of new BG-11 agar plates.

3.9.2 Biochemical methods

3.9.2.1 Heterologous protein expression

After transformation of expression plasmid into an *E. coli* expression strain, one clone was picked and suspended in 50 µl ultrapure water. The suspension was spread again onto a LB agar plate containing Amp and incubated over night at 37 °C. The bacteria were scratched from a plate with a curved and flamed glass Pasteur pipette and used to inoculate 2 liters of LB media containing Amp. Alternatively, one clone was used to inoculate 50 ml LB (Amp) and grew over night at 30 °C. The cell suspension was used to inoculate 2 liters of LB media (Amp). The bacteria were grown at 37 °C until $OD_{600} \approx 0.8$ was reached. Afterwards, protein expression was induced by adding 1 mM IPTG and expressed over night at 20-25 °C. The cells were harvested the next day by centrifugation (4,500 g, 15 min, 4 °C). The resulting pellets were snap frozen in liquid nitrogen and stored at -20 °C prior protein purification.

3.9.2.2 Protein purification

3.9.2.2.1 Cell fractionation

The *E. coli* cell pellet was suspended in lysis buffer (50 mM NaH_2PO_4, 300 mM NaCl, 10 mM imidazole, 10 % glycerol, pH 8) in a ratio of 1:25 cell culture volume. The lysis buffer included protease inhibitor (Sigma protease inhibitor cocktail, 1:1000). Cells were broken by using a microfluidizer (4 times at 18,000 PSI), including ultrasonic pretreatment (amplitude 50 V, pulse time 0.5 s, 5 min) on ice. Afterwards, the cell lysate was centrifuged (15 min, 18,000 g, 4°C). The resulting supernatant without cell debris and unbroken cells was convicted immediately onto a Ni-NTA matrix. Alternatively, the supernatant was centrifuged again to obtain membranes in the pellet (1 h, 100,000 g, 4°C).

3.9.2.2.2 Solubilization of membrane bound proteins

Membrane attached or integrated proteins were solubilized with the detergents 5 mM N,N-Dimethyldodecylamine N-oxide (DDAO) or n-Dodecyl-beta-Maltoside (DDM). Therefore, the membrane pellet was resuspended in lysis buffer with the detergents. The samples were incubated either 2 h at 37 °C or 4 °C overnight under constant inverting. Finally, the solutions were centrifuged to obtain membranes in the pellet (1 h, 100,000 g, 4°C).

3.9.2.2.3 Protein purification via Ni-NTA

His-Tag proteins were purified in a semi-batch process using a Ni-NTA matrix (centrifugation at 500 g, 5 min, 4°C). The Ni-NTA resin (usually V_{Bed} = 1.5 ml/l cell culture) was washed two times with ultrapure water ($V = V_{Bed} \times 10$) and equilibrated two times with lysis buffer ($V = V_{Bed} \times 10$). The supernatant of the cell fractionation, without cell debris and unbroken cells, was incubated with the Ni-NTA matrix for 2 h at 4°C. The matrix bound protein was recovered by centrifugation and was washed with five different wash buffers. Beside 50 mM NaH_2PO_4, 300 mM NaCl and 10 % glycerol (pH 8), the wash buffers contained an increasing concentration of imidazole (20 mM, 50 mM, 75 mM, 85 mM and 95 mM; $V = V_{Bed} \times 10$). With the last washing step, the resin was convicted into a 5-ml polypropylene column and the column was drained by gravity. The protein was eluted by using the elution buffer (50 mM NaH_2PO_4, 300 mM NaCl, 500 mM imidazole, 10 % glycerol, pH 8) in four elution steps ($V_{E1-3} = V_{Bed}$ and $V_{E4} = 0.5 \times V_{Bed}$). Protein purification was verified by sodium dodecyl sulfate polyacrylamide gel electrophoreses (SDS-PAGE) analysis (3.9.2.3).

3.9.2.2.4 Protein concentration

All proteins were concentrated using centrifugal concentrators (Sartorius) at 3,500 x g and 4°C.

3.9.2.2.5 Desalting of proteins

To change the buffer condition PD-10 columns (GE Healthcare) were used. The column was equilibrated with 25 ml of SB (20 Mm HEPES-KOH, pH 7.4). Afterwards, 2.5 ml of the protein solution was added and eluted with 3.5 ml SB.

3.9.2.3 SDS-PAGE

SDS-PAGE was utilized to separate proteins according to their mass. The separating gels were prepared with an acrylamide concentration of 8 to 14 %, the upper stacking gel with an acrylamide concentration of 6 %. The exact compositions of the SDS gels are shown in Table 13.

Table 13: SDS-PAGE separation and stacking gel composition.

Substance	**Separating gel**				**Stacking gel**
	8.0 %	10.0 %	12.0 %	14.0 %	6.0 %
H_2O	5.5 ml	5.0 ml	4.5 ml	4.0 ml	6.0 ml
Acrylamide	2.0 ml	2.5 ml	3.0 ml	3.5 ml	1.5 ml
Separating buffer (1.5 M Tris, 0.4 % (w/v) SDS, pH 8.8)	2.5 ml	2.5 ml	2.5 ml	2.5 ml	
Stacking buffer (0.5 M Tris, 0.4 % (w/v) SDS, pH 6.8)					2.5 ml
10 % (w/v) APS	50.0 µl	50.0 µl	50.0 µl	50.0 µl	50.0 µl
TEMED	20.0 µl	20.0 µl	20.0 µl	20.0 µl	20.0 µl

Under reducing conditions protein samples were treated with 5x loading buffer (0.25 M Tris, 0.5 M DTT, 50 % (v/v) glycerol, 10 % (w/v) SDS, 0.2 % bromophenol blue) and heated to 95 °C for 5 min. In cases of non-reducing conditions, no DTT was added. The proteins were separated in SDS-PAGE running buffer (25 mM Tris, 192 mM glycine, 0.1 % (w/v) SDS) at 150 to 200 V and afterwards stained with Coomassie-Brilliant Blue (CBB) or blotted (3.9.2.3.1 and 3.9.2.3.2).

3.9.2.3.1 Coomassie Brilliant Blue staining

After electrophoretic protein separation, the gels were stained and simultaneously fixed with staining solution containing Coomassie Brilliant Blue R-250 (45 % EtOH, 10 % phosphoric acid, 0.1 % (w/v) Coomassie Brilliant Blue R-250). The gels were destained with a destaining solution (45 % EtOH, 10 % phosphoric acid).

3.9.2.3.2 Western blotting

Alternative to protein staining after SDS-PAGE, the proteins were transferred onto a PVDF membrane in a Western blot (WB). Therefore, a semi dry system was used (Trans-Blot® Turbo ™, BioRad). Western blot filter papers were preequilibrated in transfer buffer (25 mM Tris, 192 mM

glycine, 20 % EtOH, ph 7.6) and a sandwich was built containing the filter papers at both sides, the blotting membrane (PVDF, activated with MeOH, preequilibrated in transfer buffer) and the SDS-PAGE gel. Proteins were transferred at a constant voltage of 25 V for 30 min. After the transfer, the PVDF membrane was blocked for 1 h at RT or overnight at 4 °C under constant moving in 5 % milk powder solved in TBST (20 mM Tris, 150 mM NaCl, 0.05 % (v/v) TWEEN 20). Afterwards, the membrane was washed three times for 10 min with TBST on an orbital shaker and incubated in primary antibody solution for 1 h at RT or overnight at 4 °C. In the next step, the membrane was washed again (3x TBST, 10 min) and incubated with the secondary antibody (1 h and RT). Finally, the membrane was washed again three times for 10 min with TBST. In case of using the anti His-Tag HRP conjugate, no second antibody was needed. The blot was developed by chemiluminescence using the Amersham GE ECL reagent following the manufactures instructions. The blot was transferred on a transparent film, covered with 200 µL of reagent A and B and closed with another transparent film. After 4 min incubation time, the liquid was squeezed out and the chemiluminescence was recorded with the imaging system STELLA 3200 from raytest and documented with AIDA imaging software.

3.9.2.4 Preparation of small unilamellar liposomes

Unilamellar liposomes were prepared by the method of Hope et al. (Hope et al., 1986). The required amount of lipid (stored in $HCCl_3$/MeOH (1:3)) was transferred into a microtube and the organic solvent was evaporated in a N_2 stream. Remaining solvents were removed by incubation in a vacuum desiccator overnight. The lipid film was rehydrated in 20 mM HEPES-KOH pH 7.4 buffer to a final concentration of 0.5 mM, resulting in formation of multilamellar liposomes. After five cycles of freeze and thaw (liquid N_2, 37 °C), the unilamellar liposomes were sized by extrusion when needed. For extrusion, membranes with a pore size of 200 nm and a mini extruder (Avanti Polar Lipids, Alabama) were used.

3.9.2.5 Sedimentation assay

Especially in the presence of nucleotides, the oligomeric state of proteins can be studied by sedimentating the protein. Therefore, 200 µl GTPase RB (3.9.3.1) with 0.34 µM protein, unilamellar DOPG liposomes (0.25 µM and sized to 200 nm) and 2 mM nucleotides were prepared

as described before. The mixture was incubated for 30 min at RT. 150 µl sample was centrifuged for 30 min, 60,000 g at 4 °C in a mini ultracentrifuge. Subsequently, 50 µL supernatant was separated, the rest was discarded. The pellet (mostly invisible) was resuspended in 150 µL GTPase RB containing 4 % (w/v) SDS. The samples were analyzed by SDS-PAGE stained with CBB and quantified using the software ImageJ.

3.9.3 (Bio)physical methods

3.9.3.1 GTPase assay

The activity of the purified GTPases was checked by a continuous, regenerative, coupled GTPase assay in which the GTP hydrolysis can be observed online. At constant GTP concentration, the turnover of NADH is detected. The composition of the samples is shown in Table 14.

Table 14: Sample compositions used in the GTPase assay.

RB			**RM**		
	V (µl)	c_{end} (mM)		V (µl)	c_{end} (mM)
$MgCl_2$ (1 M)	0.8	5	RB	127	-
NaCl (5 M)	4.5	150	PEP	2.5	1
KCl (1 M)	1.1	7.5			
20 mM HEPES pH 7.4	120.8	-	**GTP**		
			GTP (100 mM)	0 - 7.5	0 - 25
			RB	ad. 30	-
MM			**Sample**		
RM	130	-	MM	112.5	-
PK/LDH	2.6	-	GTP (0 – 25 mM)	30	0 - 5
NADH (20 mM)	4.5	0.6	Protein (5 µM)	7.5	0.25 µM

First, the reaction buffer (also called GTPase reaction buffer (RB)), which can be stored at -20 °C to 4 °C, was prepared. Immediately before use, the phosphoenolpyruvic acid (PEP) was added on ice. In the meantime, guanosine-5`-triphosphate (GTP) solutions were prepared on ice. In order to avoid self-hydrolysis of GTP, 100 mM GTP were dissolved in in 50 mM HEPES-KOH and the pH was made alkaline with NaOH. This solution can be stored over month at -20 °C, even after multiple freeze and thaw cycles. The final concentration of GTP was determined by measuring the

absorption at 253 nm (ε = 13700 $M^{-1}cm^{-1}$). The master mix (MM) was made by adding the enzyme mix containing pyruvate kinase, lactate dehydrogenase (PK/LDH) and nicotinamide adenine dinucleotide (NADH) to the RB. The NADH stock solution was prepared as the GTP stock solution. The MM solution was dispensed into the GTP solution and incubated at RT for 15 min. In this time, the PK/LDH catalyze the reaction from GDP to GTP and it can be assumed that self-hydrolyzed GDP, which was present in the GTP powder, is eliminated. Finally, the GTPase was added and the turnover of GTP was observed indirectly via the decline of NADH absorption at 340 nm in a timeframe of 1 to 2 h by a microplate reader (FLUOstar Omega, BMG Labtech). Usually, 12 GTP concentrations were simultaneously measured in 96er well plates. For every GTP concentration, a negative control or blank was measured. Here the GTPase was replaced by SB.

The decreasing absorption at 340 nm was plotted over time and the slope ΔA/min in the linear area was obtained by linear regression. The slope ΔA/min is direct proportional to the GTPase turnover rate and can be calculated with the lambert-beer law:

$$v_{GTP} = \frac{\frac{-\Delta A_{340}}{min}}{d \cdot \epsilon} \tag{2}$$

d refers to the filling height of the sample in the 96er well plate (0.38 cm) and ε is the molar extinction coefficient of NADH (6220 $M^{-1}cm^{-1}$) (Ingerman and Nunnari, 2005). The protein activity is then given by:

$$activity\ [min^{-1}] = \frac{v_{GTP}[\frac{M}{min}] \cdot MW_{Prot}[\frac{g}{mol}]}{c_{Prot}[\frac{g}{l}]} \tag{3}$$

By this procedure, a turnover rate for each GTP concentration was obtained. The resulting activities at the given GTP concentration were fitted by the Michalis-Menten (4) or the Hill equation (5) .

$$activity = \frac{activity_{max} \cdot c_{GTP}}{K_M + c_{GTP}} \quad (4)$$

$$activity = \frac{(c_{GTP})^n}{K_M + (c_{GTP})^n} \quad (5)$$

3.9.3.2 Laurdan fluorescence spectroscopy

Laurdan (1-[6-(dimethylamino)naphthalen-2-yl]dodecan-1-one), a fluorescence dye, is able to intercalate in lipid bilayers (e.g. biological membranes) due to its hydrophilic head group (benzene) and hydrophobic tail (aliphatic carbon chain).

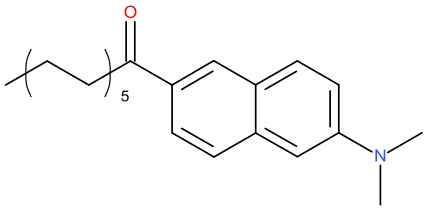

Figure 8: Structure of the Laurdan fluorescence dye.

Laurdan can be excited at 350 nm. Depending on the environment, the emission maxima shifts between 440 nm and 490 nm. When the membrane is in the gel phase (rigid membrane, less water molecules) the emission maximum is centered at 440 nm. When membrane is in the liquid phase (more water molecules), the emission maximum is shifted to 490 nm. In a polar environment, the polar solvent molecules rearrange at the Laurdan dipole, after excitation. The needed energy is taken from the excited dipole, resulting in a decreased excitation state (Sanchez et al., 2007). Thus, Laurdan fluorescence spectroscopy is used to monitor membrane phase transitions.

For the experiment, 0.5 mM unilammellar liposomes (3.9.2.4) were diluted in buffer to a final lipid concentration (c_{end}) of 0.1 mM in a volume of 200 µl. The protein concentration was variable and the proteins were incubated with die lipids for at least 30 min at RT. The samples were analyzed using a fluorescence spectrometer (Horiba, Fluoro-Max-4). λ_{ex} was set to 350 nm and the emission

spectrum was observed between 400 and 550 nm. The slit width varied depending on the signal intensity. However, the spectra were all recorded at 25 °C and automatically corrected. The background was recorded without lipid and fluorescence dye and was subtracted. To quantify the change in the peak ratio (440 nm vs. 490 nm), the so called generalized polarization (GP) value was calculated (6) (Sanchez et al., 2007).

$$GP = \frac{I_{440\ nm} - I_{490\ nm}}{I_{440\ nm} + I_{490\ nm}} \quad (6)$$

Here, I is the peak intensity at 440 nm and 490 nm, respectively. Usually, the difference or the relative amount in the GP values in presence and in absence of protein was determined.

$$\Delta GP = GP_{(+)Prot} - GP_{(-)Prot} \quad (7)$$

$$GP_{rel} = GP_{(+)Prot}/GP_{(-)Prot} \quad (8)$$

3.9.3.3 Characterization of Synechocystis cultures

At the beginning, the OD_{750} was measured and the chlorophyll content was determined. For the subsequent experiments, the chlorophyll a concentration was adjusted to 3.5 µg/ml. Aliquots were used for 77 K fluorescence spectroscopy (77 K cuvettes, lq. N_2 and stored at -80 °C), P700 re-reduction kinetics, induction curves, oxygen evolution measurements (all three in the dark, for oxygen evolution at 30 °C in addition) and for cell counting.

3.9.3.3.1 Determination of chlorophyll concentration

The chlorophyll a concentration was determined using an empiric equation (9) (Porra et al., 1989).

$$c_{Chla}[\mu\frac{g}{ml}] = 16.26 \cdot A_{665.2} - 8.54 \cdot A_{652} \quad (9)$$

The absorptions (A) at 665.2 nm and 652 nm were measured in MeOH. Therefore 1 ml cell culture was collected (1,000 g, 5 min, RT) and resuspended in 1 ml MeOH. The chlorophyll was extracted for 5 min on an orbital shaker at RT and the sample was centrifuged again (15,900 g, 5 min, RT).

The $A_{665.2}$ and A_{652} were measured using a photometer (Perkin Elmer, Lamda 435). The chlorophyll concentration of each strain was determined five times.

3.9.3.3.2 Absorption spectroscopy

Absorption spectra of *Synechocystis* cells were measured with an UV/Vis photometer (Perkin Elmer, Lamda 35 UV/VIS). The photometer was equipped an integrated sphere. All spectra were recorded between 360-800 nm. The samples were adjusted to an equal number of cells and the resulting spectra are normalized at 800 nm.

3.9.3.3.3 Determination of oxygen evolution

Oxygen evolution of *Synechocystis* WT and mutant strains was measured in a batch reactor. 1 ml dark-adapted cells containing 10 mM $NaHCO_3$ or 20 mM phenyl-p-benzoquinone (PPBQ) were placed in the reactor and the temperature was adjusted to 30 °C. The oxygen evolution was observed with an oxygen-dipping-probe (PreSens, Regensburg). The instrument was calibrated with oxygen saturated water (100 %) and oxygen free water (0 %). Oxygen-free water was obtained by adding sodium thiosulfate. Oxygen evolution was recorded in the dark for 2 min, following strong light exposure (2000 K) for another 2 min. The resulting slopes under dark (1-2 min; m_d) and light condition (3-4 min; m_L) were used to calculate oxygen evolution in µmol per ml and h, normalized to the chlorophyll concentration (c_{Chla}):

$$oxygen\ evolution\ \left(\frac{\mu mol\ O_2}{c_{Chla}\cdot ml\cdot h}\right)=\frac{(m_L-m_d)\cdot 60\frac{min}{l}}{c_{Chla}\cdot 1000\frac{mL}{l}} \qquad (10)$$

3.9.3.3.4 77 K fluorescence spectroscopy

Synechocystis cultures grown in glass bottles with gas intel were adjusted to a similar chlorophyll concentration and transferred to special glass cuvettes. Immediately afterwards, the cuvettes were frozen in lq. N_2. Fluorescence emission was measured at 77 K after the excitation of chlorophyll (435 nm) or phycobilisomes (580 nm) using a Aminco Bowman Series 2 fluorescence spectrometer, incl. 77 K accessory. The emission spectra were recorded 3 times between 630 and 760 nm and averaged.

3.9.3.3.5 Pulse-amplitude modulation (PAM) fluorescence spectroscopy

Synechocystis cultures grown in glass bottles with gas intel were adjusted to a similar chlorophyll concentration. All PAM measurements were performed using dark-adapted cells in the Dual-PAM-100 system from Walz GmbH, Effeltrich.

3.9.3.3.5.1 Induction fluorescence measurements

In order to gain information about the photosynthetic activity of PSII, dark-light induction curves were recorded. Therefore, a program and parameters predefined in the DualPAM software were used. Briefly, the measurement started by turning on the measurement light. The background fluorescence (F_0) and the maximal fluorescence (F_m) were determined by a strong saturation pulse (600 ms, 10,000 µmol photons $m^{-2}s^{-1}$). 40 s later photosynthesis was activated with actinic light and saturation light pulses were applied every 20 s to determine the maximal fluorescence in the light (F_m'). The background fluorescence (F_0') could not be measured directly, because the actin light interferes with F_0'. Thus, F_0', was calculated by the software using the variable fluorescence (F_v) and the equations (11) and (12) (Oxborough and Baker, 1997; Waltz, 2006). The effective photosynthetic activity (F_v'/F_m') of PSII is given by equation (13), and the maximal photosynthetic activity (F_v/F_m) of PSII is given by equation (14).

$$F_v = F_m - F_0 \tag{11}$$

$$F_0' = \frac{F_0}{\frac{F_v}{F_m} + \frac{F_0}{F_m'}} \tag{12}$$

$$\frac{F_v'}{F_m'} = \frac{F_m' - F_0'}{F_m'} \tag{13}$$

$$\frac{F_v}{F_m} = \frac{(F_m - F_0)}{F_m} \tag{14}$$

3.9.3.3.5.2 P700 re-reduction kinetics

To determine the re-reduction of the PSI reaction-center (P700) the entirely oxidized P700 was used. The complete oxidization of the P700 was reached by a saturating light pulse (200 ms, 10,000 µmol photons $m^{-2}s^{-1}$). Then the P700* was re-reduced by electrons provided by the electron transport chain between PSII and PSI. The measurement was repeated 15 times and the results were averaged. The resulting P700 re-reduction curve was fitted with a first order exponential function to access the half-time.

3.9.4 SFG spectroscopy

3.9.4.1 Theory

In this thesis sum frequency generation spectroscopy (SFG) was used to obtain valid and interfacial selective information about the orientation and conformation of proteins at lipid membranes. In the following, the theory of sum frequency generation spectroscopy (SFG) is hereafter described. For a more detailed description see Lambert et al. (Lambert et al., 2005).

An intrinsic property of light is the possibility to interact with matter by inducing an electric dipole moment ($\vec{\mu}$).

$$\vec{\mu} = \alpha\vec{E} \tag{15}$$

Here α is the molecular polarizability of the electrons and $\vec{E}$ is the electric field. (P) is given by the sum over all molecules.

$$\vec{P} = \varepsilon_0\chi^{(1)}\vec{E} \tag{16}$$

$\chi^{(1)}$ refers to the average of α and is called linear susceptibility. ε_0 is the permittivity of vacuum. At low electric field ($\vec{E}$) strength, the emitted light has the frequency of incident light and non-linear effects can be neglected (e.g. Rayleigh scattering). At strong electrical fields, e.g. as induced

by a pulse laser, this assumption is no longer allowed and equation (16) needs to be extended in terms of nonlinearity. Then polarization (P) is described by:

$$\vec{P} = \varepsilon_0(\chi^{(1)}\vec{E} + \chi^{(2)}\vec{E}^2 + \chi^{(3)}\vec{E}^3 \dots \chi^{(i)}\vec{E}^i) \quad (17)$$

Here $\chi^{(i)}$ is the susceptibility of i^{th} order and all i>1 are non-linear.

In the SFG setup two laser beams (infrared and visible) are used. Thus, SFG is one of the second order nonlinear optical processes. Here, the light with the frequency given by the sum of the infrared (ω_{IR}) and visible light (ω_{VIS}) of incidence overlap and result in a new SFG beam (ω_{SFG}). For SFG only the sum of both frequency of incidents are used:

$$\omega_{IR} + \omega_{VIS} = \omega_{SFG} \quad (18)$$

Consequently, the polarization (17) in case of SFG can be simplified to:

$$\vec{P}^{(2)} = \varepsilon_0\chi^{(2)}\vec{E}_{IR}\vec{E}_{VIS} \quad (19)$$

$\chi^{(2)}$ is a third rank tensor in Cartesian space, and has 27 components (3^3 different combinations) and therefore equation (19) can be expressed in individual components of Cartesian (x,y,z):

$$\vec{P}^{(2)}_{SFG} = \sum_i^{x,y,z} \vec{P}^{(2)}_{i,SFG} = \varepsilon_0 \sum_i^{x,y,z} \sum_j^{x,y,z} \sum_k^{x,y,z} \chi^{(2)}_{ijk}\, \vec{E}_{j,VIS}\vec{E}_{k,IR} \quad (20)$$

In an isotropic medium like a bulk phase, $\chi^{(2)}_{ijk}$ is symmetric, and thus all terms cancel out and $\vec{P}^{(2)}_{SFG} = 0$. $\vec{P}^{(2)}_{SFG} \neq 0$ is only the case when the material has a broken symmetry (e.g. at interfaces), but not an inversion symmetry (e.g. bulk phases). Consequently, SFG is in particular useful to investigate proteins at interfaces, because IR signals are only obtained from proteins at the interface.

Beams of incidence and the resulting SFG beam are created at the surface in an angle and can be reflected and transmitted through the interface. The reflecting angle (Θ_{SFG}) is given by the conservation of momentum (21):

$$n_{SFG}k_{SFG}\sin(\theta_{SFG}) = n_{VIS}k_{VIS}\sin(\theta_{VIS}) \pm n_{IR}k_{IR}\sin(\theta_{IR}) \quad (21)$$

Here n is the refractive index, k is the wavenumber and Θ is the angle respecting the surface.

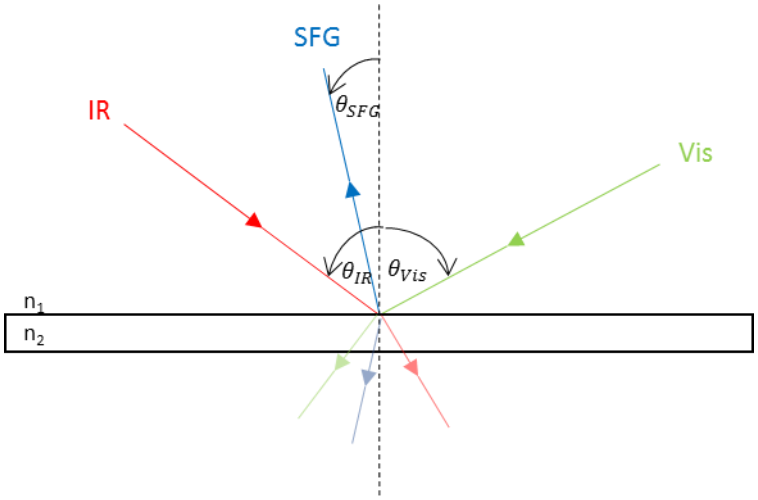

Figure 9: Schematic illustration of incoming infrared (IR) and visible (Vis) laser beams hitting an interface. The laser beams overlap at the interface between two materials with different refractive indices (n_1 and n_2), resulting in a new laser beam (SFG). All angles are referring to the z direction.

The resulting intensity of the SFG signal is proportional to the polarizability and thereby proportional to $\chi^{(2)}$ (22). A more detailed view can be found elsewhere (Lambert et al., 2005; Shen, 2012).

$$I_{SFG} \propto \left|P_{SFG}^{(2)}\right|^2 \propto \left|\chi_{SFG}^{(2)}\right|^2 I_{IR}I_{VIS} \quad (22)$$

The key factor $\chi^{(2)}$ in all directions ($\chi_{ijk}^{(2)}$) can be simplified by having a geometrical view on this problem. In a centrosymmetric environment (e.g. in a bulk phase) the average of the dipoles in every direction is equal (23).

$$\chi_{ijk}^{(2)} = \chi_{ijk}^{(2)} = -\chi_{ijk}^{(2)} = 0 \quad (23)$$

Consequently, no SFG signal should be observed. On the other side, symmetries are broken at interfaces. The dipoles are orientated in z-direction, but the surface plane is isotropic (x,y). This is described by a C_∞ rotation axis. Thus, the directions are not equivalent (x ≡ -x, y ≡ -y, z ≠ -z). In the end, only four independent compounds contribute to the SFG signal (for details please the reference (Lambert et al., 2005)). Furthermore, $\chi^{(2)}$ depends on the polarization of the laser beams and the emitted light, which are given by corresponding indices (ssp and psp).

In order to analyze the obtained spectral data, $\chi^{(2)}$ can be split into a resonant part ($\chi_R^{(2)}$) and a non-resonant part ($\chi_{NR}^{(2)}$).

$$\chi^{(2)} = \chi_R^{(2)} + \chi_{NR}^{(2)} \tag{24}$$

The tensor $\chi_R^{(2)}$ is frequency dependent and can be divided in a real part and an imaginary part:

$$\frac{\omega_q - \omega_{IR}}{(\omega_q - \omega_{IR})^2 + \Gamma^2} + i\frac{\Gamma}{(\omega_q - \omega_{IR})^2 + \Gamma^2} \tag{25}$$

ω_q is the resonant frequency, ω_{IR} is the frequency of the tunable incoming infrared beam and Γ^{-1} is the relaxation time. More simplifications and $\chi_R^{(2)}$ can be expressed as a general susceptibility:

$$\chi_R^{(2)} = \frac{A}{(\omega_q - \omega_{IR} - i\Gamma)} \tag{26}$$

A is the vibrational mode strength and is composed of the susceptibilities and hyperpolarizability part. For the fitting model, the Lorentzian spectral model was applied and thus, in terms of the Lorentzian curve, (26) is converted to:

$$\chi_R^{(2)} = \frac{\sqrt{H}W}{(\omega_q - \omega_{IR} - iW)} \tag{27}$$

A is replaced by the peak height (H) and Γ by the half peak width at half maximal height (W).

Altogether, the SFG intensity depending on the IR frequency is given by:

$$I_{SFG} = \left| \chi_{NR}^{(2)} + \sum_{q} \frac{\sqrt{H}W}{(\omega_q - \omega_{IR} - iW)} \right|^2 I_{IR} I_{VIS} \quad (28)$$

3.9.4.2 SFG setup

To generate a SFG signal two laser beams are necessary. One tunable IR laser and one constant VIS laser overlap at the sample, mix up and result in the SFG laser beam, which contains the interface selective IR information and orientation. All SFG experiments were performed at the same setup, which is descripted in detail by Smits et al. (Smits et al., 2007). A schematic illustration of the SFG setup is given in Figure 10 A. In summary, the laser beam was generated by a Ti:sapphire oscillator (Mai Tai, Spectra-Physic, Santa Clara), pumped by a Nd:YLF laser (Empower, Spectra-Physics, Santa Clara) and amplified by a femtosecond regenerative amplifier (Spitfire Ace, Spectra-Physics, Santa Clara), resulting in a 5 mJ laser pulse at 791.8 nm and a duration of 40 fs. The laser beam was guided through a beam splitter. One part of the laser beam passed through a Fabry-Perot Etalon to generate a band pulse of about 15 cm^{-1}. Thereafter, the beam reached two mirrors, which were moveable to change the delay. Then the beam passed the polarizer (P_{VIS}), a λ/2 plate and was focused on the sample, as the non-tunable visible laser. The other part of the original beam was guided through an optical parametric amplifier system (TOPAS, LightConversion, Santa Clara). During this process, the laser beam was transformed to a tunable infrared (IR) laser and went to another polarizer (P_{IR}) and a λ/2 plate. The IR beam and the VIS beam were focused on the sample by two lenses (1/2 L and ¾ L). At the sample, both beams overlap and the resulting SFG beam was guided through a third polarizer (P_{SFG}) and was focused on an electron multiplying (EMCCD) camera (Newton, Andor). A sample housing surrounds the sample itself and the last way of the beams. Thus, the area can be purged by N_2 and is protected from interfering light sources.

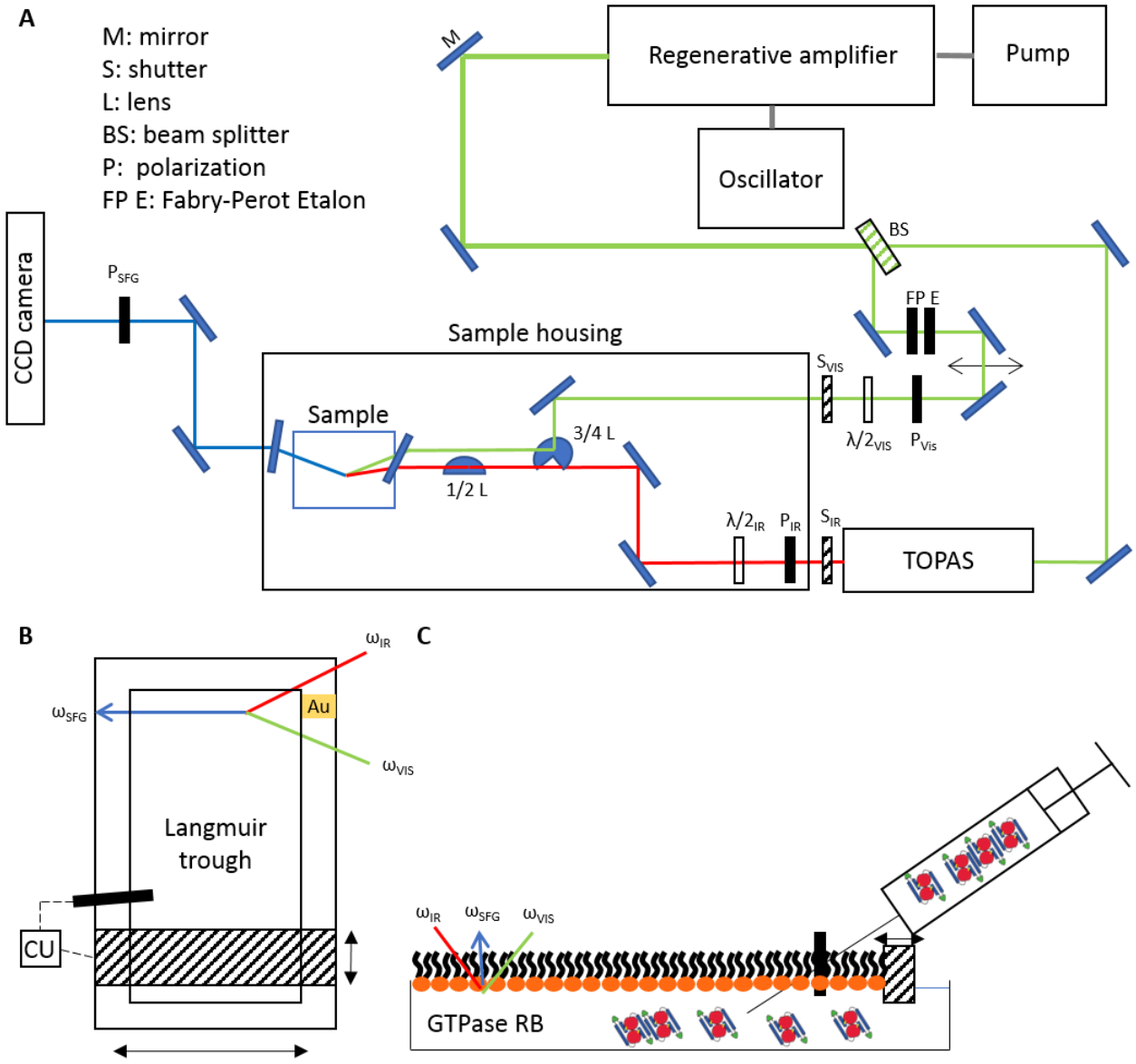

Figure 10: Schematic view of the broad-bandwidth SFG setup including the Langmuir trough. (A) The beam from the amplifier is split (BS). One part is guided through the TOPAs to generate a tunable IR laser. The other part is directed to a delay stage over a Faybry-Perot Etalon (FP E). Both beams are focused on the sample and the resulting SFG signal is collected by a CCD camera. The sample is placed in a laterally movable Langmuir trough with a tensiometer (black bar) coupled with a moveable barrier (striped bar). In addition, the trough can be moved to a gold plate to record gold reference spectra (B). The protein is injected via a syringe in the sub phase under the lipid monolayer (C). CU: control united.

The sample was placed on a Langmuir trough (Figure 10 B). The trough was complemented by a tensiometer, which was coupled over a control unit (CU) with a barrier. That system allows to monitor and manipulate the surface pressure (Π) during an experiment (Kibron, DeltaPi). In addition, the trough was modified to be laterally movable as descripted in Franz et al. to avoid laser induced temperature effects at lipid monolayers, since it ensured a continuous movement

of the laser at the lipid layer (Franz et al., 2017). Furthermore, an automatic syringe pump was refilling the trough with ultrapure water to compensate the loss of water during evaporation processes.

All SFG measurements were typically performed using ssp (P_{SFG}, P_{VIS}, P_{IR}) polarization combination. After setting up the trough and all other components, the trough was moved into the reference position (gold surface, Figure 10 B). There, the laser beams were aligned to overlap at the gold surface and the SFG signal was optimized to gain a strong SFG signal in the desired wavenumber region. The reference spectra were recorded for 60 s. For the background reference spectra, the exact same settings were used, but with IR shutter (S_{IR}) closed to block the IR beam. In the next step, the trough, the barrier, the ceramic plate, the needle (tensiometer) and the barrier were cleaned by washing them three times with ultrapure water, three times with EtOH and dried in a N_2 flow. Before use, the tensiometer needle was additionally flamed. The trough was filled with approx. 33 mL of GTPase RB, so that the buffer/air interface was at the same height as the gold reference. The needle was moved into the buffer and was calibrated to Π = 0 mN/m. Under monitoring Π the lipid was added dropwise to the buffer and spread spontaneously to a lipid monolayer (ML). Then, the pressure was constantly set to 15 mN/m and the barrier moved to decrease the ML area until the predefined Π is reached. Now, the sampling house was purged with N_2 for at least 15 min and the spectra of the ML were recorded with variable exposure times under constant moving of the trough. The protein and the GTP solution were injected in the subphase by a syringe to a final concentration of 0.05 mg/mL protein and 2 mM GTP (Figure 10 C). The energy scale in the amide I area (approx. 1600 cm^{-1} to 1800 cm^{-1}) were calibrated to the carbonyl peak at 1737 cm^{-1}.

4. Results

4.1 BDLPs in cyanobacteria

The overall knowledge of BDLPs encoded in prokaryotes and especial in cyanobacteria is limited to BDLP/NosDLP. Consequently, it was necessary to collect more information about BDLPs in cyanobacteria (cBDLPs). Therefore, a database was used, which is specialized on cyanobacteria. Run the Cyanobase (http://www.kazusa.or.jp./cyanobase/, version 2017), 121 genes in 56 different cyanobacterial strains were identified to encode cBDLPs (Fujisawa et al., 2017). A global alignment (Matrix Blossum62) showed, that all of these cBDLPs contain the highly conserved GTPase domain. As described in the introduction (1.4.1), the GTPase domain or GD harbors the nucleotide binding motif. Interestingly, the alignment revealed that all cBDLPs show an extended P-loop amino acid sequence in cyanobacteria. Beside the GxxxxGKS/T motif, the sequence is extended in cBDLPs with L/INALL/I to GxxxxGKS/TxL/INALL/I (Jilly et al., 2018). Based on the alignment, a phylogenetic tree (Neighbor-Joining method) was created (Figure 11). Within the phylogenetic tree, 5 clades are identified. The first group is termed KGK group. In the KGK clade, KGK domain proteins are encoded downstream of the cBDLP. The second group is called Tandem A. In this group, another cBDLP is encoded downstream of the Tandem A cBDLP. Consequently, the third group is called Tandem B group and is the counterpart of the Tandem A group. Noteworthy, the only yet characterized cBDLP, NosDLP, is part of this group (Low and Löwe, 2006). Beside the Tandem clades and the KGK clade, the chaperone clade and the HSR1 clade were identified. Similar to the previous clades, there are also chaperons and HSR1 proteins encoded downstream of the cBDLP (Jilly et al., 2018). A list of all identified proteins can be found in the appendix (7.7).

Especial for this study it is necessary to have a look at potential dynamin-like proteins in *Synechocystis*. In the above analysis, one potential cBDLP (AOY38_06420) was identified encoded in *Synechocystis*, which is part of the KGK clade (SynCys6302) (Fujisawa et al., 2017). This protein is also named Slr0869 and SynDLP in this thesis, while the search for dynamin-like proteins in the year 2014 resulted in six more cBDLPs (Nakamura et al., 2000).

Figure 11: Phylogenentic tree of 121 cBDLPs encoded in 56 cyanobacteria species (including NosDLP). The phylogenetic tree (model: jukes-cantor, neighbor-joining) was created based on a full-length multiprotein sequence alignment (Geneious global alignment, Matrix Blosum62). The cyanobacterial sequences were obtained from "cyanobase" (Fujisawa et al., 2017). The name of the potential dynamins is abbreviated. For full information about the strain, the gene name and the gene locus see the appendix (7.7). The cBDLPs can be classified into six different clades, depending on their sequence and genomic environment: The KGK clade (red), the HSR1 clade (orange) and the chaperone clade (brown). Upstream of the Tandem A (pink) clade another cBDLP (Tandem B, light blue) is typically encoded. cBDLPs (green) could not be further classified and thus represent a group of diverse cBDLPs. It is worth mentioning that boundaries between the cBDLPs clade and the Tandem B or HSR1 clades, respectively, are not sharp and it might be that proteins share characteristics of both clades. Furthermore, while Xen7305 3 does not show significant sequence similarity to Tandem B members, downstream of the gene the Tandem A protein Xen7305 4 is encoded. The figure is adapted from Jilly et al. (Jilly et al., 2018).

4.2 Finding, cloning, expressing and purifying potential BDLPs in Synechocystis

At the very beginning of this project, seven putative DLPs, which were predicted to be GTPases homologues to Dynamin, FZO or ADL1D had been identified in the genome of *Synechocystis*, using the database (http://www.kazusa.or.jp./cyanobase/, version 2014) (Nakamura et al., 2000). Characteristics of putative BDLPs are summarized in Table 15.

Table 15: Potential BDLPs found in the genome of *Synechocystis*.

Gene name	**Protein name**	**Gene size (bp)**	**Protein size (kDa)**	**Predicted homologue** (Nakamura et al., 2000)	**Sequencing results**
slr0179	Slr0179	1074	40.41	dynamin	Ok
slr0869	SynDLP	2439	92.54	dynamin	T780C
slr1462	Slr1462	1656	62.67	FZO	Ok
ssr0755	-	228	8.56	FZO	-
sll0503	Sll0503	1425	51.16	FZO	Ok
sll0804	Sll0804	1362	49.16	FZO	Ok
sll1225	-	450	17.30	ADL1D	-

The sizes of the potential SynDLPs range from 8 kDa up to 93 kDa. To reduce the number of potential candidates, only large GTPase in the definition of the introduction were considered and thus, the genes *ssr0755* and *sll1225* were excluded. The remaining five candidates were characterized by their domain structure and potential transmembrane regions. Furthermore, they were compared to selected and well investigated DLPs, namely dynamin, FZL and NosDLP (Figure 12 A). The GTPase domain (GD) was defined as the region beginning with the G1 motif and ending with the G4 motif, in case of the potential BDLPs. The domains structure of dynamin, FZL and NosDLP were obtained from the references (Gao et al., 2006; The UniProt Consortium, 2017). As seen in Figure 12, the GTPase part at the N-termini of the proteins is conserved through the proteins, whereas other regions or domains were not predicted. Instead, Slr1462 and Sll0804 have predicted transmembrane regions (TMHMM) (Krogh et al., 2001), like FZL. Nearly all putative *Synechocystis* DLPs share the cyanobacterial extended G1 motif, except Slr0179 and Slr1462 (Figure 12 B). Isoleucine/leucine is replaced by valine in both proteins, but valine is also a neutral nonpolar amino acid.

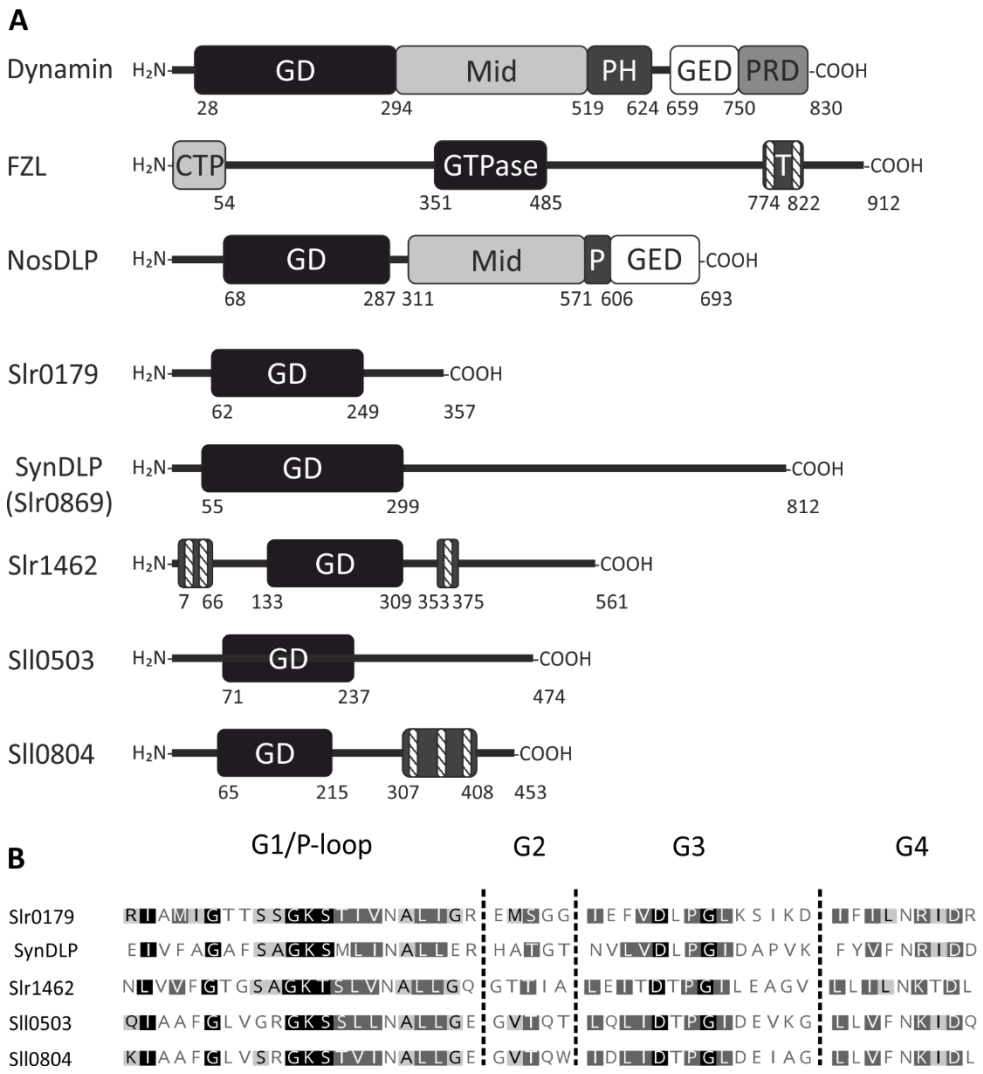

Figure 12: Potential *Synechocystis* DLPs in comparison to the known DLPs dynamin, FZL and NosDLP and the amino acid sequence of the GTPase motofs. The GTPase domain (GD) is typically highly conserved in proteins at the N-termini (GTPase), except in FZL. FZL has an additional chloroplast transit peptide (CTP) and thus the GTPase domain is localized in the middle of the protein. Other domains were not predicted, although in case of Slr1462 and Sll0804 transmembrane regions were found (striped bars) (A). All potential BDLPs in *Synechocystis* show the conserved and extended G motif, except Slr0179 and Slr1462, where valine replaces the isoleucine/leucine (B). Mid: middle domain; PH: pleckstrin homology; GED: GTPase effector domain; PRD: proline rich domain; P: paddle; T: transmembrane region.

The genes of the remaining five candidates were amplified from genomic DNA of *Synechocystis* (PCR). Thereby, two restriction sites (RS) for the restriction endonucleases (RE) per fragment were added (XhoI and XbaI or XhoI and NsiI) (Figure 13 B). The genes were cloned into the pET303-CT/His vector, which allows control of gene expression by the *lac* operon (Figure 13 A). The vector/gene fragments with the corresponding REs were restriction digested and the gene fragments were ligated into the vector. Via cloning, a His-Tag (6xHis) was added at the C-terminus of the expressed proteins. *E. coli* XL1blue cells containing the plasmid were then selected due to

the antibiotic resistance (ampicillin) encoded in the plasmid. To check whether the right plasmids were up taken by the *E. coli* cells, the plasmids were isolated and controlled via control restriction enzyme digestion and sequenced. As shown in Figure 13 C (dig), the restriction digest of the plasmids with the corresponding REs (Figure 13 B) resulted in two bands. One band at around 5000 bp, which corresponds to the vector and one band at the sizes of the different genes.

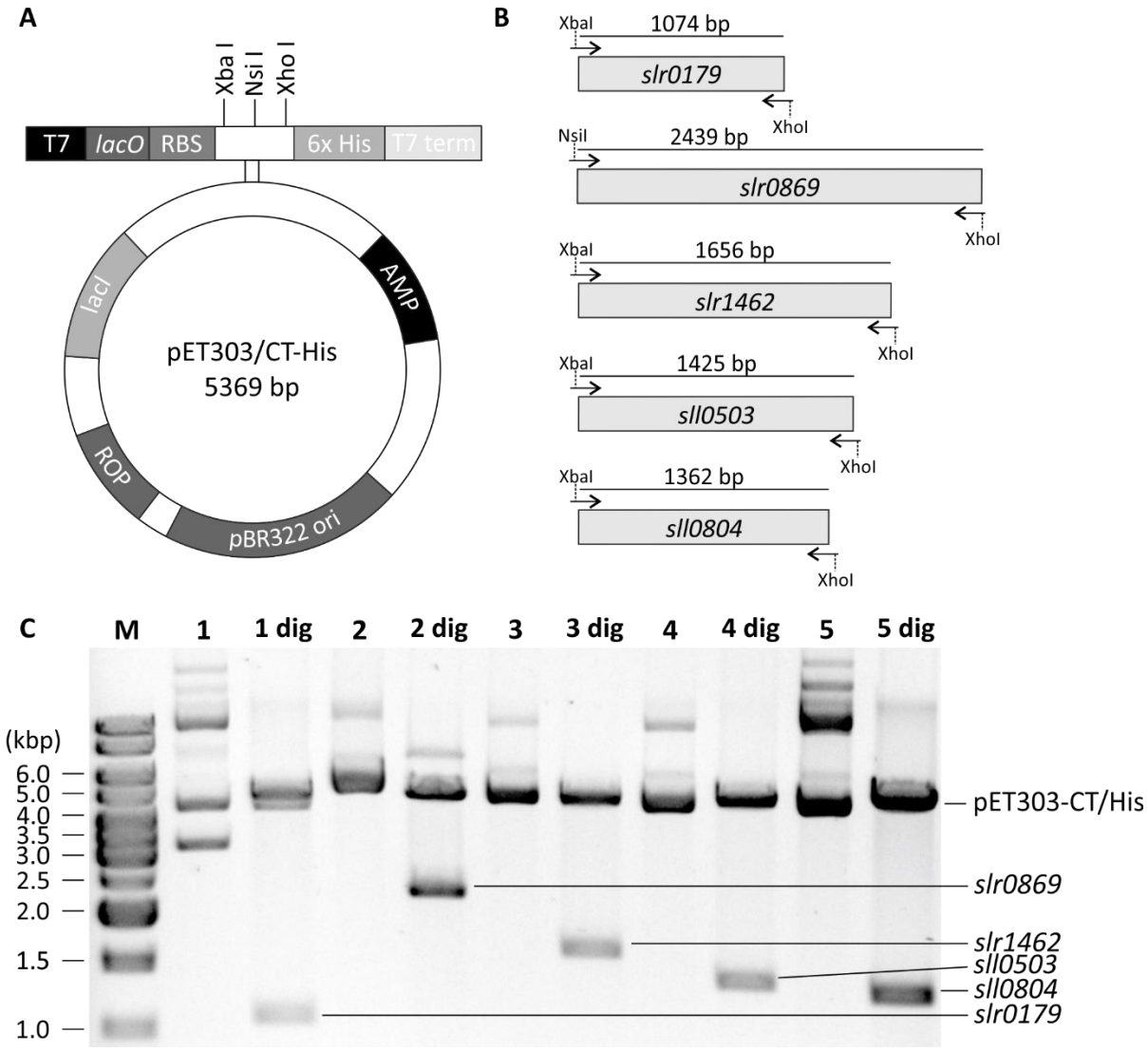

Figure 13: The vector map of pET303/CT-His and the gene fragments, which were cloned into the vector. Vector map of pET303/CT-His (A) including, the T7 binding site, the *lac* operon (*lac*O) and the multiple cloning sites (5369 bp). The genes were amplified via PCR. Restriction sites for the enzymes XhoI were inserted in all genes. Restriction sites for XbaI were inserted in all genes except *slr0869*, where the RS for XbaI was replaced by the RS for NsiI (B). (C) Agarose gel showing the plasmids (1: pET303-*slr0179/*CT-His, 2: pET303-*slr0869/*CT-His, 3: pET303-*slr1462/*CT-His, 4: pET303-*sll0503/*CT-His, 5: pET303-*sll0804/*CT-His) before and after restriction digestion (dig). l*ac*O: *lac* operon; RBS: ribosome binding side; AMP: ampicillin; M: Marker.

The sequencing results confirmed successful cloning of the genes *slr0179*, *slr1462*, *sll0503* and *sll0804*. In case of pET303-*slr0869*-CT/His, the sequencing result showed a difference to the sequence provided by Nakamura *et al.* (2000). In the gene *slr0869* at position 781 the base thymine is replaced by a cytosine (T780C), but in the base triplet context (TGT to TGC) both encode for a cysteine residue. Thus, it was decided to work with that clone.

Thus, five potential genes, which encodes for potential DLPs in *Synechocystis,* were identified and cloned into the expression vector pET303-CT/His for heterologous expression of the proteins. The five candidates were expressed in *E. coli*. optimizing expression conditions followed a similar procedure and thus the detailed procedure is exemplary described only for Slr0179 in the following.

4.2.1 Expression

The plasmid pET303-*slr0179*-CT/His was transformed in several different *E. coli* expression strains (Figure 14 C) and protein expression was induced with 1 mM Isopropyl-β-D-thiogalactopyranosid (IPTG) at an OD_{600} of 0.8-1. After induction, the protein was expressed for 4 h at 37 °C. The cells were broken (microfluidizer) and several centrifugation steps at increasing speed allowed to fractionate the lysate in low speed (containing all unbroken cells and aggregates), cytoplasm (containing soluble proteins) and membrane (containing membrane bound and/or associated proteins) fractions. The presence of the protein was analyzed by SDS-PAGE with CBB staining and WB using an antibody directed the His-Tag. The results are shown in Figure 14.

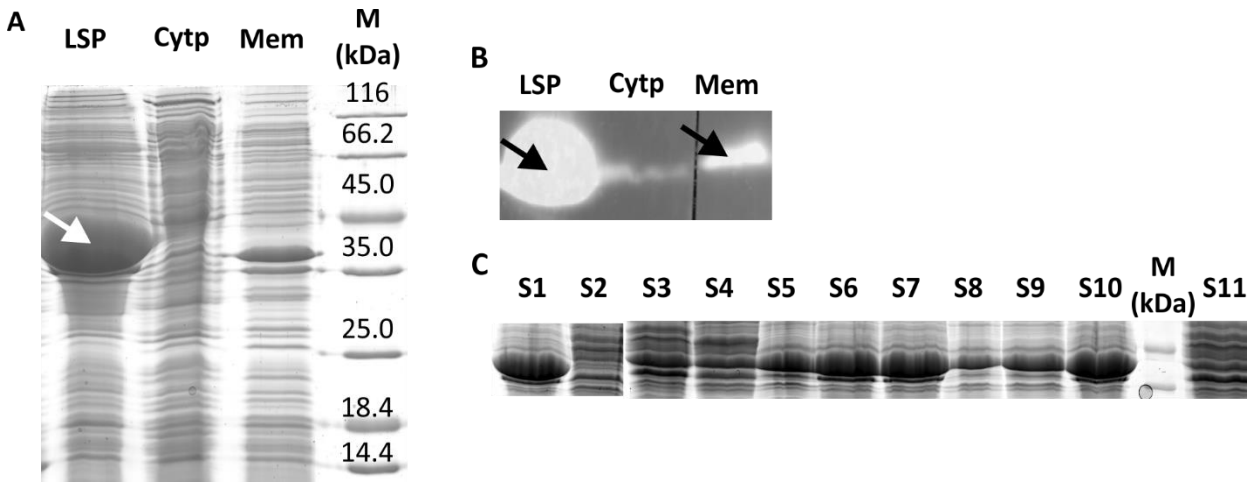

Figure 14: Analyzation of *E. coli* cell fractions and identification of the most powerful expression strain of Slr0179 via CBB staining and WB. (A) SDS PAGE gel stained with CBB showing samples after fractionation into the low-speed pellet (LSP), cytoplasm (Cytp) and membrane (Mem) fractions. Slr0179 is marked with a white arrow. In addition, the presence of Slr0179 (black arrow) was confirmed by WB analysis using a α-His-Tag HRP conjugate (B). SDS-PAGE gel stained with CBB, showing the expression level of Slr0179 in different *E. coli* strains (C). S1: Bl21(DE3); S2: Bl21(De3)pLysE; S3: Bl21(De3)pLysS; S4: HMS174(DE3)pLysS; S5: Orgami(DE3)pLysS; S6: Rosetta2(DE3); S7: Rosetta2(DE3)pLysS; S8: Rosetta-gami2(DE3); S9: Rosetta-gami2(DE3)pLysS; S10: Tuner(DE3); S11: Tuner(DE3)pLysS, M: marker

When expression in BL21(DE3) for 4 h at 37 °C, Slr0179 was nearly exclusively found in the low speed pellet (LSP) fraction, indicating that the protein was expressed mainly in inclusion bodies. To obtain soluble protein, 11 different *E. coli* expression strains were tested at different temperatures, IPTG concentrations and varied expression times. As seen in Figure 14 C, the most powerful expression level was reached with the strains Bl21(DE3) and Tuner(DE3), but again no protein was detected in the cytoplasm. Instead, some Slr0179 was detected in the membrane fraction (Mem), indicating that Slr0179 is a membrane associated protein. Heterologous expression was optimized for all remaining proteins in a similar way. The corresponding parameters are summarized in Table 16.

Table 16: Conditions used for expression of the five potential *Synechocystis* BDLPs.

Name	Expression strain	Temperature (°C) / time	C_{IPTG} (mM)
Slr0179	BL21(DE3)	37 / 4 h	1
SynDLP	Rosetta-gami2(DE3)pLysS	20 / O/N	1
Slr1462	Rosetta2(DE3)	37 / 3 h	0.5
Sll0503	Rosetta-gami2(DE3)pLysS	37 / 4 h	1
Sll0804	Rosetta2(DE3)pLysS	37 / 4 h	0.5

In the end, all five potential BDLPs of *Synechocystis* could be expressed heterologously in *E. coli*. Western blot (WB) analyzes using α-His-Tag HRP conjugate detected the five proteins (Figure 15). Samples taken before the induction do not show any signal, whereas after the induction, signals at the corresponding sizes become visible, indicating successful expression of the proteins.

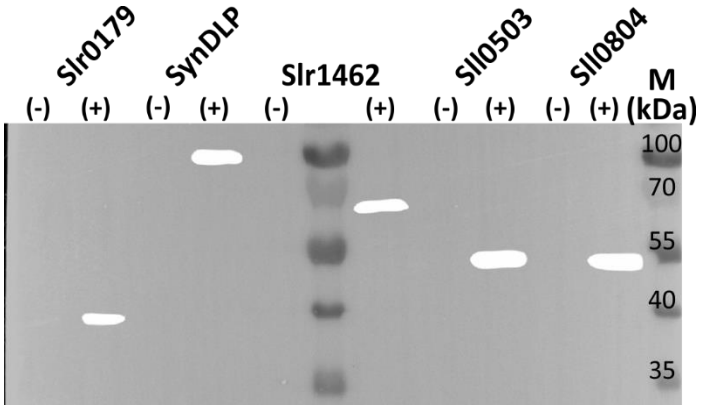

Figure 15: WB analysis of the expression of the five different hypothetical *Synechocystis* DLPs. Samples were taken before induction (-) with IPTG and after the expression for 4 h (+). The samples were adjusted to the same OD_{600}, separated on an SDS-PAGE gel, blotted and the proteins were detected by α-His-Tag HRP conjugates. Signals were obtained at the expected protein size: Slr0179 (~40 kDa), SynDLP (~100 kDa), Slr1462 (~65 kDa), Sll0503 (~50 kDa) and Sll0804 (~50 kDa), as are marked by the white signals. M: marker

4.2.2 Solubilization

The proteins Slr1462 and Sll0804 harbor a predicted transmembrane domain. Consequently, it was obvious to find them exclusively in the membrane fraction. A transmembrane domain in Slr0179 is not predicated, thus the presence of Slr0179 partially in the membrane fraction, indicating membrane interaction of this protein. For *in vitro* studies, the proteins have to solubilized with detergents. To find the most suitable detergent, six different detergents were tested. As an example, the solubilization is shown for Slr1462 in Figure 16, as a representative of all three proteins. Beside using SDS (positive control) and the strong detergent Triton, solubilization was also effective working for the more gently detergent DDAO. Thus, the downstream purification steps were performed using buffer with 5 mM DDAO. It was also tried to solubilize Slr0179 in detergents, but the amount of extracted protein was always too low for subsequent analyses steps. Solubilization conditions of Sll0804 were tested by Vladislava Schulz, resulting in DDM as the most powerful detergent for Sll0804.

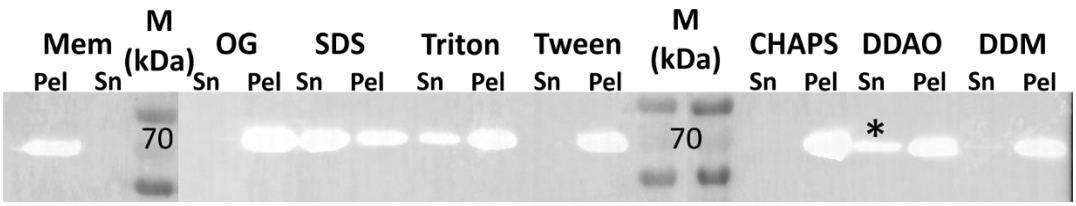

Figure 16: WB to analyze the solubilization of Slr1462. The signal of Slr1462 is localized in the membranes (Mem, Pel). To solubilize Slr1462 the detergents N-octyl-β-D-glucoside (OG), Trition-X (Triton), Tween-20 (Tween), 3-[(3-cholamidopropyl)dimethylammonio]-1-propanesulfonate (CHAPS), N,N-Dimethyldodecylamine N-oxide (DDAO) and *n*-Dodecyl-β-D-maltopyranoside (DDM) were used. As a positive control sodium dodecyl sulfate (SDS) and as a negative control, buffer without detergent (Mem, Sn) were used. The samples were incubated for 2 h at 37 °C and were centrifuged to separate the membranes from the solubilized proteins (1 h, 100,000 g, 4°C). The supernatant (Sn) represents the solubilized fraction, whereas the pellet (Pel) represent the non-solubilized fraction. The black star marks the protein solubilized in mild detergent.

4.2.3 Purification

After the expression and, in some cases, solubilization, the proteins were purified. First, ion metal exchange chromatography was used to bind the proteins via their His-Tags to the NTA matrix loaded with Ni^{2+} ions. The bound proteins were eluted using an imidazole gradient. During the experiments, the number of wash fraction and the imidazole concentration was optimized to get the proteins as pure as possible. From every fraction, loading (L), wash (W), elution (E) and flow through (FT) samples were taken and separated on an SDS-PAGE gel and stained with CBB. The proteins of interest are highlighted with an arrow. The Ni-NTA purification was successful only for SynDLP, where the gel shows a dominant SynDLP band at approx. 90 kDa, which correspond to the theoretical mass of the protein (93 kDa) (Figure 17). In the next step, SynDLP was concentrated and the buffer was changed to the storage buffer (20 mM HEPES-KOH, pH 7.4) using a PD-10 desalting column. Finally, the protein was concentrated again, resulting in a yield of approx. 800 µg protein per liter culture. Additionally, the protein identity was confirmed by WB analysis using an α-His-Tag HRP conjugate.

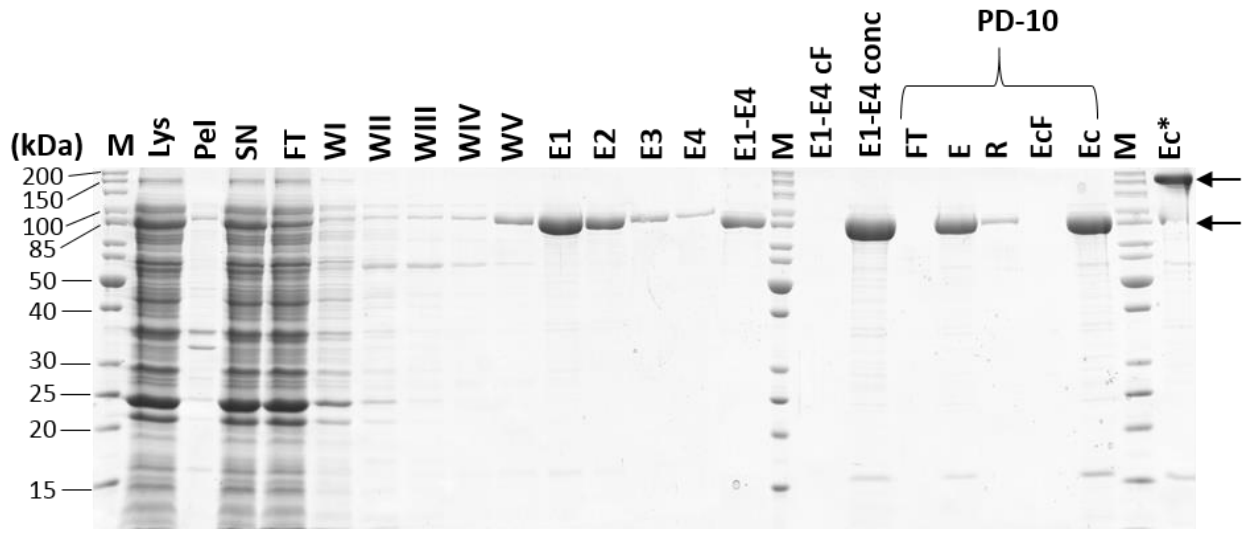

Figure 17: CBB stained SDS-PAGE gel showing purification of SynDLP. The cell lysate (Lys) was centrifuged to remove cell debris and unbroken cells (Pel). The supernatant (SN) was applied onto a Ni-NTA matrix, the components, which did not bind to the matrix also called flow through (FT) were discarded and the matrix was washed with 20 mM (WI), 50 mM (WII), 75 mM (WIII), 85 mM (WIV) and 95 mM (WV) imidazole containing buffer. SynDLP was eluted from the matrix in four steps with 500 mM imidazole containing buffer (E1-E4). The united fractions (E1-E4) were concentrated (E1-E4c) and desalted via a PD-10 column. The concentrated eluate (Ec) contained the purified protein. All samples were prepared under reducing conditions, except Ec*. Ec* was prepared under non-reducing condotions. SynDLP is indicated by an arrow at approx. 90 kDa (Ec) and approx. 175 kDa (Ec*).

Routinely, all samples were reduced by DTT (dithiothreitol) to break any disulfide bonds. Since SynDLP harbors cysteine residues, a sample was also analyzed without preincubation the sample with DTT to check whether the protein might form disulfide bonds or not. Indeed, under non-reducing conditions, SynDLP migrates at higher molecular weights (Ec* in Figure 17), indicating that SynDLP is a disulfide-linked dimer, at least *in vitro*. This issue is discussed in greater detail in chapter 4.3.1.

On the other SDS-PAGE gels stained with CBB and showing the NI-NTA purification, no dominate protein band were detected. Instead, the presence of multiple bands indicated an insufficient purification. Thus, the purity of Slr1462 and Sll0804 was further improved by size exclusion chromatography (SEC). As can been seen in Figure 18 A (CBB) and B (WB) purification was successful only in case of Slr1462. This purification yielded of 300 µg/ml protein. In contrast, Sll0804 was still impure (Figure 18 C).

To sum up, Slr0179 could be expressed solely in inclusion bodies. Since a control for Slr0179 activity and the correct folding is missing, a purification under denaturation conditions was not

done and thus it was decided to shelve this project. Purification of Sll0804 was not sufficient enough for further experiments. Nevertheless, SynDLP and Slr1462 were purified successfully.

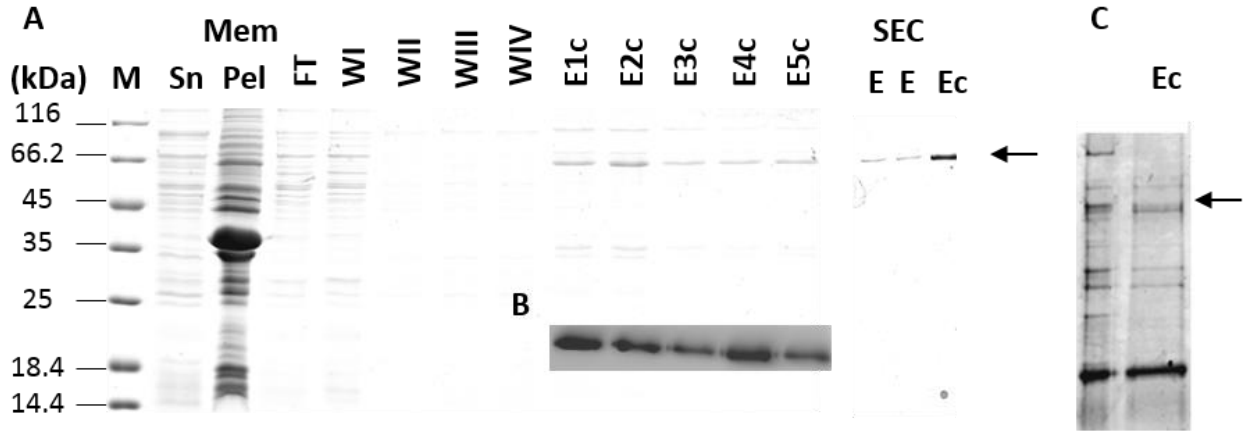

Figure 18: SDS-PAGE gel of the solubilization of Slr1462 (Mem, Sn) and the following purification with Ni-NTA. (A) the solubilized membrane fraction (Mem, Sn) were applied onto a Ni-NTA column, washed with 20 mM (WI), 50 mM (WII), 75 mM (WII) and 100 mM (WIV) imidazole containing buffer and eluted with 500 mM imidazole containing buffer five times (WB in (B)). The eluates were concentrated (Ec) and separated by SEC. The SEC fractions containing the protein (SEC, E) were united and concentrated again (SEC, Ec). (C) shows the insufficient purification of Sll0804 by a stained SDS-PAGE gel. This gel sector was taken from the diploma thesis of Vladislava Schultz.

4.3 SynDLP is mainly α-helical

The secondary structure of SynDLP was analyzed by CD (circular dichroism) and FTIR (Fourier-transform infrared) spectroscopy. The SynDLP structure was predicted with I-TASSER (Iterative Threading ASSEmbly Refinement) provided by the Zhang Lab. The program identifies structure templates from the PDB and models the new structure by iterative template fragment simulations (Yang et al., 2015). The predicted structure (Figure 19 B) reveals a high α-helical content (blue) and some β-sheets in the GTPase domain (red). The potential region, which interacts with membranes was predicted by a hydrophobicity blot analysis using the amino acid hydrophobic scale of Kyte and Doolittle (Kyte and Doolittle, 1982). In addition, a CD spectrum (Figure 19 D) and a FTIR spectrum (Figure 19 E) were recorded. The CD data confirm, a high content of a α-helical secondary structure. In addition, the FTIR spectrum shows the amide I band of SynDLP. The FTIR measurements were done in cooperation with Dr. EL Khoury the group of Prof. Dr. Hellwig (University Strassburg). The amide I band was deconvoluted by assuming that it is composed out

of four peaks. One for the helical part, one for the random coil part and two for the β-sheets. Subsequently, the spectrum was deconvoluted with the second derivate finally resulting in peak centers of 1654 cm^{-1} (α-helical), 1633 cm^{-1}, 1680 cm^{-1} and 1693 cm^{-1} (β-sheet). Interestingly, a random coil part was not integrated. Due to this combined information, the overall α-helical content is approx. 76 ± 10 % and consequently the remaining structural components are β-sheets. Because of simplification and to highlight further important functions and findings in this thesis, SynDLP is cartooned with its key domains. The GTPase domain (GD, red), the membrane interacting domain (MID, green) and the regions, which are α-helical bundles (Bundle, blue).

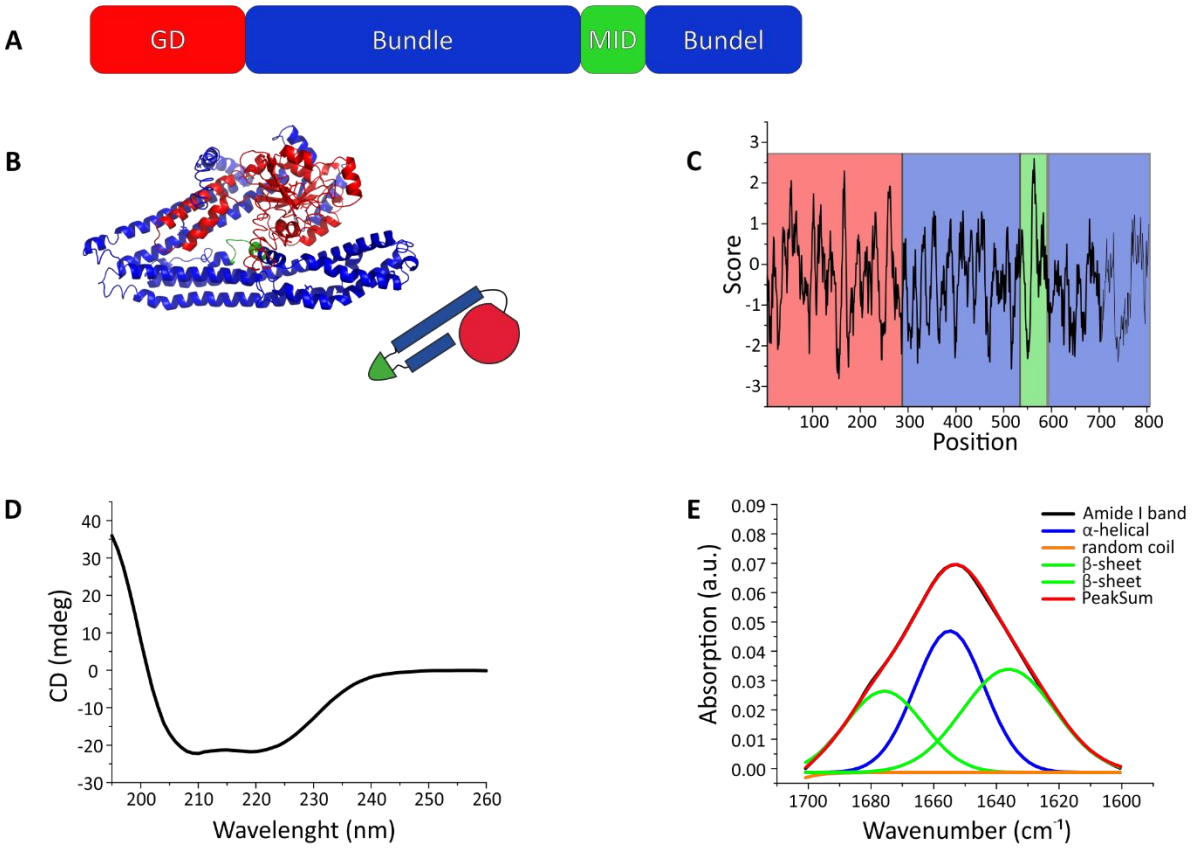

Figure 19: The protein structure of SynDLP. (A) shows the assumed domain arrangement and (B) the predicted structure (I-Tasser) of SynDLP. In addition, the predicted structure is simplified as a cartoon. (C) is a hydrophobic plot using the hydrophobic amino acid scale of Kyte and Doolittle. (D) and (E) show a CD spectrum and a FTIR spectrum of the Amide I band, respectively. The G-domain (GD) is colored in red and harbors the β-sheets, the helical bundles are colored in blue and the potential membrane interacting domain is colored in green.

4.3.1 Disulfide bridges

SynDLP contains 10 cysteine residues and thus it might form intra- or/and intermolecular disulfide bridges. Disulfide bridges (R-S-S-R') are covalent bonds between two thiol groups (R-SH), in case of proteins between two cysteines. Disulfide bonds are widely known to have a key role in the folding, stabilization and structure function of proteins (Sevier and Kaiser, 2002). However, to investigate the role of cysteines in SynDLP, the sample preparation for SDS-PAGE gels were performed without DTT (dithiothreitol), i.e. under non-reducing conditions. Usually, DTT or other reducing agents are added to sample prior loading. In this reducing environment, all inter- and intramolecular disulfide bonds are broken and thus the protein migrates only depending on its size. As shown in Figure 17, SynDLP migrates at a higher molecular weight under non-reducing conditions, indicating that SynDLP might be present as a dimer, at least *in vitro*. To test this hypothesis, 2 µg SynDLP were incubated together with different DTT concentrations. As shown in Figure 20, with an increasing amount of DTT, the ratio of monomer (above 90 kDa) to dimer (above 120 kDa) increases. At low DTT concentrations the predominate band corresponds to the dimer at approx. 120 kDa and starting from 50 mM DTT no dimer signal was observed.

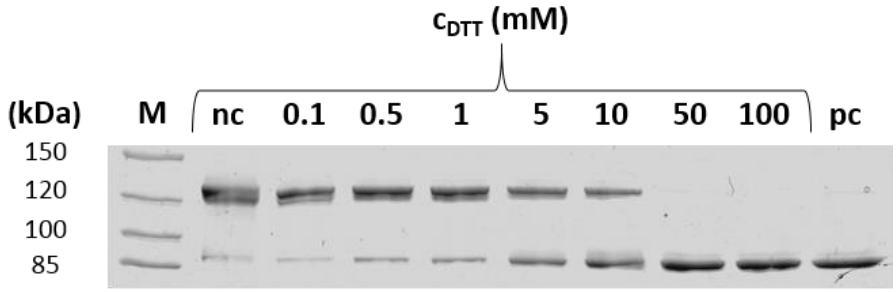

Figure 20: The influence of different DTT concentration on the monomer/dimer ratio of SynDLP. SDS-PAGE gel containing 2 µg SynDLP per lane and an increasing DTT concentration (left to right). The negative control (nc) does not contain any reducing agent in the loading dye, whereas the positive control (pc) contains 500 mM DTT. M: marker

Next the position of the disulfide bond was identified. To do so, 10 SynDLP cysteine mutants were created. In each mutant, a different cysteine residue was replaced by an alanine. The SynDLP mutants were created by PCR site-directed mutagenesis using the plasmid previously created (chapter 4.2).

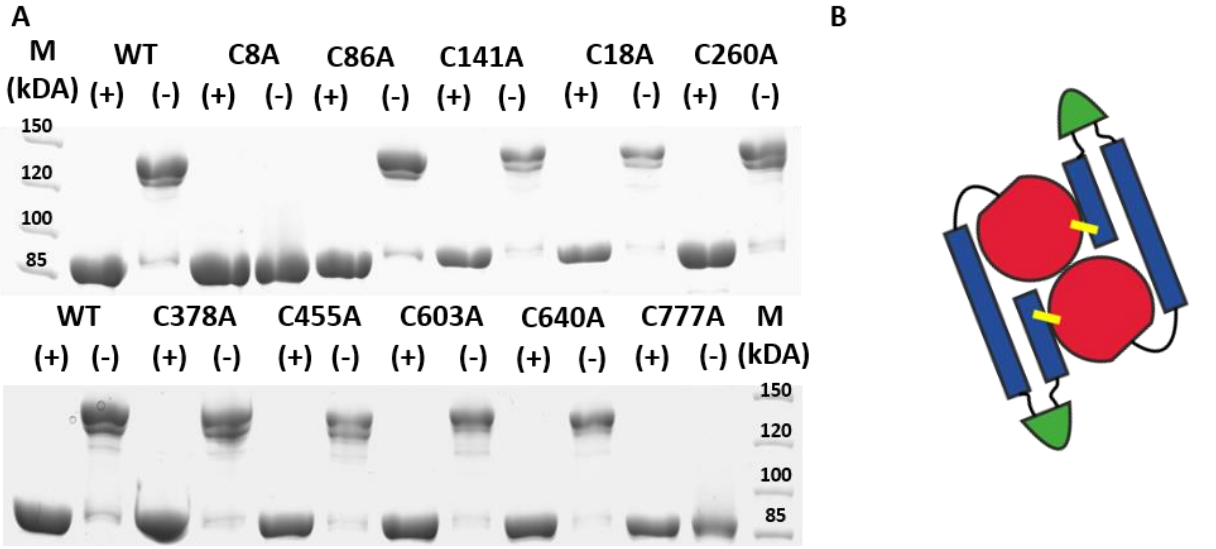

Figure 21: Identification of cysteine residues involved in dimer formation. (A) SDS-PAGE gels stained with CBB showing 1.5 µg WT as well as ten mutants under reducing (+) and non-reducing (-) conditions. In the mutants the SynDLP cysteine residues were individually replaced by alanine. All proteins form dimers, except the mutants C8A and C777A, indicating an asymmetric dimerization between C8 and C777. A possible arrangement of two monomer to a dimer is cartooned in (B). The G domain is colored red, the α helical bundles are colored blue and the potential MID is colored green.

The triplets coding for cysteines (TGC) have been replaced by one coding for alanine (GCC). All mutants were expressed and purified, like the WT. As in the previous DTT experiments, 1.5 µg of each mutant were loaded on an SDS-PAGE gel and stained with CBB. The proteins were pretreated with (+DTT) and without (-DTT) to reach reducing or non-reducing conditions, respectively. The results are presented in Figure 21. Besides the WT, all mutants form potential dimers under non-reducing conditions, except the mutants C8A and C777A. Thus, the dimer is linked between the cysteines 8 and 777, indicating an asymmetric arrangement (Figure 21 B).

From the previous experiments two important information about the structure can be obtained: (i) SynDLP is a predominantly α-helical protein and (ii) the WT forms an asymmetric dimer between the cysteine residues C8 and C777 at least *in vitro*. Consequently, further studies were typically performed with the WT and the non-dimer forming mutant C777A, since it is necessary to know how the presence or absence of a covalently linked dimer influences the activity, oligomerization and membrane interaction properties.

4.4 Membrane interaction of SynDLP WT and C777A

One main key property of DLPs is the ability to interact with biological membranes. Consequently, the membrane interaction properties of SynDLP WT (dimer) and the mutant C777A (non-dimer) were investigated. The first upcoming question, which had to be resolved, was whether SynDLP can interact with model membrane systems containing TM lipids or not. Therefore, liposomes containing 80 % DOPC (as a neutral background lipid) and 20 % of a thylakoid lipid (DOPG, MGDG, SQDG or DGDG) were prepared. In addition, Laurdan was incorporated into the liposomes. Laurdan intercalates into a lipid bilayer and its fluorescence properties are sensitive to the environment. Thus, the assay can detect changes in the lipid order (chapter 3.9.3.1). The results are summed up in Figure 22. The prepared liposomes were incubated with SynDLP or with SynDLP storage buffer.

After 30 min, the Laurdan emission fluorescence was measured in presence and absence of SynDLP. Figure 22 A shows a typical of Laurdan spectrum in the presence and in the absence of WT SynDLP. Upon WT SynDLP addition, the Laurdan fluorescence emission spectrum shows an increase at 490 nm and a decrease at 440 nm. Thus, the GP value decreases (equation (6)). To quantify the differences between the GP in presence (+) and absence (-) of SynDLP, equation (8) was used. The normalized GP+/GP- ratio for all four TM lipids are shown in Figure 22 B, together with the negative control (DOPC). The most pronounced differences were observed with lipids containing PG and SQDG. Interestingly, these are the two negatively charged TM lipids. Subsequently, it was tested whether the negative charges have an influence on the protein binding. Therefore, DOPC liposomes containing an increasing amount of DOPG were prepared and the GP values were determined relative to the GP value of pure DOPC. Figure 22 C shows that the interaction of SynDLP with membranes increases with an increasing amount of DOPG and it was concluded that SynDLP interacts with negatively charged lipids. The SynDLP mutant, which does not form disulfide linked dimers shows the same membrane interacting properties compared to the WT (appendix 7.5), indicating that the disulfide bonds do not have any influence on the membrane interaction.

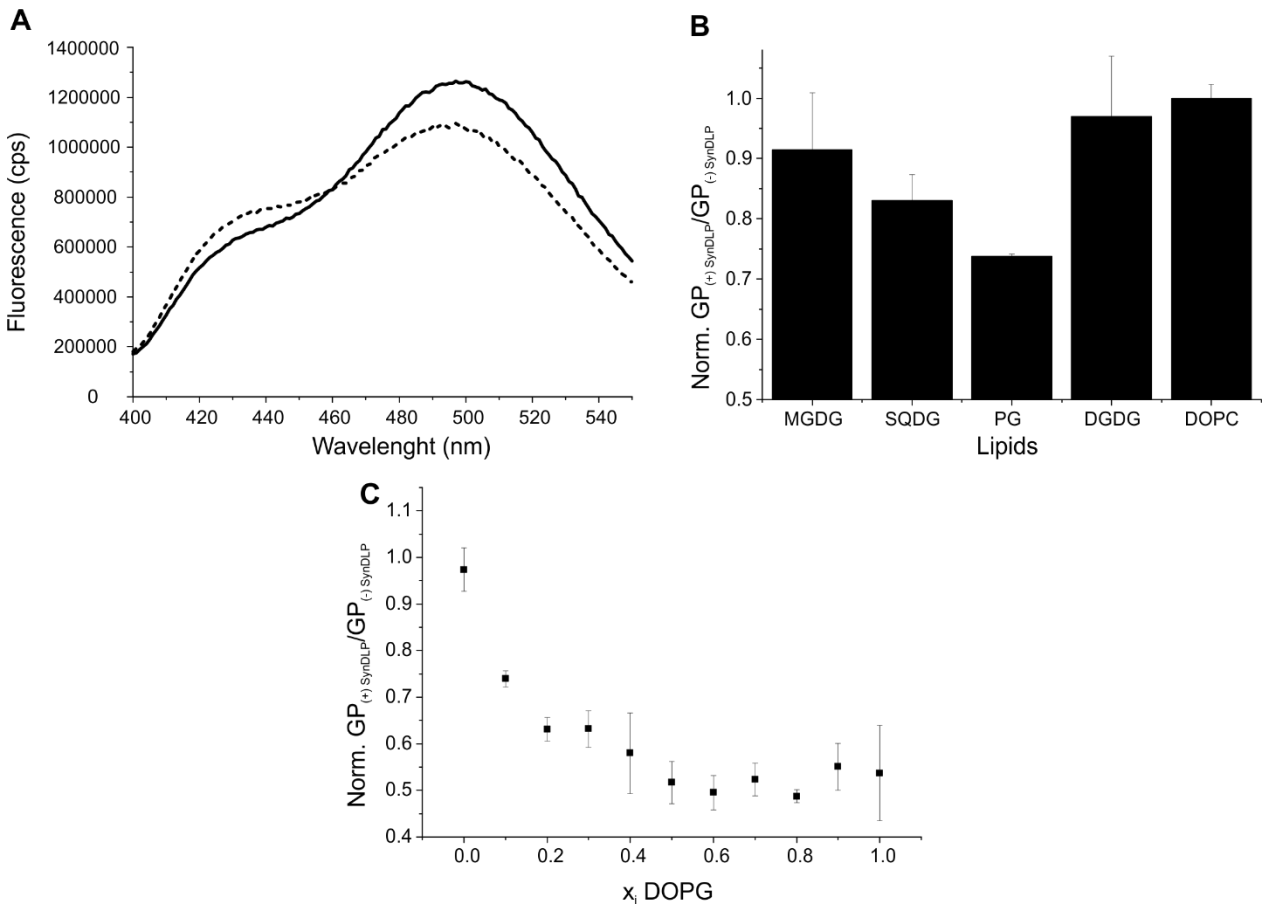

Figure 22: Membrane interaction properties of SynDLP. The spectrum of Laurdan incorporated into DOPG liposomes (line) is blue shifted in the presences of SynDLP (dotted line) (A). The negatively charged thylakoid lipids PG and SQDG induce the most prominent shift in the Laurdan spectra, indicated by the lowest normalized GP+/GP- ratio (B). Moreover, with an increasing amount DOPG, the normalized GP+/GP- ratio decreases, revealing an increasing Laurdan spectra shift (C). All GP+/GP- ratios are normalized to the GP+/GP- ratio of 100 % DOPC (negative control).

4.5 The formation of higher ordered aggregates – oligomerization of SynDLP

It is widely known that DLPs form higher ordered oligomeric structures in presence of lipids (Daumke and Praefcke, 2016). Especially, for (B)DLPs it was shown that they can tubulate liposomes *in vitro* when GMPPnP ((Guanosine 5'-[β,γ-imido]triphosphate) is present and form big protein/lipid complexes (Accola et al., 2002; Bürmann et al., 2011; Daumke et al., 2007; Low and Löwe, 2006; Reubold et al., 2015). In GMPPnP the oxygen between the β and γ phosphate is replaced by an amine. Thus, a GTPase is not able to split it, but GMPPnP remains tightly bound in

an enzymes' binding pocket. There it freezes the active state of the GTPase. To investigate whether SynDLP forms higher ordered oligomers or aggregates or not, three methods were used.

4.5.1 Sedimentation assay

SynDLP WT and the mutant C777A were mixed with either GTP or GMPPnP in the presence or absences of DOPG liposomes. After incubation, the liposomes were separated from the solution by ultracentrifugation and the amount of protein, in the liposomes (pellet fraction) and in the supernatant, was analyzed using SDS-PAGE with CBB staining (Figure 23 A). In addition, higher ordered oligomers may also be found in the pellet fraction. It should be noted that in this assay it is not possible to discriminate between the quantity and the quality of oligomers. For example, an increase in the oligomeric state can be caused by both, an increase in the number of monomers per oligomer or an increase of the number of oligomers with the same number of monomers. Thus, the term "oligomeric state" always refers to both in this work. However, SynDLP WT is mostly found in the pellet when GMPPnP is present (Figure 23 A), indicating a higher oligomeric state, in comparison to sole SynDLP WT. Here, a nearly equivalent distribution of protein in the supernatant (S) or the pellet (P) fraction can be observed. Interestingly, in presence of GTP, more protein appears in the supernatant, indicating a lowered oligomeric state. The presence of DOPG liposomes does not have any influence on the oligomeric state.

To quantify band intensities, the software ImageJ was used. The signals of the protein found in the pellet (P) or the supernatant (S) are always given relative to the signal of the sample before they were separated by ultracentrifugation (SP) (Figure 23 B).

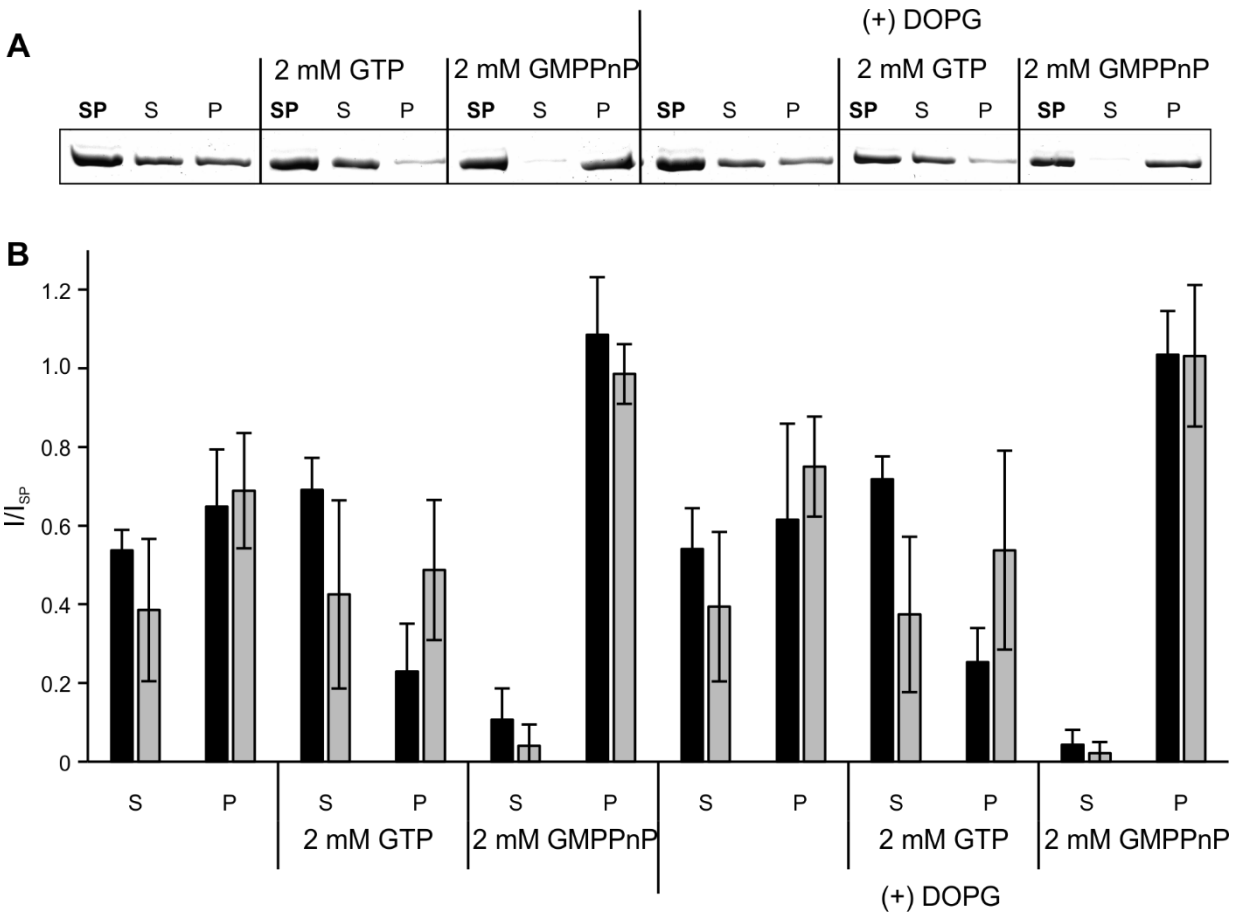

Figure 23: Sedimentation assay of SynDLP WT and C777A. (A) SDS-PAGE gel stained with CBB showing one representative example of the pellet assay. Samples were taken before ultracentrifugation (SP) and of the supernatant (S) and the pellet fraction after ultracentrifugation(P). All samples were prepared in LD buffer and heated to 95 °C for 5 min. The total protein amount before ultracentrifugation was 0.32 µg SynDLP. In presence of GMPPnP, SynDLP WT is exclusively present in the pellet fraction. In (B), three independent experiments of SynDLP WT (black) and C777A (grey) are averaged. The SDS-PAGE gels were analyzed using the software ImageJ and the intensities S and P are relative to SP. The error bars represent the standard derivation of 3 experiments.

SynDLP WT and SynDLP C777A are nearly equally distributed between the supernatant and the pellet, indicating an equilibrium between higher and lower ordered oligomeric states. The addition of GTP as well as the presence of DOPG does not influence SynDLP C777A. But in case of the WT protein and in the presence of GTP, there is a significantly higher amount of protein in the soluble fraction than in the pellet. By adding GMPPnP, nearly the whole amount of protein (WT and C777A) ended up in the pellet fraction, independent from DOPG. Thus, the formation of higher ordered oligomeric structures is most certainly mediated by GMPPnP.

4.5.2 SEC

Based on the sedimentation assay, it is reasonable to assume the formation of high molecular weight SynDLP complexes. To gain further information on the size of each oligomers, the WT and mutant proteins were analyzed by gel filtration. Therefore, the prepacked column HiLoad™ 16/600 Superdex™ 200 (GE Healthcare) was utilized to ensure the coverage of wide molecular weight range. The column was loaded with 500 µl of a 0.85 mg/ml protein solution and protein separation was observed by measuring the absorption at 280 nm. Fractions of 500 µl were collected and pooled in correspondence to the peaks. The pooled fractions were analyzed by a CBB stained SDS-PAGE gel under non-reducing conditions. Figure 24 shows the elution profile of the two proteins. Both chromatograms have an essentially identical shape with at least one strong peak at approximately 36 ml elution volume (V_E) and a small peak at approx. 105 ml V_E. For SynDLP WT and C777A, fractions before the strong peak (a), at the peak (b) and after the peak (c) were collected and pooled. The analysis via SDS-PAGE detected the proteins in the strong peak, indicated by a band at around 95 kDa for the non-dimer forming mutant (C777A) and a band at around 200 kDa for the SynDLP dimer (WT). In the small peaks, no protein band could be detected and is most likely caused by imidazole traces (see also appendix 7.2). However, both proteins eluted in the void volume, where a separation of different sizes is not possible. As the columns specific parameters indicate molecular weight ranges from 10,000 up to 600,000, it is very likely that SynDLP WT and C777A form oligomers with higher molecular masses. Due to the maximal separation size (600,000 kDa), at least octamers (8 x 93.6 kDa = 748.8 kDa) form. Moreover, formation of higher ordered oligomers was not dependent on disulfide bond formation.

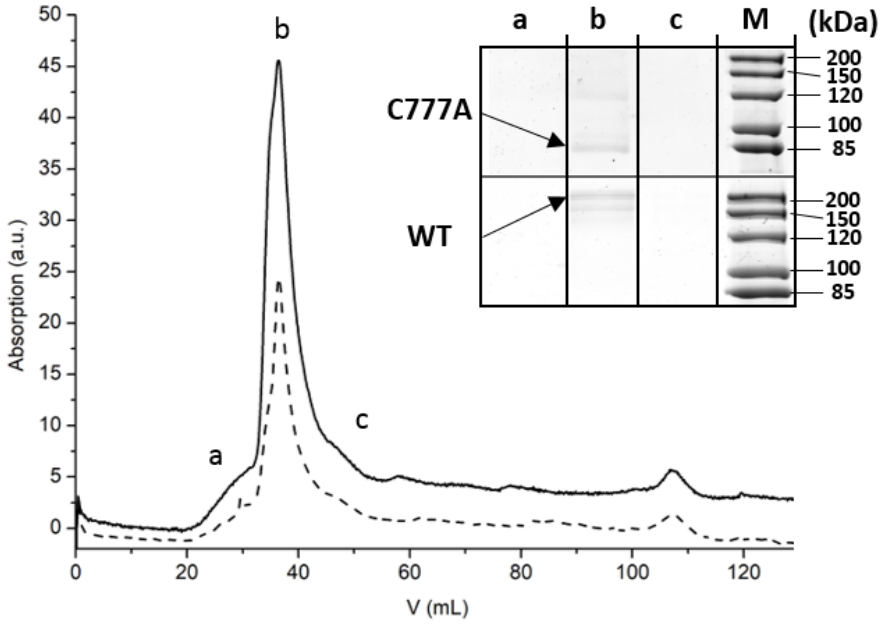

Figure 24: Gel filtration chromatogram to identify and quantify the higher oligomeric structure of the proteins SynDLP WT and C777A. 425 µg SynDLP WT (straight line) and SynDLP C777A (dashed line) were separated in RB utilizing the prepacked column HiLoad™ 16/600 Superdex™ 200 (GE Healthcare) (A). The samples of the pooled fractions (a-c) were pretreated under non-reducing conditions loaded on an SDS-PAGE gel. The proteins are marked with a black arrow. Note that the gel image was cropped and merged in a different sequence to show only the important lanes. The full and raw gels are in the appendix. M: marker

4.5.3 TEM

To further analyze whether SynDLP WT and SynDLP C777A form organized quaternary structures, transmission electron microscopy (TEM) was used. TEM is widely used to clarify the structures of proteins and, more important for (B)DLPs, to visualize tubulated liposomes, which is an *in vitro* key feature shared by many (B)DLPs (Accola et al., 2002; Bürmann et al., 2011; Daumke et al., 2007; Low and Löwe, 2006; Reubold et al., 2015). Negative stained TEM samples were prepared with the WT protein and the mutant C777A in cooperation with Dr. Rusitzka and Dr. Haugewitz. The samples were analyzed in presence of DOPG liposomes sized to 200 nm, in presence and absence of 2 mM GTP and 2 mM GMPPnP, respectively. To ensure a fully functional protein, all samples were prepared in GTPase RB. Selected micrographs are shown in Figure 25. Besides unregular aggregates, SynDLP WT forms two differently sized structures.

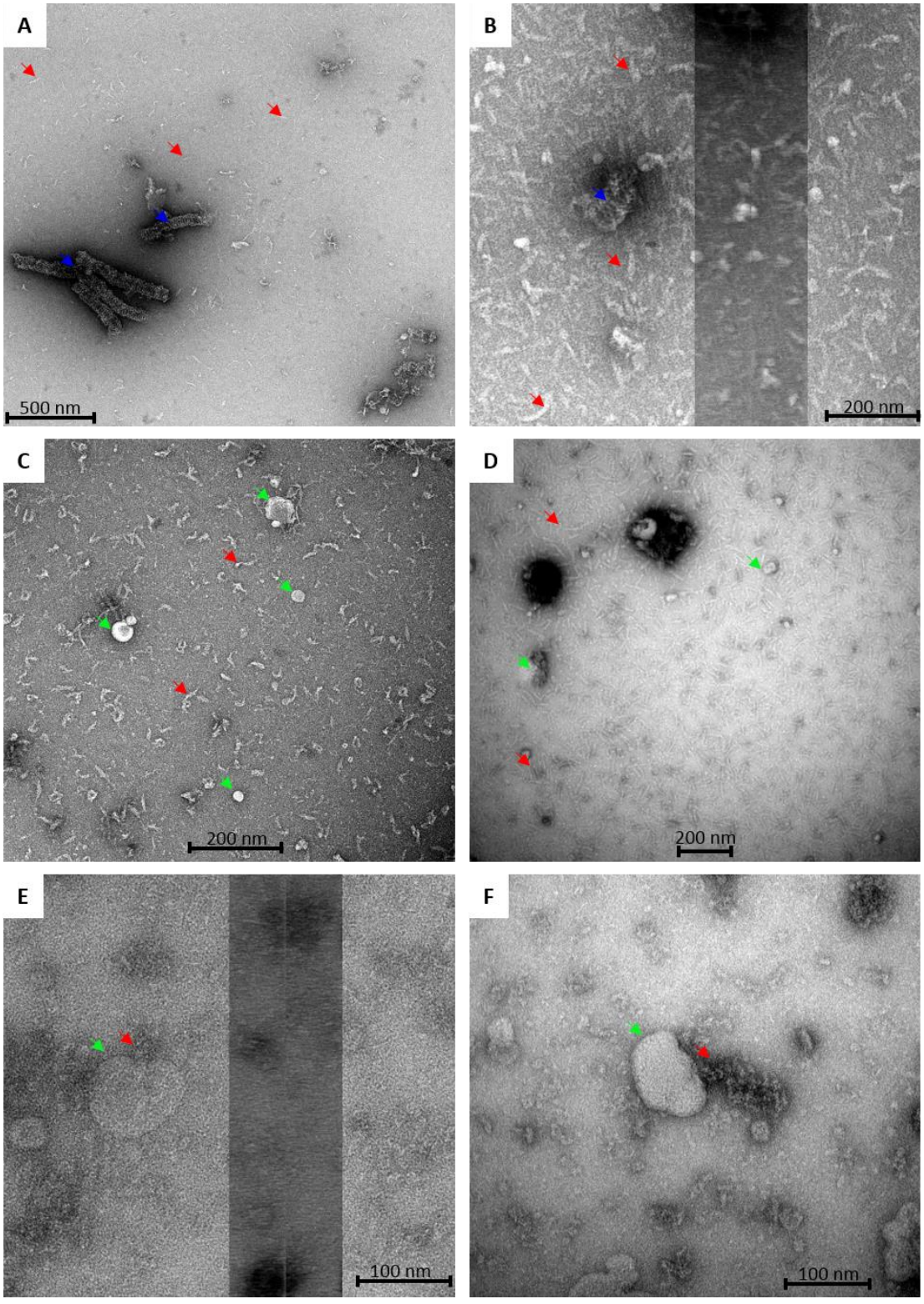

Figure 25:Selected TEM micrographs (negative staining) of SynDLP WT (left) vs. C777A (right). Without any additions ((A) and (B)), in the presence of DOPG and GTP ((C) and (D)) as well as in the presence of DOPG and GTP ((E) and (F)). Blue arrows mark big helical protein structures, red arrows mark the small protein structures and green arrows the liposomes. Note the different scale bars.

Table 17: Summary of the measured sizes of SynDLP WT and C777A.

Micrographs	Protein	Nucleotide	Size		
				length (nm)	width (nm)
A	WT	-	Small units	35-70	10
			Big units	Up to 1000	65
B	C777A	-		40-50	20
C	WT	GTP		55	10
D	C777A	GTP		50	10
E	WT	GMPPnP		-	25
F	C777A	GMPPnP		-	25-30

The sizes of the different protein structures were analyzed by ImageJ as summarized in Table 17. On the one hand, small tubulated structures (named here small units, red arrow in Figure 25 A) with a length of 35-70 nm and a width of approx. 10 nm were identified. On the other hand, there are long helical or rod like tubes with different length of up to 1000 nm and a diameter of approx. 65 nm (big units, blue arrows Figure 25 A). In the presence of liposomes, the diameter of the big rods increases to 85 nm and the liposomes close to the big rods show strong deformation, whereas the size of the small units remains unchanged (appendix 7.3). Interestingly, the C777A mutant shape differs from WT shape. Large helical structures were not identified and some small helical structures were only observed rarely (blue arrows, Figure 25 B). Like the WT, C777A forms small units, but smaller and more unregularly formed, with a length distribution of 40-50 nm and a doubled width (20 nm). In the presence of GTP (Figure 25 C and D) both proteins seem to affect liposomes, since in the micrographs intact liposomes are absence (micrograph showing intact liposomes can be found in the appendix 7.3). Instead, potential liposome/lipid fragments are observable (green arrows in Figure 25 Cand D). In addition, SynDLP WT does not longer form helical/rod like structures and the small units are unregular formed. In opposite, the small units of SynDLP C777A become more uniform and rod-shaped.

Moreover, TEM micrographs were recorded in the presence of GMPPnP and DOPG liposomes (Figure 25 E and F). For several DLPs this results in the tubulated liposomes in the presence of GMPPnP (Accola et al., 2002; Bürmann et al., 2011; Daumke et al., 2007; Low and Löwe, 2006; Reubold et al., 2015). Consequently, TEM samples with SynDLP WT and C777A were also prepared

in the presence of GMPPnP and DOPG liposomes. The results are shown in Figure 25 E and F. In both cases, the liposomes might be tubulated, as evidenced by large cylindrical rod structures growing out of the liposome (blue arrows in Figure 25 E and F). Beside the potential tubes, the free SynDLP WT and C777A form large irregular structures (red arrow in Figure 25 E and F). The formation of higher ordered aggregates and/or oligomers in the presence of GMPPnP was also revealed by the sedimentation assay.

Taken together, the presence of nucleotides strongly influences the oligomeric state of SynDLP WT and C777A. Nucleotide-depending conformational changes might be responsible for a structural reorganization. The DOPG liposomes do not influences the oligomeric state of SynDLP, but the liposomes themselves are disrupted, once SynDLP WT or C777A are present (appendix 7.3). Differences between the dimer forming protein and the non-dimer forming mutant are limited to a different conformation. In the TEM micrographs it was shown that the SynDLP WT and C777A do not have the same oligomeric structure, although they both affect DOPG liposomes in the presences of GTP and tubulate DOPG liposomes in the presence of GMPPnP.

4.6 Establishing a continuous, regenerative coupled GTPase assay

The GTPase activity is a key marker for the majority of DLPs. The GTP hydrolysis to GDP and inorganic phosphate provides the energy, which is necessary for remodeling membranes (described in greater detail in chapter 1.4.2 of the introduction) (Daumke and Praefcke, 2016). In principle, two non-radioactive methods are described in the literature to determine GTPase activity. The more commonly used method bases on the determination of free P_i. P_i builds a complex with malachite green molybdate under acidic conditions (D'Angelo et al., 2001; Itaya and Ui, 1966), whereby the amount of P_i is directly related to the color intensity. But for this procedure samples must be taken and the enzyme activity must be stopped. The second assay is a continuous, regenerative coupled GTPase assay. It is based on a protocol from Renosto *et al*. for a ATP kinase (Renosto et al., 1984) and was adapted and modified to determine GTPase activities (Ingerman and Nunnari, 2005). The assay includes two coupled reactions (Figure 26). The active

protein turns over the substrate GTP to GDP and P_i. The pyruvate kinase (PK) recovers GTP by transferring a phosphoryl group from phosphoenolpyruvate (PEP) to GDP. The resulting product is pyruvate. In another reaction, the pyruvate is consumed with $NADH/H^+$ by the lactate dehydrogenase (LDH), which catalysis the production of lactate and NAD^+. The reaction scheme shows explicitly that the turnover of one GTP results in an oxidization of one $NADH/H^+$. $NADH/H^+$ has a strong absorption maximum at 340 nm (A_{340}) and thus, while observing the decrease of $NADH/H^+$, the activity of the GTPase is given indirectly, as it is proportional to the decrease of A_{340}.

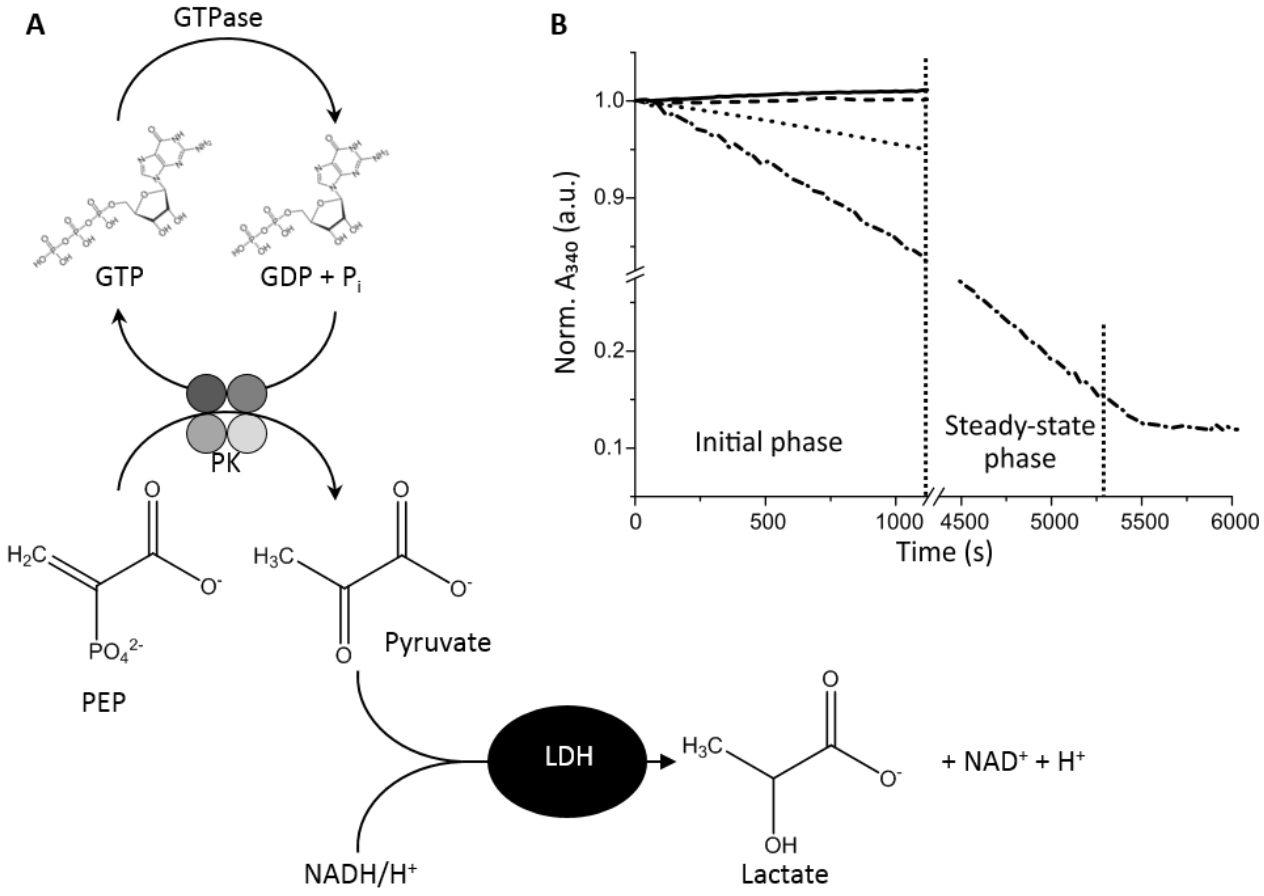

Figure 26: Principle of the continues regenerative coupled GTPase assay (A) and typical A_{340} curves over the time (B). The GTPase hydrolysis GTP to GDP and P_i The pyruvate kinase (PK) recovers GTP by the consumption of phosphoenolpyruvate (PEP) to pyruvate. The pyruvate can be turned over into lactate by the lactate dehydrogenase with the simultaneous oxidization of $NADH/H^+$ to NAD^+. (B) Typical curves of the GTPase assay measuring the absorption at 340 nm over the time. A sample, where the proteins are replaced by storage buffer (straight line) is the negative control. Slr1462 (dashed line) does not show any difference to the control, whereas in case of SynDLP (0.1 µM, dotted line and 2 µM, dashed/dotted line) the absorption at 340 nm decreases significantly.

The protocol was adapted and modified from Ingerman et al., which is specialized on DLPs (Ingerman and Nunnari, 2005). Contrary to this protocol, the master mix (every component except protein) was incubated for 15 min at RT, in order to first convert any free GDP into GTP. Thus, no GDP interferes with the assay. Typical curves are shown in Figure 26 B. The A_{340} was measured in RB containing 0.9 µM Slr1462 (dashed line), 0.1 µM (dotted line) and 2 µM SynDLP (dashed/dotted line), respectively and 1.5 mM GTP for up to 100 min. Furthermore, a control, which contained only storage buffer ((SB); 20 mM HEPES-KOH pH 7.4) and Slr1462 do not show any enhanced A_{340} decrease. In contrast, A_{340} declines significantly in presence of SynDLP, in a SynDLP concentration-dependent manner. Based on this data, only SynDLP is an active GTPase at the chosen conditions. Its activity can be divided into three phases: At the beginning, the curve declines moderately (initial phase), followed by a long linear decrease (steady-state) and no changes are observed when all $NADH/H^+$ is turned over.

Some DLPs, like dynamin, show a strong increase of the GTPase activity in presence of lipids (Ford et al., 2011). Thus, the shape of a kinetic curve might provide information about the binding mechanism of GTP and involved conformational changes. However, to measure such enzyme kinetic curves, the activity of SynDLP at different substrate concentrations has to be calculated. Therefore, the method of Ingerman et al. was used (Ingerman and Nunnari, 2005). Exemplarily, the calculation is shown for a c_{SynDLP} of 0.5 µM in 150 µl and in the presence of 1 mM GTP.

The slope is given by linear regression of the steady-state phase (-0.03 ΔA_{340}/min) and is corrected by the subtraction of a blank sample. The blank sample is free of any protein to consider the auto hydrolysis of GTP and NADH. Because the correlation of NADH to GTP is proportional, the turnover can be described by the absolute value, which is given by Δ0.03 A_{340}/min. Using equation (2), the molar attenuation coefficient (6220 $M^{-1}cm^{-1}$) and the buffer height (0.38 cm) (Ingerman and Nunnari, 2005) the velocity of the GTP hydrolysis is:

$$v_{GTP} = \frac{0.03 \frac{\Delta A_{340}}{min}}{0.38\ cm \cdot 6220 A_{340} M^{-1} cm^{-1}} = 1.2x10^{-5} \frac{M}{min} \qquad (29)$$

With equation (3) a molar mass of SynDLP of 93,000 g/mol and a mass concentration of 0.047 g/l, the activity is given by:

$$Activity\ [min^{-1}] = \frac{1.2x10^{-5}\ \frac{M}{min} \cdot 93{,}000[\frac{g}{mol}]}{0.047[\frac{g}{l}]} = 23.74\ min^{-1} \qquad (30)$$

To obtain a suitable protein concentration, the activity was studied at different protein concentrations (WT and C777A) and at constant GTP concentration of 1 mM. The results are shown in Figure 27. The WT activity as well as the mutant activity increase steeply at low protein concentrations and no significant difference in the activity can be observed, until a saturation level at a c_{Prot} of approx. 0.2 µM is reached. Interestingly, the mutant maximal activity (17 min^{-1}) is only 70 % of the WT maximal activity (24 min^{-1}).

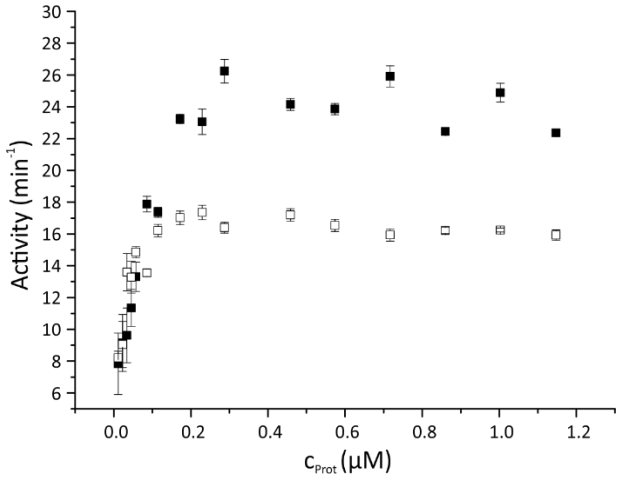

Figure 27: The activity of SynDLP WT and C777A at various c_{Prot}. The activity of SynDLP WT (filled squares) and the mutant C777A (non-filled squares) were calculated as descripted in the text. The error indicates the average of three independent experiments.

Subsequently, all further GTPase activity measurements were performed at a protein concentration of 0.5 µM, thus the activity difference is maximal and the activities can be compared to the C777A mutant.

One SynDLP WT enzyme hydrolysis approx. 24 GTP molecules per minute. These calculations were done for different substrate concentrations from 0 to 5 mM GTP. In addition, a non-hydrolysable

analogue of GTP, GMPPnP was added. The results of these experiments are shown in (Figure 28). Moreover, the influence of DOPG liposomes on the hydrolysis rate was tested.

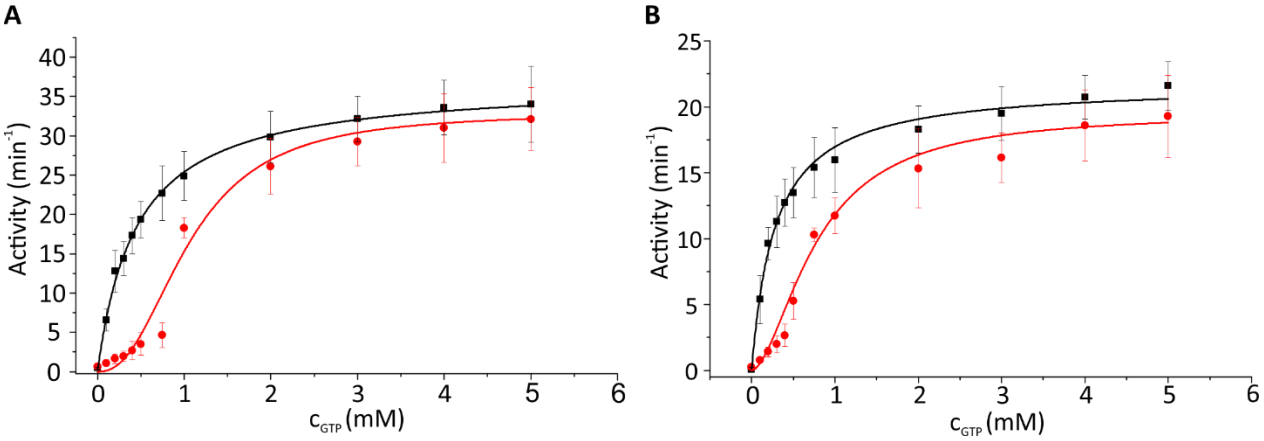

Figure 28: The activity of SynDLP WT and C777A depend on the substrate concentration (c_{GTP}). The black squares indicate the activity of SynDLP WT (A) and C777A (B) in absence of GMPPnP, whereas the red points indicate the activity in presence of GMPPnP. The data points were fitted by Michaelis-Menten (black line) and Hill equation (red line), respectively. The error bars indicate the average of at least three independent experiments, at least.

Figure 28 illustrates the activity of the proteins SynDLP WT and C777A in presence of GMPPnP at various GTP concentrations. When comparing the activities of the WT with C777A, both (black line) show classical Michaelis-Menten kinetics, where at low substrate concentrations the activity increases strongly and reaches a saturation level. But evidently, the maximal activity is inhibited in case of C777A ($Actv_{max}$ (WT) = 37 ± 3 min^{-1} and $Actv_{max}$ (C777A) = 21.8 ± 0.4 min^{-1}) and the K_m value is slightly reduced (K_m (WT) = 0.5 ± 0.1 mM and K_m (C777A) = 0.23 ± 0.02 mM). The presence of DOPG does not influences the SynDLP WT and C777A activity (appendix 7.6.1). Interestingly, in the presence of GMPPnP the kinetics changes. In both cases, the enzyme activity follows a more sigmoid curve, which can be describe by e.g. the Hill equation. Note that the here used Hill equation does not perfectly describe the best model for kinetics in presence of GMPPnP and it was carefully used here to obtain an estimation of the kinetic parameters. However, the sigmoidal shaped curves are also an indicator for allosteric inhibition or a completely different model (discussed later in chapter 5.3.1 of the discussion). $Actv_{max}$ is not influenced by GMPPnP and the K_m value as well as the Hill slope (n) do not differ significantly. All parameters are summed up in Table 18.

Table 18: The maximal activity ($Actv_{max}$) and Michaelis-Menten constant (K_m) as well as the Hill coefficient (n) of SynDLP WT and C777A. The parameters are the result from fitting enzyme activity with the Michaelis-Menten or Hill equation.

	Model	$Actv_{max}$ (min^{-1})	K_m (mM)	n
SynDLP WT	Michaelis-Menten	36 ± 3	0.5 ± 0.1	-
SynDLP WT + GMPPnP	Hill	33 ± 5	1.1 ± 0.2	2.4 ± 0.6
SynDLP C777A	Michaelis-Menten	21.8 ± 0.4	0.28 ± 0.02	-
SynDLP WT + GMPPnP	Hill	19 ± 3	0.8 ± 0.2	1.7 ± 0.2

In summary, the GTPase assay provides some useful information: (i) SynDLP and its non-dimer forming mutant are active GTPases, (ii) in presence of GMPPnP the enzyme kinetic changes fundamental and (iii) the presence of DOPG does not influence the activity in case of the WT and the non-dimer forming mutant.

4.7 SynDLP at membrane interfaces

Membrane remodeling implicates a membrane interaction of SynDLP, which was already suggested by Laurdan fluorescence spectroscopy. As SynDLP is not a membrane protein, it is necessary to obtain buffer/ML interface selective information, which can be provided by SFG. In addition, SFG is related to IR spectroscopy and thus includes information about the secondary structure of the protein. Moreover, it is possible to calculate the orientation of proteins with respect to the ML (Weidner and Castner, 2013).

As known from previous experiments (GTPase assay and Laurdan fluorescence spectroscopy), SynDLP is active in RB and can interact with negatively charged lipids. Therefore, a DMPG (1,2-ditetradecanoyl-*sn*-glycero-3-phospho-(1'-*rac*-glycerol)) monolayer (ML) was used for SFG experiments. Note that DMPG was used because it is a saturated lipid and cannot be oxidized easily, such as DOPG, which would influence the ML order especially over long-time experiments. After adding the lipid to the buffer, the ML was compressed to a surface pressure (Π_0) of 15 mN/m and which was held constant, while a first SFG spectra in the amide I area (1600-1800 cm^{-1}) was recorded. Thereafter, Π was released and SynDLP was added to a final concentration of approx. 0.05 mg/ml. Lastly, GTP was added to a final concentration of 1 mM. SFG spectra were recorded

before adding the protein, after adding the protein and after adding the GTP. It should be highlighted, that the measuring of the surface pressure and the recording of the SFG spectra were performed always simultaneous.

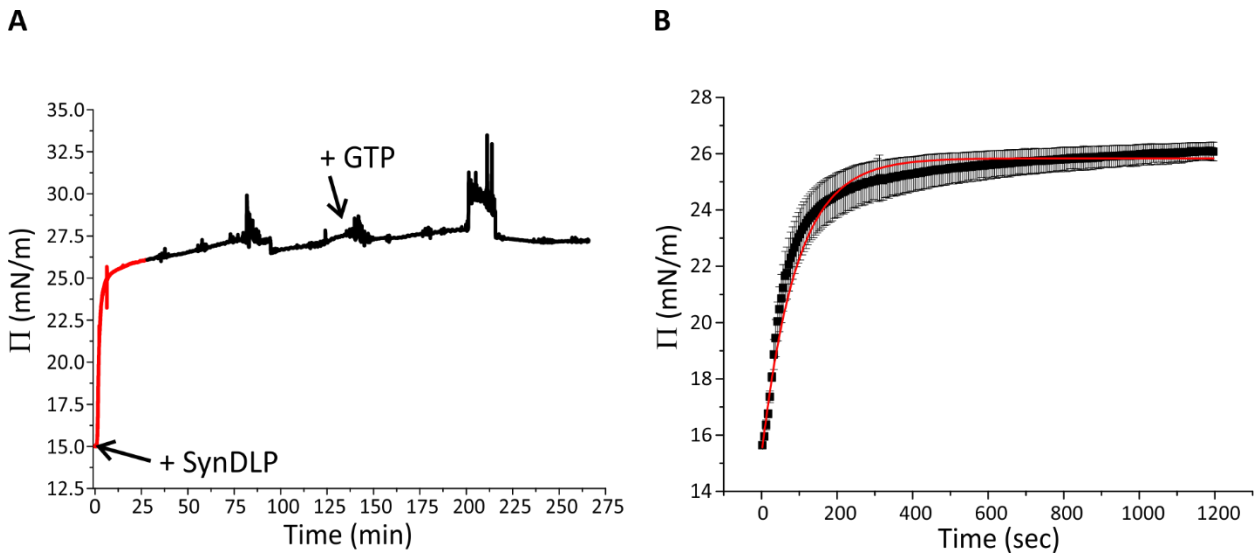

Figure 29: The progression of the surface pressure (Π) over the whole experiment (A) and the initial increase of Π in the first 1200 seconds (B). After setting the Π to 15 mN/m protein (SynDLP) was added. Approx. 150 min later GTP was added (A). The red part of the curve indicates the data points, which were used for the fitting procedure. Similar results were obtained from three independent experiments. The initial slope (B) are averaged and fitted by a mono exponential function (red curve). The error bars are the result of the three independent experiments.

As can been seen in Figure 29 A, directly after adding SynDLP, the surface pressure increased from 15 mN/m to approx. 26 mN/m and further increased slightly. The initial increase in the surface pressure, reflecting protein adsorption at the DMPG ML, can be approximately descripted by a mono exponential fit within the first 1200 sec (Khattari, 2016; Nordera et al., 1997), yielding to a Π_{max} of 25.83 ± 0.02 mN/m and a growth rate constant of 92 ± 2 sec (Figure 29 B). Moreover, the protein had to penetrate the membrane in a certain depth, since only an electrostatic interaction would not explain the pronounced increase of the surface pressure. The addition of 1 mM GTP did not significantly change the surface pressure. The slight increased Π afterwards can be neglected, because it probably was caused by technical factors, e.g. vaporization of water. In addition, the little peaks attribute to the sensitivity of the Π measurements, which recognizes every change in the experimental setup, such as adding GTP or changing the polarization. The small fluctuations and peaks can be explained by the great sensitivity of measuring Π. Every touch

of the laser setup (e.g. injecting of GTP in the sub phase) and even the rotation of the through due to a light fluctuation in the Π level.

The first SFG spectra were recorded at a constant Π = 15 mN/m only in the presence of the ML. The example spectrum shows the characteristic carbonyl stretching vibrations (C=O) of a lipid monolayer at ~1738 cm^{-1} in the amide I region (Figure 30 C). Upon adding SynDLP the surface pressure increased and in the amide I SFG spectra region a new band arose, which correspond to the SynDLP amide I band. Over time the band became more pronounced and in good agreement with the surface pressure data a saturation level was reached after ca. 30 min (Figure 31 A). After the addition of 1 mM GTP, the amide I band decreased (Figure 31 B), which reveals a nucleotide depending conformational change at membrane surfaces.

To quantify the changes in the amide I band, the positions of the different contributed peaks had to be determined. Therefore, the second derivate approached was applied on the deconvoluted SynDLP amide I band (see appendix 7.4.2, done by Dr. Youssef, University of Strasbourg). The approach resulted in four peaks, which contribute to the amide I band. The alpha helical peak resonance is at 1654 cm^{-1} and the beta sheets have resonances at 1633 cm^{-1}, 1680 cm^{-1} and 1693 cm^{-1}. This result was incorporated into the fitting routine and a spectra before adding GTP and after adding GTP were recorded. Figure 30 (red lines) illustrates the three fitted SFG spectra (details to the fitting routine and the fitting parameters can be found in the appendix 7.4.3) and it was shown that the fitting routine describes the data well. The arising amide I band indicated that the SynDLP is able to order itself at the DMPG monolayer, which underlines the orientated membrane interaction property of it. Moreover, after the addition of GTP the amid I band seems to be lower and indeed all amplitudes of the peaks contribute to the amide I band are reduced. In more detail, the β-sheets amplitudes were between 12 and 13 % lower and interestingly, the α-helical amplitude was even reduced to 50 %. Revealing that, the difference in the SFG spectra might be the consequence of a conformational change in presence of DMPG, which not can be observed without the monolayer (appendix 7.4.4). To determine the angle between the monolayer and SynDLP (θ), Steven Roeters calculated theoretical spectra (Figure 30 A (-GTP) and B (+GTP), green line), which fits best to both experimental data (presence and absence of

GTP) when assuming a θ of 89 °. Only in the region above 1750 cm^{-1} the calculated spectra do not describe the experimental data well. Nevertheless, the orientation of SynDLP regarding the DMPG ML is illustrated in Figure 30 D. Note that the Ψ angle (the side of SynDLP, which facing the membrane) is not orientated and is consequently not defined. The definition of θ and Ψ as well as the calculation procedure are described by Roeters *et al.* (Roeters et al., 2013).

In summary, the observation of the surface pressure revealed an interaction of SynDLP with a DMPG ML, which is in good agreement with Laurdan fluorescence spectroscopy. Beyond that, the increased surface pressure may also include an intercalating of SynDLP in the ML, otherwise the surface pressure would not be affected. The SFG spectra analysis indicate, that the protein binds to the membrane in a highly oriented way with a calculated Θ of 89 °. Moreover, potential change in the secondary structure after GTP hydrolysis occur, which do not influence the orientation with respect to the membrane.

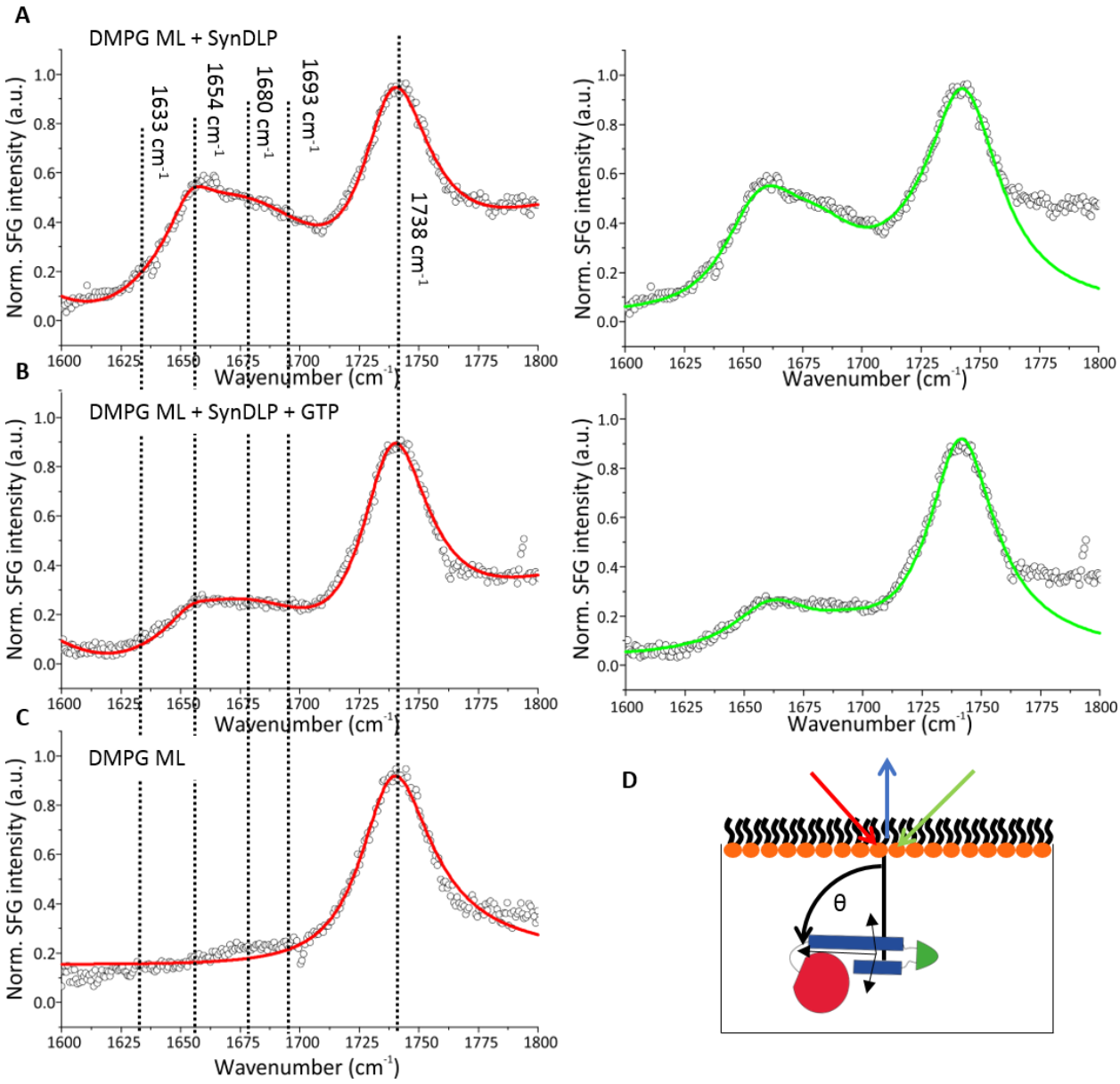

Figure 30: SFG spectra of SynDLP at DMPG monolayer (A), in the presence of SynDLP and GTP (B) and without SynDLP (C). The predicted orientation of SynDLP is cartooned in (D). All experimental SFG spectra are the average of at least three independent experiments (cycles) and were recorded at a DMPG ML, after adding 0.05 mg/mL SynDLP (A) and after adding 1 mM GTP (B). The red line (panel (A)-(C) left) corresponds to the secondary structure analysis based on the deconvoluted amid I band from IR spectroscopy (Dr. Youssef, University of Strasbourg). The green lines (A)-(B), right) correspond to calculated spectra for a protein orientation of 89 °C (Θ) with respect to the ML (kindly provided by Steven Roeters). A schematic cartoon in (D) shows the orientation of SynDLP regarding the DMPG ML. Θ is the Euler angle between the SynDLP and the ML. The red, green and light blue arrows represent IR/VIS laser beams of incident and the resulting SFG laser beam, respectively.

4.8 Working in vivo: SynDLPs knock out strains

To understand molecular details of proteins, structure and biochemical activity, *in vitro* studies are important and necessary. However, to understand the biological function of a protein, *in vivo* studies are mandatory. Therefore, the genes encoding for potential DLPs are deleted or depleted in *Synechocystis* (*slr0179*, *slr0869*, *slr1462*, *sll0503* and *sll0804*) and the generated mutant strains were characterized. Especially, the *slr0869* mutant (encodes SynDLP and thus named Δ*syndlp*) was studied.

4.8.1 Generating knock out strains

As discussed before, the genome of *Synechocystis* encodes five potential BDLPs. That directly lead to the question, if these genes/proteins are essential for *Synechocystis*. To investigate such a question, depletion or deletion mutants of *Synechocystis* were generated by replacing the respective genes (*bdlps*) with an antibiotic resistance cassette (kanamycin resistance cassette, kan^R). To do so, forward and reverse primers were designed appropriately to matching approx. 200 bp upstream (UP) and 200 bp downstream (DS) of the gene, respectively. In addition, RE sites were added to the primers and the upstream and downstream regions of the *bdlps* were amplified via PCR (see also Figure 31). The upstream fragment and the vector pBluescript II KS(+) were individually restriction digested by the corresponding REs and ligated. In the next step, the downstream regions were restriction digested and ligated into the vector containing the upstream region. Finally, the kan^R was restriction digested and inserted between the upstream and the downstream region in the vector (for more details see Figure 31).

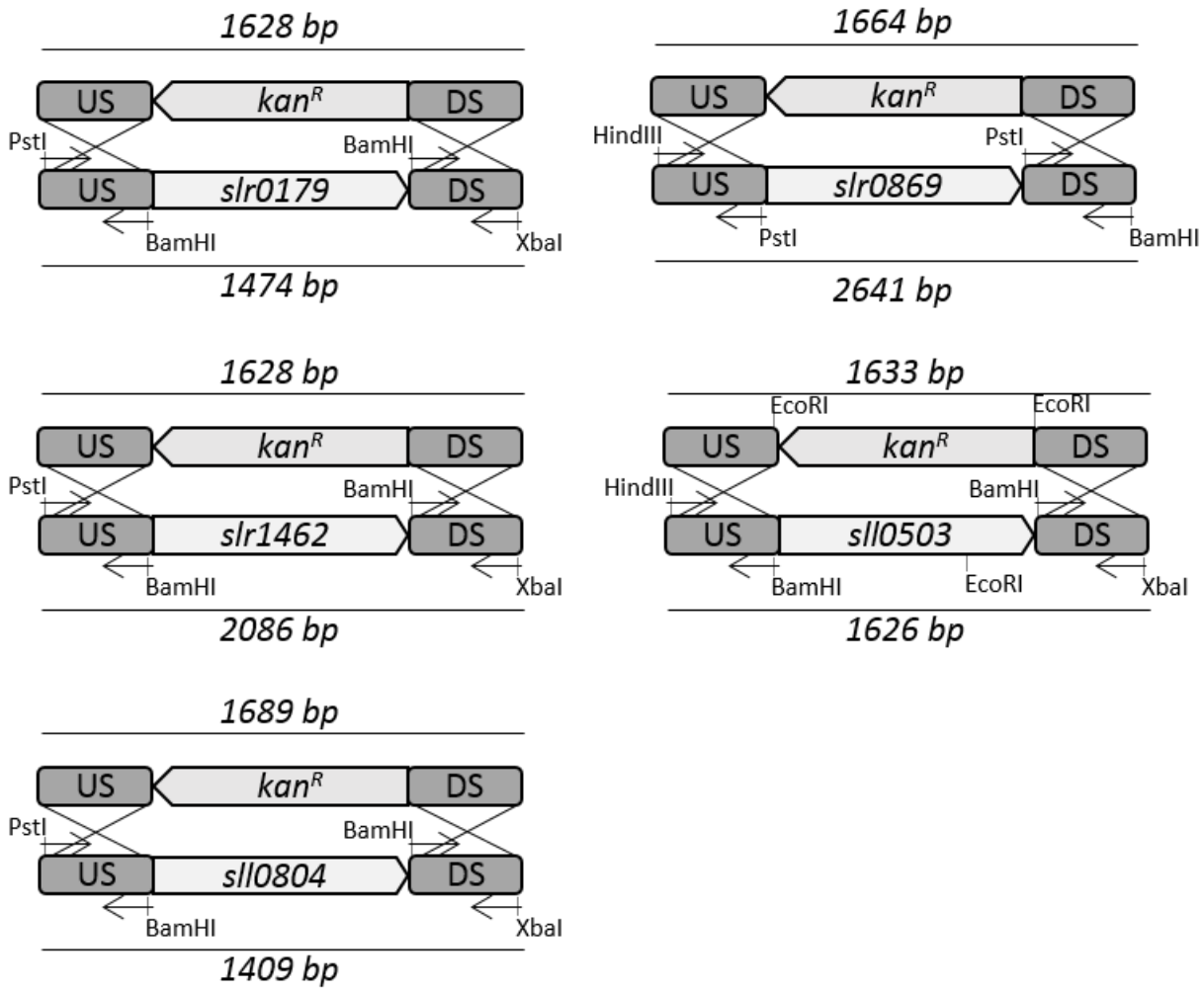

Figure 31: Schematic view on the cloning procedure. The upstream (US) and downstream (DS) region of the *bdlp* genes were amplified using the *Synechocystis* WT gDNA and using primers, which insert RE sites. The DNA fragments and the vector pBluescript II KS(+) were restriction digested with the corresponding REs. First the US, then the DS and finally the kanamycin resistance gene (*kan*^{R}) were inserted into the vector. The identical DNA from the plasmids (above) and the gDNA is marked with cross lines. The total sizes of the US, DS and *kan*^{R} DNA fragment in the plasmid are indicated by a line above the illustrations and the total sizes of the US, DS and corresponding gene DNA fragments are indicated by a line under the illustrations. The black arrows indicate the primers.

The plasmids pBluescript II KS(+)-Δ*bdlps-kan*^{R} were individually transformed into *Synechocystis* WT. *Synechocystis* is naturally competent, and via homologous recombination foreign DNA can integrated into its genome. The UP and DS region of the BDLPs in the genome are identical with the UP and DS region of the deletion plasmids. That is why, *kan*^{R} can be inserted exactly between the both regions and replace the original gene. *Synechocystis* harbors several identical copies of its gDNA , and thus several copies of each gene (Labarre et al., 1989). To select only the clones that had taken up the *kan*^{R} and thereby replaced the *bdlp* genes, Kanamycin had

to be added. Furthermore, to replace every gene copy, it was necessary to increase the selection pressure by increasing the concentration of kanamycin. After the transformation, the strains were grown on agarose plates containing increasing kanamycin concentration of up to 200 µg/ml to obtain a fully segregated strain individually. Clones were transferred from the plate in liquid cultures, and the gDNA were extracted. Afterwards it was checked whether the genes were fully segregated or not via PCR using the US forward primer and the DS reverse primer of the respective genes. In case of a fully segregated strain, the *kan*^{R} with the US and DS region (1200 bp + 400 bp = 1600 bp) are amplified. In case of a non-full segregation, the corresponding gene and the US and DS region (gene bp +400 bp) are amplified. The amplified genomic region of each mutant strain was loaded on an agarose gel and stained with EtBr. As a control, the gDNA of *Synechocystis* WT was also amplified using the US forward primer and the DS reverse primer of the respective genes. Figure 32 shows an agarose gel loaded with the PCR products obtained by amplification of the *Synechocystis* mutant strains Δ*slr0179*, Δ*slr0869*, Δ*slr1462*, Δ*sll0503*, and Δ*sll0804*. In addition, the restriction digested PCR products of Δ*sll0503* were loaded (marked with a star).

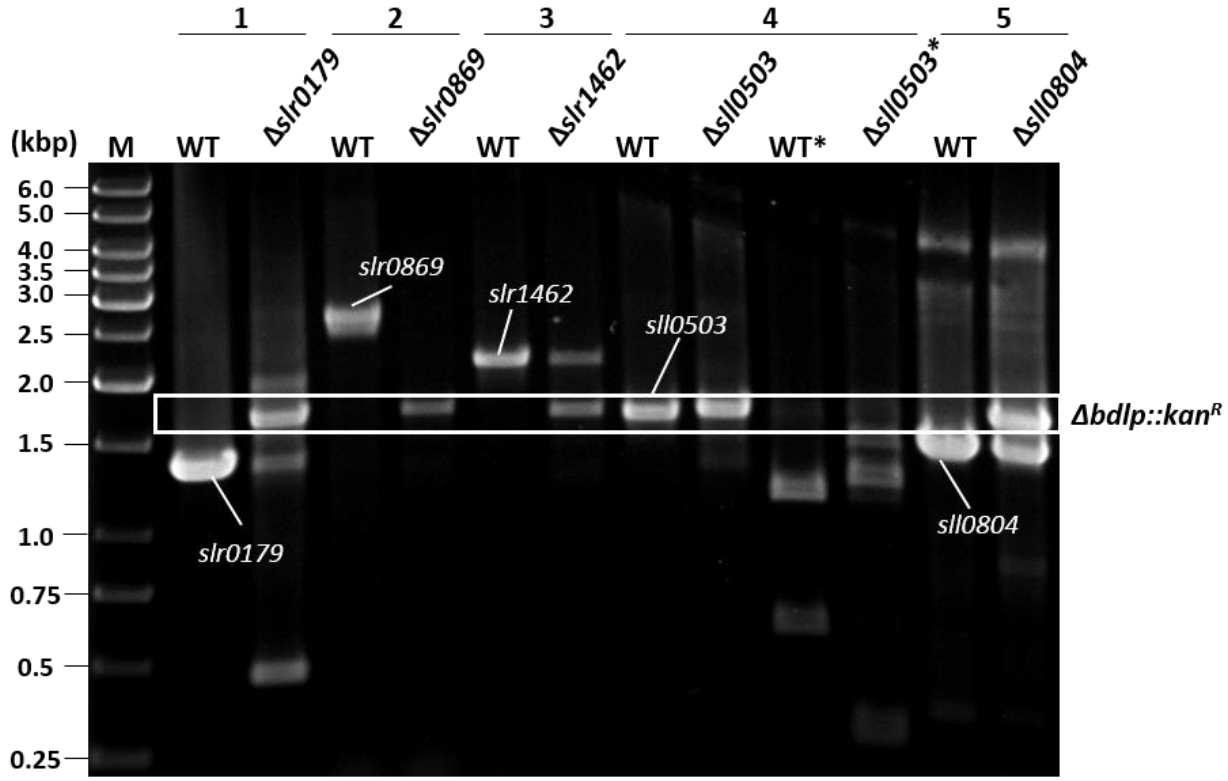

Figure 32: Agarose gel showing the PCR products of *Synechocystis* WT and five mutant strains to test fully segregation of the five different *bdlps*. The numbers 1 to 5 indicate different primer sets that were used to amplify the DNA between the upstream and downstream region of the *bdlp* genes in the *Synechocystis* WT (WT) strain or in the mutant strains (Δ*slr0179*, Δ*slr0869*, Δ*slr1462*, Δ*sll0503* and Δ*sll0804)*. In addition, the amplified PCR products of the primer set 4 were restriction digested with EcoRI (4*). The whit box highlights the total size (ca. 1600 bp) of the kanamycin resistance cassette and the US/DS regions. M: marker; *Δbdlp::kan*^{R}: *bdlp* gene replaced by an kanamycin resistance gene.

The PCR products of all five mutant strains show a band at the size of the resistance cassette at approx. 1600 bp in the agarose gel (Figure 32, white box). Using the gDNA of the mutant strains Δ*slr0179*, Δ*slr1462* and Δ*sll0804* the amplification resulted in a second DNA fragment corresponding to the respective gene sizes, revealing a non-fully gene segregation. In case of Δ*sll0503,* it is not possible to identify whether the gene or *kan*^{R} including the US and DS regions were amplified, because the size of both fragments is nearly the same. Thus, the amplified gene fragments were restriction digested by EcoRI to get a unique DNA fragment fingerprint. Theoretical, a single EcoRI side in the WT PCR product should yield two DNA fragments of 1071 bp and 523 bp, and two EcoRI sides in the *Δsll0503* PCR product should yield in three DNA fragments of 1180 bp, 232 bp and 221 bp. Indeed, these fragments can be found in the WT* lane and in the Δ*sll0503** lane. But in addition, in case of Δ*sll0503** another fragment at approx. 1600 bp can be

observed, which the origin of is mysterious. However, no fragments of the WT digested can be seen, indicating full segregation. Additionally, the results are summed up in Table 19.

Table 19: Summary of theoretical and observed size of PCR product to verify that the genes are partially or fully deleted. The star marks the PCR products, which were restriction digested with EcoRI.

No.	Primer	gDNA	Theoretical size (bp)	Observed size (bp)	Result
1	fPstIslr0179up	WT	1474	~1400	**Partial**
	rXbaIslr0179down	Δ*sll0179*	1628	~1400 and ~1600	**deletion**
2	fHindIIIslr0869up	WT	2641	~2600	**Full**
	rBamHIslr0869down	Δ*syndlp*	1664	~1600	**deletion**
3	fPstIslr1462up	WT	2086	~2100	**Partial**
	rXbaIslr1462down	Δ*slr1462*	1628	~2100 and ~1600	**deletion**
4	fHindIIIsll0503up	WT	1626	~1600	**Full**
		Δ*sll0503*	1623	~1600	
	rXbaIsll0503down	WT*	1071 and 523	~1100 and ~550	**deletion**
		Δ*sll0503**	1180, 232 and 221	~1200 and ~260	
5	fPstIsll0804up	WT	1409	~1400	**Partial**
	rXbaIsll0804down	Δ*sll0804*	1689	~1400 and ~1600	**deletion**

The PCR analysis indicates that solely Δ*syndlp and Δsll0503* are fully segregated. In contrast, Δ*slr0179*, Δ*slr1462* and Δ*sll0804* are not fully segregated, since *bdlp* genes could not be replaced by *kan*^{R} in every gene copy. Thus, the results show a complete deletion of Δ*syndlp* (Δ*slr0869*) and Δ*sll0503*, whereas the other three genes are not fully deleted, e.g. "just" depleted. In the end, this result suggests that the genes *slr0179*, *slr1462*, and *sll0804* are essential for *Synechocystis* at least under the chosen growth conditions.

4.8.2 In vivo characterization of a Δsyndlp knock out strain

The main protein of this study is SynDLP and consequently, the in *vivo* characterizations are focused on the *Synechocystis* mutant strain Δ*syndlp*, where the gene of SynDLP was replaced by a kanamycin resistance cassette. In the next chapters, the phenotype of the *Δsyndlp* mutant is discussed. All *in vivo* experiments were always performed with the *Synechocystis* WT strain for comparison.

4.8.2.1 Deletion of SynDLP does not influence the growth rate

Because (B)DLPs are usually involved in diverse membrane remodeling processes, it might be possible that absence of SynDLP influences the growth of *Synechocystis*. However, as can been seen in Figure 33 A, the growth of the mutant is not impaired under normal liquid growth conditions (BG11, 5 mM glucose at 30 °C) when compared to the WT strain.

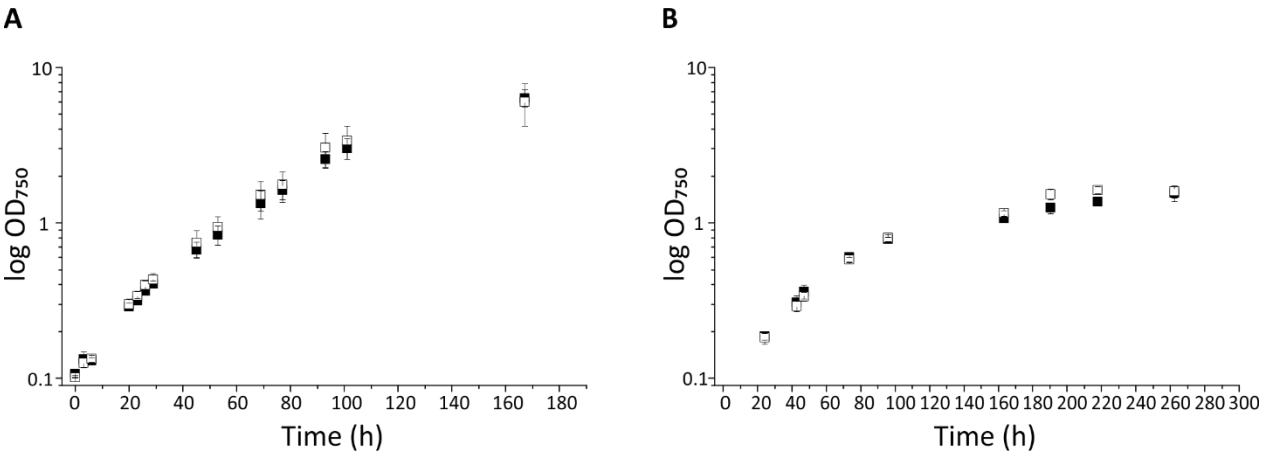

Figure 33: *Synechocystis* growth measured under normal cultivation conditions and phosphate depletion. The OD_{750} was set to 0.1 (A) and 0.2 (B) and observed for 7 days (A) or 11 days (B). Filled squares: WT; empty squares: *Δsyndlp*. The error bars indicate the standard derivation of at least three independent experiments**.**

Thus, I searched literature for conditions, which offered the transcription of *syndlp*. Kopf et al. suggested an upregulation of *syndlp* transcription under phosphate depletion (Kopf et al., 2014). Consequently, the WT and *Δsyndlp* strain were diluted in phosphate free BG-11. As under standard growth conditions, the growth of the WT and the mutant strain do not differ (Figure 33 B) under phosphate depletion. The overall slower growth rates are likely due to phosphate starvation.

However, more recently it was shown that transcription of *syndlp* (*slr0869*) might be regulated by an antisense RNA (asRNA) (Hu et al., 2017). The expression of the asRNA is halved under highlight conditions. Simultaneously, the transcription of *syndlp* mRNA is doubled (Hu et al., 2017). With that information, the influence of high light (24 h, 1200 µE) conditions on the growth rates was tested. For these experiments, the strains were cultivated in gas flasks, bubbled with CO_2 (2 %) enriched air. At the beginning, all four cultures (2x WT and 2x Δ*syndlp*) grew under NL conditions.

After 2 days, they were diluted to an OD_{750} of 0.5 and one culture of each strain (1x WT and 1x Δ*syndlp*) was cultivated under HL conditions for 24 h.

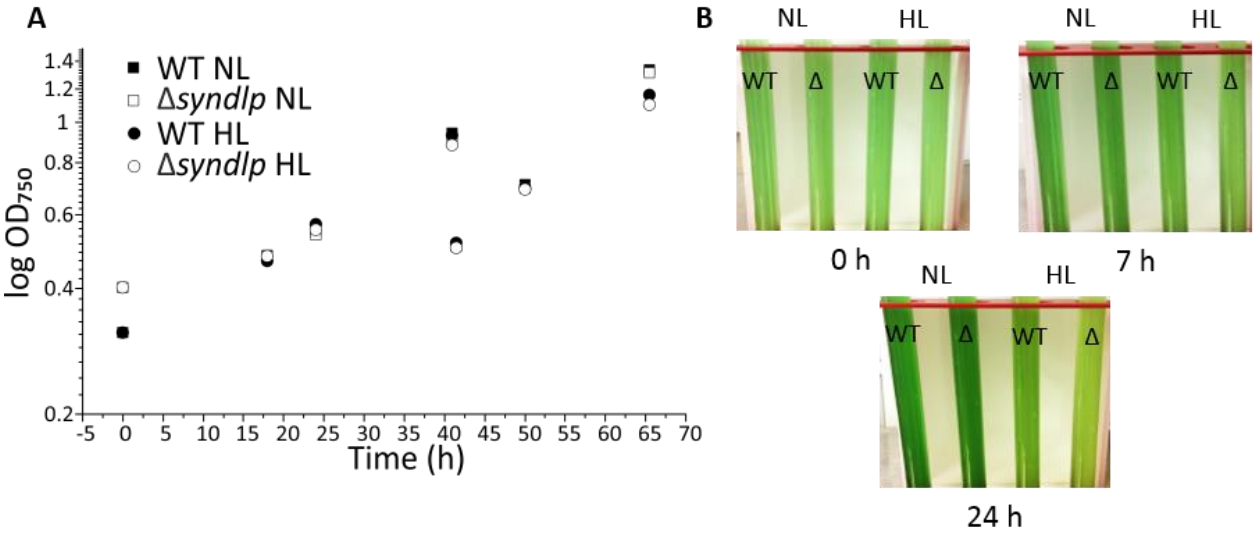

Figure 34: Influence of high light conditions on the *Synechocystis* WT and Δ*syndlp* mutant strains. Two WT cultures and two Δ*syndlp* cultures were grown under NL conditions for 40 h. After 40 h, one WT culture and one Δ*syndlp* culture were exposed to HL for 24 h. The OD_{750} (A) and the appearance (B) for all four cultivating conditions were determined.

As can been seen in Figure 34 A, the growth rate was not influenced by the high light treatment. The culture growth rate of the mutant strain and the WT strain is nearly the same. In contrast, after 24 h under HL conditions, the mutant strain appeared to be less greenish than the WT strain (Figure 34 B). To quantify this observation, the chlorophyll a concentration (c_{Chla}) and the OD_{750} were determined. After setting the c_{Chla} to 3.5 µg/ml, also the number of cells was counted and the number of chlorophyll molecules was (N_{Chla}) calculated.

Table 20: Summary of parameters characterizing the appearance of *Synechocystis* WT and Δ*syndlp* mutant strain.

	c_{Chla} (µg/ml)	OD_{750}	N_{Cells} ($x10^5$)	N_{Chla}/N_{Cell} ($x10^{12}$)	c_{Chla}/OD_{750}
WT NL	2.7 ± 0.7	1.1 ± 0.1	1.5 ± 0.2	1.5 ± 0.2	2.4 ± 0.4
***Δsyndlp* NL**	2.3 ± 0.8	1.1 ± 0.2	1.1 ± 0.3	2.3 ± 0.8	2.0 ± 0.4
WT HL	1.3 ± 0.2	1.0 ± 0.1	2.4 ± 0.8	1.0 ± 0.3	1.3 ± 0.2
***Δsyndlp* HL**	1.0 ± 0.2	0.9 ± 0.2	1.7 ± 0.7	1.5 ± 0.6	1.0 ± 0.1

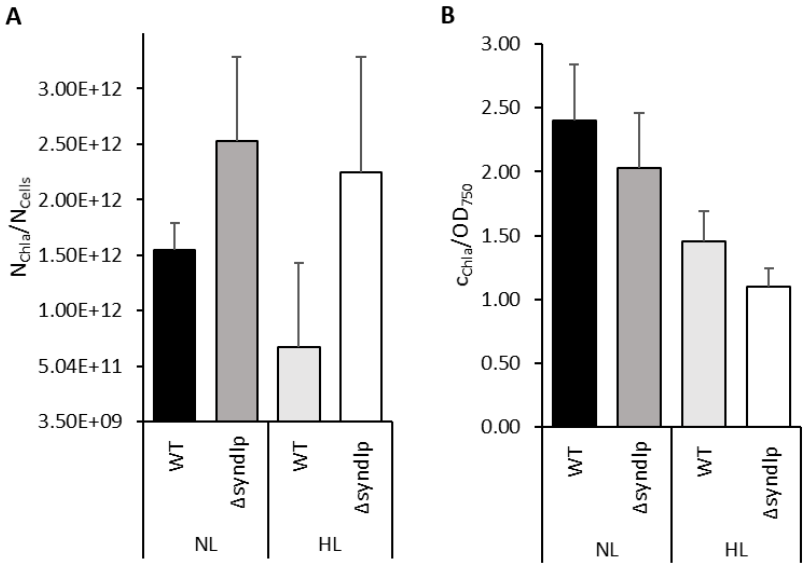

Figure 35:The chlorophyll a content of *Synechocystis* WT and Δ*syndlp* mutant strains. The number of molecules (N_{Chla}) per number of cells (N_{cells}) (A) and the chlorophyll a concentration (c_{Chla}) per OD_{750} (B). The N_{Chla}/ N_{cells} and c_{Chla}/ OD_{750} of WT NL, Δ*syndlp* NL, WT NL and Δ*syndlp* HL are colored black, dark grey, light grey and white, respectively. The error bars indicate the standard derivation of at least three independent experiments.

The chlorophyll a concentration of *Synechocystis* Δ*syndlp* is reduced when compared to the WT strain, while the OD is nearly the same. Moreover, at an identical chlorophyll a concentration the number of mutant cells is lower when compared to the WT. Consequently, and as can been seen in Figure 35 A the number of chlorophyll molecules per cell is higher in case of the mutant strain, but chlorophyll a concentration per OD is lower, under both growth conditions (Figure 35 B).

4.8.2.2 The pigment content and ratio

To determine the relative pigment content in the *Synechocystis* Δ*syndlp* mutant and WT, absorption spectra of whole *Synechocystis* cells were performed. *Synechocystis* absorption spectra have characteristics due the presence of the antenna pigment-protein phycocyanin (PhyC), carotenoids (Car) and chlorophyll a (Chla). All cultures were diluted to the same number of cells and the absorption were measured from 350 nm to 800 nm, using an integrated sphere to reduce light scattering. All spectra are characterized by four major absorption peaks. Chlorophyll a has its two characteristic absorption maxima around 440 and 680 nm, the carotenoids around 490 nm and phycocyanin (PhyC) around 625 nm (Figure 36 A). By comparing WT NL absorption with Δ*syndlp* NL absorption, the absorption level is slightly decreased, alike the phycocyanin to chlorophyll a ratio (PhyC/Chla) and the carotenoid to chlorophyll a ratio (Car/Chla)

do not change significantly (Figure 36 B). In contrast, both HL grown strains show an increased PhyC/Chla and Car/Chla ratio, but again, between the WT and the mutant no significant differences can be observed. Noteworthy, the overall absorption level of the mutant strains is reduced, although the pigment ratio is not influenced.

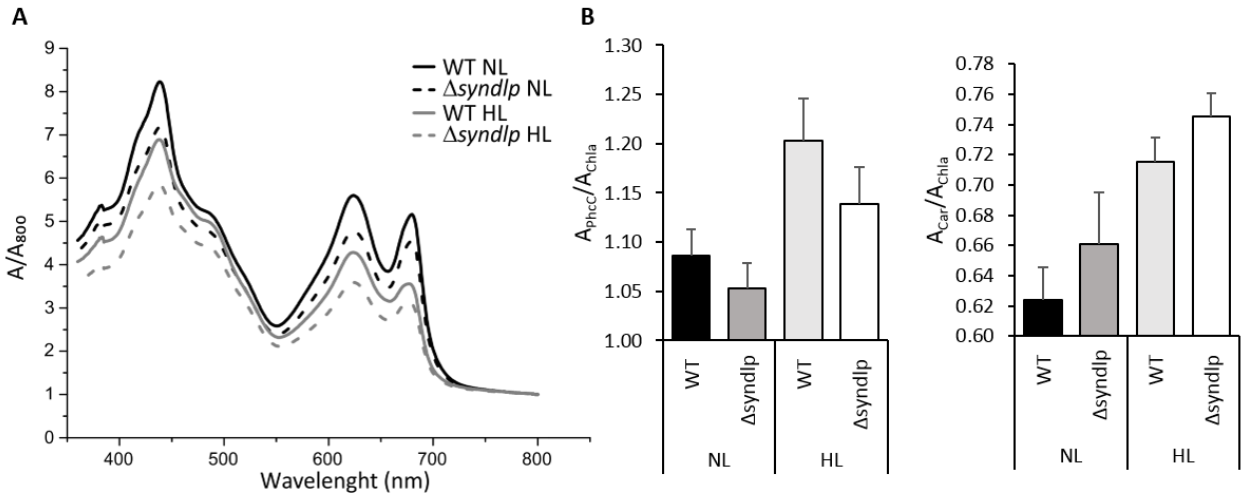

Figure 36: Pigment content of *Synechocystis* WT and *Δsyndlp* strains. (A) Averaged absorption spectra of three independent experiments under normal light (NL) or high light (HL) conditions. All spectra were normalized to A_{800}. WT NL, Δ*syndlp* NL, WT NL and Δ*syndlp* HL are colored black, dark grey, grey and light grey, respectively. The spectra were utilized to calculate the pigment ratio. The error bars indicate the standard derivation of at least three independent experiments (B). PhyC: phycocyanin; Chla: chlorophyll a; Car: carotenoids

4.8.2.3 The Δsyndlp mutant strain has an impaired oxygen production

The production of oxygen is an indicator for the photosynthetic activity of cyanobacteria cells and thus was measured using dark adapted strains (WT and Δ*syndlp*, NL and HL) in the presence of $NaHCO_3$ (CO_2 is not limited and the whole photosynthetic chain is involved) or PPBQ (accepts electrons directly from PSII and the PSII activity is not limited by the PQ pool). Figure 37 shows the oxygen production per an hour normalized to the chlorophyll concentration.

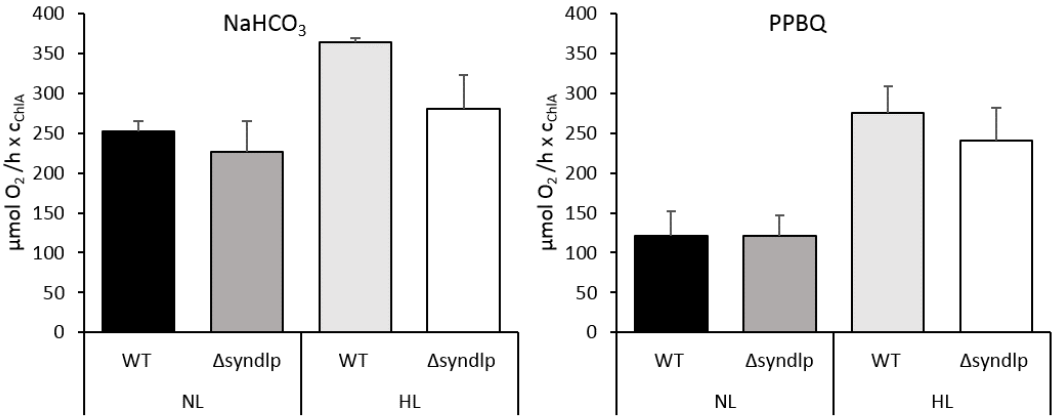

Figure 37: Oxygen evolution of *Synechocystis* WT and *Δsyndlp* strains. The oxygen evolution in the presence $NaHCO_3$ (CO_2 saturation) and PPBQ (only PSII activity) per hour and normalized to the Chla concentration. The error bars indicate the standard derivation of at least three independent experiments.

Altogether, the oxygen production level is higher under HL conditions than under NL conditions. In presence of $NaHCO_3$, the oxygen production of Δ*syndlp* HL is reduced compared to the WT HL. Whereas, under NL conditions and in the presence of PPBQ no differences were observed.

4.8.2.4 Determination of the PSI to PSII ration

By the previous experiments it was shown that the chlorophyll content differs in the mutant strain in comparison to the WT strain. 80 % to 85 % of the chlorophyll is associated at PSI in *Synechocystis* and thus a reduced pigment content indicates a reduced PSI content (Shen et al., 1993). To test this assumption, 77 K fluorescence spectra were recorded. While exciting chlorophyll at 435 nm information about the relative PSI to PSII stoichiometry can be obtained. PSII has two fluorescence emission maxima at 684 nm and 693 nm, and PSI has one emission maximum at 721 nm. Typical spectra are shown in Figure 38 A.

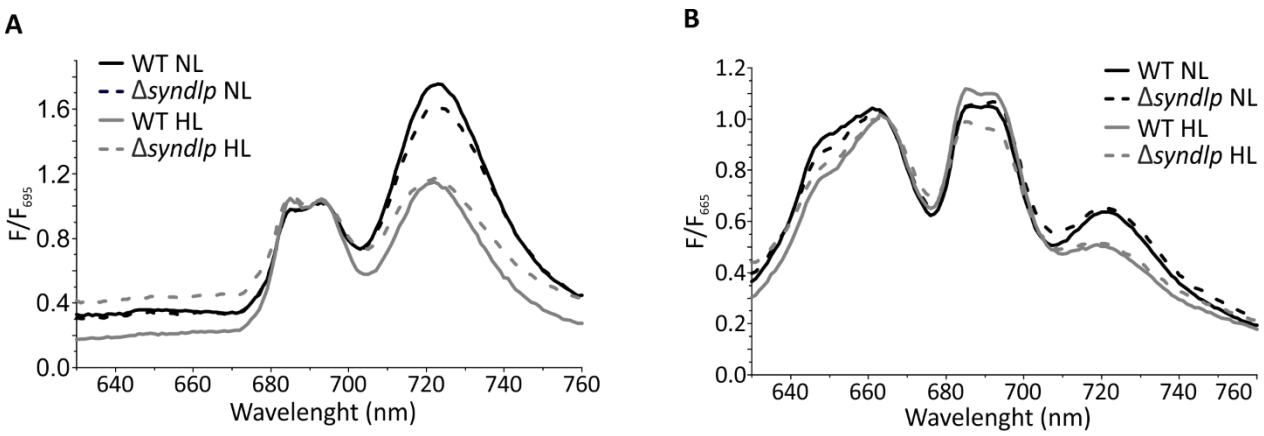

Figure 38: 77 K fluorescence emission spectra of *Synechocystis* WT and *Δsyndlp* strains to determine the PSI/PSII ratio and the energy transfer from the phycobilisomes to PSI and PSII. Chlorophyll can be excited at 435 nm to obtain the and the emission spectra are normalized at 695 nm (A). In (B) the phycobilisomes are excited at 580 nm and the emission spectra are normalized to 665 nm (B). All spectra represent the average of three independent measurements.

The fluorescence emission spectra of *Synechocystis* WT and Δ*syndlp* are very similar after the exaction of chlorophyll. Under NL conditions, the PSI to PSII ratio is on the PSI side and under HL conditions both strains show a reduced PSI to PSII ratio compared to the PSI/PSII under NL conditions, as can be seen by the decreased PSI peak at 725 nm. Moreover, Δ*syndlp* NL has a slightly decrease PSI/PSII ratio, as the PSI peak is lower than the PSI peak of the WT NL. In a second experiment (Figure 38 B), the phycobilisomes were exited at 580 nm and the energy transfer from the phycobilisomes to PSI and PSII, can be quantified. While comparing the WT NL with the mutant NL strains, the energy transfer to PSI (emission at 720 nm) is similar. Under HL conditions, the energy transfer to PSI is decreased, indicated by the decrease emission peak at 720 nm in both cases. The energy transfer from the phycobilisomes to PSII is visible by the PSII emission at 693 nm. The mutant NL energy transfer is not different when compare to the WT NL strain. In contrast, the mutant strain grown under HL conditions shows a slightly reduced energy transfer to the PSII, indicated by a declined PSII emission.

4.8.2.5 Determination of the PSII activity

The oxygen production of Δ*syndlp* is reduced when compared to the WT under HL conditions and in the presence of $NaHCO_3$ (see Figure 37). To get a more detailed view on the activity of PSII, PSII was tested by using pulse amplitude modulated fluorescence spectroscopy (PAM). PAM fluorescence spectrometers are specialized instrument to investigate the photosynthetic activity

of plants, algae or cyanobacteria. In dark-light induction curves, alternating light pulses are applied to determine the maximal activity of PSII. Therefore, *Synechocystis* cells were first dark adapted, which stops the photosynthetic activity. A very weak measuring light, which cannot trigger the light reaction, was used to monitor the background fluorescence level (**F_0**). The PSII reaction centers are open and photochemical quenching (q_p, energy transfer to the electron transport chain) is maximal, whereas the non-photochemical quenching (q_N, energy levy by other processes e.g. heat release) is minimal. The first saturated light pulse (SP) reduces PSII completely, all PSII reaction centers are closed, and the maximal fluorescence of PSII in the dark (**F_m**) is measured. After 40 s, actinic light was switched on to ensure the full re-oxidation of PSII, and the background fluorescence upon actinic light was measured (**F_0'**). Then, SPs were given every 20 s twelve times to measure the maximal fluorescence after illumination (**F_m'**). From the measured parameters, maximal photosynthetic activity (F_v/F_m) and the effective photosynthetic activity (F_v'/F_m') were calculated using equation (14) and (13), respectively.

Figure 39 A shows typical dark-light induction curves from the cells. All four curves have a similar shape. After the first SP and the following dark phase, actinic light was switched on, followed by an immediate increase of F_0 to F_0'. The increase in the background fluorescence might be due to phycobilisome fluorescence emission, which was also excited. F_m' and F_0' slightly increases up to the 3rd or 4th SP, and afterwards both parameters decrease over time, albeit the difference between F_0' and F_m' remain nearly constant. The decline of F_m' and $F_0'$and can be explained e.g. by non-photochemical quenching processes. However, the course of the curves is very similar for WT NL, Δ*syndlp* NL and WT HL strains. In contrast, the strain Δ*syndlp* HL shows significant lower differences between F_0' and F_m'. Moreover, in Figure 39 B it is revealed that F_v/F_m and F_v'/F_m' is also affected, as the mutant strains under NL and HL conditions are significantly reduced compared to the WT strains under NL and HL conditions. This reveals that the maximal and effective PSII activity of the mutant strains Δ*syndlp* NL and Δ*syndlp* HL is significantly reduced when compared to WT NL and HL, respectively.

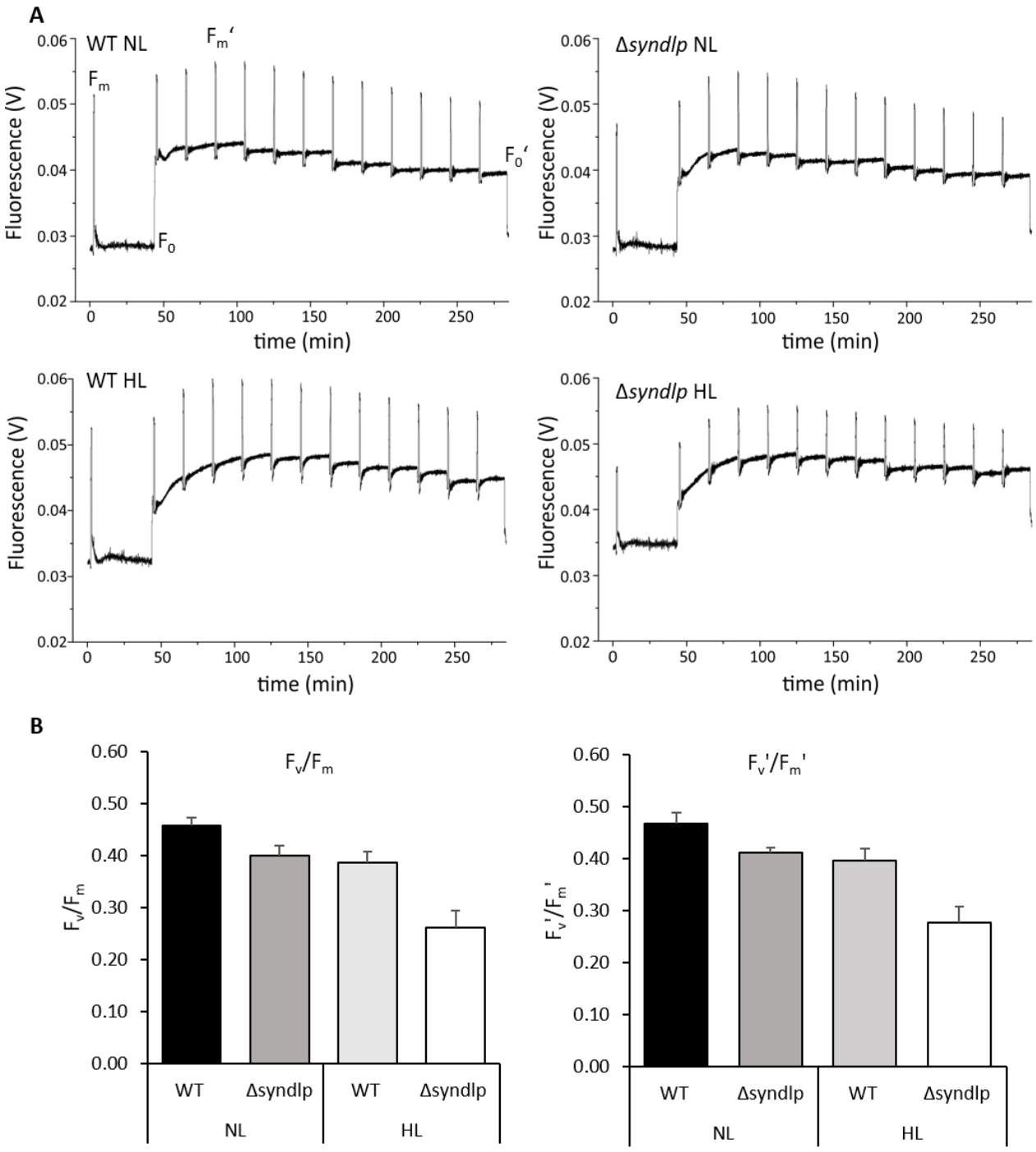

Figure 39:Dark-light induction curves to determine the PSII activity of *Synechocystis* WT and Δ*syndlp* strains. The dark-light induction curves are the average of three independent measurements for the WT and mutant strains under NL and HL growth conditions. One peak is the result of one saturation light pulse (A). In (B) F_v/F_m describes the maximum photochemical activity and F_v'/F_m' the effective photochemical activity of PSII. F_m: maximal fluorescence; F_o: Background fluorescence; F_0': Background fluorescence (light); F_m': maximal fluorescence light

4.8.2.6 P700 re-reduction kinetics

Electrons from PSII reduce the PQ pool. However, especially in cyanobacteria the PQ pool is also reduced by the cyclic electron flow (CEF) and other processes (Bernát et al., 2009). The reduced PQ pool is then used as reductive power by the PSI. Thus, information about the redox state of the PQ pool can be obtained by measuring the PSI re-reduction time. Different inhibitors can block the electron transfer. DCMU (3-(3,4-Dichlorophenyl)-1,1-dimethylurea) inhibits electron flow from PSII to PQ, whereas Paraquat (1,1'-Dimethyl-4,4'-bipyridinium dichloride) inhibits the cycle electron flow (Fan et al., 2007; Huber and Edwards, 1975; Yu et al., 1993).

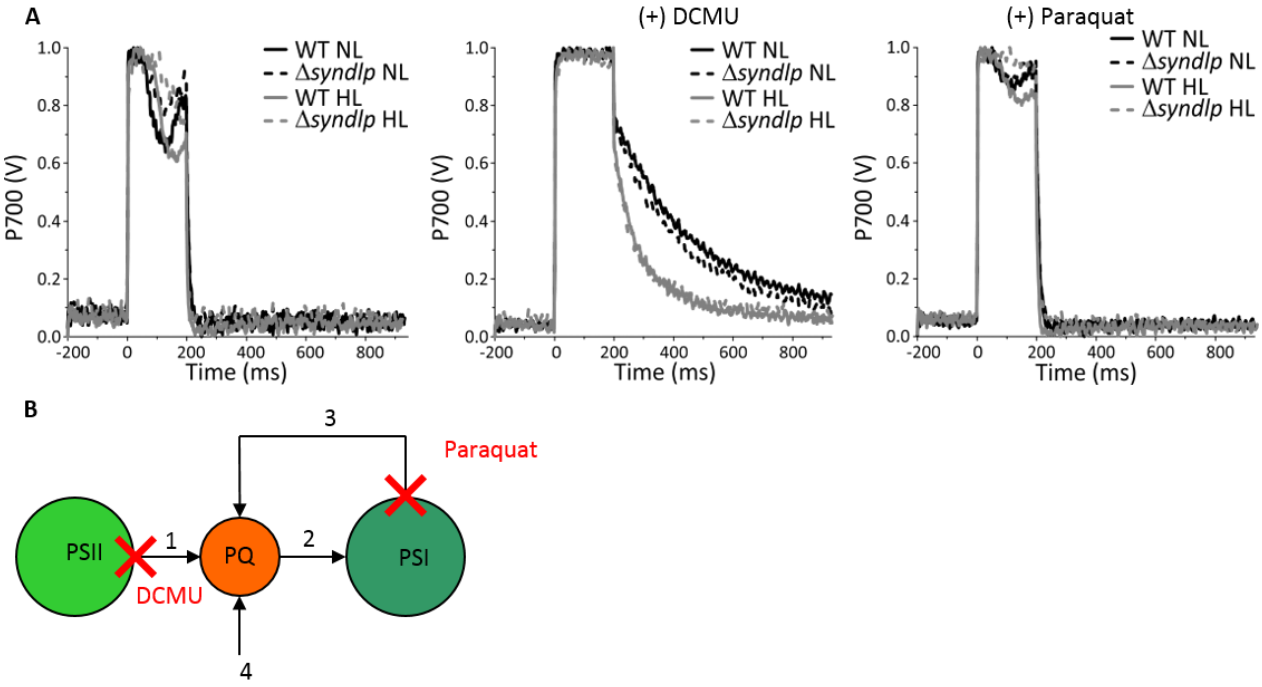

Figure 40: P700 re-reduction curves of *Synechocystis* WT and the Δ*syndlp* mutant in presence of DCMU and Paraquat. The re-reduction curves were recorded in absence of additives, in the presence of DCMU and in the presence of Paraquat (A). (B) The electrons can linear flow to PSI from PSII via PQ (1) to PSI (2) or about the cyclic electron flow back to the PQ (3) as well as directly to the PQ via other processes (4). The electrons from the PSII are directly transferred to DCMU and cannot reach the PQ pool, which blocks the linear electron flow (route 1). Paraquat inhibits the PQ reduction by the cyclic electron flow (route 3), since it is PSI electron acceptor.

When a saturation light was turned on (time 0 ms to 200 ms on Figure 40), P700 was fully oxidized (P700*). Oxidized P700 has a strong absorbance peak at around 820 nm. After a short delay time, P700* was re-reduced by electrons from the electron transport chain. This was observed by an absorption decay back to the original level. Typical curves of all four cultures are shown in Figure

40, in absence and in presence of DCMU or Paraquat. By comparing the P700 re-reduction kinetics, no differences between the WT and mutant strains was detectable, in any cases. The significantly slower re-reduction in presence of DCMU, indicates a more oxidized electron transport chain without the linear electron flow. However, in case of the both HL strains (+DCMU) the re-reduction is faster, revealing a more reduced electron transport chain compared to NL conditions. In no cases (without additives and in the presence of DCMU or Paraquat) could a difference be observed between the WT strain and the mutant strain, revealing that it is not very likely that SynDLP has direct impact on the cyclic or linear electron flow.

5. Discussion

5.1 Potential DLPs in cyanobacteria

(B)DLPs were identified or at least predicted in eukaryotes, over bacteria and archaea and even in one virus (Pfam entry: PF00350) (Finn et al., 2014; Van Der Bliek, 1999). Remarkable, only four BDLPs DynA/DynB (*S. venezuelae*), LeoA (*E. coli*), DynA (*B. subtilis*) and NosDLP (*N. punctiforme*) were extensively studied (Bürmann et al., 2011; Low and Löwe, 2006; Michie et al., 2014; Schlimpert et al., 2017), although in the Pfam database (PF00350) 1932 sequences with the dynamin specific "Dynamin-N" domain in prokaryotes are predicted. This domain corresponds to the dynamin specific GTPase domain. A particularly large number of such proteins was identified in cyanobacteria: In 56 species, 121 sequences are predicted as potential DLPs, which we could categorized in several different clades via phylogenetic analysis (Figure 11) (Jilly et al., 2018). The thus far only analyzed cBDLP, NosDLP, is a representative of the Tandem B group and was suggested to remodel membranes, *in vitro* (Low and Löwe, 2006). Thus, it might be reasonable to assume, that also the other members of the Tandem B group remodel membranes. Subsequent, cBDLPs of the other clades might be involved in other processes at membranes. Such activities might involve membrane repair/protection (Sawant et al., 2016), vesicle release (Michie et al., 2014) and/or cytokinesis (Schlimpert et al., 2017). The cytokinesis is a process in cell division in which the cell cytoplasm is divided. In addition, it should be mentioned that in (http://www.kazusa.or.jp./cyanobase/, version 2014), also FZO-like cBDLPs were identified and FZL, the FZO homolog of *Arabidopsis*, was directly linked to TM biogenesis (Gao et al., 2006). However, based on the previously described properties of (B)DLPs, potential functions in cyanobacteria can be suggested, as summarized in Figure 41 (Jilly et al., 2018).

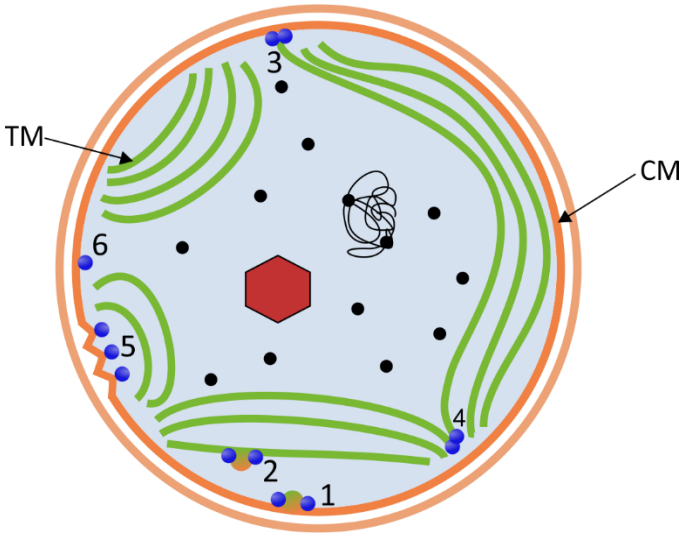

Figure 41: Potential functions of cBDLPs in cyanobacteria membrane dynamics. cBDLPs might be involved in the release or fusion of vesicles to the CM (1) or TMs (2), in the fusion/constriction of CM and TM (3) or in the fusion/constriction of TM layers (4). In addition, they may help to repair (5) and protect membranes (6). These figure is adapted and modified from Jilly et al. (Jilly et al., 2018).

In this work, the role of *Synechocystis* BDLPs for TM biogenesis was investigated. In detail, the genome of *Synechocystis* contains 5 potential DLPs, two of which are predicted to be homologues to dynamin (Slr0179 and SynDLP) and three are FZO-like (Slr1462, Sll0503 and Sll0804). However, since the purification and activity test were only successful for SynDLP, I will mainly focus on SynDLP in the discussion.

At the beginning the overall structure of SynDLP should be compared with the prototypical DLPs. The average number of amino acids of the previously described (B)DLPs is about 700. SynDLP has 812 aa and is thus perfectly in a line with the typical size of dynamin (830 aa), FZL (855 aa) and OPA1 (847 aa). Consequently, much of the sequence is free to harbor another domain besides the G domain, such as the middle domain, which has also around 300 aa. Moreover, SynDLP could be categorized being within the KGK clade and thus three KGK proteins are encoded downstream (Figure 11) (Jilly et al., 2018). KGK domain containing proteins are not characterized so far (Finn et al., 2017). However, underlined by an analysis of the *Synechocystis* transcriptome (Kopf et al., 2014), it is likely that SynDLP is expressed together with the KGK proteins. The gene *slr0869* (the gene of SynDLP) belongs to the transcription unit TU1409, together with the genes of the three potential KGK proteins and one gene encoding a hypothetical protein (Slr0872), which shows sequence homology to LptC (lipopolysaccharide export system protein) (Kopf et al., 2014). As the

name suggests LptC is involved in the export of lipopolysaccharides (LPS) from the inner membrane to the outer *E. coli* membrane in (Tran et al., 2010). In this previous analysis SynDLP seems to have clear BDLP characteristics based on the predicted domain structure and bioinformatic studies. The other four candidates need to be further analyzed, as the high diversity in the DLP family suggests that they also have some DLP properties.

5.2 SynDLP can be expressed and purified

In order to analyze the structure and activity of BDLPs, the proteins were first aimed to express and purify. A common and well-established method is the expression in *E. coli*, which was also often used for (B)DLPs (Gao et al., 2010; Low and Löwe, 2006; Reubold et al., 2015). After a successful cloning the gene individually into a plasmid, different expression conditions were tested. It was shown, that the proteins were expressed to different extents. Under the tested expression conditions, Slr0179 was expressed in high amount, but nearly exclusively in inclusion bodies (Figure 14). Inclusion bodies are misfolded proteins, which form aggregates. To reduce the amount of aggregates and express Slr0179 in the cytoplasm several different *E. coli* strains were tested. In the literature, several ways to refold denatured proteins from inclusion bodies are described (Alibolandi and Mirzahoseini, 2011; Singh and Panda, 2005). Nevertheless, I decided not to use these methods. Since no similar protein exists to compare the refolded protein with, it would never be clear if Slr0179 is 100 % correctly folded or not. Beside occurrence in inclusion bodies, Slr0179 was also expressed in the membrane fraction, as was the case for Sll0804 and Slr1462, which have predicted transmembrane domains. In addition, the presence of Slr0179 in the membrane fraction, revealing that Slr0179 is a membrane associated proteins. Solubilization of Slr0179 from membranes was not successful, since the amount of protein was always too low for further downstream applications. Sll0804 could be solubilized by DDM and Slr1462 by DDAO. The solubilized proteins were subsequent purified via Ni-NTA affinity chromatography. However, the elution fractions of the Ni-NTA purification of Slr1462 and Sll0804 remained contaminated by several other proteins (Figure 18). Thus, a SEC step was added as a further purification step. Slr1462 was successfully be purified with this additional step, but the purification of Sll0804 was

still insufficient. One reason for this might be the low expression level and a potentially in the protein enclosed His-Tag. For Slr0179 and Sll0804 more optimizations (e.g. cell free expression) are necessary to obtain sufficient pure protein. In contrast to that, SynDLP and its CxxxA mutants were finally purified in a single step (Figure 17). The conditions crucial for expression and purification were established within several experiments. The expression at 20 °C O/N increased the amount of soluble protein and the use of the Rosetta-gami™ 2 *E. coli* expression strain helped to reduce unfolded proteins (Betz, 1993). The following Ni^{2+} affinity chromatography was optimized to obtain almost pure protein. Finally, 0.75 mg to 1 mg SynDLP per liter of cell culture were obtained having purity of 98 % based on SDS-PAGE analysis. A cleavage of the His-Tag was not performed, assuming that the relative small size of the 6x His-Tag in comparison to the protein size does not influence behavior of the protein (Kimple et al., 2013).

5.3 SynDLP is a bacterial DLP

As described in chapter 1.4, (B)DLPs share common features. As discussed below in detail, in this thesis, SynDLP was shown to be most likely a BDLP. The other potential candidates could not be further investigated, because the purification was insufficient (Slr0179 and Sll0804) or the purified protein did not show any GTPase activity (Slr1462) under the chosen conditions (Figure 18 and Figure 26). However, this does not exclude that they are BDLPs or have some BDLP properties, but that must be further analyzed.

SynDLP shows structural elements, which are very common for (B)DLPs: The GTPase domain that harbors the cyanobacterial extended P-loop and the G2 to G4 motifs can be found. Beside the typical GTPase domain, a predicted region in the amino acid sequence could be identified, which exhibits a high hydrophobicity (Figure 19). This domain might be involved in membrane interaction, like the Tip region in LeoA (Michie et al., 2014). But, it should be noted that the localization of the MID of SynDLP must also be confirmed experimentally. The potential MID is flanked by α-helical bundles. α-helical content of SynDLP of approx. 75 % was determined by CD and FTIR spectroscopy (Figure 19). The localization of the other domains (GED and MD), as far as

they exist, and especially the involved aa sequences has to be solved experimentally in further work.

5.3.1 A model for the SynDLP GTPase activity

One key element of (B)DLPs is the GTPase activity. In contrast to DLPs, BDLPs do not show an increased hydrolysis rate in presence of lipids (Bürmann et al., 2011; Low and Löwe, 2006), which is also the case for SynDLP (appendix 7.6.1). Without an inhibitor, the activity of SynDLP follows a classical Michaelis-Menten enzyme kinetic, but in presence of the inhibitor GMPPnP, the enzyme activity changed to a sigmoidal shaped curve, indicating cooperativity or cooperativity-like effects, such as slow conformational changes (Figure 28). This is very uncommon, because a competitive inhibitor would not change the curve shape and cooperative enzymes should also be cooperative without an inhibitor (Nagar et al., 2014). In principle, two models could explain this behavior: The first one assumes binding sites in a protein complex, which are independent from each other (no cooperativity), but a slow transition from a less active to a more active enzyme conformation can result in a cooperativity-like behavior (Ainslie Jr. et al., 1972). The second model assumes cooperativity and a strongly bound inhibitor. Fitting the activities with the slow transition model, revealed an insufficient fit, especially at low substrate concentrations and during the rapid increase to higher activities (appendix 7.6.2) (Ainslie Jr. et al., 1972). The strong increase in the activity cannot be only explained by the substrate concentration squared terms of the numerators and denominators, and at very low substrate concentrations (up to 0.75 mM), the fitted curve increases much stronger as the experimental data suggest. Consequently, a completely new model must be developed to explain this behavior (see Figure 42). At first, a higher oligomeric state of SynDLP is assumed (e.g. 10 units with 10 binding sites), because SEC suggested an oligomer with at least 8 protein monomers. Second, a low K_d of GMPPnP is assumed. In the equilibrium state, nearly all bindings sites are blocked by GMPPnP. This complex has a low activity. At low GTP concentration, GTP can be hydrolyzed at a free binding site (which can always occur in an equilibrium), indicated by a low hydrolysis rate. A conformational change at one binding site, due to GTP hydrolysis, does not influence the overall low activity of the whole complex. As the GTP concentration increases further, the probability increases that a new free binding site is

directly occupied by a GTP and not by a GMPPnP. This situation leads to the nearly hyperbolic behavior of data points up to c_{GTP} = 0.75 mM. At one point (e.g. 5x GMPPnP and 5x GTP are bound), the hydrolysis of GTP releases enough energy to induce a conformational change and the total complex changes to a complex with higher activity. This complex of higher activity, has a lower affinity to GMPPnP and can hydrolyze GTP much faster, which can be observed by a very strong increase of the activity. At high GTP concentrations, the complex of high activity has the same behavior as without inhibitor. A test of this hypothesis might include the development of new kinetic models and GTPase assays with a stronger focus on the effect of different GMPPnP concentrations.

The resulting question is why this cooperativity cannot be observed in the absence of GMPPnP. Here, it is useful to have a look at the curves with focus on the time dependence of the absorption at 340 nm. Before the steady-state phase, an initial phase or lag phase can be observed (Figure 26). With increasing GTP concentrations, these initial phases become more pronounced. GTP induces the formation of a complex of enhanced activity and thus, the activity increases until the steady-state level is reached. Since the initial phase was not used for activity calculation, an impact on the kinetic curve was not given.

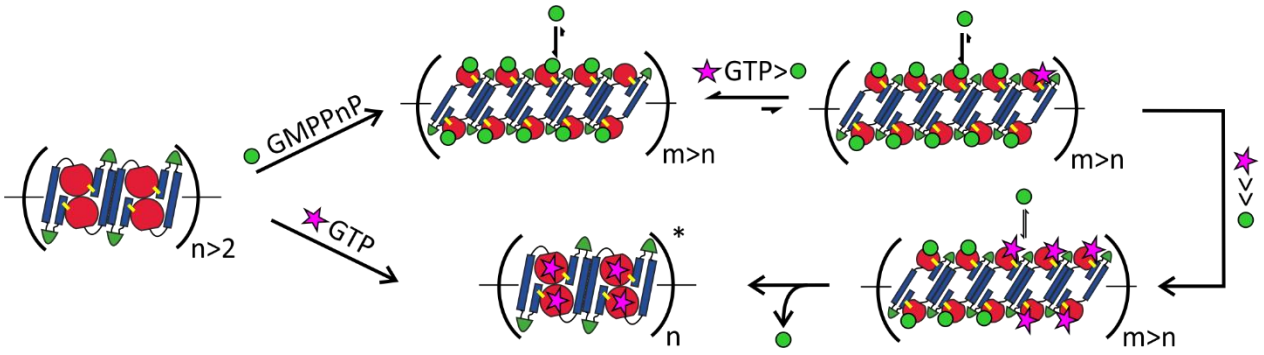

Figure 42: A model to describe the activity of SynDLP. SynDLP WT is linked by disulfide bonds (yellow bars) and is present as an oligomer of at least four dimer units (n>2). Upper route: The addition of GMPPnP (green sphere) increases the oligomeric state (m>n>2) and blocking the binding sites in an equilibrium state, which is subsequent strongly shifted to the GMPPnP-SynDLP complex. At a c_{GTP} slightly higher than c_{GMPPnP} GTP hydrolysis is inhibited, since nearly all binding sides are blocked by GMPPnP. At c_{GTP} several orders of magnitudes higher than c_{GMPPnP}, the chance of GTP occupying a binding side is higher. At one point enough GTP binding and hydrolysis induce a conformational change to a complex of higher activity. Consequently, the activity reaches a level like in the absence of GMPPnP (*). Lower route: the SynDLP oligomer is activated (*) by GTP. n: number of double dimer units (bigger than 2); m: number of oligomer units bigger than n

This model might also explain differences between SynDLP WT and C777A in presence of GMPPnP. Since it was shown before that the WT is a disulfide-linked dimer (Figure 21), it can be speculated that formation of the disulfide bonds induces a conformation, which is more rigid compared to a conformation without disulfide bonds. Thus, higher GTP concentrations are needed to activate the enzyme complex (higher K_m), whereas in case of the mutant the conformation transition is not inhibited by the disulfide bonds (lower K_m) (Figure 28). However, that would not explain the differences in the maximal activity, but it is widely known that the presence or absence of disulfide bonds can influence the activity of enzymes in many ways. (Chang et al., 2003; Trivedi et al., 2009). In chapter 5.6 the influence of the disulfide bond and the differences between disulfide-linked dimer and the non-dimer forming mutant C777A are discussed in more detail. In this chapter a kinetic model is suggested to describe the GTPass activity of SynDLP WT in detail, while uniting cooperativity effects in presence of an inhibitor with non-cooperativity in absence of an inhibitor and including two complexes of different activities.

5.3.2 SynDLP interacts with membranes

The membrane remodeling activity of (B)DLPs is a key feature and was suggested for all (B)DLPs discussed in this thesis (Bian et al., 2011; DeVay et al., 2009; Frezza et al., 2006; Gao et al., 2006, 2010; Low and Löwe, 2006; Mettlen et al., 2009; Nantais et al., 1996; Sawant et al., 2016; Shah et al., 2014; Smirnova et al., 2001). First, Laurdan fluorescence studies with liposomes suggested an interaction of SynDLP specifically with negatively charged lipids (Figure 22). This result might indicate a potential interaction of SynDLP with the TM and CM of *Synechocystis*, as a similar behavior was shown for the protein IM30, which is potentially involved in the TM biogenesis (Hennig et al., 2015). The interaction might be electrostatically controlled, since an interaction with DOPS (1,2-dioleoyl-sn-glycero-3-phospho-L-serine) could also be observed (appendix 7.5). Like DOPG, DOPS is a lipid with a negatively charged headgroup, but it is not a TM lipid. It should be remembered that the buffer used in Laurdan fluorescence spectroscopy studies does not contain any salts. Thus, additional experiments should include variations in the ionic strength to analyze the influence of ions on the membrane interaction properties.

Not only the electrostatic interaction might trigger the membrane interaction of SynDLP, also it is more than likely that for a membrane remodeling process the protein must intercalated into the membrane. The increasing surface pressure (Π) in a Langmuir trough at a DMPG monolayer (ML), indicates that the protein attaches to and/or intercalated into the ML. While adding the protein, the Π increased up to approx. 26 mN/m and remained nearly stable over the whole experiment, indicating a stable ML and an overall stable system. Since SynDLP has been injected in the sub phase, it started to adsorb at the ML. While the surface area remains constant, Π increased as a result of reduced space at the surface (Figure 29) and that indicates a binding of SynDLP at least in between the lipid headgroups. This is also confirmed by SFG spectra with SynDLP at d_{54}-DMPG ML in the CD region (appendix 7.4.4). An increased CD_3/CD_2 ratio (symmetric stretch vibration 2078 cm^{-1} and 2114 cm^{-1}), revealing that binding of SynDLP induces more orientated lipid tails (cartooned in Figure 43) (Franz et al., 2016; Guyot-Sionnest et al., 1987).

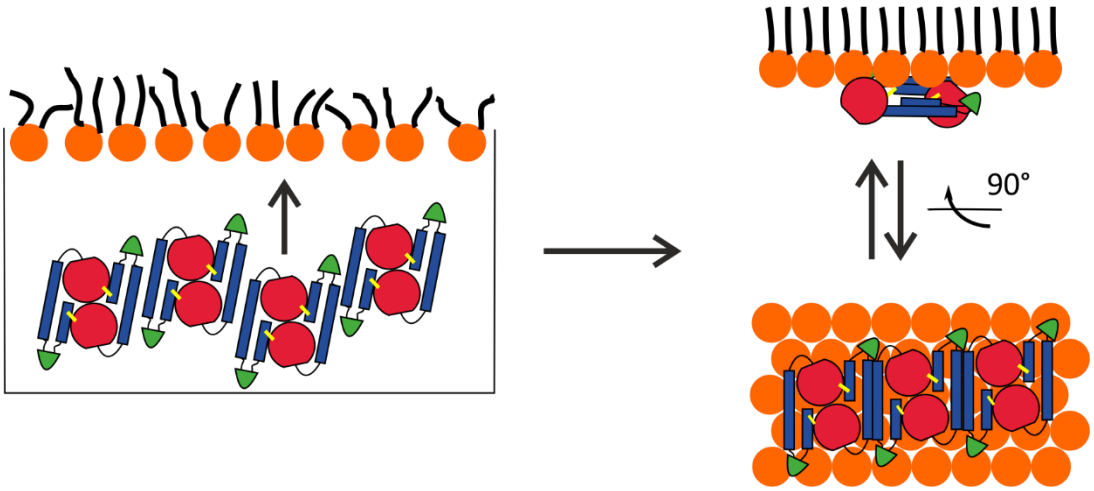

Figure 43: SynDLP orders itself at ML/buffer interface. After the injection, SynDLP starts to arrange at the ML/buffer interface (left panel). This results in an increased ML order and an orientated SynDLP (Θ = 89°)at the interface (right panel).

This raises the question how SynDLP behaves at the ML and how GTP hydrolysis influences the interaction. After addition of SynDLP to the ML, a strong amid I band arises from 1620 cm^{-1} to 1710 cm^{-1}. This strong amid I band indicates the adsorption of SynDLP at the buffer/ML interface in an oriented manner. It should be noted that a signal does not necessarily represent a high order in the protein itself, but a defined orientation between the buffer and the ML (e.g. reviewed here (Fu et al., 2011b)).

Some DLPs display enhanced GTPase activity in the presence of lipids (chapter 1.4.2). Although SynDLP does not exhibit this behavior, a conformational change and/or reorientation is suggested by the SFG experiments. After addition of GTP clear changes became visible. The amide I band decreased, which could be due to two reasons. The protein might desorb from the ML or it might adept another conformation. Although the exact reason for the observed decrease is unknown, it is remarkable that the decrease was not equal amongst all amide I components. While the β-sheet amplitudes were reduced to ca. 87 %, the α-helical amplitude was even halved. That observation would favor the conformation change as a possible explanation. Moreover, it can be speculated that the conformational alteration forces the ML in a more ordered structure (the amplitude growth of C=O is about 18 %), whereas the orientation of the helical bundles changes, which can also influence the SFG signal (Xiao et al., 2012). Noteworthy, the SFG experiments revealed a nucleotide induced structural change. But this do not influence the GTPase activity as it is known from the GTPase assay (4.6). However, the calculated spectra revealed an 89 ° angle of SynDLP with respect to the ML interface (Θ) in presence and in absence of GTP, indicating that the orientation toward the ML did not change during the GTP hydrolysis.

As it was mentioned before, the in this study used SFG was not able to distinguish between a disordered protein oriented at the interface or a well order protein oriented at the interface. To clarify this, Fu et al. suggested to perform chiral SFG (using the polarization psp) to distinguish between several secondary structure elements, which they tested for several model proteins and peptides (Fu et al., 2011a). α-helices and disordered regions are not chiral and consequently they should not be observable in the psp polarization, whereas beta sheets should give a signal (Fu et al., 2011a). In sps polarization (achiral SFG), every secondary structure element contributes to the amid I band (Fu et al., 2011a). Consequently, only a signal of the 25 % β-sheets in SynDLP was expected, but a low signal to noise ration impeded the data evaluation (appendix 7.4.4). Besides a small C=O signal, a very weak signal in the amide I region might be observable, but this is speculative. Longer exposure times and averaging more spectra could be helpful to solve this problem.

A very critical point of the calculated orientation was the underlying protein structure. The predict crystal structure (chapter 4.3) based on the crystal structure of a non-membrane associated NosDLP (PDB 2J69) (Low and Löwe, 2006) and subsequently the predicted SynDLP is also non-membrane associated, which might reduce the significance of the calculated Θ. At this point molecular dynamics simulation could help to calculate a proper SynDLP structure reflecting a membrane associated protein. That could improve the results and might help to answer the question of the non-orientated Ψ. Anyway, there might also exist another explanation for the non-orientated Ψ. As known from previous experiments, SynDLP forms dimers and oligomers. Depending on the orientation of these dimers or oligomers the Ψ orientation averages out. E.g., when one SynDLP is facing the membrane and the next SynDLP is facing away from the membrane, this might also result in a non-oriented Ψ.

Although the SFG studies were done at a lipid monolayer, which is a different and more artificial system than a lipid bilayer (e.g. liposomes), the SFG experiments confirmed, that SynDLP interacts with negatively charged lipids. Moreover, the SFG experiment suggested that SynDLP enters the membrane and the conformation of the protein changes in the presence of GTP. The calculated spectra revealed a nearly flat position (θ = 89 °) of SynDLP with respect to the membrane.

5.3.3 SynDLP is a highly ordered oligomer

The third feature of (B)DLPs is the ability to oligomerize. The oligomeric state was analyzed by FPLC in order to separate different SynDLP oligomers. SynDLP eluates only in the void volume and therefore an exact statement about oligomeric state could not be made. It can only safety be said that SynDLP forms higher oligomers/aggregates and a unit number of $n \geq 8$ can be assumed, as the column separation limit suggests a separation up to 600,000 kDa.

The formation of higher ordered oligomers is also supplemented by the established sedimentation assay. Without a nucleotide, SynDLP is nearly equivalently distributed between the pellet and the supernatant (Figure 23). Thus, at least two oligomeric states can be assumed. One oligomeric state of high molecular weights can be sedimentated and one oligomeric state of lower molecular weights remains in the supernatant. Note that an oligomeric state of lower

molecular weight still implies molecular weights above 600,000 kDa. A similar behavior was found for the DLP MxA. MxA WT is equivalently distributed between the pellet and the supernatant in the absence of a non-hydrolysable GTP analogue (Gao et al., 2010). In contrast, NosDLP was mainly found in the supernatant (Low et al., 2009). The addition of GTP to SynDLP shifts the pellet to supernatant ration, to more protein in the supernatant, indicating a change in the oligomeric state and most likely due to lower oligomers. Interestingly, in the presence of GMPPnP the pellet to supernatant ratio completely shifts to the SynDLP in the pellet, and it can be concluded that GMPPnP stabilizes the oligomeric state of high molecular weights. This was also observed for NosDLP, but not for DynA (Burmann et al., 2012; Low et al., 2009). It was shown for DynA that the presence of liposomes induces a sedimentation of the protein after centrifugation. Consequently, an influence of DOPG liposomes on the oligomeric state was tested, but was not observed. In summary, SynDLP shows nucleotide depending changes in the oligomeric state, whereas liposomes have no influence on the oligomeric state. This makes SynDLP unique in the field of BDLPs.

In this context TEM micrographs gave a more pronounced and detailed look on the oligomeric state. In addition to that, TEM micrographs were able to show tubulated liposomes. Again, SynDLP seems to form two kinds of oligomers, one with higher molecular weights, and one with lower molecular weights. GTP inhibits the formation of oligomers with higher molecular weights and in addition the liposomes seem to be affected as no intact liposomes were observed (Figure 25 C vs. appendix 7.3). In the presence of GMPPnP, tubs/aggregates seems to grow out of liposomes (Figure 25 E), like it is observed e.g. for dynamin, DynA, Nos*D*LP and Drp1 (Bürmann et al., 2011; Ferguson and De Camilli, 2012; Marin et al., 2006; Pucadyil and Schmid, 2008; Ugarte-Uribe et al., 2014). Thus, it can be concluded that the oligomeric state is strongly influenced by the nucleotide, but not by DOPG liposomes, although a membrane interaction/remodeling activity of SynDLP was observed in the TEM micrographs. However, further TEM studies should be performed as cryogenic TM. The better resolution might help to see the protein/lipid interaction in more detail.

5.4 SynDLP forms a disulfide linked asymmetric dimer in vitro

Experiments under reducing and non-reducing conditions suggested the formation of two inter-protein disulfide bonds. The position of the disulfide bond was determined by introducing point mutations. Ten mutants were created in which a single cysteine was replaced by an alanine. It was shown that the mutants C8A and C777A do not form dimers. In a disulfide linked dimer, in which the same cysteine residues are covalently linked, mutation of one cysteine residue will likely result in monomerization. In case of SynDLP, two mutations are resulting in protein monomerization, although two different cysteine residues were mutated. If these two cysteine residues form disulfide bonds with their direct counterpart in the other protein (symmetric disulfide bond formation), replacing one cysteine residue would not change the covalently bound dimer state (Figure 44 A). Only if the two cysteine residues form disulfide bonds with the second essential cysteine residue adjacent SynDLP (asymmetric), replacing one of the two critical cysteines monomerize the protein (Figure 44 B). Note that the shown arrangement of the monomers to a dimer is one possibility and should only illustrate the asymmetric dimer formation.

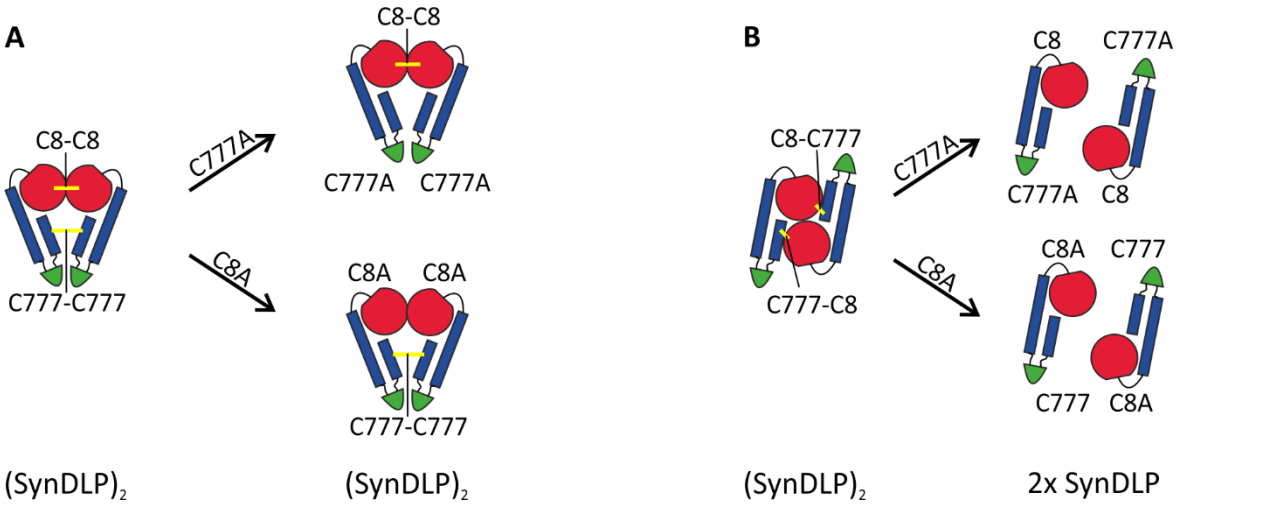

Figure 44: The influence of point mutations on the SynDLP monomer/dimer. The replacing of Cys to Ala do not change the dimer state in a symmetric disulfide linked dimer (A), but in the asymmetric disulfide linked dimer (B).

The *E. coli* strain used for SynDLP expression was Rosetta-gami™ 2 (Novagen). According to the manufacturer, it is known for an enhanced disulfide bond formation even in the cytoplasm (discussed in 5.6). In addition, and from an *in vivo* point of view, protein expression in the

cytoplasm of *Synechocystis* is not the right environment for the formation of disulfide bonds. Nevertheless, this *E. coli* strain was used, because the protein expression was best in this strain. Nonetheless, disulfide bonds only form, if both cysteine residues are in very close contact (Qin et al., 2015). Therefore, an inter protein disulfide bond between C8 and C777 is not likely, when two SynDLP proteins do not interact asymmetrically. Consequently, the SynDLP WT might also arrange asymmetrically under reducing conditions, but without the covalent disulfide bond. Moreover, the differences between SynDLP WT (covalent dimer) and SynDLP C777A (non-covalent dimer) are marginal in the experiments performed in this thesis (e.g. Membrane interaction, GTPase assay, sedimentation assay). Thus, it reasonable to work with SynDLP WT, although the dimer formation is most likely an *in vitro* artefact.

5.5 The Δsyndlp strain has a stronger phenotype under HL conditions

In this thesis, pioneer work was done in studying a new *Synechocystis* BDLP systematically. As it was discussed before, the proteins Slr0179, Slr1462, Sll0503 and Sll0803 must be analyzed in more extend, whereas SynDLP is most likely a BDLP. Anyway, all potential BDLPs might have an important *in vivo* function. Therefore, *Synechocystis* mutant strains were generated, lacking in respective genes. Via PCR amplification it was shown that *slr0179*, *slr1462* and *sll0804* are not completely deleted, whereas *syndlp* and *sll0503* are even deleted (Figure 32). *Synechocystis* contains several identical genomic copies (Labarre et al., 1989). Consequently, a full segregation of the genes can only be reached in case of gene deletion in every genomic copy. If it is not possible to replace the gene in each genomic copy, it indicates that in absence of the gene the cell cannot survive and it can be concluded that the gene is essential for Synechocystis. Thus, under the chosen growth conditions *slr0179*, *slr1462* and *sll0804* are essential for *Synechocystis*, indicating that the three encoded proteins have important functions for the cell survival. However, information about these genes in the literature are very rare. *sll0804* was found to be important for the photoautotrophic growth (Zhang et al., 2004). Later on, this result was specified and *Synechocystis* mutants, which have an unfunctional *sll0804* gene show an impaired affinity for inorganic carbon. Thus, *sll0804* was proposed to be part of carbon-concentrating mechanism

(Zhang et al., 2008). The genes *slr0179* and *slr1462* are not discussed in the literature so far. A transcriptome analysis showed an increased transcription of *slr1462* and *slr0179* after CO_2 and phosphate depletion, respectively (Kopf et al., 2014). In addition, *slr0179* is part of a gene cluster together with *slr0180* (a hypothetical transposase). The genes *syndlp* and *sll0503* appears not to be essential for *Synechocystis*. The reasons for this could be manifold. It might be possible that other genes are upregulated to perform the same tasks. Another reason could be that the gene is only essential under certain conditions, which has to be investigated in further studies. As discussed above, *syndlp* is part of a gene cluster together with KGK proteins and a lipid transporter (Kopf et al., 2014). This gene cluster is under control of an asRNA (Mitschke et al., 2011). A recent publication reveals a reduced expression of the asRNA and consequently an enhances expression of *syndlp/slr0869* under moderate HL conditions (Hu et al., 2017). In summary, the potential *Synechocystis* BDLP candidates are very different in their genetic environment and thus it might be very likely that they also have different *in vivo* functions. A first hint, if the here discussed BDLPs are involved in the TM biogenesis can be given by searching for the potential *Synechocystis* BDLPs homologues in the genome of the only cyanobacterium, that does not contain TMs, namely *Gloebacter violaceus* (Rippka et al., 1974). Indeed, in *G. violaceus* no homologues could be found and thus no candidate can be excluded from being important for TM biogenesis (Nakamura et al., 2003). Further studies should include TEM analyzes to identify the localization of the potential BDLPs within the *Synechocystis* cell, e.g. with immunogold labeling.

However, to get an idea about potential *in vivo* functions of SynDLP studies were performed with a *Synechocystis* strain lacking the gene of SynDLP. Under normal growth conditions, the growth of the Δ*syndlp* strain did not differ from the WT strain (Figure 33). Because it was suggested that expression of SynDLP increases under HL conditions, the cells were grown at NL and HL exposure, respectively. These conditions did not influence the growth rates of the strains, but after 24 h (HL) the mutant strain showed a different phenotype compared to WT (HL) (Figure 34). While the OD_{750} was similar, the chlorophyll content and the number of cells per chlorophyll concentration were reduced in case of the mutant strain. But the number of chlorophyll molecules per cell was higher (Figure 35). Regarding this information, the mutant cells appear bigger, due to the higher

turbidity at the same number of cells. Further experiments should include e.g. TEM analysis of whole *Synechocystis* cells to get an idea about the cell size and shape.

Other physiological parameters were also slightly influenced. It is known that *Synechocystis* responses to HL stress via downregulation its light harvesting capacity and the upregulation of general light protection mechanisms (Muramatsu and Hihara, 2012). Furthermore, the amount of chlorophyll and phycocyanin are reduced, albeit the relative carotenoid content is enhanced to avoid photodamage (Muramatsu and Hihara, 2012; Zakar et al., 2017). These effects were observed in case of the WT HL and the mutant HL strains (Figure 36 A). In addition, the mutant strain exhibited a lower phycocyanin-to-chlorophyll ratio, but a higher carotenoid-to-chlorophyll ratio (Figure 36 B), both, under NL and under HL conditions. This indicates that the mutant strain has a different pigment composition, including an enhanced relative content of carotenoids and a lower chlorophyll content.

In Figure 38 it is shown that after excitation of phycobilisomes the PSII emission of WT HL at 693 nm is significantly more increased than the mutant HL emission. When phycobilisomes are coupled to the PSII, the energy is transferred to PSII and the phycobilisomes fluorescence is quenched, whereas the PSII fluorescence is enhanced. The phycobilisomes are degraded or uncoupled from the TM under HL condition (Muramatsu and Hihara, 2012; Pojidaeva et al., 2004). Consequently, the energy cannot be transferred to the photosystems and the energy is released as fluorescence (Rakhimberdieva et al., 2007). Interestingly, this is the case for WT HL, but it is not the case for the mutant under HL conditions. Here is PSII emission at 693 nm is reduced. The enhanced energy transfer from the phycobilisomes to the PSII under HL conditions might suggest that the phycobilisomes are not uncoupled from the PSII. Alternatively, a relative higher amount of PSII could absorb more energy, but especial under HL conditions no significant difference in the PSI to PSII ratio was observed (Figure 38). Further experiments should include WB analyzes with antibodies directed against PSI and PSII subunits should quantify the exact PSI to PSII ratio.

In summary, the *in vivo* studies reveal a slight different phenotype of the Δ*syndlp* mutant strain compared to the WT strain. Especially, the cell size and the electron transfer from the phycobilisomes to the PSII are affected under HL conditions.

The investigation of SynDLP are at the beginning and thus more *in vivo* studies are necessary to uncover the role of SynDLP in *Synechocystis*. Potential functions can be presumed by having a look at the three other BDLPs and their functions in the cells. Unfortunately, two of them share the same name (DynA), although one is of *Bacillus subtilis* and one is of *Streptomyces venezuelae* (Bürmann et al., 2011; Schlimpert et al., 2017). Thus, they are named SubDynA and VenDynA, in the following. SubDynA repairs membrane as a stress response protein (Sawant et al., 2016) and ValDynA is playing a role in bacterial cytokinesis (Schlimpert et al., 2017). In addition, LeoA, also in cooperation with LeoB/C, is suggested to be involved in the release of membrane vesicles (Michie et al., 2014). They all have different *in vivo* functions, albeit they share the feature that they do not act on their own, but in cooperation with at least one other BDLP. ValDynA needs ValDynB and 3 other proteins, DynA directly contains two BDLP like subunits and LeoA is part of a gene cluster with LeoBC (Bürmann et al., 2011; Michie et al., 2014; Schlimpert et al., 2017). Therefore, it is very likely that also SynDLP need a supporter protein for its *in vivo* function, which might be the KGK proteins or Slr0872. The comparison to other BDLPs reveals that also SynDLP might be part of a protein complex. However, since in all *in vivo* studies no evidence was observed that SynDLP influences the TM biogenesis, SynDLP is most likely not essential for the TM biogenesis. Nevertheless, the lack of the protein result in a phenotype that differs from the WT. The phenotype is more pronounced under HL conditions, indicating an involvement in the stress response of SynDLP. Thus, potential functions of SynDLP might be the organization/reorganization or repair of TMs/CMs in *Synechocystis*, upon stress induced defects.

5.6 SynDLP in vitro vs. in vivo

The remaining and not solved question concerns the SynDLP, which is encode in the living *Synechocystis* WT cells. Although the absence of SynDLP affects the phenotype, WB analyzes were not able to detect the protein in *Synechocystis* cell extract. The expression conditions do not lead to a detectable amount of SynDLP. Beside phosphate depletion and HL, other conditions can be tested (e.g. cold stress) (Hernández-Prieto et al., 2016; Hernández-Prieto and Futschik, 2012; Kopf et al., 2014). Moreover, it is conceivable to use reverse transcription polymerase chain reaction,

for quantifying the expression on a RNA level. In this context, it is important to know if the protein forms disulfide bonds *in vivo*. On the one hand, disulfide bonds help to stabilize the protein, and even in *Synechocystis* the presence of a mechanisms is discussed, which trigger formation of disulfide bonds, at least in the extra cytoplasmic space (Singh et al., 2008). On the other hand, no single (B)DLP has ever been suggested to contain disulfide bonds as they are mainly expressed in the cytoplasm and to my knowledge, no protein in *Synechocystis* has ever been described which has inter or intra protein disulfide bonds. Thus, it is reasonable to assume that SynDLP does not form disulfide bonds, *in vivo*. Consequently, the covalently linked dimer might be an *in vitro* artefact and thus, it was important to create a non-covalently linked dimer (C777A). And that case might also explain the slight differences between the WT and C777A. In some experiments differences occur, such as a slightly reduced GTPase activity of C777A, another behavior in the sedimentation assay (presence of GTP) and a different shape in the TEM images. The slight differences might be explained by a more rigid structure of the WT protein. The disulfide bonds might fix the asymmetrical conformation, whereas the non-fixed mutant is more flexible and can reach transitions states faster or even other transitions states. However, since the differences between SynDLP WT and the mutant C777A are small, it is reasonable to assume that the artificial disulfide bonds did not interfere with the performed experiments.

6. Conclusion

Oxygenic photosynthesis is ubiquitously distributed. From plants, algae to cyanobacteria, the photosynthetic light reaction is localized in a special membrane system, the TMs, which biogenesis is still a mystery. Thus, one aspect of current research is to find new proteins, which are potentially involved in the TM biogenesis. In addition, new models were developed in order to describe the *in vivo* and *in vitro* function of potential *Synechocystis* DLPs. In the end, in this thesis three main question should be answered: (i) Are there potential BDLPs in *Synechocystis*? (ii) Are they real BDLPs? (iii) Can they be linked to TM biogenesis?

Consequently, the hypothesis of this thesis was that BDLPs in *Synechocystis* are involved in the TM biogenesis. Five potential candidates were identified. Out these five candidates, SynDLP was proven to be very likely a "real" BDLP, as it has at least three of the four DLP key features: SynDLP is (i) an active GTPase with a low binding affinity to nucleotides, (ii) it interacts with and remodels membranes and (iii) self-assemblies into higher oligomers. In further studies the domains and especially the amino acid sequences, which are involved in the self-assembly or membrane binding must be analyzed e.g. by point mutations. Still unclear is a potential involvement of SynDLP in the TM biogenesis. An impact on the phenotype reveals that the absence of the protein is not essential for the TM biogenesis, but it is very likely that SynDLP might be involved in the reorganization or repair of membranes within *Synechocystis*, as a stress responses protein. Finally, I was able to answer two of the three main question in this thesis: (i) There are potential BDLPs in *Synechocystis* and (ii) SynDLP is most likely a BDLP.

7. Appendix

7.1 Amino acid sequences of analyzed proteins and mutants

The amino acid sequences were obtained from “Cyanobase” (Nakamura et al., 2000). All proteins were expressed carrying a His-Tag at the C-terminus.

7.1.1 Slr0179

MNIEAKLSQARSWLDELGNAISDLVGVASEVFEDEKLKQDLADFRRAYDQAVLDLANPSL
RIAMIGTTSSGKSTIVNALIGRRIAPIEAGEMSGGVLRIKHGEGSHLKIEETEGAVWETG
EWSGLSDEEIYNRIHQVMQKYHETKKRKIYISPQIEVRLPLLPGYDRALSGLPEELAIEF
VDLPGLKSIKDSKNLKVIQSLVGNAFCLVALDYSHVDEEHRQVLLNELKDVVEYLHGSTE
SMIFILNRIDRRSSDDFPLNKRVNLLKDEIKSTLKLSSKPYIMPLNALLLYNAQCAWGYN
FTDNSLNCHEKFKSDFIKNLLIKSSEIIQIKALESEDIKLFSWFTHLSLSFAQKQKC

7.1.2 SynDLP

MSKIAPQ**C**QNLREQVNQLIELLRQEPTLRSQQDTSIVETALGKALSPRFEIVFAGAFSAG
KSMLINALLERELLYSAEGHATGTE**C**HIEYANANEERVVLTFLSEAEIRQQALILAKYLN
VNVGDLNINQPEAVKVVSQY**C**QKIIAEEGGENKSERAKQANALHLLLIGFEQNRERINTV
QNSTYSMDQLNFSSLAEAAGYARRGANSAVLKRLDYF**C**NHSLLKDGNVLVDLPGIDAPVK
EDAERAYRKIESPDTSAVI**C**VLKPAAAGDMSAEETQLLERISKNHGIRDRVFYVFNRIDD
TWYNTQLRQRLEGLIQSQFRDNSRVYKTSGLLGFYGSQVKQTNSSTRFGLDSIFATTIKG
FDGEEETPQFVSEFNNY**C**ANSGKLLSTAFRVSVNGYETSNENYVRILSEWGIPLVDQLIH
DSGIESFRSGIGLYLAEEKYPELFATLANDLQPL**C**IALRQFYLENYRQLDSQPREIAAMK
AQELTLLNQEMQNLGIEFKKYMSAQINDVVIGNDREFDQDFTKLKARMVARLDELLKTFS
VMNAYKRATESHPRNSTAPFIAVLVEALYYLANELEDAFIEAIHELVKNFFQRLGDRLRK
VD**C**YHQVYRLVGNDGGIEQLLRRAEEDITKALVNEARTE**C**DRYVRESPRFYDEGTFSIYQ
FRQTLQQTSQGYDAQAIVEAEPAIKELLKLDFEPKVFNTVRKNFRQTVNNTLKTHLLPMA
EEQAQIILEQYDVARKYREQTLEQDAEEKIARNSRLQSEIKQKIDLYQTSIVSINE**C**LKA
MQIFEQLPVITESDITKQAEIVADADFVEIVE

7.1.3 Slr1462

MPLPRLLTIVLAVSFILGMVIWLIDAILRLYSQVAWTSPFLANIVILLVIAVLALLIATF
FYYFNLANQPKDSSGKKRRRIKLPEQKNETAAANLQAVRRQMQQIQDQVAQKALLEKTRL
IEAQLKRGNLNLVVFGTGSAGKTSLVNALLGQIQGEVAPTMGTTIAGEKYYLYLDGVSRD
LEITDTPGILEAGVRGTERETAARQLATEADLLLFVVDNDLRQSEYEPLQALAKIGKRSL
LILNKTDLYPPDEVEVLLQTLRQRVKAFIPPEDVLAIAARPQDVAIQPGLLMRPEPEIEP
LVKRLVSVLRSDGDDLMADNILLQSQRLGDEARQIIEQQRQREAMKIIDRYQWIGAGAIA
VTPLPVIDLLATTAINAQMVVEIGRVYGCEIDGDRGKELAISLGKTFVGLGIVKGAVELM
AQAMQLQLTTYIIGKAIQGITAAYLTRIAGKSFIQYFRQDQDWGDGGVAQVVEQQFQLSR
KDEFIQAFVKQAIAKVVEPLEDFWGKESPDTTPEQLEPLPELRDLTPLEEEFIEAILPEP
EVYHTRYADWDSPRPQRQDDW

7.1.4 Sll0503

MNNNSLTDLDQTLDIISAIQEDLNYQQAQASLTAIVEQIDLDTTEKQGLEKEISHLCTML
ENLNQGVVQIAAFGLVGRGKSSLLNALLGEQVFTTGPVHGVTQTQQSASWQLNQADGLST
VTISGWGNAQLQLIDTPGIDEVKGQEREQLAIAVAQQVDLILFVIAGDMSQVEFQALSRL
RAVGKPMLLVFNKIDQYPATDQQLIYEKIRDERVKELLSPEEIVLVSASPLVTELRENTQ
GKLERYQYRGEAKVDNLRLKIIDLLQREGKSLVALNTLLCADNLNDKLVQQKMRLRDSQA
NTILQKAVMVKATAIALNPVTVLDLFSGAVVDVALIISLSKLYGLPMTQTAAIALLQKIG
VSMGGITASEFLAGLGLSSLKGLLGLTVPLTGGLALAPYISVALTQASVAGVSTLAIGQV
TKTYLANGAAWGETGPRTVVRDILNSLDQNSVMARIKQELQEKLTPERIVSPSP

7.1.5 Sll0804

MNSPAPDPALSTAIASIQQSLNWYASQRRHWNYPPNLELQGAVRQDIQAMHQALAKLEQR
VFKIAAFGLVSRGKSTVINALLGEKRLETGPLHGVTQWPQSVRWCSNDKIQIDLIDTPGL
DEIAGGARAAMAQTVAHQADLILFVIAGDITQTEFTALQTLRQAQKPLLLVFNKIDLYPE
QDQQQIFAQLQSLTPDGEDSPIFSAEDIVLVAAEPPPIMVRVEYGNSPKGSRPSPALEER
WEKPAPKLDQLRQKIFTILNQDGSQLLALNALRQVEQAEKNIATKTIEIRTAEADQLISK
YMRYKALAIAVNPIGLLDLAASVITDLLLIRNLARIYGLPITSYEAGRIWKKVLIGAGGI
LLSQWVSALFLGLQKTASLVENPGNLAAYAGGALLQGGVAAYSTYIVGEGAKIYLAQGAS
WGNAGTSTAIAKIKNDAPPDSMLRRLDDVGGEG

7.2 SDS-PAGE gel

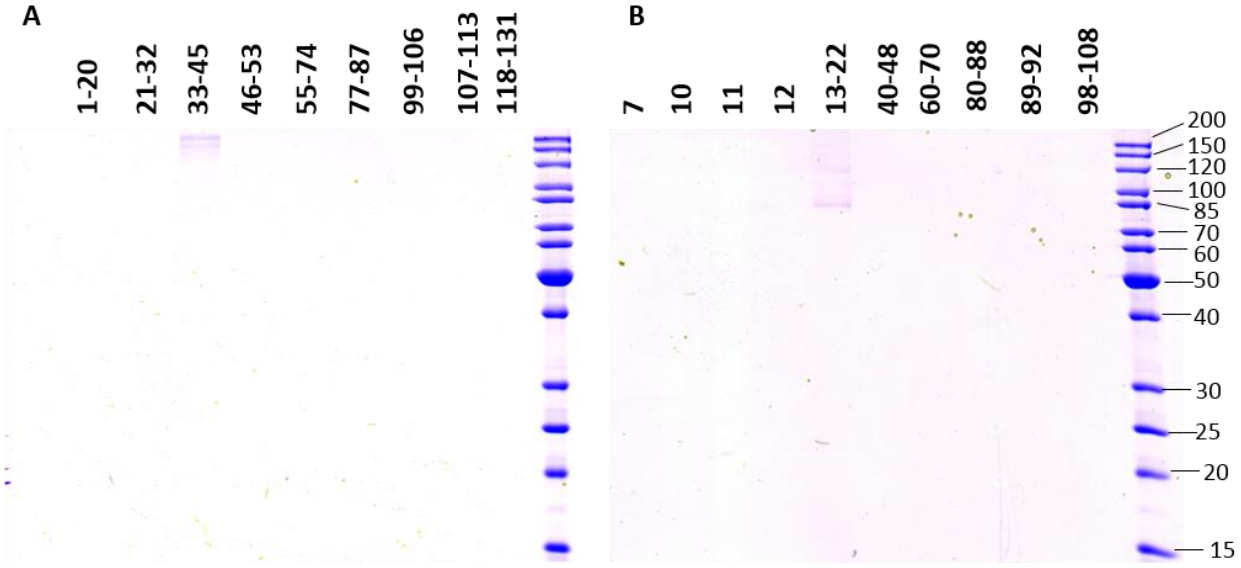

Figure 45: SDS-PAGE gels of SEC fractions. 0.85 mg/ml SynDLP WT (A) and SynDLP C777A (B) were injected and separated by SEC. The numbers represent the collected fractions.

7.3 TEM micrographs

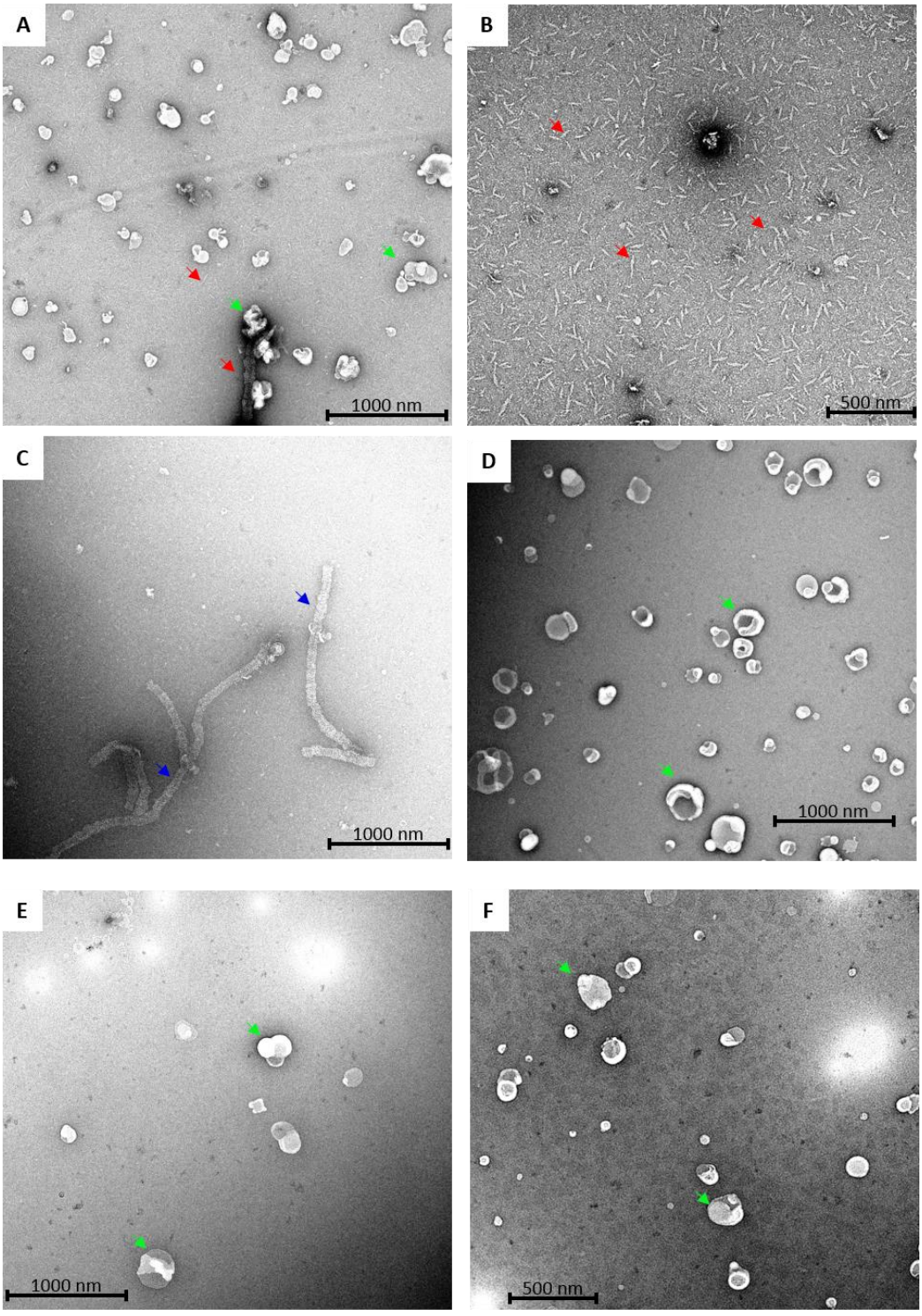

Figure 46: Selected TEM micrographs of SynDLP WT and isolated DOPG liposomes. (A) shows SynDLP in presence of DOPG, GTP (B) and GMPPnP (C). Isolated DOPG liposomes are shown in (D), liposomes in the presence of GTP (E) and liposomes in the presence of GMPPnP (E). Blue arrows mark big helical protein structures, red arrows mark the small protein structures and green arrows the liposomes. Note the different scale bars.

7.4 SFG spectroscopy

7.4.1 Fitting of the surface pressure

The surface pressure (Π) was fitted using an exponential function.

$$\Pi = \Pi_{max} - Ae^{-\frac{t}{k_t}}$$

7.4.2 FTIR second derivate approach

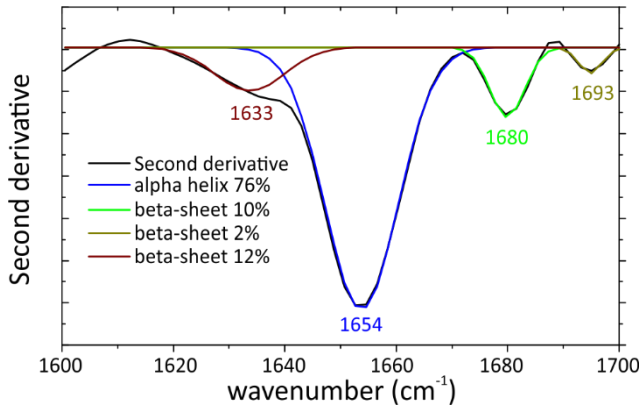

Figure 47: Deconvoluted amide I band FTIR spectrum of SynDLP in the second derivate approach. The FTIR spectrum was kindly provided by Dr. Youssef from the University of Strasbourg and shows the contributions of alpha helices and beta sheets to the amid I band including the positions of the resonances.

7.4.3 Fitting routine for the SFG spectra in the amide I area

The SFG spectra fitting routine assumes the presence of 6 resonances at 1737 cm^{-1} (C=O), 1654 cm^{-1} (α-helical), 1633 cm^{-1}, 1680 cm^{-1} and 1693 cm^{-1} (β-sheet), based on FTIR measurements due to FTIR. The resonances and the full width at half height (FWHH) were kept constant. All fits were done with Origin 8.6 pro and the following equation:

$$I_{SFG} = \left(NR_{Real} + \sum_{q=1}^{6} \frac{A_n(w_n - w_{IR})}{(w_q - w_{IR})^2 + \Gamma_n^2} \right)^2 + \left(NR_{Img} + \sum_{q=1}^{6} \frac{A_n\Gamma_n}{(w_q - w_{IR})^2 + \Gamma_n^2} \right)^2$$

A is the amplitude, I the SFG intensity, NR the non-resonance background, w is the frequency and Γ the phase or, in terms of the Lorentzian model, the full width at half height.

Table 21: Parameters used and obtained to fit the SFG spectra.

Mode		ML	SynDLP	SynDLP+GTP
C=O	A (a.u.)	10.3	10.1	11.9
	Freq. (cm^{-1})	1737	1737	1737
	FWHH (cm^{-1})	18.3	18.3	18.3
α-helical	A (a.u.)	0	1.6	0.8
	Freq. (cm^{-1})	1654	1654	1654
	FWHH (cm^{-1})	0	11.2	11.2
β-sheet	A (a.u.)	0	1860	1608
	Freq. (cm^{-1})	1680	1680	1680
	FWHH (cm^{-1})	0	111	111
	A (a.u.)	0	-407	-358
	Freq. (cm^{-1})	1633	1633	1633
	FWHH (cm^{-1})	0	97	97
	A (a.u.)	0	-1404	-1225
	Freq. (cm^{-1})	1693	1693	1693
	FWHH (cm^{-1})	0	105	105

7.4.4 SFG spectra

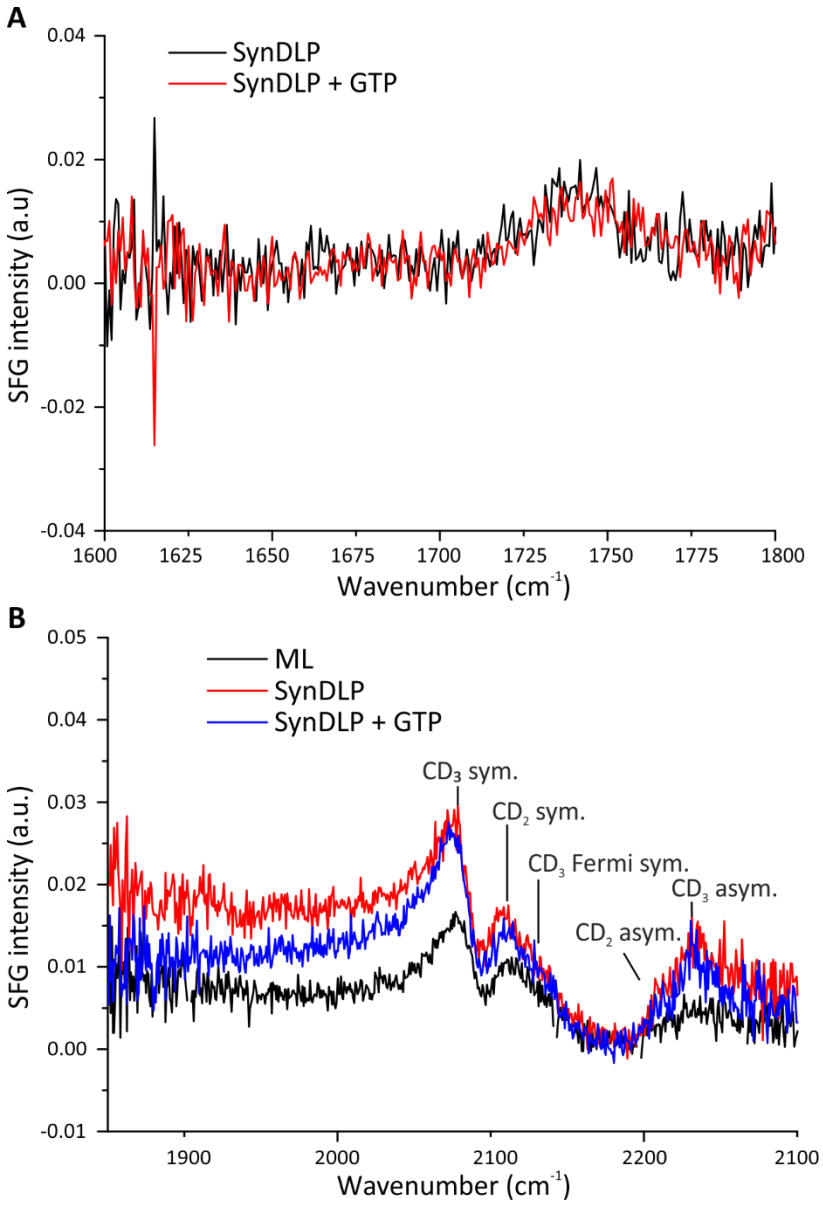

Figure 48: Recorded SFG spectra. (A) Chiral SFG spectra (psp polarization) at the DMPG/buffer interfaces in absence (SynDLP) and presence of SynDLP and GTP (SynDLP+GTP). (B) SFG spectra in the CD region at the DMPG/buffer interface, only with a d_{54}-DMPG monolayer (ML), with the addition of SynDLP (SynDLP) and SynDLP in presence of GTP (+GTP). CD_3 sym. stretch (2078 cm^{-1}), CD_2 sym. stretch (2114 cm^{-1}), CD_3 Fermi sym. stretch (2137 cm^{-1}), CD_2 asym. stretch (2213 cm^{-1}) and CD_3 asym. stretch (2239 cm^{-1}).

7.5 Laurdan fluorescence spectroscopy

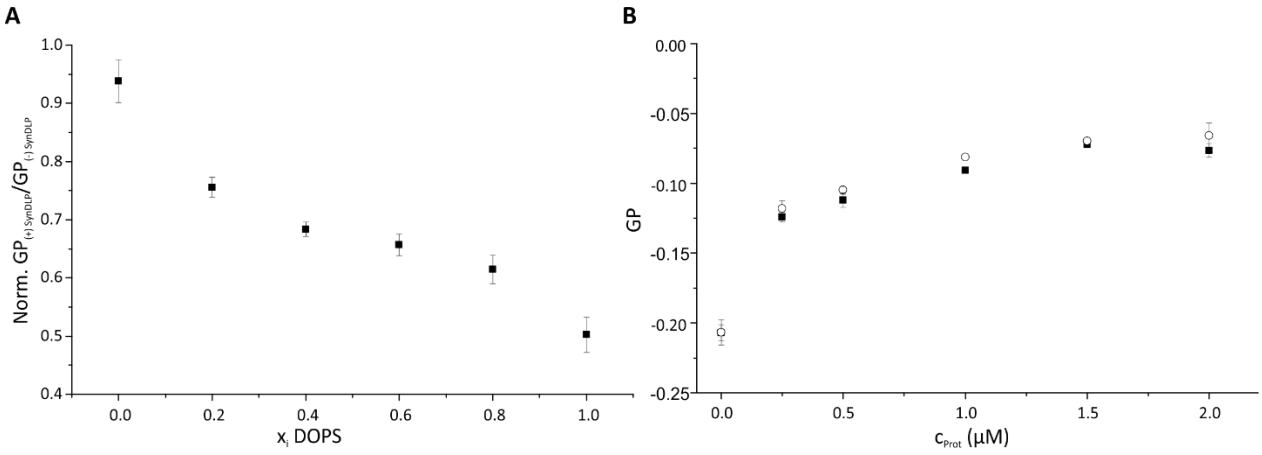

Figure 49: Laurdan fluorescence spectroscopy to determine the influence of the lipid headgroups and the membrane interaction properties of SynDLP C777A. (A) Rel. GP values ($GP_{(+)SynDLP}/GP_{(-)SynDLP}$) depending on the amount of DOPS in DOPC. The values were normalized on $GP_{(+)SynDLP}/GP_{-)SynDLP}$ with 100 % DOPC. (B) GP values of SynDLP WT (black squares) and SynDLP C777A (open cycles) at different protein concentrations. No differences in the GP values (calculated with equation (6)) of SynDLP WT and SynDLP C777A were observed.

7.6 GTPase Assay

7.6.1 Influence of DOPG on the activity of SynDLP WT and C777A

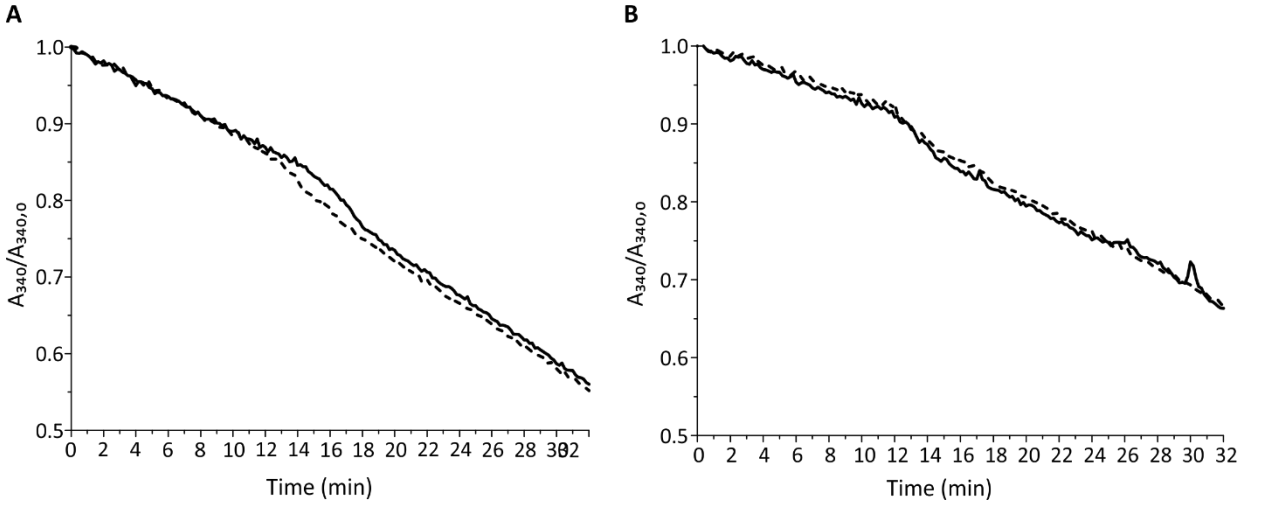

Figure 50: Absorption curves (A_{340}) normalized to the absorption at t=0 min ($A_{340,0}$) over the time. Absorption curves resulting from a continues, regenerative coupled GTPase assay. The samples containing 1 mM GTP, 0.5 µM SynDLP WT (A) and C777A (B), respectively. In addition, the assay was performed in the absence (straight line) and in the presence (dashed line) of 20 µM DOPG liposomes.

7.6.2 A slow transition model

The slow transition model described by (Ainslie Jr. et al., 1972).

$$activity\ [min^{-1}] = \frac{d(c_{GTP})^2 + ec_{GTP}}{a(c_{GTP})^2 + bc_{GTP} + c}$$

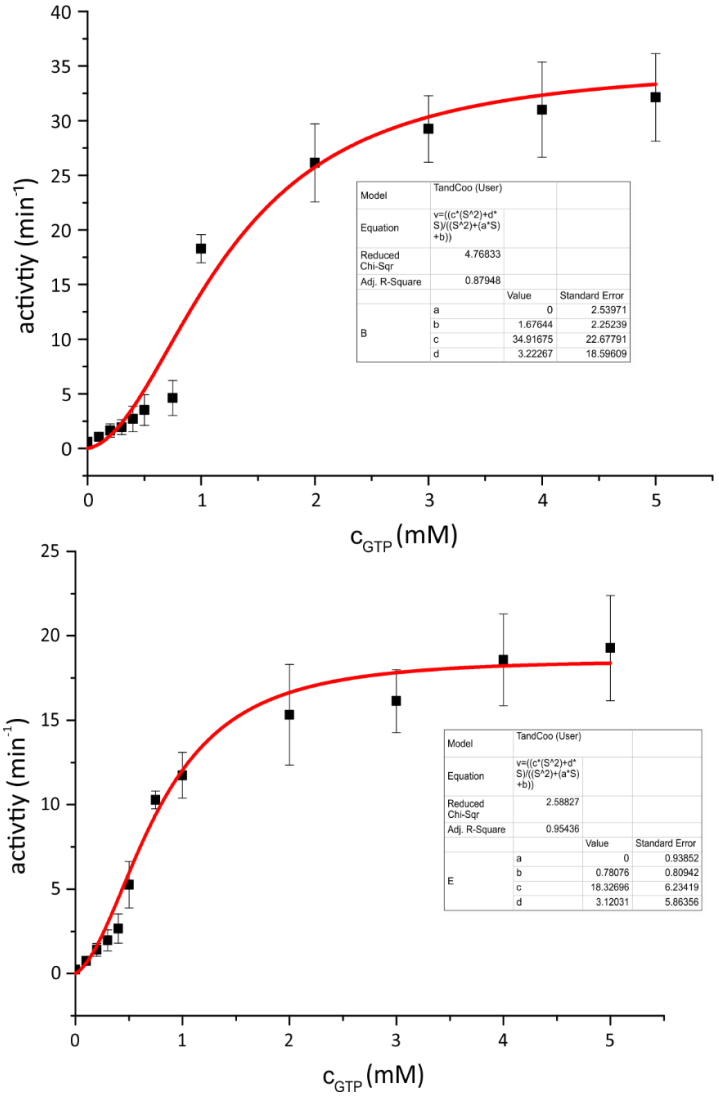

Figure 51: SynDLP WT (upper panel) and C777A (lower panel) activity fitted with the slow transition model.

7.7 List of identified cBDLPs

The here presented list is also part of the publication (Jilly et al., 2018).

Synonym	Strain	Gene Name	Cyanobase Group	Cluster in read direction		
				up	down	clade name
LynAes 1	Lyngbya aestuarii BL J	M595_0809	Dynamin Family protein		HP	cBDLPS
LynAes 2	Lyngbya aestuarii BL J	M595_1406	Dynamin Family protein	HP	HP	cBDLPS
Pho 1	Phormidium sp. OSCR	HLUCCO16_05220	Dynamin Family	P of UH	HP	cBDLPS
Xen7305 1	Xenococcus sp. PCC 7305	Xen7305DRAFT_00007930	Dynamin Family protein	HP	DNA replication and repair prot	cBDLPS
MicAer777 1	Microcystis aeruginosa SPC777	MAESPC_02002	Dynamin Family protein	HP		cBDLPS
MicAer777 2	Microcystis aeruginosa SPC777	MAESPC_04016	Dynamin Family protein	HP		cBDLPS
Gloe73106 2	Gloeocapsa sp. PCC 73106	GLO73106DRAFT_00033050	Dynamin Family protein	HP	molecular chaperone	cBDLPS
ScyMil11283 2	Scytonema millei VB511283	QH73_38235	Dynamin Family protein	DNA methyltransferase		cBDLPS
LimRob 4	Limnoraphis robusta	WN50_20835	Dynamin Family protein		HP	cBDLPS
ChroCya 5	Chroococcales cyanobacterium CENA595	UH38_23205	Dynamin Family protein		HP	cBDLPS
Xen7305 2	Xenococcus sp. PCC 7305	Xen7305DRAFT_00010220	Dynamin Family protein			cBDLPS
AnaWa102 1	Anabaena sp. wa102	AA650_07240	Dynamin Family protein	HP	HP	cBDLPS
OscNigro7112 4	Oscillatoria nigro-viridis PCC 7112	Osc7112_5337	Dynamin Family protein		HSR1-related	cBDLPS
PhoPri 2	Phormidesmis priestleyi Ana	HLUCCA11_23840	Dynamin family		HP	cBDLPS
TriEry101 2	Trichodesmium erythraeum IMS101	Tery_2545	Dynamin	HP	dynamin?	cBDLPS
ChroThe7203 1	Chroococcidiopsis thermalis PCC 7203	Chro_0749	Dynamin Family protein			cBDLPS
PhoPri 1	Phormidesmis priestleyi Ana	HLUCCA11_23170	Dynamin family		HP	cBDLPS
ColCht7420 3	Coleofasciculus chthonoplastes PCC 7420	MC7420_4217	Dynamin Family protein	Predicted GTPases (dynamin-related		cBDLPS
CylSta7417 5	Cylindrospermum stagnale PCC 7417	Cylst_6624	Dynamin Family protein		HP	cBDLPS
Cal7507 4	Calothrix sp. PCC 7507	Cal7507_5390	Dynamin Family protein	Dynamin Family protein	peptidase M48 Ste24p	cBDLPS
Cal7507 5	Calothrix sp. PCC 7507	Cal7507_5391	Dynamin Family protein	small GTP-binding protein	Dynamin Family protein	cBDLPS
ColCht7420 2	Coleofasciculus chthonoplastes PCC 7420	MC7420_4072	Dynamin Family protein		HP	cBDLPS
Hapa220 1	Hapalosiphon sp. MRB220	AMR41_08345	Dynamin Family protein	HP	GTP-binding protein	cBDLPS
Cal7507 3	Calothrix sp. PCC 7507	Cal7507_5388	Dynamin Family protein	peptidase M48 Ste24p		cBDLPS
Xen7305 3	Xenococcus sp. PCC 7305	Xen7305DRAFT_00033290	Dynamin Family protein		dynamin family protein	cBDLPS
SynCho7335 1	Synechococcus sp. PCC 7335	S7335_2274	Dynamin Family protein		HP	cBDLPS
DynA a	Bacillus subtilis subsp. subtilis 168	BSU22030				cBDLPS
LeoA	Escherichia coli ETEC strain H10407					cBDLPS
Riv7116	Rivularia sp. PCC 7116	Riv7116_0755	Dynamin Family protein			cBDLPS
NodSpu9414	Nodularia spumigena CCY9414	NSP_34240	putative GTPases (**dynamin**-like)	HP	HP	Chaparone
CylSta7417 1	Cylindrospermum stagnale PCC 7417	Cylst_0498	Dynamin Family protein		molecular chaperone	Chaparone
Nos7524 3	Nostoc sp. PCC 7524	Nos7524_3124	Dynamin Family protein		Virulence factor SrfB	Chaparone
TolBou 4	Tolypothrix bouteillei VB521301	DA73_0244415	Dynamin Family protein			Chaparone
ScyToly 1	Scytonema tolypothrichoides VB-61278	SD80_16940	Dynamin Family protein			Chaparone
TolyCam 1	Tolypothrix campylonemoides VB511288	SD81_03565	Dynamin Family protein		molecular chaperone	Chaparone
MasTes008 1	Mastigocoleus testarum BC008	BC008_02845	Dynamin Family protein		four helix bundle protein	Chaparone
CalThrix 1	Calothrix sp. 336/3	IJ00_17090	Dynamin Family protein		HP	Chaparone
Hapa220 3	Hapalosiphon sp. MRB220	AMR41_22450	Dynamin Family protein		molecular chaperone	Chaparone
MasLam774 2	Mastigocladus laminosus UU774	SP67_08100	Dynamin Family protein		molecular chaperone	Chaparone
Riv7119	Rivularia sp. PCC 7116	Riv7116_6519	Dynamin Family protein	HP	HP	Chaparone
Cya7424 1	Cyanothece sp. PCC 7424	PCC7424_2424	Dynamin Family protein	HP	HSR1-related	HSR1
Cya7822 1	Cyanothece sp. PCC 7822	Cyan7822_4416	Dynamin Family protein	HP	HSR1-related	HSR1
Ana90 1	Anabaena sp. 90	ANA_P10081	Dynamin Family protein	HP	HSR1-related	HSR1
TriEry101 1	Trichodesmium erythraeum IMS101	Tery_1654	Dynamin	HP	HSR1-related	HSR1
MicAer9809 1	Microcystis aeruginosa PCC 9809	MICAH_4710016	Dynamin Family protein	HP	HSR1-related	HSR1
MicAer9808	Microcystis aeruginosa PCC 9808	MICAG_3110011	Dynamin Family protein	HP	HSR1-related	HSR1
LimRob 1	Limnoraphis robusta	WN50_01000	Dynamin Family protein			KGK
Pho 5	Phormidium sp. OSCR	HLUCCO16_19355	Dynamin Family	TPR repeat	Restriction endonuclease	KGK
ChaMin6605 1	Chamaesiphon minutus PCC 6605	Cha6605_3278	Dynamin Family protein		HP	KGK
Gloe73106 1	Gloeocapsa sp. PCC 73106	GLO73106DRAFT_00002440	Dynamin Family protein	Toxin with endonuclease activity	quinolinate synthetase	KGK
Cya8802 1	Cyanothece sp. PCC 8802	Cyan8802_4244	GTPase (**dynamin**-related)-like protein		KGK	KGK
Plank 5	Planktothricoides sp. SR001	AM228_07300	Dynamin Family protein	phosphate permease	HNH nucleas	KGK
Mic7113 1	Microcoleus sp. PCC 7113	Mic7113_0538	Dynamin Family protein	amino acid transporter	KGK	KGK
OscAcu6304 1	Oscillatoria acuminata PCC 6304	Oscil6304_4435	Dynamin Family protein	Glycosyl hydrolases family	KGK	KGK
CylSta7417 3	Cylindrospermum stagnale PCC 7417	Cylst_3537	Dynamin Family protein	collagenase-like protease	KGK	KGK
ChroCya 2	Chroococcales cyanobacterium CENA595	UH38_12875	Dynamin Family protein		KGK	KGK
Hapa220 4	Hapalosiphon sp. MRB220	AMR41_25555	Dynamin Family protein		HNH nuclease	KGK
MasLam774 1	Mastigocladus laminosus UU774	SP67_07900	Dynamin Family protein	modification methylase	HNH nuclease	KGK
TolBou 1	Tolypothrix bouteillei VB521301	DA73_0213440	Dynamin Family protein			KGK
CalThrix 2	Calothrix sp. 336/3	IJ00_25925	Dynamin Family protein	serine/threonine protein kinase	HP	KGK

HassBys 1	Hassallia byssoidea VB512170	PI95_04005	Dynamin Family protein		HP	KGK
Nos7524 2	Nostoc sp. PCC 7524	Nos7524_0596	putative GTPase (dynamin-related)		KGK	KGK
Riv7117	Rivularia sp. PCC 7116	Riv7116_3732	putative GTPase (**dynamin**-related)		KGK	KGK
SynCho6312 1	Synechococcus sp. PCC 6312	Syn6312_2093	Dynamin Family protein		KGK	KGK
SynCys 6803 1	Synechocystis sp. PCC 6803	AOY38_06420	Dynamin Family protein	HP	HP (KGK)	KGK
TriEry101 3	Trichodesmium erythraeum IMS101	Tery_2547	Dynamin	dynamin?		Tandem A
Lep7375 2	Leptolyngbya sp. PCC 7375	Lepto7375DRAFT_2244	Dynamin Family protein	HP		Tandem A
LepHerJ 4	Leptolyngbya sp. Heron Island J	N836_32075	Dynamin Family protein	Dynamin Family protein		Tandem A
Xen7305 4	Xenococcus sp. PCC 7305	Xen7305DRAFT_00033300	Dynamin Family protein	dynamin family protein		Tandem A
TolBou 2	Tolypothrix bouteillei VB521301	DA73_0229115	Dynamin Family protein	Dynamin		Tandem A
HassBys 3	Hassallia byssoidea VB512170	PI95_57350	Dynamin Family protein	dynamin		Tandem A
Toly7601 1	Tolypothrix sp. PCC 7601	FDUTEX481_07820	Dynamin Family protein	Dynamin Family protein	HP	Tandem A
Cal7507 2	Calothrix sp. PCC 7507	Cal7507_2364	Dynamin Family protein	Dynamin family protein	HP	Tandem A
Nostoc7107 1	Nostoc sp. PCC 7107	Nos7107_3291	Dynamin Family protein	HP		Tandem A
MooPro 1	Moorea producens 3L	LYNGBM3L_16350	Dynamin Family protein		HP	Tandem A
ChaMin6605 3	Chamaesiphon minutus PCC 6605	Cha6605_3927	Dynamin Family protein	putative nucleic acid-binding protein, contains PIN domain		Tandem A
OscAcu6304 4	Oscillatoria acuminata PCC 6304	Oscil6304_5113	Dynamin Family protein	HP	Dynamin family protein (HSP Dna	Tandem A
ColCht7420 1	Coleofasciculus chthonoplastes PCC 7420	MC7420_2927	Dynamin Family protein			Tandem A
Mic7113 2	Microcoleus sp. PCC 7113	Mic7113_1346	Dynamin Family protein	HP		Tandem A
Plank 2	Planktothricoides sp. SR001	AM228_02150	Dynamin	Dynamin		Tandem A
AcaMar11017 2	Acaryochloris marina MBIC11017	AM1_1423	bacterial dynamin-like protein	HP	HP	Tandem A
ChroCya 4	Chroococcales cyanobacterium CENA595	UH38_17700	Dynamin	Dynamin	HP	Tandem A
MicVaFGP-2 1	Microcoleus vaginatus FGP-2	MicvaDRAFT_4172	Dynamin Family protein	Dynamin family protein		Tandem A
OscNigro7112 1	Oscillatoria nigro-viridis PCC 7112	Osc7112_2088	Dynamin Family protein	Dynamin Family protein	HP	Tandem A
AnaCyl7122 1	Anabaena cylindrica PCC 7122	Anacy_3863	Dynamin Family protein	Dynamin family protein		Tandem A
NosPunc73102 2	Nostoc punctiforme PCC 73102	Npun_R6512	Dynamin Family protein	Dynamin family protein (BDLP)	P of UF	Tandem A
AcaMar11017 1	Acaryochloris marina MBIC11017	AM1_1263	bacterial dynamin-like protein			Tandem B
AcaMar11017 4	Acaryochloris marina MBIC11017	AM1_2720	bacterial dynamin-like protein			Tandem B
Lep7375 1	Leptolyngbya sp. PCC 7375	Lepto7375DRAFT_1514	Dynamin Family protein	transcriptional regulator	esponse regulator containing a CI	Tandem B
LepHerJ 1	Leptolyngbya sp. Heron Island J	N836_00865	Dynamin Family protein	family transcriptional regulator		Tandem B
Lep7375 3	Leptolyngbya sp. PCC 7375	Lepto7375DRAFT_2396	Dynamin Family protein	HP	P of UF	Tandem B
LepHerJ 2	Leptolyngbya sp. Heron Island J	N836_32005	Dynamin Family protein		sam-dependent methyltransfera	Tandem B
LepHerJ 3	Leptolyngbya sp. Heron Island J	N836_32070	Dynamin Family protein	HP	Dynamin Family protein	Tandem B
AcaMar11017 3	Acaryochloris marina MBIC11017	AM1_1426	bacterial dynamin-like protein	phosphoglycolate phosphatase, putative		Tandem B
ChaMin6605 2	Chamaesiphon minutus PCC 6605	Cha6605_3923	Dynamin Family protein	HP	HP	Tandem B
Mic7113 4	Microcoleus sp. PCC 7113	Mic7113_1349	Dynamin Family protein	FHA domain-containing protein	dynamin family protein	Tandem B
OscAcu6304 2	Oscillatoria acuminata PCC 6304	Oscil6304_5110	Dynamin Family protein	P of UF	Dynamin Family protein	Tandem B
ColCht7420 5	Coleofasciculus chthonoplastes PCC 7420	MC7420_5930	Dynamin Family protein	HP	Dynamin family protein	Tandem B
LimRob 2	Limnoraphis robusta	WN50_11780	Dynamin		dynamin	Tandem B
Plank 4	Planktothricoides sp. SR001	AM228_02175	Dynamin	HP		Tandem B
LimRob 3	Limnoraphis robusta	WN50_11785	Dynamin	dynamin	HP	Tandem B
CroWat8502 1	Crocosphaera watsonii WH 8502	CWATWH8502_1561	Dynamin	HP	Dynamin family protein (HSP Dna	Tandem B
CroWat8501 1	Crocosphaera watsonii WH 8501	CwatDRAFT_0874	dynamin	HP	HP	Tandem B
CroWat003 1	Crocosphaera watsonii WH 0003	CWATWH0003_0845	Dynamin		HP	Tandem B
CroWat005 1	Crocosphaera watsonii WH 0005	CWATWH0005_2075	dynamin	HP	DnaJ-class molecular chaperone	Tandem B
ChroCya 3	Chroococcales cyanobacterium CENA595	UH38_17695	Dynamin	HP	Dynamin	Tandem B
ColCht7420 4	Coleofasciculus chthonoplastes PCC 7420	MC7420_5753	Dynamin Family protein	Dynamin family protein	HP	Tandem B
Plank 3	Planktothricoides sp. SR001	AM228_02155	Dynamin		Dynamin	Tandem B
MicVaFGP-2 2	Microcoleus vaginatus FGP-2	MicvaDRAFT_4173	Dynamin Family protein	HP	Dynamin Family protein	Tandem B
OscNigro7112 2	Oscillatoria nigro-viridis PCC 7112	Osc7112_2089	Dynamin Family protein	HP	Dynamin Family protein	Tandem B
OscAcu6304 3	Oscillatoria acuminata PCC 6304	Oscil6304_5111	Dynamin Family protein	Dynamin Family protein	P of UF	Tandem B
Mic7113 3	Microcoleus sp. PCC 7113	Mic7113_1348	Dynamin Family protein	Dynamin Family protein (phosph	HP	Tandem B
ScyMil11283 1	Scytonema millei VB511283	QH73_23255	Dynamin		HP	Tandem B
TolBou 3	Tolypothrix bouteillei VB521301	DA73_0229120	Dynamin	HP	Dynamin family protein	Tandem B
Toly7601 2	Tolypothrix sp. PCC 7601	FDUTEX481_07821	Dynamin Family protein	HP	Dynamin Family protein	Tandem B
HassBys 4	Hassallia byssoidea VB512173	PI95_57355	dynamin	HP	Dynamin family protein	Tandem B
Cal7507 1	Calothrix sp. PCC 7507	Cal7507_2363	Dynamin Family protein	HP	Dynamin family protein (HSP Dna	Tandem B
CylSta7417 2	Cylindrospermum stagnale PCC 7417	Cylst_3143	Dynamin Family protein	HP	Dynamin family protein (HSP Dna	Tandem B
AnaVar 29413 1	Anabaena variabilis ATCC 29413	Ava_1350	dynamin			Tandem B
Nos7524 1	Nostoc sp. PCC 7524	Nos7524_0028	Dynamin Family protein	P of UF	Dynamin family protein (HSP Dna	Tandem B
AnaCyl7122 2	Anabaena cylindrica PCC 7122	Anacy_3864	Dynamin Family protein	HP	Dynamin family protein	Tandem B
NosDLP	Nostoc punctiforme PCC 73102	Npun_R6513 (BDLP)	Dynamin Family protein (BDLP)	HP	Dynamin family protein (HSP Dna	Tandem B
Riv7118	Rivularia sp. PCC 7116	Riv7116_4642	Dynamin Family protein		Dynamin family; DnaJ domain	Tandem B
ChroCya 1	Chroococcales cyanobacterium CENA595	UH38_07380	Dynamin Family protein		fatty-acid oxidation protein subu	not sorted
CrinEpi 1	Crinalium epipsammum PCC 9333	Cri9333_2354	Dynamin Family protein			not sorted
CyaApo 1	Cyanobacterium aponinum PCC 10605	Cyan10605_0425	Dynamin Family protein	Uncharacterized protein family U	HP	not sorted
CylSta7417 4	Cylindrospermum stagnale PCC 7417	Cylst_5480	Dynamin Family protein	HP		not sorted
Hapa220 2	Hapalosiphon sp. MRB220	AMR41_16410	Dynamin Family protein			not sorted
HassBys 2	Hassallia byssoidea VB512170	PI95_07810	Dynamin Family protein			not sorted
MicVaFGP-2 3	Microcoleus vaginatus FGP-2	MicvaDRAFT_4804	Dynamin Family protein		naphthoate synthase	not sorted
NosPunc73102 1	Nostoc punctiforme PCC 73102	Npun_F0558	Dynamin Family protein			not sorted
OscNigro7112 3	Oscillatoria nigro-viridis PCC 7112	Osc7112_2521	Dynamin Family protein		1,4-Dihydroxy-2-naphthoyl-CoA s	not sorted
Pho 2	Phormidium sp. OSCR	HLUCCO16_05230	Dynamin Family	HP	putativ ATPae	not sorted
Pho 3	Phormidium sp. OSCR	HLUCCO16_05285	Dynamin Family	HP	ABC transporter	not sorted
Pho 4	Phormidium sp. OSCR	HLUCCO16_06290	Dynamin Family			not sorted
Plank 1	Planktothricoides sp. SR001	AM228_01520	Dynamin Family protein	HP		not sorted
ProHoll9006 1	Prochlorothrix hollandica PCC 9006	PROH_02620	Dynamin Family protein	GTPase		not sorted
PseBic7429 1	Pseudanabaena biceps PCC 7429	Pse7429DRAFT_4458	Dynamin Family protein		HP	not sorted
AnaCyl7122 3	Anabaena cylindrica PCC 7122	Anacy_5476	Dynamin Family protein			not sorted

Abbreviations

°C	Degree Celsius
A	Alanine
ADL	*A. thaliana* dynamin-like protein
Amp	Ampicillin
approx.	Approximately
BDLP	Bacterial dynamin-like protein
bp	Base pair
C	Cytosine
CBB	Coomassie Brilliant Blue
cBDLP	Cyanobacterial dynamin-like protein
CD	Circular dichroism
CEF	Cyclic electron flow
CHAPS	3-[(3-cholamidopropyl)dimethylammonio]-1-propanesulfonate
Chla	Chlorophyll a
CTAP	Cetrimonium bromide
CT	C terminus
CTP	Chloroplast transit peptide
Cyt	Cytochrome
Cytp	Cytoplasm
CM	Cytoplasmic membrane
DCMU	3-(3,4-dichlorophenyl)-1,1-dimethylurea
DDAO	N,N-Dimethyldodecylamine N-oxide
DDM	n-Dodecyl-β-D-maltopyranoside
DGDG	1,2-dioleoyl-sn-glycero-3-phospho-(1'-rac-glycerol)
dig	Digestion
DLP	Dynamin-like protein
DMPG	1,2-Dimyristoyl-sn-glycero-3-phosphorylglycerol
DNA	Deoxyribonucleic acid
DOPG	1,2-dioleoyl-sn-glycero-3-phospho-(1'-rac-glycerol)
DRP	Dynamin-related protein
DS	Downstream
DTT	Dithiothreitol
E	Elution
E	Einstein
E. coli	*Escherichia coli*
e.g.	*Exempli gratia*
EHD	Eps15 homology domain-containing proteins
EtBR	Ethidium bromide
EtOH	Ethanol
Ex	Extract

F0	Background fluorescence (dark)
F0'	Background fluorescence (actin light)
Fm	Maximal fluorescence (dark)
Fm'	Maximal fluorescence (actin light)
FT	Flow through
FTIR	Fourier-transform infrared spectroscopy
Fv	Variable fluorescence (dark)
Fv'	Variable fluorescence (actin light)
FZL	Fuzzy onion like protein
FZO	Fuzzy onion protein
G	Glycine
G	Guanine
GBP	Guanyl-binding protein
GD	GTPase domain or G-domain
gDNA	Genomic DNA
GDP	Guanosine diphosphate
GED	GTPase effector domain
GMPPnP	Guanosine 5′-[β,γ-imido]triphosphate
GOE	Great Oxygen Event
GP	Generalized polarization
GTP	Guanosine-5'-triphosphate
HEPES	4-(2-hydroxyethyl)-1-piperazineethanesulfonic acid
His-Tag	Histidine tag
HL	High light
HRP	Horse radish peroxidase
I	Isoleucine
IE	Inner envelope
IMS	Inner membrane space
IPTG	Isopropyl-β-D-thiogalactopyranosid
IR	Infrared
I-TASSER	Iterative Threading Assembly Refinement
K	Lysine
k	Kilo-
kanR	Kanamycin resistance cassette
L	Leucine
L	Loading
LD	Loading dye
LDH	Lactate dehydrogenase
LSP	Low speed pellet
M	Marker
mcs	Multiple cloning side
MD	Middle domain
Mem	Membrane

MeOH	Methanol
MGDG	Monogalactosyldiacylglycerol
MID	Membrane interacting domain
MIS	Mitochondrial interaction side
N	Asparagine
NADH	Nicotinamide adenine dinucleotide (reduced)
nc	Negative control
NL	Normal light
O/N	Over night
OD	Optical density
OE	Outer envelope
OG	N-octyl-β-D-glucoside
OM	Outer membrane
P	Paddle
P	Pellet
P680	Reaction center PSII
P700	Reaction center PSI
pc	Positive control
PCR	Polymerase chain reaction
Pel	Pellet
Peri	Periplasm
Pi	Inorganic phosphate
PK	Pyruvate kinase
P-loop	Phosphate-binding loop
PQ	Plastoquinone
PRD	Proline rich domain
PSI	Photosystem I
PSII	Photosystem II
RB	Reaction buffer
RBS	Ribosome binding side
RE	Restriction enzyme
RS	Restriction site
RT	Room temperature
S	Serine
S	Supernatant
SB	Storage buffer
SDM	Site-directed mutagenesis
SDS	Sodium dodecyl sulfate
SDS-PAGE	Sodium dodecyl sulfate polyacrylamide gel electrophoresis
SEC	Size exclusion
SP	Saturation pulse
SQDG	Sulfoquinovosyl diacylglycerols
T	Threonine

T	Thymine
T	Transmembrane helix
TEM	Transmission electron microscopy
TM	Thylakoid membrane
US	Upstream
UV	Ultraviolet
VIS	Visible
W	Wash
WB	Western blot
WT	Wild type
X	Any amino acid

References

Accola, M.A., Huang, B., Masri, A. Al, McNiven, M.A., 2002. The antiviral dynamin family member, MxA, tubulates lipids and localizes to the smooth endoplasmic reticulum. J. Biol. Chem. 277, 21829–21835. doi:10.1074/jbc.M201641200

Adam, Z., Charuvi, D., Tsabari, O., Knopf, R.R., Reich, Z., 2011. Biogenesis of thylakoid networks in angiosperms: Knowns and unknowns. Plant Mol. Biol. 76, 221–234. doi:10.1007/s11103-010-9693-5

Ainslie Jr., G.R., Shill, J.P., Neet, K.E., 1972. Transients and Cooperativity. J. Biol. Chem. 247, 7088–7096.

Al-Haj, L., Lui, Y., Abed, R., Gomaa, M., Purton, S., 2016. Cyanobacteria as Chassis for Industrial Biotechnology: Progress and Prospects. Life 6, 42. doi:10.3390/life6040042

Alibolandi, M., Mirzahoseini, H., 2011. Chemical assistance in refolding of bacterial inclusion bodies. Biochem. Res. Int. 2011, 631607. doi:10.1155/2011/631607

Anderson, S.L., McIntosh, L., 1991. Light-activated heterotrophic growth of the cyanobacterium Synechocystis sp. strain PCC 6803: a blue-light-requiring process. J. Bacteriol. 173, 2761–7.

Antonny, B., Burd, C., De Camilli, P., Chen, E., Daumke, O., Faelber, K., Ford, M., Frolov, V.A., Frost, A., Hinshaw, J.E., Kozlov, M.M., Lenz, M., Low, H.H., Mcmahon, H., Merrifield, C., Pollard, T.D., Robinson, P.J., 2016. Membrane fission by dynamin: what we know and what we need to know. EMBO J. 35, 2270–2284. doi:10.15252/embj

Arimura, S., Tsutsumi, N., 2002. A dynamin-like protein (ADL2b), rather than FtsZ, is involved in Arabidopsis mitochondrial division. Proc. Natl. Acad. Sci. U. S. A. 99, 5727–5731. doi:10.1073/pnas.082663299

Arimura, S.I., Aida, G.P., Fujimoto, M., Nakazono, M., Tsutsumi, N., 2004. Arabidopsis Dynamin-Like Protein 2a (ADL2a), Like ADL2b, is Involved in Plant Mitochondrial Division. Plant Cell Physiol. 45, 236–242. doi:10.1093/pcp/pch024

Aung, K., Hu, J., 2012. Differential Roles of Arabidopsis Dynamin-Related Proteins DRP3A, DRP3B, and DRP5B in Organelle Division. J. Integr. Plant Biol. 54, 921–931. doi:10.1111/j.1744-7909.2012.01174.x

Aung, K., Hu, J., 2009. The Arabidopsis peroxisome division mutant pdd2 is defective in the dynamin-

related protein3A (DRP3A) gene. Plant Signal. Behav. 4, 542–544. doi:10.4161/psb.4.6.8699

Awai, K., Kakimoto, T., Awai, C., Kaneko, T., Nakamura, Y., Takamiya, K., Wada, H., Ohta, H., 2006. Comparative Genomic Analysis Revealed a Gene for Monoglucosyldiacylglycerol Synthase, an Enzyme for Photosynthetic Membrane Lipid Synthesis in Cyanobacteria. Plant Physiol. 141.

Awai, K., Xu, C., Tamot, B., Benning, C., 2006. A phosphatidic acid-binding protein of the chloroplast inner envelope membrane involved in lipid trafficking. Proc. Natl. Acad. Sci. 103, 10817–10822. doi:10.1073/pnas.0602754103

Barten, R., Lill, H., 1995. DNA-uptake in the naturally competent cynaobacterium, Synechocystis sp. PCC 6803. FEMS Microbiol. Lett. 129, 83–88.

Barthel, S., Bernát, G., Seidel, T., Rupprecht, E., Kahmann, U., Schneider, D., 2013. Thylakoid membrane maturation and PSII activation are linked in greening Synechocystis sp. PCC 6803 cells. Plant Physiol. 163, 1037–46. doi:10.1104/pp.113.224428

Belenguer, P., Pellegrini, L., 2013. The dynamin GTPase OPA1: More than mitochondria? Biochim. Biophys. Acta - Mol. Cell Res. 1833, 176–183. doi:10.1016/j.bbamcr.2012.08.004

Benning, C., 2009. Mechanisms of Lipid Transport Involved in Organelle Biogenesis in Plant Cells. Annu. Rev. Cell Dev. Biol. 25, 71–91. doi:10.1146/annurev.cellbio.042308.113414

Bernát, G., Waschewski, N., Rögner, M., 2009. Towards efficient hydrogen production: the impact of antenna size and external factors on electron transport dynamics in Synechocystis PCC 6803. Photosynth. Res. 99, 205–216. doi:10.1007/s11120-008-9398-7

Betz, S.F., 1993. Disulfide bonds and the stability of globular proteins. Protein Sci. 2, 1551–8. doi:10.1002/pro.5560021002

Bian, X., Klemm, R.W., Liu, T.Y., Zhang, M., Sun, S., Sui, X., Liu, X., Rapoport, T.A., Hu, J., 2011. Structures of the atlastin GTPase provide insight into homotypic fusion of endoplasmic reticulum membranes. Proc. Natl. Acad. Sci. U. S. A. 108, 3976–81. doi:10.1073/pnas.1101643108

Blankenship, R.E., 2010. Early evolution of photosynthesis. Plant Physiol. 154, 434–8. doi:10.1104/pp.110.161687

Block, M.A., Douce, R., Joyard, J., Rolland, N., 2007. Chloroplast envelope membranes: a dynamic interface between plastids and the cytosol. Photosynth. Res. 92, 225–244. doi:10.1007/s11120-007-9195-8

Boudière, L., Michaud, M., Petroutsos, D., Rébeillé, F., Falconet, D., Bastien, O., Roy, S., Finazzi, G., Rolland, N., Jouhet, J., Block, M.A., Maréchal, E., 2014. Glycerolipids in photosynthesis: Composition, synthesis and trafficking. Biochim. Biophys. Acta - Bioenerg. 1837, 470–480. doi:10.1016/j.bbabio.2013.09.007

Bramkamp, M., 2012. Structure and function of bacterial dynamin-like proteins. Biol. Chem. 393, 1203–14. doi:10.1515/hsz-2012-0185

Brown, E.A., Hardwidge, P.R., 2007. Biochemical characterization of the enterotoxigenic Escherichia coli LeoA protein. Microbiology 153, 3776–3784. doi:10.1099/mic.0.2007/009084-0

Bryan, S.J., Burroughs, N.J., Evered, C., Sacharz, J., Nenninger, A., Mullineaux, C.W., Spence, E.M., 2011. Loss of the SPHF Homologue Slr1768 Leads to a Catastrophic Failure in the Maintenance of Thylakoid Membranes in Synechocystis sp. PCC 6803. PLoS One 6, e19625. doi:10.1371/journal.pone.0019625

Büdel, B., 2011. Cyanobacteria: Habitats and Species. Springer, Berlin, Heidelberg, pp. 11–21. doi:10.1007/978-3-642-19106-0_2

Bürmann, F., Ebert, N., van Baarle, S., Bramkamp, M., 2011. A bacterial dynamin-like protein mediating nucleotide-independent membrane fusion. Mol. Microbiol. 79, 1294–304. doi:10.1111/j.1365-2958.2011.07523.x

Burmann, F., Sawant, P., Bramkamp, M., 2012. Identification of interaction partners of the dynamin-like protein DynA from Bacillus subtilis. Commun Integr Biol 5, 362–369.

Bustillo-Zabalbeitia, I., Montessuit, S., Raemy, E., Basañez, G., Terrones, O., Martinou, J.-C., 2014. Specific interaction with cardiolipin triggers functional activation of Dynamin-Related Protein 1. PLoS One 9, e102738. doi:10.1371/journal.pone.0102738

Byrnes, L.J., Sondermann, H., 2011. Structural basis for the nucleotide-dependent dimerization of the large G protein atlastin-1/SPG3A. Proc. Natl. Acad. Sci. U. S. A. 108, 2216–21. doi:10.1073/pnas.1012792108

Cao, Y.L., Meng, S., Chen, Y., Feng, J.X., Gu, D.D., Yu, B., Li, Y.J., Yang, J.Y., Liao, S., Chan, D.C., Gao, S., 2017.

MFN1 structures reveal nucleotide-triggered dimerization critical for mitochondrial fusion. Nature 542, 372–376. doi:10.1038/nature21077

Chang, S.-G., Choi, K.-D., Jang, S.-H., Shin, H.-C., 2003. Role of disulfide bonds in the structure and activity of human insulin. Mol. Cells 16, 323–30.

Chapman, D.J., De-Felice, J., Barber, J., 1983. Growth temperature effects on thylakoid membrane lipid and protein content of pea chloroplasts. Plant Physiol. 72, 225–8.

Chappie, J.S., Acharya, S., Leonard, M., Schmid, S.L., Dyda, F., 2010. G domain dimerization controls dynamin's assembly-stimulated GTPase activity. Nature 465, 435–440. doi:10.1038/nature09032

Chappie, J.S., Acharya, S., Liu, Y.-W., Leonard, M., Pucadyil, T.J., Schmid, S.L., 2009. An intramolecular signaling element that modulates dynamin function in vitro and in vivo. Mol. Biol. Cell 20, 3561–71. doi:10.1091/mbc.E09-04-0318

Chappie, J.S., Mears, J.A., Fang, S., Leonard, M., Schmid, S.L., Milligan, R.A., Hinshaw, J.E., Dyda, F., 2011. A pseudoatomic model of the dynamin polymer identifies a hydrolysis-dependent powerstroke. Cell 147, 209–222. doi:10.1016/j.cell.2011.09.003

Charuvi, D., Kiss, V., Nevo, R., Shimoni, E., Adam, Z., Reich, Z., 2012. Gain and Loss of Photosynthetic Membranes during Plastid Differentiation in the Shoot Apex of Arabidopsis. Plant Cell Online 24.

Cho, B., Choi, S.Y., Cho, H.M., Kim, H.J., Sun, W., 2013. Physiological and pathological significance of dynamin-related protein 1 (drp1)-dependent mitochondrial fission in the nervous system. Exp. Neurobiol. 22, 149–57. doi:10.5607/en.2013.22.3.149

Choi, H., Mascuch, S.J., Villa, F.A., Byrum, T., Teasdale, M.E., Smith, J.E., Preskitt, L.B., Rowley, D.C., Gerwick, L., Gerwick, W.H., 2012. Honaucins A-C, potent inhibitors of inflammation and bacterial quorum sensing: synthetic derivatives and structure-activity relationships. Chem. Biol. 19, 589–98. doi:10.1016/j.chembiol.2012.03.014

Chuartzman, S.G., Nevo, R., Shimoni, E., Charuvi, D., Kiss, V., Ohad, I., Brumfeld, V., Reich, Z., 2008. Thylakoid Membrane Remodeling during State Transitions in Arabidopsis. PLANT CELL ONLINE 20, 1029–1039. doi:10.1105/tpc.107.055830

Chung, C.T., Niemela, S.L., Miller, R.H., 1989. One-step preparation of competent Escherichia coli: transformation and storage of bacterial cells in the same solution. Proc. Natl. Acad. Sci. U. S. A. 86, 2172–5.

Cook, T.A., Urrutia, R., McNiven, M.A., 1994. Identification of dynamin 2, an isoform ubiquitously expressed in rat tissues. Proc. Natl. Acad. Sci. U. S. A. 91, 644–8.

Cook, T., Mesa, K., Urrutia, R., 1996. Three dynamin-encoding genes are differentially expressed in developing rat brain. J. Neurochem. 67, 927–31.

D'Angelo, E., Crutchfield, J., Vandiviere, M., 2001. Rapid, Sensitive, Microscale Determination of Phosphate in Water and Soil. J. Environ. Qual. 30, 2206. doi:10.2134/jeq2001.2206

Daumke, O., Lundmark, R., Vallis, Y., Martens, S., Butler, P.J.G., McMahon, H.T., 2007. Architectural and mechanistic insights into an EHD ATPase involved in membrane remodelling. Nature 449, 923–927. doi:10.1038/nature06173

Daumke, O., Praefcke, G.J.K., 2016. Invited review: Mechanisms of GTP hydrolysis and conformational transitions in the dynamin superfamily. Biopolymers 105, 580–593. doi:10.1002/bip.22855

Daumke, O., Roux, A., Haucke, V., 2014. BAR Domain Scaffolds in Dynamin-Mediated Membrane Fission. Cell 156, 882–892. doi:10.1016/j.cell.2014.02.017

de Beer, T., Carter, R.E., Lobel-Rice, K.E., Sorkin, A., Overduin, M., 1998. Structure and Asn-Pro-Phe binding pocket of the Eps15 homology domain. Science 281, 1357–60. doi:10.1126/science.281.5381.1357

de los Ríos, A., Grube, M., Sancho, L.G., Ascaso, C., 2007. Ultrastructural and genetic characteristics of endolithic cyanobacterial biofilms colonizing Antarctic granite rocks. FEMS Microbiol. Ecol. 59, 386–95.

DeVay, R.M., Dominguez-Ramirez, L., Lackner, L.L., Hoppins, S., Stahlberg, H., Nunnari, J., 2009. Coassembly of Mgm1 isoforms requires cardiolipin and mediates mitochondrial inner membrane fusion. J. Cell Biol. 186, 793–803. doi:10.1083/jcb.200906098

Dörmann, P., Hoffmann-Benning, S., Balbo, I., Benning, C., 1995. Isolation and characterization of an Arabidopsis mutant deficient in the thylakoid lipid digalactosyl diacylglycerol. Plant Cell 7, 1801–10.

doi:10.1105/tpc.7.11.1801

Dorne, A.-J., Joyard, J., Douce, R., 1990. Do thylakoids really contain phosphatidylcholine? Proc. Natl. Acad. Sci. U. S. A. 87, 71–74. doi:10.1073/pnas.87.1.71

Eckhardt, U., Grimm, B., Hörtensteiner, S., 2004. Recent advances in chlorophyll biosynthesis and breakdown in higher plants. Plant Mol. Biol. 56, 1–14. doi:10.1007/s11103-004-2331-3

Engel, B.D., Schaffer, M., Kuhn Cuellar, L., Villa, E., Plitzko, J.M., Baumeister, W., 2015. Native architecture of the Chlamydomonas chloroplast revealed by in situ cryo-electron tomography. Elife 4. doi:10.7554/eLife.04889

Essigmann, B., Güler, S., Narang, R.A., Linke, D., Benning, C., 1998. Phosphate availability affects the thylakoid lipid composition and the expression of SQD1, a gene required for sulfolipid biosynthesis in Arabidopsis thaliana. Proc. Natl. Acad. Sci. U. S. A. 95, 1950–5.

Faelber, K., Held, M., Gao, S., Posor, Y., Haucke, V., Noé, F., Daumke, O., 2012. Structural insights into dynamin-mediated membrane fission. Structure 20, 1621–1628. doi:10.1016/j.str.2012.08.028

Faelber, K., Posor, Y., Gao, S., Held, M., Roske, Y., Schulze, D., Haucke, V., Noé, F., Daumke, O., 2011. Crystal structure of nucleotide-free dynamin. Nature 477, 556–60. doi:10.1038/nature10369

Fan, D.-Y., Nie, Q., Hope, A.B., Hillier, W., Pogson, B.J., Chow, W.S., 2007. Quantification of cyclic electron flow around Photosystem I in spinach leaves during photosynthetic induction. Photosynth. Res. 94, 347–357. doi:10.1007/s11120-006-9127-z

Ferguson, S.M., De Camilli, P., 2012. Dynamin, a membrane-remodelling GTPase. Nat. Rev. Mol. Cell Biol. 13, 75–88. doi:10.1038/nrm3266

Finn, R.D., Attwood, T.K., Babbitt, P.C., Bateman, A., Bork, P., Bridge, A.J., Chang, H.Y., Dosztanyi, Z., El-Gebali, S., Fraser, M., Gough, J., Haft, D., Holliday, G.L., Huang, H., Huang, X., Letunic, I., Lopez, R., Lu, S., Marchler-Bauer, A., Mi, H., Mistry, J., Natale, D.A., Necci, M., Nuka, G., Orengo, C.A., Park, Y., Pesseat, S., Piovesan, D., Potter, S.C., Rawlings, N.D., Redaschi, N., Richardson, L., Rivoire, C., Sangrador-Vegas, A., Sigrist, C., Sillitoe, I., Smithers, B., Squizzato, S., Sutton, G., Thanki, N., Thomas, P.D., Tosatto, S.C.E., Wu, C.H., Xenarios, I., Yeh, L.S., Young, S.Y., Mitchell, A.L., 2017. InterPro in 2017-beyond protein family and domain annotations. Nucleic Acids Res. 45, D190–D199.

doi:10.1093/nar/gkw1107

Finn, R.D., Bateman, A., Clements, J., Coggill, P., Eberhardt, R.Y., Eddy, S.R., Heger, A., Hetherington, K., Holm, L., Mistry, J., Sonnhammer, E.L.L., Tate, J., Punta, M., 2014. Pfam: the protein families database. Nucleic Acids Res. 42, D222-30. doi:10.1093/nar/gkt1223

Fleckenstein, J.M., Lindler, L.E., Elsinghorst, E.A., Dale, J.B., 2000. Identification of a gene within a pathogenicity island of enterotoxigenic Escherichia coli H10407 required for maximal secretion of the heat-labile enterotoxin. Infect. Immun. 68, 2766–2774. doi:10.1128/IAI.68.5.2766-2774.2000

Ford, M.G.J., Jenni, S., Nunnari, J., 2011. The crystal structure of dynamin. Nature 477, 561–6. doi:10.1038/nature10441

Franz, J., Lelle, M., Peneva, K., Bonn, M., Weidner, T., 2016. SAP(E) - A cell-penetrating polyproline helix at lipid interfaces. Biochim. Biophys. Acta - Biomembr. 1858, 2028–2034. doi:10.1016/j.bbamem.2016.05.021

Franz, J., Van Zadel, M.J., Weidner, T., 2017. A trough for improved SFG spectroscopy of lipid monolayers. Rev. Sci. Instrum. 88. doi:10.1063/1.4982050

Frezza, C., Cipolat, S., Martins de Brito, O., Micaroni, M., Beznoussenko, G. V., Rudka, T., Bartoli, D., Polishuck, R.S., Danial, N.N., De Strooper, B., Scorrano, L., 2006. OPA1 Controls Apoptotic Cristae Remodeling Independently from Mitochondrial Fusion. Cell 126, 177–189. doi:10.1016/j.cell.2006.06.025

Fröhlich, C., Grabiger, S., Schwefel, D., Faelber, K., Rosenbaum, E., Mears, J., Rocks, O., Daumke, O., 2013. Structural insights into oligomerization and mitochondrial remodelling of dynamin 1-like protein. EMBO J. 32, 1280–1292. doi:10.1038/emboj.2013.74

Fu, L., Liu, J., Yan, E.C.Y., 2011a. Chiral sum frequency generation spectroscopy for characterizing protein secondary structures at interfaces. J. Am. Chem. Soc. 133, 8094–8097. doi:10.1021/ja201575e

Fu, L., Wang, Z., Yan, E.C.Y., 2011b. Chiral vibrational structures of proteins at interfaces probed by sum frequency generation spectroscopy. Int. J. Mol. Sci. 12, 9404–9425. doi:10.3390/ijms12129404

Fuhrmann, E., Bultema, J.B., Kahmann, U., Rupprecht, E., Boekema, E.J., Schneider, D., 2009. The Vesicle-

inducing Protein 1 from Synechocystis sp. PCC 6803 Organizes into Diverse Higher-Ordered Ring Structures. Mol. Biol. Cell 20, 4620–4628. doi:10.1091/mbc.E09-04-0319

Fuhrmann, E., Gathmann, S., Rupprecht, E., Golecki, J., Schneider, D., 2009. Thylakoid membrane reduction affects the photosystem stoichiometry in the cyanobacterium Synechocystis sp. PCC 6803. Plant Physiol. 149, 735–744. doi:10.1104/pp.108.132373

Fujimoto, M., Arimura, S. -i., Ueda, T., Takanashi, H., Hayashi, Y., Nakano, A., Tsutsumi, N., 2010. Arabidopsis dynamin-related proteins DRP2B and DRP1A participate together in clathrin-coated vesicle formation during endocytosis. Proc. Natl. Acad. Sci. 107, 6094–6099. doi:10.1073/pnas.0913562107

Fujimoto, M., Arimura, S.I., Mano, S., Kondo, M., Saito, C., Ueda, T., Nakazono, M., Nakano, A., Nishimura, M., Tsutsumi, N., 2009. Arabidopsis dynamin-related proteins DRP3A and DRP3B are functionally redundant in mitochondrial fission, but have distinct roles in peroxisomal fission. Plant J. 58, 388–400. doi:10.1111/j.1365-313X.2009.03786.x

Fujisawa, T., Narikawa, R., Maeda, S.-I., Watanabe, S., Kanesaki, Y., Kobayashi, K., Nomata, J., Hanaoka, M., Watanabe, M., Ehira, S., Suzuki, E., Awai, K., Nakamura, Y., 2017. CyanoBase: a large-scale update on its 20th anniversary. Nucleic Acids Res. 45, D551–D554. doi:10.1093/nar/gkw1131

Gao, H., Kadirjan-Kalbach, D., Froehlich, J.E., Osteryoung, K.W., 2003. ARC5, a cytosolic dynamin-like protein from plants, is part of the chloroplast division machinery. Proc. Natl. Acad. Sci. 100, 4328–4333. doi:10.1073/pnas.0530206100

Gao, H., Sage, T.L., Osteryoung, K.W., 2006. FZL, an FZO-like protein in plants, is a determinant of thylakoid and chloroplast morphology. Proc Natl Acad Sci USA 103, 6759–6764. doi:10.1073/pnas.0507287103

Gao, S., Von der Malsburg, A., Dick, A., Faelber, K., Schröder, G.F., Haller, O., Kochs, G., Daumke, O., 2011. Structure of Myxovirus Resistance Protein A Reveals Intra- and Intermolecular Domain Interactions Required for the Antiviral Function. Immunity 35, 514–525. doi:10.1016/j.immuni.2011.07.012

Gao, S., von der Malsburg, A., Paeschke, S., Behlke, J., Haller, O., Kochs, G., Daumke, O., 2010. Structural basis of oligomerization in the stalk region of dynamin-like MxA. Nature 465, 502–506. doi:10.1038/nature08972

Giordano, M., Beardall, J., Raven, J.A., 2005. CO2 concentrating mechanisms in algae: Mechanisms, Environmental Modulation, and Evolution. Annu. Rev. Plant Biol. 56, 99–131. doi:10.1146/annurev.arplant.56.032604.144052

Gounaris, K., Sundby, C., Andersson, B., Barber, J., 1983. Lateral heterogeneity of polar lipids in the thylakoid membranes of spinach chloroplasts. FEBS Lett. 156, 170–174. doi:10.1016/0014-5793(83)80271-3

Güler, S., Seeliger, A., Härtel, H., Renger, G., Benning, C., 1996. A null mutant of Synechococcus sp. PCC7942 deficient in the sulfolipid sulfoquinovosyl diacylglycerol. J. Biol. Chem. 271, 7501–7.

Guyot-Sionnest, P., Hunt, J.H., Shen, Y.R., 1987. Sum-frequency vibrational spectroscopy of a Langmuir film: Study of molecular orientation of a two-dimensional system. Phys. Rev. Lett. 59, 1597–1600. doi:10.1103/PhysRevLett.59.1597

Heidrich, J., Thurotte, A., Schneider, D., 2017. Biochimica et Biophysica Acta Speci fi c interaction of IM30 / Vipp1 with cyanobacterial and chloroplast membranes results in membrane remodeling and eventually in membrane fusion ☆. BBA - Biomembr. 1859, 537–549. doi:10.1016/j.bbamem.2016.09.025

Hennig, R., Heidrich, J., Saur, M., Schmu, L., Roeters, S.J., Hellmann, N., Schneider, D., Woutersen, S., Bonn, M., Weidner, T., 2015. IM30 triggers membrane fusion in cyanobacteria and chloroplasts. doi:10.1038/ncomms8018

Herbstova, M., Tietz, S., Kinzel, C., Turkina, M. V., Kirchhoff, H., 2012. Architectural switch in plant photosynthetic membranes induced by light stress. Proc. Natl. Acad. Sci. 109, 20130–20135. doi:10.1073/pnas.1214265109

Hernández-Prieto, M.A., Futschik, M.E., 2012. CyanoEXpress: A web database for exploration and visualisation of the integrated transcriptome of cyanobacterium Synechocystis sp. PCC6803. Bioinformation 8, 634–638. doi:10.6026/97320630008634

Hernández-Prieto, M.A., Semeniuk, T.A., Giner-Lamia, J., Futschik, M.E., 2016. The Transcriptional Landscape of the Photosynthetic Model Cyanobacterium Synechocystis sp. PCC6803. Sci. Rep. 6, 22168. doi:10.1038/srep22168

Herrero, A., Flores, E. (Flores G., 2008. The cyanobacteria : molecular biology, genomics, and evolution. Caister Academic Press.

Hinshaw, J.E., 2000. Dynamin and Its Role in Membrane Fission. Annu. Rev. Cell Dev. Biol. 16, 483–519.

Hinshaw, J.E., Schmid, S.L., 1995. Dynamin self-assembles into rings suggesting a mechanism for coated vesicle budding. Nature. doi:10.1038/374190a0

Hohmann-Marriott, M.F., Blankenship, R.E., 2011. Evolution of Photosynthesis. Annu. Rev. Plant Biol. 62, 515–548. doi:10.1146/annurev-arplant-042110-103811

Holland, H.D., 2006. The oxygenation of the atmosphere and oceans. Philos. Trans. R. Soc. Lond. B. Biol. Sci. 361, 903–915. doi:10.1007/3-540-33088-7_2

Hoober, J.K., Boyd, C. 0, Paavola, L.G., 1991. Origin of Thylakoid Membranes in Chiamydomonas reinhardtii y-1 at 38°C. Plant Physiol 96, 1321–1328.

Hope, M.J., Bally, M.B., Mayer, L.D., Janoff, A.S., Cullis, P.R., 1986. Generation of multilamellar and unilamellar phospholipid vesicles. Chem. Phys. Lipids 40, 89–107. doi:10.1016/0009-3084(86)90065-4

Hu, J., Li, T., Xu, W., Zhan, J., Chen, H., He, C., Wang, Q., 2017. Small Antisense RNA RblR Positively Regulates RuBisCo in Synechocystis sp . PCC 6803 8, 1–14. doi:10.3389/fmicb.2017.00231

Huber, S.C., Edwards, G.E., 1975. Effect of DBMIB, DCMU and antimycin A on cyclic and noncyclic electron flow in C4 mesophyll chloroplasts. FEBS Lett. 58, 211–214. doi:10.1016/0014-5793(75)80261-4

Ingerman, E., Nunnari, J., 2005. A continuous, regenerative coupled GTPase assay for dynamin-related proteins. Methods Enzymol. 404, 611–9. doi:10.1016/S0076-6879(05)04053-X

Itaya, K., Ui, M., 1966. A new micromethod for the colorimetric determination of inorganic phosphate. Clin. Chim. Acta. 14, 361–366.

Itsui, Y., Sakamoto, N., Kakinuma, S., Nakagawa, M., Sekine-Osajima, Y., Tasaka-Fujita, M., Nishimura-Sakurai, Y., Suda, G., Karakama, Y., Mishima, K., Yamamoto, M., Watanabe, T., Ueyama, M., Funaoka, Y., Azuma, S., Watanabe, M., 2009. Antiviral effects of the interferon-induced protein guanylate

binding protein 1 and its interaction with the hepatitis C virus NS5B protein. Hepatology 50, 1727–1737. doi:10.1002/hep.23195

Iwai, M., Yokono, M., Nakano, A., 2015. Visualizing structural dynamics of thylakoid membranes. Sci. Rep. 4, 3768. doi:10.1038/srep03768

Jilly, R., Khan, N.Z., Aronsson, H., Schneider, D., 2018. Dynamin-Like Proteins Are Potentially Involved in Membrane Dynamics within Chloroplasts and Cyanobacteria. Front. Plant Sci. 9, 1–13. doi:10.3389/fpls.2018.00206

Jin, J.B., Kim, Y.A., Kim, S.J., Lee, S.H., Kim, D.H., Cheong, G.W., Hwang, I., 2001. A New Dynamin-Like Protein, ADL6, Is Involved in Trafficking from the trans-Golgi Network to the Central Vacuole in Arabidopsis. Plant Cell Online 13, 1511–1526. doi:10.1105/tpc.13.7.1511

Jouhet, J., Maréchal, E., Block, M.A., 2007. Glycerolipid transfer for the building of membranes in plant cells. Prog. Lipid Res. 46, 37–55. doi:10.1016/j.plipres.2006.06.002

Joyard, J., Ferro, M., Masselon, C., Seigneurin-Berny, D., Salvi, D., Garin, J., Rolland, N., 2010. Chloroplast proteomics highlights the subcellular compartmentation of lipid metabolism. Prog. Lipid Res. 49, 128–158. doi:10.1016/j.plipres.2009.10.003

Kanehisa, M., Furumichi, M., Tanabe, M., Sato, Y., Morishima, K., 2017. KEGG: new perspectives on genomes, pathways, diseases and drugs. Nucleic Acids Res. 45, D353–D361. doi:10.1093/nar/gkw1092

Kaneko, T., Sato, S., Kotani, H., Tanaka, A., Asamizu, E., Nakamura, Y., Miyajima, N., Hirosawa, M., Sugiura, M., Sasamoto, S., Kimura, T., Hosouchi, T., Matsuno, A., Muraki, A., Nakazaki, N., Naruo, K., Okumura, S., Shimpo, S., Takeuchi, C., Wada, T., Watanabe, A., Yamada, M., Yasuda, M., Tabata, S., 1996. Sequence analysis of the genome of the unicellular cyanobacterium Synechocystis sp. strain PCC6803. II. Sequence determination of the entire genome and assignment of potential protein-coding regions. DNA Res. 3, 109–36.

Kang, B.-H., Busse, J.S., Bednarek, S.Y., 2003. Members of the Arabidopsis Dynamin-Like Gene Family, ADL1, Are Essential for Plant Cytokinesis and Polarized Cell Growth. Plant Cell Online 15, 899–913. doi:10.1105/tpc.009670

Keller, R., Schneider, D., 2013. Homologs of the yeast Tvp38 vesicle-associated protein are conserved in chloroplasts and cyanobacteria. Front. Plant Sci. 4, 467. doi:10.3389/fpls.2013.00467

Khan, N.Z., Lindquist, E., Aronsson, H., Preisinger, C., Fuchs, E., 2013. New Putative Chloroplast Vesicle Transport Components and Cargo Proteins Revealed Using a Bioinformatics Approach: An Arabidopsis Model. PLoS One 8, e59898. doi:10.1371/journal.pone.0059898

Khattari, Z., 2016. Adsorption kinetics of low-density lipoproteins with Langmuir monolayer. J. Biol. Phys. 42, 539–550. doi:10.1007/s10867-016-9422-7

Kimple, M.E., Brill, A.L., Pasker, R.L., 2013. Overview of affinity tags for protein purification. Curr. Protoc. protein Sci. 73, Unit 9.9. doi:10.1002/0471140864.ps0909s73

Kirchhoff, H., Hall, C., Wood, M., Herbstova, M., Tsabari, O., Nevo, R., Charuvi, D., Shimoni, E., Reich, Z., 2011. Dynamic control of protein diffusion within the granal thylakoid lumen. Proc. Natl. Acad. Sci. 108, 20248–20253. doi:10.1073/pnas.1104141109

Kochs, G., Haller, O., 1999. Interferon-induced human MxA GTPase blocks nuclear import of Thogoto virus nucleocapsids. Proc. Natl. Acad. Sci. U. S. A. 96, 2082–6.

Kopf, M., Klähn, S., Scholz, I., Matthiessen, J.K.F., Hess, W.R., Voß, B., 2014. Comparative Analysis of the Primary Transcriptome of Synechocystis sp. PCC 6803. DNA Res. 21, 527–539. doi:10.1093/dnares/dsu018

Krogh, A., Larsson, B., von Heijne, G., Sonnhammer, E.L.., 2001. Predicting transmembrane protein topology with a hidden Markov model: application to complete genomes. J. Mol. Biol. 305, 567–580. doi:10.1006/jmbi.2000.4315

Kroll, D., Meierhoff, K., Bechtold, N., Kinoshita, M., Westphal, S., Vothknecht, U.C., Soll, J., Westhoff, P., 2001. VIPP1, a nuclear gene of Arabidopsis thaliana essential for thylakoid membrane formation. Proc. Natl. Acad. Sci. U. S. A. 98, 4238–42. doi:10.1073/pnas.061500998

Kyte, J., Doolittle, R.F., 1982. A simple method for displaying the hydrophobic character of a protein. J. Mol. Biol. 157, 105–132. doi:10.1016/0022-2836(82)90515-0

Labarre, J., Chauvat, F., Thuriaux, P., 1989. Insertional mutagenesis by random cloning of antibiotic

resistance genes into the genome of the cyanobacterium Synechocystis strain PCC 6803. J. Bacteriol. 171, 3449–57.

Lambert, A.G., Davies, P.B., Neivandt, D.J., 2005. Implementing the Theory of Sum Frequency Generation Vibrational Spectroscopy: A Tutorial Review. Appl. Spectrosc. Rev. 40, 103–145. doi:10.1081/ASR-200038326

Lea-Smith, D.J., Bombelli, P., Vasudevan, R., Howe, C.J., 2016. Photosynthetic, respiratory and extracellular electron transport pathways in cyanobacteria. Biochim. Biophys. Acta - Bioenerg. 1857, 247–255. doi:10.1016/j.bbabio.2015.10.007

Lee, A.G., 2000. Membrane lipids : It ' s only a phase 377–380.

Leipe, D.D., Wolf, Y.I., Koonin, E. V, Aravind, L., 2002. Classification and evolution of P-loop GTPases and related ATPases. J. Mol. Biol. 317, 41–72. doi:10.1006/jmbi.2001.5378

Li, Z., Ding, B., Zhou, X., Wang, G.-L., 2017. The Rice Dynamin-Related Protein OsDRP1E Negatively Regulates Programmed Cell Death by Controlling the Release of Cytochrome c from Mitochondria. PLOS Pathog. 13, e1006157. doi:10.1371/journal.ppat.1006157

Liberton, M., Austin, J.R., Berg, R.H., Pakrasi, H.B., 2011a. Unique Thylakoid Membrane Architecture of a Unicellular N2-Fixing Cyanobacterium Revealed by Electron Tomography. Plant Physiol. 155, 1656–1666. doi:10.1104/pp.110.165332

Liberton, M., Austin, J.R., Berg, R.H., Pakrasi, H.B., Pakrasi, H.B., 2011b. Insights into the complex 3-D architecture of thylakoid membranes in unicellular cyanobacterium Cyanothece sp. ATCC 51142. Plant Signal. Behav. 6, 566–9. doi:10.4161/psb.6.4.14946

Lindquist, E., Solymosi, K., Aronsson, H., 2016. Vesicles Are Persistent Features of Different Plastids. Traffic 17, 1125–1138. doi:10.1111/tra.12427

Liu, L.-N., 2016. Distribution and dynamics of electron transport complexes in cyanobacterial thylakoid membranes. Biochim. Biophys. Acta 1857, 256–65. doi:10.1016/j.bbabio.2015.11.010

Liu, T.Y., Bian, X., Romano, F.B., Shemesh, T., Rapoport, T.A., Hu, J., 2015. Cis and trans interactions between atlastin molecules during membrane fusion. Proc. Natl. Acad. Sci. U. S. A. 112, E1851-60.

doi:10.1073/pnas.1504368112

Low, H.H., Löwe, J., 2006. A bacterial dynamin-like protein. Nature 444, 766–9. doi:10.1038/nature05312

Low, H.H.H., Sachse, C., Amos, L.L.A. LA, Löwe, J., 2009. Structure of a Bacterial Dynamin-like Protein Lipid Tube Provides a Mechanism For Assembly and Membrane Curving. Cell 139, 1342–1352. doi:10.1016/j.cell.2009.11.003

Lu, B., Xu, C., Awai, K., Jones, A.D., Benning, C., 2007. A small ATPase protein of Arabidopsis, TGD3, involved in chloroplast lipid import. J. Biol. Chem. 282, 35945–53. doi:10.1074/jbc.M704063200

Lu, S., Jang, H., Gu, S., Zhang, J., Nussinov, R., 2016. Drugging Ras GTPase: a comprehensive mechanistic and signaling structural view. Chem. Soc. Rev. 45, 4929–4952. doi:10.1039/C5CS00911A

Mano, S., Nakamori, C., Kondo, M., Hayashi, M., Nishimura, M., 2004. An Arabidopsis dynamin-related protein, DRP3A, controls both peroxisomal and mitochondrial division. Plant J. 38, 487–98. doi:10.1111/j.1365-313X.2004.02063.x

Marin, K., Stirnberg, M., Eisenhut, M., Krämer, R., Hagemann, M., 2006. Osmotic stress in Synechocystis sp. PCC 6803: low tolerance towards nonionic osmotic stress results from lacking activation of glucosylglycerol accumulation. Microbiology 152, 2023–30. doi:10.1099/mic.0.28771-0

Martin, W., Rujan, T., Richly, E., Hansen, A., Cornelsen, S., Lins, T., Leister, D., Stoebe, B., Hasegawa, M., Penny, D., 2002. Evolutionary analysis of Arabidopsis, cyanobacterial, and chloroplast genomes reveals plastid phylogeny and thousands of cyanobacterial genes in the nucleus. Proc. Natl. Acad. Sci. U. S. A. 99, 12246–51. doi:10.1073/pnas.182432999

Mattila, J.P., Shnyrova, A. V, Sundborger, A.C., Hortelano, E.R., Fuhrmans, M., Neumann, S., Muller, M., Hinshaw, J.E., Schmid, S.L., Frolov, V.A., 2015. A hemi-fission intermediate links two mechanistically distinct stages of membrane fission. Nature 524, 109–113. doi:10.1038/nature14509

McCollom, T.M., Seewald, J.S., 2006. Carbon isotope composition of organic compounds produced by abiotic synthesis under hydrothermal conditions. Earth Planet. Sci. Lett. 243, 74–84. doi:10.1016/J.EPSL.2006.01.027

Mears, J.A., Lackner, L.L., Fang, S., Ingerman, E., Nunnari, J., Hinshaw, J.E., 2011. Conformational changes

in Dnm1 support a contractile mechanism for mitochondrial fission. Nat. Struct. Mol. Biol. 18, 20–6. doi:10.1038/nsmb.1949

Mendiola-Morgenthaler, L., Eichenberger, W., Boschetti, A., 1985. Isolation of chloroplast envelopes from Chlamydomonas. Lipid and polypeptide composition. Plant Sci. 41, 97–104. doi:10.1016/0168-9452(85)90109-8

Merchant, S.S., Prochnik, S.E., Vallon, O., Harris, E.H., Karpowicz, S.J., Witman, G.B., Terry, A., Salamov, A., Fritz-Laylin, L.K., Marechal-Drouard, L., Marshall, W.F., Qu, L.-H., Nelson, D.R., Sanderfoot, A.A., Spalding, M.H., Kapitonov, V. V., Ren, Q., Ferris, P., Lindquist, E., Shapiro, H., Lucas, S.M., Grimwood, J., Schmutz, J., Cardol, P., Cerutti, H., Chanfreau, G., Chen, C.-L., Cognat, V., Croft, M.T., Dent, R., Dutcher, S., Fernandez, E., Fukuzawa, H., Gonzalez-Ballester, D., Gonzalez-Halphen, D., Hallmann, A., Hanikenne, M., Hippler, M., Inwood, W., Jabbari, K., Kalanon, M., Kuras, R., Lefebvre, P.A., Lemaire, S.D., Lobanov, A. V., Lohr, M., Manuell, A., Meier, I., Mets, L., Mittag, M., Mittelmeier, T., Moroney, J. V., Moseley, J., Napoli, C., Nedelcu, A.M., Niyogi, K., Novoselov, S. V., Paulsen, I.T., Pazour, G., Purton, S., Ral, J.-P., Riano-Pachon, D.M., Riekhof, W., Rymarquis, L., Schroda, M., Stern, D., Umen, J., Willows, R., Wilson, N., Zimmer, S.L., Allmer, J., Balk, J., Bisova, K., Chen, C.-J., Elias, M., Gendler, K., Hauser, C., Lamb, M.R., Ledford, H., Long, J.C., Minagawa, J., Page, M.D., Pan, J., Pootakham, W., Roje, S., Rose, A., Stahlberg, E., Terauchi, A.M., Yang, P., Ball, S., Bowler, C., Dieckmann, C.L., Gladyshev, V.N., Green, P., Jorgensen, R., Mayfield, S., Mueller-Roeber, B., Rajamani, S., Sayre, R.T., Brokstein, P., Dubchak, I., Goodstein, D., Hornick, L., Huang, Y.W., Jhaveri, J., Luo, Y., Martinez, D., Ngau, W.C.A., Otillar, B., Poliakov, A., Porter, A., Szajkowski, L., Werner, G., Zhou, K., Grigoriev, I. V., Rokhsar, D.S., Grossman, A.R., 2007. The Chlamydomonas Genome Reveals the Evolution of Key Animal and Plant Functions. Science (80-.). 318, 245–250. doi:10.1126/science.1143609

Mettlen, M., Pucadyil, T., Ramachandran, R., Schmid, S.L., 2009. Dissecting dynamin's role in clathrin-mediated endocytosis. Biochem. Soc. Trans. 37, 1022–6. doi:10.1042/BST0371022

Michie, K. a, Boysen, A., Low, H.H., Møller-Jensen, J., Löwe, J., 2014. LeoA, B and C from enterotoxigenic Escherichia coli (ETEC) are bacterial dynamins. PLoS One 9, e107211. doi:10.1371/journal.pone.0107211

Miller J H, 1972. Experiments in molecular genetics. Cold Spring Harb. Lab. Press. Cold Spring Harb. NY.

Mimuro, M., Tomo, T., Tsuchiya, T., 2008. Two unique cyanobacteria lead to a traceable approach of the first appearance of oxygenic photosynthesis. Photosynth. Res. 97, 167–176. doi:10.1007/s11120-008-9311-4

Mitschke, J., Georg, J., Scholz, I., Sharma, C.M., Dienst, D., Bantscheff, J., Voss, B., Steglich, C., Wilde, A., Vogel, J., Hess, W.R., 2011. An experimentally anchored map of transcriptional start sites in the model cyanobacterium Synechocystis sp. PCC6803. Proc. Natl. Acad. Sci. U. S. A. 108, 2124–2129. doi:10.1073/pnas.1015154108

Mizusawa, N., Wada, H., 2012. The role of lipids in photosystem II. Biochim. Biophys. Acta - Bioenerg. 1817, 194–208. doi:10.1016/j.bbabio.2011.04.008

Moren, B., Shah, C., Howes, M.T., Schieber, N.L., McMahon, H.T., Parton, R.G., Daumke, O., Lundmark, R., 2012. EHD2 regulates caveolar dynamics via ATP-driven targeting and oligomerization. Mol. Biol. Cell 23, 1316–1329. doi:10.1091/mbc.E11-09-0787

Morishima, K., Yoshida, M., Furuya, A., Moriuchi, T., Ota, M., Furukawa, Y., 2007. Improving the performance of a direct photosynthetic/metabolic bio-fuel cell (DPBFC) using gene manipulated bacteria. J. Micromechanics Microengineering 17, 2391–2391. doi:10.1088/0960-1317/17/11/C01

Morlot, S., Roux, A., 2015. Europe PMC Funders Group Mechanics of Dynamin-Mediated Membrane Fission 629–649. doi:10.1146/annurev-biophys-050511-102247.Mechanics

Mullineaux, C.W., 2014. Electron transport and light-harvesting switches in cyanobacteria. Front. Plant Sci. 5, 1–6. doi:10.3389/fpls.2014.00007

Muramatsu, M., Hihara, Y., 2012. Acclimation to high-light conditions in cyanobacteria: From gene expression to physiological responses. J. Plant Res. 125, 11–39. doi:10.1007/s10265-011-0454-6

Nagar, S., Argikar, U.A., Tweedie, D.J., 2014. Enzyme kinetics in drug metabolism: fundamentals and applications., Methods in molecular biology (Clifton, N.J.). doi:10.1007/978-1-62703-758-7_1

Nakamura, Y., Kaneko, T., Sato, S., Mimuro, M., Miyashita, H., Tsuchiya, T., Sasamoto, S., Watanabe, A., Kawashima, K., Kishida, Y., Kiyokawa, C., Kohara, M., Matsumoto, M., Matsuno, A., Nakazaki, N., Shimpo, S., Takeuchi, C., Yamada, M., Tabata, S., 2003. Complete Genome Structure of Gloeobacter violaceus PCC 7421, a Cyanobacterium that Lacks Thylakoids. DNA Res. 10, 137–145.

doi:10.1093/dnares/10.4.137

Nakamura, Y., Kaneko, T., Tabata, S., 2000. CyanoBase, the genome database for Synechocystis sp. strain PCC6803: status for the year 2000. Nucleic Acids Res. 28, 72.

Nantais, D.E., Schwemmle, M., Stickney, J.T., Vestal, D.J., Buss, J.E., 1996. Prenylation of an interferon-gamma-induced GTP-binding protein: the human guanylate binding protein, huGBP1. J. Leukoc. Biol. 60, 423–31.

Nevo, R., Charuvi, D., Shimoni, E., Schwarz, R., Kaplan, A., Ohad, I., Reich, Z., 2007. Thylakoid membrane perforations and connectivity enable intracellular traffic in cyanobacteria. EMBO J. 26, 1467–1473. doi:10.1038/sj.emboj.7601594

Nickelsen, J., Rengstl, B., Stengel, A., Schottkowski, M., Soll, J., Ankele, E., 2011. Biogenesis of the cyanobacterial thylakoid membrane system - an update. FEMS Microbiol. Lett. 315, 1–5. doi:10.1111/j.1574-6968.2010.02096.x

Nordera, P., Dalla Serra, M., Menestrina, G., 1997. The adsorption of Pseudomonas aeruginosa exotoxin A to phospholipid monolayers is controlled by pH and surface potential. Biophys. J. 73, 1468–1478. doi:10.1016/S0006-3495(97)78179-7

Orso, G., Pendin, D., Liu, S., Tosetto, J., Moss, T.J., Faust, J.E., Micaroni, M., Egorova, A., Martinuzzi, A., McNew, J.A., Daga, A., 2010. Homotypic fusion of ER membranes requires the dynamin-like GTPase Atlastin. Nature 464, 942–942. doi:10.1038/nature08886

Oxborough, K., Baker, N.R., 1997. Resolving chlorophyll a fluorescence images of photosynthetic efficiency into photochemical and non-photochemical components – calculation of qP and Fv-/Fm-; without measuring Fo-; Photosynth. Res. 54, 135–142. doi:10.1023/A:1005936823310

Park, J.M., Cho, J.H., Kang, S.G., Jang, H.J., Pih, K.T., Piao, H.L., Cho, M.J., Hwang, I., 1998. A dynamin-like protein in Arabidopsis thaliana is involved in biogenesis of thylakoid membranes. EMBO J. 17, 859–867. doi:10.1093/emboj/17.4.859

Peschek, G.A., Hinterstoisser, B., Wastyn, M., Kuntner, O., Pineau, B., Missbichler, A., Lang, J., 1989. Chlorophyll precursors in the plasma membrane of a cyanobacterium, Anacystis nidulans. Characterization of protochlorophyllide and chlorophyllide by spectrophotometry,

spectrofluorimetry, solvent partition, and high performance liquid chromatography. J. Biol. Chem. 264, 11827–32.

Pojidaeva, E., Zinchenko, V., Shestakov, S. V., Sokolenko, A., 2004. Involvement of the SppA1 Peptidase in Acclimation to Saturating Light Intensities in Synechocystis sp. Strain PCC 6803. J. Bacteriol. 186, 3991–3999. doi:10.1128/JB.186.12.3991-3999.2004

Porra, R.J., Thompson, W.A., Kriedemann, P.E., 1989. Determination of accurate extinction coefficients and simultaneous equations for assaying chlorophylls a and b extracted with four different solvents: verification of the concentration of chlorophyll standards by atomic absorption spectroscopy. Biochim. Biophys. Acta - Bioenerg. 975, 384–394. doi:10.1016/S0005-2728(89)80347-0

Praefcke, G.J.K., McMahon, H.T., 2004. The dynamin superfamily: universal membrane tubulation and fission molecules? Nat. Rev. Mol. Cell Biol. 5, 133–47. doi:10.1038/nrm1313

Pucadyil, T.J., Schmid, S.L., 2008. Real-Time Visualization of Dynamin-Catalyzed Membrane Fission and Vesicle Release. Cell 135, 1263–1275. doi:10.1016/j.cell.2008.11.020

Qin, M., Wang, W., Thirumalai, D., 2015. Protein folding guides disulfide bond formation. Proc. Natl. Acad. Sci. U. S. A. 112, 11241–6. doi:10.1073/pnas.1503909112

Rakhimberdieva, M.G., Vavilin, D. V., Vermaas, W.F.J., Elanskaya, I. V., Karapetyan, N. V., 2007. Phycobilin/chlorophyll excitation equilibration upon carotenoid-induced non-photochemical fluorescence quenching in phycobilisomes of the cyanobacterium Synechocystis sp. PCC 6803. Biochim. Biophys. Acta - Bioenerg. 1767, 757–765. doi:10.1016/j.bbabio.2006.12.007

Rast, A., Heinz, S., Nickelsen, J., 2015. Biogenesis of thylakoid membranes. Biochim. Biophys. Acta 1847, 821–830. doi:10.1016/j.bbabio.2015.01.007

Renosto, F., Seuberts, P.A., Segele, I.H., 1984. Adenosine 5’-Phosphosulfate Kinase from. Society 259, 2113–2123.

Reubold, T.F., Faelber, K., Plattner, N., Posor, Y., Ketel, K., Curth, U., Schlegel, J., Anand, R., Manstein, D.J., Noé, F., Haucke, V., Daumke, O., Eschenburg, S., 2015. Crystal structure of the dynamin tetramer. Nature 525, 404–408. doi:10.1038/nature14880

Rexroth, S., Mullineaux, C.W., Ellinger, D., Sendtko, E., Rögner, M., Koenig, F., 2011. The plasma membrane of the cyanobacterium Gloeobacter violaceus contains segregated bioenergetic domains. Plant Cell 23, 2379–2390. doi:10.1105/tpc.111.085779

Rippka, R., Deruelles, J., Waterbury, J.B., Herdman, M., Stanier, R.Y., 1979. Generic assignments, strain histories and properties of pure cultures of cyanobacteria. J. Gen. Microbiol. 111, 1–61. doi:10.1099/00221287-111-1-1

Rippka, R., Waterbury, J., Cohen-Bazire, G., 1974. A cyanobacterium which lacks thylakoids. Arch. Microbiol. 100, 419–436. doi:10.1007/BF00446333

Roeters, S.J., Van Dijk, C.N., Torres-Knoop, A., Backus, E.H.G., Campen, R.K., Bonn, M., Woutersen, S., 2013. Determining in situ protein conformation and orientation from the amide-I sum-frequency generation spectrum: Theory and experiment. J. Phys. Chem. A 117, 6311–6322. doi:10.1021/jp401159r

Rolland, N., Curien, G., Finazzi, G., Kuntz, M., Maréchal, E., Matringe, M., Ravanel, S., Seigneurin-Berny, D., 2012. The Biosynthetic Capacities of the Plastids and Integration Between Cytoplasmic and Chloroplast Processes. Annu. Rev. Genet. 46, 233–264. doi:10.1146/annurev-genet-110410-132544

Roston, R., Gao, J., Xu, C., Benning, C., 2011. Arabidopsis chloroplast lipid transport protein TGD2 disrupts membranes and is part of a large complex. Plant J. 66, 759–769. doi:10.1111/j.1365-313X.2011.04536.x

Rupprecht, E., Gathmann, S., Fuhrmann, E., Schneider, D., 2007. Three different DnaK proteins are functionally expressed in the cyanobacterium Synechocystis sp. PCC 6803. Microbiology 153, 1828–1841. doi:10.1099/mic.0.2007/005876-0

Sánchez, M., Bernal-Castillo, J., Rozo, C., Rodríguez, I., 2003. Spirulina (arthrospira): an edible microorganism: a review. Univ. Sci. 8, 7–24.

Sanchez, S.A., Tricerri, M.A., Gunther, G., Gratton, E., 2007. Laurdan Generalized Polarization: from cuvette to microscope. Mod. Res. Educ. Top. Microsc. 2, 1007–1014.

Santel, A., Fuller, M.T., 2001. Control of mitochondrial morphology by a human mitofusin. J. Cell Sci. 114, 867–874. doi:mitochondrial fusion fzo human gtpase dynamin related protein mitofusin outer-

membrane protein dynamin-related gtpase saccharomyces-cerevisiae coiled coils fusion yeast reticulum fzo1p maintenance fission

Sawant, P., Eissenberger, K., Karier, L., Mascher, T., Bramkamp, M., 2016. A dynamin-like protein involved in bacterial cell membrane surveillance under environmental stress. Environ. Microbiol. 18, 2705–2720. doi:10.1111/1462-2920.13110

Schaller-Laudel, S., Latowski, D., Jemioła-Rzemińska, M., Strzałka, K., Daum, S., Bacia, K., Wilhelm, C., Goss, R., 2017. Influence of thylakoid membrane lipids on the structure of aggregated light-harvesting complexes of the diatom *Thalassiosira pseudonana* and the green alga *Mantoniella squamata*. Physiol. Plant. 160, 339–358. doi:10.1111/ppl.12565

Schaller, S., Latowski, D., Jemioła-Rzemińska, M., Dawood, A., Wilhelm, C., Strzałka, K., Goss, R., 2011. Regulation of LHCII aggregation by different thylakoid membrane lipids. Biochim. Biophys. Acta - Bioenerg. 1807, 326–335. doi:10.1016/j.bbabio.2010.12.017

Schaller, S., Richter, K., Wilhelm, C., Goss, R., 2014. Influence of pH, Mg2+, and lipid composition on the aggregation state of the diatom FCP in comparison to the LHCII of vascular plants. Photosynth. Res. 119, 305–317. doi:10.1007/s11120-013-9951-x

Schlimpert, S., Wasserstrom, S., Chandra, G., Bibb, M.J., Findlay, K.C., Flärdh, K., Buttner, M.J., 2017. Two dynamin-like proteins stabilize FtsZ rings during *Streptomyces* sporulation. Proc. Natl. Acad. Sci. 201704612. doi:10.1073/pnas.1704612114

Schneider, D., Fuhrmann, E., Scholz, I., Hess, W.R., Graumann, P.L., 2007. Fluorescence staining of live cyanobacterial cells suggest non-stringent chromosome segregation and absence of a connection between cytoplasmic and thylakoid membranes. BMC Cell Biol. 8, 39. doi:10.1186/1471-2121-8-39

Schopf, J.W., 1993. Microfossils of the Early Archean Apex chert: new evidence of the antiquity of life. Science 260, 640–646. doi:10.1126/science.260.5108.640

Schottkowski, M., Ratke, J., Oster, U., Nowaczyk, M., Nickelsen, J., 2009. Pitt, a Novel Tetratricopeptide Repeat Protein Involved in Light-Dependent Chlorophyll Biosynthesis and Thylakoid Membrane Biogenesis in Synechocystis sp. PCC 6803. Mol. Plant 2, 1289–1297. doi:10.1093/mp/ssp075

Selão, T.T., Zhang, L., Ariöz, C., Wieslander, Å., Norling, B., 2014. Subcellular Localization of

Monoglucosyldiacylglycerol Synthase in Synechocystis sp. PCC6803 and Its Unique Regulation by Lipid Environment. PLoS One 9, e88153. doi:10.1371/journal.pone.0088153

Sevier, C.S., Kaiser, C.A., 2002. Formation and transfer of disulphide bonds in living cells. Nat. Rev. Mol. Cell Biol. 3, 836–847. doi:10.1038/nrm954

Shah, C., Hegde, B.G., Morén, B., Behrmann, E., Mielke, T., Moenke, G., Spahn, C.M.T.T., Lundmark, R., Daumke, O., Langen, R., Mor??n, B., Behrmann, E., Mielke, T., Moenke, G., Spahn, C.M.T.T., Lundmark, R., Daumke, O., Langen, R., 2014. Structural insights into membrane interaction and caveolar targeting of dynamin-like EHD2. Structure 22, 409–420. doi:10.1016/j.str.2013.12.015

Shen, G., Boussiba, S., Vermaas, W.F., 1993. Synechocystis sp PCC 6803 strains lacking photosystem I and phycobilisome function. Plant Cell 5, 1853–63.

Shen, Y.R., 2012. Basic Theory of Surface Sum-Frequency Generation. J. Phys. Chem. C. doi:10.1021/jp305539v

Shevela, D., Pishchalnikov, R., Eichacker, L., 2013. Oxygenic Photosynthesis in Cyanobacteria. Stress Biol. Cyanobacteria 3–40. doi:10.1201/b13853-3

Shnyrova, A. V, Bashkirov, P. V, Akimov, S. a, Pucadyil, T.J., Zimmerberg, J., Schmid, S.L., Frolov, V. a, 2013. Geometric catalysis of membrane fission driven by flexible dynamin rings. Science 339, 1433–6. doi:10.1126/science.1233920

Shpetner, H.S., Vallee, R.B., 1992. Dynamin is a GTPase stimulated to high levels of activity by microtubules. Nature 355, 733–735. doi:10.1038/355733a0

Shpetner, H.S.H.S.S., Vallee, R.B., Paschal, B.P., Shpetner, H.S.H.S.S., Reese, T.S., Sheetz, M.P., Fujimoto, E.K., Goeke, N.M., Olson, B.J., Klenk, D.C., 1989. Identification of dynamin, a novel mechanochemical enzyme that mediates interactions between microtubules. Cell 59, 421–432. doi:10.1016/0092-8674(89)90027-5

Simidjiev, I., Stoylova, S., Amenitsch, H., Javorfi, T., Mustardy, L., Laggner, P., Holzenburg, A., Garab, G., 2000. Self-assembly of large, ordered lamellae from non-bilayer lipids and integral membrane proteins in vitro. Proc. Natl. Acad. Sci. U. S. A. 97, 1473–6.

Singh, A.K., Bhattacharyya-Pakrasi, M., Pakrasi, H.B., 2008. Identification of an atypical membrane protein involved in the formation of protein disulfide bonds in oxygenic photosynthetic organisms. J. Biol. Chem. 283, 15762–15770. doi:10.1074/jbc.M800982200

Singh, S.M., Panda, A.K., 2005. Solubilization and refolding of bacterial inclusion body proteins. J. Biosci. Bioeng. 99, 303–310. doi:10.1263/jbb.99.303

Siva Kiran, R., Madhu, G., Satyanarayana, S., 2015. Spirulina in combating Protein Energy Malnutrition (PEM) and Protein Energy Wasting (PEW) - A review. J. Nutr. Res. 3, 62–79.

Smirnova, E., Griparic, L., Shurland, D.-L., van der Bliek, A.M., 2001. Dynamin-related Protein Drp1 Is Required for Mitochondrial Division in Mammalian Cells. Mol. Biol. Cell 12, 2245–2256. doi:10.1091/mbc.12.8.2245

Smits, M., Sovago, M., Wurpel, G.W.H., Kim, D., Müller, M., Bonn, M., 2007. Polarization-resolved broad-bandwidth sum-frequency generation spectroscopy of monolayer relaxation. J. Phys. Chem. C 111, 8878–8883. doi:10.1021/jp067453w

Song, B.D., Leonard, M., Schmid, S.L., 2004. Dynamin GTPase domain mutants that differentially affect GTP binding, GTP hydrolysis, and clathrin-mediated endocytosis. J. Biol. Chem. 279, 40431–40436. doi:10.1074/jbc.M407007200

Staeheli, P., Haller, O., Boll, W., Lindenmann, J., Weissmann, C., 1986. Mx protein: Constitutive expression in 3T3 cells transformed with cloned Mx cDNA confers selective resistance to influenza virus. Cell 44, 147–158. doi:10.1016/0092-8674(86)90493-9

Studier, F.W., Moffatt, B.A., 1986. Use of bacteriophage T7 RNA polymerase to direct selective high-level expression of cloned genes. J. Mol. Biol. 189, 113–130. doi:10.1016/0022-2836(86)90385-2

Summons, R.E., Jahnke, L.L., Hope, J.M., Logan, G.A., 1999. 2-Methylhopanoids as biomarkers for cyanobacterial oxygenic photosynthesis. Nature 400, 554–557. doi:10.1038/23005

The UniProt Consortium, 2017. UniProt: The universal protein knowledgebase. Nucleic Acids Res. 45, D158–D169. doi:10.1093/nar/gkw1099

Tran, A.X., Dong, C., Whitfield, C., 2010. Structure and Functional Analysis of LptC, a Conserved Membrane

Protein Involved in the Lipopolysaccharide Export Pathway in *Escherichia coli*. J. Biol. Chem. 285, 33529–33539. doi:10.1074/jbc.M110.144709

Trivedi, M. V, Laurence, J.S., Siahaan, T.J., 2009. The role of thiols and disulfides on protein stability. Curr. Protein Pept. Sci. 10, 614–25.

Ugarte-Uribe, B., Müller, H.M., Otsuki, M., Nickel, W., García-Sáez, A.J., 2014. Dynamin-related protein 1 (Drp1) promotes structural intermediates of membrane division. J. Biol. Chem. 289, 30645–30656. doi:10.1074/jbc.M114.575779

Uniacke, J., Zerges, W., 2007. Photosystem II Assembly and Repair Are Differentially Localized in Chlamydomonas. Plant Cell Online 19, 3640–3654. doi:10.1105/tpc.107.054882

Van De Meene, A.M.L., Hohmann-Marriott, M.F., Vermaas, W.F.J., Roberson, R.W., 2006. The three-dimensional structure of the cyanobacterium Synechocystis sp. PCC 6803. Arch. Microbiol. 184, 259–270. doi:10.1007/s00203-005-0027-y

Van Der Bliek, A.M., 1999. Functional diversity in the dynamin family. Trends Cell Biol. 9, 96–102. doi:10.1016/S0962-8924(98)01490-1

Vermass, W.F., Rutherford, A.W., Hansson, O., 1988. Site-directed mutagenesis in photosystem II of the cyanobacterium Synechocystis sp. PCC 6803: Donor D is a tyrosine residue in the D2 protein. Proc. Natl. Acad. Sci. U. S. A. 85, 8477–81.

Verseux, C., Baqué, M., Lehto, K., de Vera, J.-P.P., Rothschild, L.J., Billi, D., 2016. Sustainable life support on Mars – the potential roles of cyanobacteria. Int. J. Astrobiol. 15, 65–92. doi:10.1017/S147355041500021X

Vestal, D.J., Jeyaratnam, J.A., 2011. The Guanylate-Binding Proteins: Emerging Insights into the Biochemical Properties and Functions of This Family of Large Interferon-Induced Guanosine Triphosphatase. J. Interf. Cytokine Res. 31, 89–97. doi:10.1089/jir.2010.0102

Waltz, 2006. Dual-PAM-100 Measuring System for Simultaneous Assessment of P700 and Chlorophyll Fluorescence. System.

Wang, Z., Xu, C., Benning, C., 2012. TGD4 involved in endoplasmic reticulum-to-chloroplast lipid trafficking

is a phosphatidic acid binding protein. Plant J. 70, 614–623. doi:10.1111/j.1365-313X.2012.04900.x

Weidner, T., Castner, D.G., 2013. SFG analysis of surface bound proteins: a route towards structure determination. Phys. Chem. Chem. Phys. 15, 12516–24. doi:10.1039/c3cp50880c

Westphal, S., Soll, J., Vothknecht, U.C., 2001. A vesicle transport system inside chloroplasts. FEBS Lett. 506, 257–61.

Xiao, D., Fu, L., Liu, J., Batista, V.S., Yan, E.C.Y., 2012. Amphiphilic adsorption of human islet amyloid polypeptide aggregates to lipid/aqueous interfaces. J. Mol. Biol. 421, 537–547. doi:10.1016/j.jmb.2011.12.035

Xu, C., Fan, J., Cornish, A.J., Benning, C., 2008. Lipid trafficking between the endoplasmic reticulum and the plastid in Arabidopsis requires the extraplastidic TGD4 protein. Plant Cell 20, 2190–204. doi:10.1105/tpc.108.061176

Xu, C., Fan, J., Riekhof, W., Froehlich, J.E., Benning, C., 2003. A permease-like protein involved in ER to thylakoid lipid transfer in Arabidopsis. EMBO J. 22, 2370–2379. doi:10.1093/emboj/cdg234

Yang, J., Yan, R., Roy, A., Xu, D., J, P., Zhang, Y., 2015. The I-TASSER Suite: Protein structure and function prediction. Nat. Methods 12, 7–8. doi:10.1038/nmeth.3213

Yu, L., Zhao, J., Muhlenhoff, U., Bryant, D.A., Golbeck, J.H., 1993. PsaE Is Required for in Vivo Cyclic Electron Flow around Photosystem I in the Cyanobacterium Synechococcus sp. PCC 7002. Plant Physiol. 103, 171–180.

Zakar, T., Herman, E., Vajravel, S., Kovacs, L., Knoppová, J., Komenda, J., Domonkos, I., Kis, M., Gombos, Z., Laczko-dobos, H., 2017. Biochimica et Biophysica Acta Lipid and carotenoid cooperation-driven adaptation to light and temperature stress in Synechocystis sp . PCC6803. BBA - Bioenerg. 1858, 337–350. doi:10.1016/j.bbabio.2017.02.002

Zhang, S., Laborde, S.M., Frankel, L.K., Bricker, T.M., 2004. Four Novel Genes Required for Optimal Photoautotrophic Growth of the Cyanobacterium Synechocystis sp. Strain PCC 6803 Identified by In Vitro Transposon Mutagenesis. J. Bacteriol. 186, 875–879. doi:10.1128/JB.186.3.875-879.2004

Zhang, S., Spann, K.W., Frankel, L.K., Moroney, J. V, Bricker, T.M., 2008. Identification of two genes, sll0804

and slr1306, as putative components of the CO2-concentrating mechanism in the cyanobacterium Synechocystis sp. strain PCC 6803. J. Bacteriol. 190, 8234–7. doi:10.1128/JB.01126-08

Zhang, X., Hu, J., 2010. The Arabidopsis chloroplast division protein DYNAMIN-RELATED PROTEIN5B also mediates peroxisome division. Plant Cell 22, 431–442. doi:10.1105/tpc.109.071324

Zheng, J., Cahill, S.M., Lemmon, M.A., Fushman, D., Schlessinger, J., Cowburn, D., 1996. Identification of the Binding Site for Acidic Phospholipids on the PH Domain of Dynamin: Implications for Stimulation of GTPase Activity. J. Mol. Biol. 255, 14–21. doi:10.1006/jmbi.1996.0002

Declaration

I hereby declare that I wrote the dissertation submitted without any unauthorized external assistance and used only sources acknowledged in the work. All textual passages which are appropriated verbatim or paraphrased from published and unpublished texts as well as all information obtained from oral sources are duly indicated and listed in accordance with bibliographical rules. In carrying out this research, I complied with the rules of standard scientific practice as formulated in the statutes of Johannes Gutenberg-University Mainz to insure standard scientific practice.

_____ Mainz, den _____

Ruven Jilly